MOLECULAR MECHANISMS OF SELECTIVE AUTOPHAGY IN INNATE IMMUNITY

A thesis submitted in fulfilment of the requirements for the degree of Doctor of Philosophy in Life Sciences

PANAGIOTIS TSAPRAS

University ID: 1591990

University of Warwick, School of Life Sciences
May 2021

TABLE OF CONTENTS

PART II — MATERIALS & METHODS

LIST OF FIGURES

INTRODUCTION

MATERIALS & METHODS

RESULTS

Chapter 5

Chapter 6

Chapter 7

DISCUSSION

APPENDIX

LIST OF TABLES

INTRODUCTION

MATERIALS & METHODS

APPENDIX

DECLARATION & CONTRIBUTIONS

Declaration: This thesis is submitted to the University of Warwick in support of my application for the degree of Doctor of Philosophy. It has been composed by the author (Panagiotis Tsapras) and has not been submitted in any previous application for any degree.

Contributions: All work presented here (including data generated and data analysis) was carried out by the author except in the cases outlined below:

Prof. Terje Johansen

Figure 1.5 (Adapted from existing publication with permission)

Prof. Pascal Meier

Figure 7.1 (A)

Dr. Anne-Claire Jacomin

Creation of FLPout-mCherry-Atg8a flies

Creation of Atg8a plasmid for Yeast-2-Hybrid Screen

Dr. Radu Tusco

Compilation of Ref(2)P-like UBD protein list

ACKNOWLEDGMENTS

This PhD work would not have been made into reality, had it not been for a large number of people who helped me both at the professional and personal level. Due to space limitations, I apologise to everyone not mentioned by name here, but I would like to affirm that their aid is under no circumstance, any less appreciated.

First, I would like to thank my PhD supervisor Prof. Ioannis Nezis for not only offering me a fascinating science topic to work on, but also challenging me to improve step by step as a researcher. It is in large part due to his ceaseless support throughout this 4-year journey (5 if also counting the COVID-19 lockdown), that I have emerged as a more complete scientist and person. Second, Dr. Anne-Claire Jacomin, to whom I owe a debt of gratitude that will never be fully repaid; for her otherworldly support and level of patience with me and my never-ending barrage of questions. I apologise, thank, and hope rum is a good start for paying-off that debt.
I have been fortunate enough to not only work alongside, but also develop lasting friendships with fantastic people in both our lab, and the School of Life Sciences as a whole. I thank from the bottom of my heart Dr. Stavroula Petridi from our team, for her aid and comments in various aspects of my work, as a professional and as a friend. Special thanks go out in particular to fellow PhD sufferers-turned Drs, Marisa, and Bhavini; who have been by side throughout this endeavour as trusted colleagues, and valued friends. A special mention also goes to Ash for having single-handedly kept the lab running along with my fly stocks, during my time away.
I express my sincere gratitude to my PhD advisory panel members, Dr. Kristen Panfilio and Dr. Mark Wall, whose always accurate comments and alternative perspective on my work during our meetings, provided a much-needed, refreshing outlook that kept me from losing focus of my research. I would also like to thank the entire Media Prep Team and especially Akos Torok, for preparing the fly food on time and putting up with me and my at-times ludicrous requests.

Finally, the people who have suffered and laughed the most with me, my Mum, Dad and Brother Nikos. No words of gratitude are enough to do their love and support justice, which carried me through at the times of greatest professional and personal turmoil. And to Konstantina, I hope to return in kind the love and encouragement she has given me, in spite of her own PhD struggles. Thank you for being a constant source of my happiness and personal development through these years.

ABBREVIATIONS

3xFLAG	3 Repeats of DYKDDDDK
6xHis	6 Repeats of Histidine
aa	Amino-Acid
Abs	Antibodies
AMP	Anti-Microbial-Peptide
Atg/ATG	Autophagy-related protein
Atg8a	Autohagy-related protein 8a
$Atg8a^{LDS}$	Atg8a LIR Docking Site
AttA	*Attacin, isoform A*
BSA	Bovine Serum Albumin
CMA	Chaperone-Mediated Autophagy
DAPI	4′,6-Diamidino-2-Phenylindole
DptB	*Diptericin, isoform B*
Dro	*Drosocin*
Drosophila	*Drosophila melanogaster*
dTAB2	*Drosophila* TAK1 Binding Protein 2
dTAK1	*Drosophila* TAK1
E. coli	*Escherichia Coli*
Ecc15	*Erwinia Carotovora Carotovora* 15
EM	Electron Microscopy
FLAG®	Sigma Aldrich trademark name of the DYKDDDDK sequence
FT	Flow-Through
GABARAP	Gamma-Aminobutyric Acid Receptor-Associated Protein
GAL4	Galactose-induced 4 transcription factor
GST	Glutathione S-Transferase
Hsc70	Heat shock cognate protein of 70 kDa
HSPA8	Heat shock protein family A [Hsp70] member 8
IF	Immuno-Fluorescence
IKKb	Inhibitor of NF-kB kinase subunit beta (β)
iLIR™	Interactive LIR Software
Imd/IMD	Immune Deficiency
Ird5	Immune Response Deficient 5
JNK	c-Jun N-Terminal Kinase
Kenny	Inhibitor of NFkB kinase subunit gamma/IKKgamma (γ)
LAMP-2A	Lysosome-associated membrane protein type 2A
LB	Lysogeny Broth
LDS	LIR-Docking Site
LIR	LC3-Interacting Region
mA	Micro-autophagy

MAP1LC3 (also LC3)	Microtubule-Associated Protein 1 Light Chain 3
mCherry	Mammalian Cherry
mRNA	Messenger RNA
NBR1	Neighbour Of BRCA1 Gene 1
NDP52	Nuclear Domain 10 Protein 52
NEMO	Nfkb Essential Modulator
NF-κB	Nuclear Factor Kappa (K) Beta
OPTN	Optineurin
PD	Pull-Down
PE	Phosphatidylethanolamine
PGN	Peptidoglycan
PGRP-LC	Peptidoglycan-Recognition Protein Long, Isoform C
PGRP-SA/B/C/D	Peptidoglycan-Recognition Protein Short, Isoform A/B/C/D
pH3	Phospho-Histone 3
Phospho/p	Phosphorylated
PI3K	Phosphoinositide 3-Kinase
PI3P	Phosphatidylinositol-3-Phosphate
Pirk	Poor Imd Response Upon Knock-In
PSSM	Position Specific Scoring Matrix
qPCR	Quantitative Polymerase Chain Reaction
Ref(2)P	Refractory to sigma P
Relish	Nuclear factor NF-kB p110 subunit
S. cerevisiae	*Saccharomyces cerevisiae*
SAR	Selective Autophagy Receptor
SDS	Sodium Dodecyl Sulfate
SDS-PAGE	SDS Polyacrylamide Gel Electrophoresis
SH3PX1	Src Homology 3 And Phox Domain-Containing 1
SID	Specific Interaction Domain
SNX	Sorting Nexin
TAK1	Transforming Growth Factor B-Activated Kinase 1
TCT	Tracheal Cytotoxin
TNFR	Tumor Necrosis Factor Receptor
TNFα	Tumor Necrosis Factor Alpha (A)
UAS	Upstream Activating Sequence
Ub	Ubiquitin
UBD	Ubiquitin Binding Domain
WB	Western Blot
WT	Wild Type
Y2H	Yeast-2-Hybrid

Author's Note 1: For the purpose of this manuscript, where a given name for a protein is the same between the fruit fly and other organisms e.g mammals, the fruit fly proteins are distinguished by the use of either of the prefixes "*Drosophila*", "*Dm*" (from ***D****rosophila* ***m****elanogaster*), or "d", followed by the protein name in regular capital case. Where the surrounding content of the text leaves no expected room for confusion that it refers to the fruit fly system, the standardized *Drosophila* nomenclature for genes (Capitalized first letter and italics font) and phenotypes (Capitalized first letter, normal font) is followed. As an example of the above, the names "*Drosophila* TAK1", "*Dm*TAK1", and "dTAK1" refer to the TAK1 protein of the fruit fly; while the names "*Tak1"* and "Tak1" denote the TAK1 gene and the phenotype (details of phenotype given in text) respectively.

Author's Note 2: The term "autophagy" used throughout this manuscript refers to ***macro-autophagy***; a specialized form of the autophagic process. Where other forms of autophagy are discussed, these are explicitly referred to by name and explained in text.

ABSTRACT

Selective autophagy is a catabolic route that engulfs cellular material on specialized vesicles called "*autophagosomes*" before turning them over to lysosomes for degradation. Such degradation substrates often interact and are anchored by the autophagosome-localized core autophagy protein LC3 (Atg8a in *Drosophila*). Autophagy is a pivotal process that helps in maintaining a homeostatic intracellular environment by contributing, among other functions, to the attenuation of innate immune signalling for several pathways, such as the IMD response in *Drosophila*. The IMD pathway, which this work focused on, is among the innate immune cascades that become increasingly harder to terminate with age; correlating with a concomitant waning of autophagy's functions. The exact regulatory interactions between IMD pathway components and the autophagy machinery remain largely unknown.

This work identified that the apical kinase of the *Drosophila* IMD pathway, dTAK1, as well as its co-activator dTAB2, interact with the autophagy protein Atg8a as examined by GST-pulldown experiments and confocal microscopy colocalization studies. Furthermore, the interaction between dTAK1 and Atg8a seems to rely on the functional LIR motif harboured in the C-terminal of dTAK1, that binds its cognate LDS region on Atg8a. Observations from qPCR assays that were employed to measure mRNA expression levels of the IMD-regulated genes *AttA*, *DptB* and *Dro* in conventionally reared young and old adult flies, suggest that the dTAK1 LIR motif prevents at least partly, the chronic overactivation of the IMD pathway. This study also further delineates the role of the Atg8a-interacting protein SH3PX1 in downregulating the IMD pathway, by characterizing the interaction between dTAB2 and SH3PX1, assessed by mass-spectroscopy and GST pulldown experiments. Genetic ablation of *Sh3px1* correlates with both, increased levels of *AttA*, *DptB* and *Dro* that suggest overactivation of the IMD pathway in young and old *Sh3px1*-deficient flies, as well as their overall markedly reduced lifespan compared to controls in survival assays.

Based on the insight gleaned by this study, I propose a mechanistic model for the dTAK1/dTAB2/SH3PX1 interactions with Atg8a, which may collectively mediate the selective autophagic degradation of the dTAK1/dTAB2 complex, and prevent in turn the constitutive activation of the IMD pathway in *Drosophila*. The conservation of all components in mammals provides encouraging evidence for potential similarities with the human condition as well.

Part I

INTRODUCTION

Chapter 1

An Outline of Ageing: Setting the Stage of the Study

The "Tragedy of Tithonus" is an ancient Greek mytheme, illustrating how eternal life is wasted without the corresponding health to match. According to the story, the goddess Eos pleads with Zeus to grant her handsome but mortal lover, Tithonus, the gift of immortality. Jealous of Eos's infatuation with a mortal, Zeus grants the prince eternal life — but in an act of deceit— not eternal youth. Unable to die, Tithonus grows increasingly decrepit; losing all of his once striking visage and vitality and ultimately, the love of the goddess as well [1].

Attaining immortality and remaining forever vigorous, are two concepts which galvanized humanity since ancient times. Our pursuit for eternal life and the proverbial fountain of youth has only grown more sophisticated with time, so that nowadays immortality and eternal youth are represented by the research aimed at extending our overall "lifespan" and "healthspan" respectively. As of to date, there are many promising drug targets and therapeutic strategies in development which attempt to fulfil both of these criteria [2]. Present day investigations of ageing focus on delineating the mechanisms behind the process, pinpoint its roots, and ameliorate its more detrimental side-effects to the largest possible extent. However, ageing is a multifactorial process that involves an intricate cross-talk of cellular pathways between each other and with environmental factors and as such, it is a challenge for any study to thoroughly address any aspect at length. This project focuses on the interplay between just two processes that affect ageing: inflammation and autophagy. More specifically it deals with how autophagy can regulate the innate immune-signalling pathway through sequestration of specific components, and how this may contribute towards increasing the window of overall good health in one's lifespan.

To better contextualize the findings discussed herein, it is important to present at first a working definition for ageing, along with the main schools of thought for its onset and the impact of chronic inflammation in its propagation. Autophagy and inflammation are each presented in their own introductory chapters.

1.1 *Ageing: Definition & Prevalent Theories for its Onset*

In the context of homeostasis, "ageing" may be described as the time-dependent functional decline and deregulation of cellular mechanisms, which progressively tips the scale from a balanced and optimal working cellular environment, to one favouring the accumulation of internal damage [3]. This damage can propagate to nearby or distant tissues and eventually lead to the organism-wide deterioration in function [3]. The progressive functional decline can manifest as decreased adaptability to intrinsic, as well as extrinsic stresses and reduced reproductive capacity; further accompanied by an increased risk of susceptibility to disease and mortality [3]. Ageing is almost always observably accompanied by frailty; overall muscle weakness, unintentional weight-loss, and low capacity for physical activity [4], and the rather more innocent by-standers for mammals; progressive greying and loss of hair and reduced skin elasticity [5].

Most theories regarding the onset of ageing seem to stem primarily from two schools of thought according to the primary causality model they support: "damage/ internal error" and "programme-based". The first group gives more weight to the damage accumulated within cells over time, which eventually becomes unsustainable, and in the upper hierarchy results in tissue and organ failure. More specifically, proponents within the group argue that it is the combination of a chronic build-up of metabolic by-products to toxic levels, together with the progressive failure of maintenance and repair mechanisms to clear out such by-products, which accounts for most of the deleterious aspects of ageing [6]. The binding theme of all the different theories in this class is that cellular damage can occur at random. As such they consider ageing as a stochastic process, largely influenced by the interplay between internal biochemical reactions and external environmental factors [6].

On the other end of the spectrum, "programme-based" theories place more emphasis on the genetic component, by arguing that ageing is a somewhat pre-determined process, driven primarily by genes and as an extent, the pathways their products regulate [6]. From an evolutionary standpoint according to this group, it is not in evolution's best interest to maintain repair systems in perfect working order, once an organism has passed its reproductive prime. In this regard, ageing can be thought of as a built-in countdown timer, where biological mechanisms purposefully fail, or deterioration over time is increasingly allowed to propagate. This would make ageing a cost-effective method for organisms to obtain an evolutionary benefit by limiting lifespan of each species around its optimal reproductive range [6].

There are many overlapping concepts between both theory camps; Damage-based theories recognize the roles of certain genes in delaying or contributing to ageing, and vice-versa; programme-based theories acknowledge that some forms of damage and environmental factors do indeed exert varying degrees of influence on the outcome of ageing [6]. As is the case with testing hypotheses, there are caveats in both camps [6], and this is mainly due to the fact that each attempts to pinpoint the cause for ageing to only a subset of functions going awry; either via randomly accumulated damage, or in a deterministic manner. As the quote from statistics states: "*association does not necessarily imply causation*", and it may be erroneous to attempt and explain the full aetiology of ageing through assigning only certain factors as its primary causes. A more unifying perspective that combines the genetic control of maintenance and repair mechanisms, as well as the stochastic nature of damage from internal errors and environmental factors has been gaining ground in the recent decade, favouring instead the complex interplay between the two that ultimately dictates the outcome of ageing with regards to health [7]. Ageing is as such, a multifactorial process that demands the implementation of more systematic and integrative approaches for understanding its biology.

But why the apparent overabundance of ageing theories? A potential explanation might simply boil down to us being — ironically enough — still young in our majority to the concept of "old age". By that is meant that the limitations of past periods in important areas for one's wellbeing such as medicine, healthcare, and the socio-economic infrastructure, as well as the often tumultuous times in each era, largely accounted for the high morbidity rates experienced among children and adults at the time. As such, even though an individual's maximum lifespan, might have remained relatively unchanged since ancient times, the population's average life expectancy as whole was significantly shorter compared to today's standards [8]. In fact due to such limitations, as recently as the 1800s an average individual was expected to live until around 40-50 years [9]. The overall stability of the modern era and advancements in sectors important for the quality of life, make it that the privilege of an extended life expectancy — currently around 80 years [9] — is now enjoyed by the majority of the global population. Since this is a relatively late phenomenon, emerged within the last 200 years, it may be argued that it is not until recently that the reproductive and survival programming have firmly taken a backseat, and more of us reach old age to experience the full extent that our inherent systems fail us over time, and are consequently afforded the luxury to ponder on the root of the problem.

1.2 *"Inflamm-Ageing" & The Protective Role of Autophagy*

Low-grade chronic inflammation has been positively associated with the more detrimental side-effects of ageing in humans, as well as in several invertebrate animal models used for studying aspects of the process in relative lower complexity systems [10]–[12]. Among the sources for this chronic inflammation that seem to be the most directly relevant to ageing and can have a large impact on the process are cell senescence, the imbalance between adaptive and innate immune responses, and the perturbed relationship between the gut microbiome and the host [13]–[16]. Irrespective of source, a common characteristic is that all such inflammatory signals start localized but become progressively persistent with age and eventually converge, resulting in propagation of the age-related deterioration in a system-wide manner [17]. At the turn of the millennium Franceschi and colleagues coined the term "*inflamm-ageing*" to emphasize the importance of such low-grade inflammatory signals in collectively driving the ageing process [10].

Without going into much detail, it is important to note that cell senescence is regarded as an initially protective response against the onset of cancer, as it arrests proliferation of defective cells [18], [19]. However, the secretome of senescent cells is particularly enriched in pro-inflammatory cytokines that exacerbates inflammatory responses of nearby cells [18], [19]. This characteristic marker is known as the "senescence-associated secretory phenotype" and is the most likely cause of inflammation associated with cell senescence during ageing [18], [19]. With respect to the gut microbiome, observations from studies comparing the gut flora composition of centenarians with that of other elderly individuals, agree that preservation of commensal gut microbiota populations reduces the risk of deregulated inflammatory responses in the tissue, and overall promotes healthy ageing [16], [20]. The importance of maintaining a balanced and proportionate activation of inflammatory responses in the gut with regards to homeostasis and ageing is further discussed in Introductory Section 3.3.

Progressive overactivation of the innate immune system is a characteristic feature of ageing and for organisms with adaptive immunity as well — such as humans — this is accompanied by a parallel steady decline of adaptive immune responses [11], [13], [21]. Innate immune signalling is primarily mediated by the evolutionarily conserved transcription factor NF-κB [11], [22]. With regards to how inflammatory cues become increasingly frequent and progressively harder to terminate with age, some of the primary contributing factors can be traced back to mitochondrial deficiencies, which result in the overactivation of

inflammasomes [23], [24]. These multimeric signalling complexes are fundamental in mounting of the innate immune defence mechanisms as they integrate cues from extrinsic and intrinsic sources, and their prototypic mode of operation involves activation of caspase-1, which in turn mediates the release of pro-inflammatory cytokines interleukin-1β and -18 [25], [26]. Inflammasomes can be upregulated by ROS (***R****eactive* ***O****xygen* ***S****pecies*) signals, or the release of mtDNA and other mitochondrial constituents in the cytoplasm; which result from disruption of mitochondrial membrane integrity and similar perturbations that derail normal functionality of these organelles [23], [24]. By extension, impaired clearance of defective mitochondria by a cell's trafficking and degradation pathways exacerbates inflammasome activation, which in turn contributes to an increase in innate immune responses [23], [24].

Misfolded or long-lived proteins, as well as protein aggregates and obsolete organelles, are primarily removed by the quintessential housekeeping activities of autophagy, and the proteasome systems (and certain routes of endocytosis). The age-associated rise in systemic pro-inflammatory markers consequently correlates with these processes' gradual reduction in their efficiency. For instance, elevated expression levels of the immune-proteasome — a sign of neuro-inflammation — were observed in the brains of elderly Alzheimer's patients, but not healthy subjects [27]. Autophagy has already been established to be responsible for shaping the inflammatory response by removing defective mitochondria [23], [24]. Furthermore, the deregulated neuroendocrine signalling, which causes the system-wide ageing deterioration has also been demonstrated to result from aberrant inflammatory responses in the brain [28], largely attributed to defective autophagy [29]. As an example, the recycling pathway was found to be downregulated in the hypothalamus of mice on high-fat diet, which correlated with increased NF-κB-mediated inflammatory signals from the structure and exacerbated the systemic built-up of insulin resistance and development of diabetes [29]. When function of IKKβ (**i**nhibitor of NF-**κ**B **k**inase-**β**); the main NF-κB activator kinase, was impaired in autophagy-deficient mice, they were in turn largely spared from obesity and inflammatory markers [29]. In addition, autophagy's regulatory role in NF-κB signalling has been further highlighted by the research team of I. Nezis and others, demonstrating that the regulatory subunit of the IKKβ kinase mediates the degradation of the IKK complex by selective autophagy [30]–[33]; a type of autophagy explained in further detail in section 2.6.

Keeping the focus on inflammation, it is evident that systematic failure of intracellular trafficking and recycling pathways — such as autophagy — in maintaining homeostasis by regulating immune responses, is a central component in propagating the inflammatory phenotype of ageing. Maintaining the regulatory controls that keep the balance between pro- and anti-inflammatory responses is therefore key to extending the overall window of health well into old age [34], [35]. As such, nowadays the majority of anti-ageing drug discovery and research revolves around utilizing autophagy-activators and NF-κB inhibitors [11], [35]. In terms of individual-driven changes to lifestyle habits, dietary restriction is the most well-characterized, simple, and arguably most cost-effective method to reduce some of the detrimental side-effects of ageing [11], [35]. Its autophagy-inducing and inflammation-dampening properties are well-documented in literature, and remains to-date the most consistently employed strategy for increasing overall life- and health-span in all animal models studied so far [11], [36], [37].

A considerable amount of effort is targeted towards delineating the different stages of ageing, that also offers prospects for identifying early markers with potential prognostic value. An extensive review on this subject utilizing all relevant data from existing literature, breaks down the ageing process into nine characteristic hallmarks [17]. While discussing these hallmarks here is beyond the main focus of this work, it is important to note that many of them are either the direct result of, or strongly correlate with deregulated immune signalling, or impaired autophagic clearance, or finally, the perturbed crosstalk between the two [17].

The above further underpin the importance of understanding the mechanism behind the regulation of inflammation by autophagy and fuel the scientific efforts to uncover promising novel targets for integrative anti-ageing strategies (Figure 1.1).

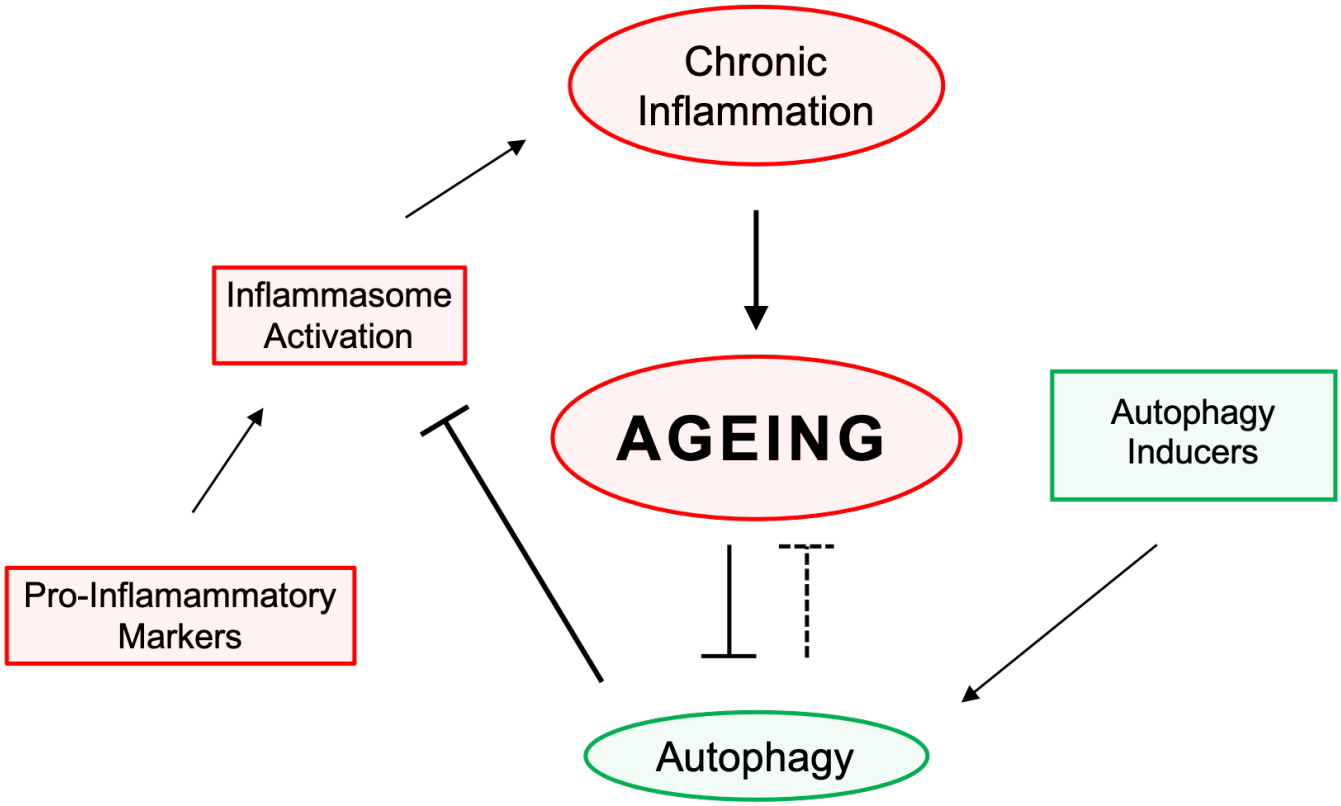

Figure 1.1. ***Ageing as a Function of Inflammation and Autophagy***. Pro-inflammatory markers, e.g invading pathogens, aggregate formations, and ROS or mtDNA release from defective mitochondria, trigger inflammasomes and subsequent mounting of innate immune responses. Normally, these responses are transient in nature and the source of their activation is cleared by the upkeep mechanisms of cells, such as autophagy. However, as efficiency of autophagy wanes with age, innate immune responses become progressively harder to terminate and are maintained at a low-grade level. This low-grade chronic inflammation exacerbates the ageing process and the accompanying decline of cellular, tissue and organ functions (represented with **bold black arrow**). In contrast, many promising anti-ageing strategies and drug development approaches, revolve around inducing, or maintaining autophagy efficiency in late age, as under these circumstances autophagy can dampen chronic inflammatory signaling and delay the ageing process (dotted "**T**"-shaped line).

Chapter 2

Autophagy & Endocytic Trafficking

Intracellular trafficking of membrane-coated vesicles is mediated together by autophagy and endocytosis; with the former being more degradation-oriented, while the latter also carries out sorting and recycling activities [38]. Because of their very similar mechanism of action, many of their individual components overlap and function in both pathways, with the lysosome acting as the final common endpoint where autophagy and endocytosis converge to deliver their cargo for degradation [38]. Several landmark studies identified the key structures and principles for autophagy activation, as well as the genetic component of its regulation. A cursory overview of the main findings from these early investigations would aid in providing additional sub-context for this current work, since their discoveries have also served in conjunction with other studies, to separate the processes of autophagy and endocytosis from each other.

With regards to endocytosis, my interest is on the sorting nexin (SNX) family of endocytic trafficking regulators [39]. More specifically, I focus on the *Drosophila* SNX18 homologue, SH3PX1. As it will be expanded further below, SNX18/SH3PX1 is one of many endocytic proteins that crosstalk with the autophagy apparatus. Therefore, to better understand how it is involved in both pathways I provide a short overview of endocytosis (Introductory section 2.7.1), and then briefly describe the properties of the specific SNX-family group that SNX18/SH3PX1 belongs to, which make its members interesting with regards to how they may promote the autophagic process (Introductory section 2.7.3).

In addition, this investigative work used the fruit fly as a model system to recapitulate key aspects of ageing, innate immune signalling, and autophagy as observed in higher complexity organisms. There are certain benefits justifying the use of *Drosophila* as a basis for certain types of studies such as this, which are presented here; prior to discussing the autophagy process in reasonable — yet not exhaustive — detail, along with a complementary view of endocytosis.

2.1 *Drosophila as A Model To Study Cellular Pathways*

"[…] s*ometimes these dollars, they go to projects having little or nothing to do with the public good, things like fruit fly research in Paris, France. I kid you no*t."

Sarah Palin,
Vice-Presidential Candidate, 2008 US Elections

The above infamous quote by Ms. Palin [40], encapsulates the inherent risks of perpetuating misconceptions regarding the perceived importance of certain model organisms in science, which can sometimes influence vital decisions on research funds allocation. The "common fruit fly" (*Drosophila melanogaster*) has been in fact an invaluable model system to researchers for well over a century now; earning itself several Nobel Prizes along the way. When interest into Mendel's theory of heredity was re-kindled during the early 19th century, there was a need for a complex yet easy to manipulate organism to test the newly proposed principles of inheritance on. *Drosophila* was distinctly selected among other candidate organisms for this purpose, as it was found to combine many desired properties which are still relevant to this day, making it a popular choice among different research disciplines.

Fruit flies have a very short life cycle of 10-12 days from egg to adult at 25^{o}C, and produce a large number of eggs per generation, rendering them ideal for lineage studies. Their small size and cost-effective maintenance allow their cultivation in large numbers. *Drosophila* combines the benefits of being simple enough to manipulate with relative ease, while also retaining a great level of the complexity found in higher metazoans, favouring *in vivo* work. Many pathways and their components are functionally conserved between fruit flies and mammals. This large degree of homology has in turn enabled researchers to use the fruit fly extensively as a cheaper and more easily accessible resource than mammalian models, and often serves as a starting point of investigations before moving onto higher and more complex eukaryote systems. In early 2000, the fly genome was fully sequenced [41] and found to share ~60% similarity to human, with less redundancy [41]. This means there are fewer genetic duplication events found throughout the fly genome compared to humans, which makes genetic studies easier. Because of the high degree of similarity shared between the fly and human genomes, nearly 65% of the human genes associated with a known disease are also expressed in the fruit fly [42]. Finally, the genome of *Drosophila* is distributed between just 4 chromosomes, compared to 23 for humans, which greatly

simplifies genetic studies. Furthermore, there are generally fewer limitations regarding the use of fruit flies in a laboratory setting compared to mammalian cell lines or live organisms.

The relative ease of working with *Drosophila* has created a positive feedback loop, where more advanced genetic tools are developed in order to further facilitate finer manipulation of this model organism. The UAS-GAL4 and FLP-FRT systems for targeted gene expression (further explained in Materials & Methods section 4.3.1.) are routinely used in fruit flies, allowing mosaic analysis of phenotypes that might otherwise be lethal under whole-tissue conditions [43], [44]. This is further simplified with the creation of balancer chromosomes, which are modified chromosomes that carry large inversions across their sequence to supress homologous crossover. Balancer chromosomes were first developed in the fly by H. Muller [45], as a way to preserve mutations which would otherwise be lethal in homozygosity. In this manner, instead of being lost after several generations, such mutations remain in the gene pool through the heterozygotes of the population. A balancer chromosome often additionally carries one or more dominant marker mutations, that result in the manifestation of a distinct phenotype in heterozygotes, and as such makes the screening of individuals with the desired genotype in a fly population easier. The development of targeted gene editing technologies such as RNA interference [46] and more recently, CRISPR-Cas9 [47], has refined the available toolkit for researchers to allow for the generation of fly lines carrying specific point mutations. Combined with the existing targeted expression systems such as UAS-GAL4 and FLP-FRT, the diverse arsenal of genetic tools that scientists have at their disposal enables the creation of multiple different combination of mutations in a single fly. The fly research community is fortunate enough to boast one of the largest extents of unrestricted access to commonly available resources, as individual labs and large stock centres create fly stocks with particular characteristics, most of which are easily obtainable. Finally, the modern fly researcher benefits from the existence of “Flybase”; a large online and publicly accessible datahub containing annotations for every gene in *Drosophila*, together with associated mutations, homologues in other organisms, and available stocks to order as needed.

2.2 *Discovery of Autophagy & Autophagy-Related Genes*

The characterization of the lysosome in 1955 by Christian de Duve [48] spearheaded research aimed into identifying intracellular degradation pathways and their mechanism of action. In these early stages of the field, electron microscopy (EM) imaging contributed significantly towards this endeavour. A year later, driven from preliminary observations in lysosome-rich rat liver fractions, A. Novikoff would comment on the presence of "*dense-bodies*", with elevated acid phosphatase-activity and at times containing identifiable cytoplasmic components [49]. As they would state on that same paper, further work would be warranted to confirm whether these "*dense-bodies*" are distinct from lysosomes [49]. In 1957, while studying differentiation in murine kidney tubule cells, S. Clark reported that, in addition to lysosomes, cells also contained irregularly-shaped vacuoles of amorphous material, with encapsulated mitochondria on occasion [50]. Perhaps unknown to him at the time, with this report S. Clark would provide the first line of evidence for the existence of autophagy in cells. T.P Ashford and K.R Porter would follow in 1962 with their work on rat liver cells describing a time-dependent increase in the number of lysosomes, and their translocation towards the centre of the cell, following treatment with glucagon [51]. As the concept of autophagy was still unknown, they would label some of these membranous structures containing cytoplasmic components like mitochondria, as nascent lysosomes, when in fact they had captured autophagosomes on image [51].

Prompted by all the above major findings, while attending a symposium on lysosomes in London, de Duve would finally introduce the term "*autophagy*" to the scientific community in 1963 [52]. Inspired by the ancient Greek word "*αὐτόφαγος*", which translates to "self-devouring", he used this expression to denote the delivery route for lysosomal degradation of material originating from within the cell, therefore distinguishing it from the other major protein trafficking route known at the time; "*heterophagy*" [52]. The latter term was used to place emphasis on the extracellular source of the degradation substrates that are delivered to lysosomes in a highly similar manner, and that pathway was itself later renamed "*endocytosis*". Shortly thereafter, A.U Arstila and B.F Trump would study "*autophagocytosis*" and publish their extensive work in 1968, within which they defined the "autophagosome" as a double-membrane organelle without hydrolase activity, where cytoplasmic material is retained without being degraded [53]. In the same work they further coined the terms "*autophagic vacuoles*" and "*autolysosomes*" to refer to the double-

or single-membrane vesicles respectively and which contained material in various stages of degradation, or displayed hydrolase activity in turn [53].

These important findings provided an early roadmap for identifying and ordering the most characteristic stages of autophagy. The process begins with the formation of a crescent-shaped, double-membrane structure known as the phagophore. The phagophore grows and expands to eventually encircle itself and close maturing to a double-membrane vesicle called an autophagosome. A signature group of autophagy proteins; the Atg8-family (discussed in further detail in Introduction section 2.5.1), is crucial during the entire process of expansion and maturation, as well as tethering cargo labelled for degradation which is continuously delivered to the vesicle. The autophagosome subsequently fuses with a lysosome and it, along with all its contents, are completely broken down by the resident proteolytic enzymes. Any leftover building block material, such as amino-acids, can then be recycled back to the cytoplasm where it is taken up by other metabolic pathways (Figure 1.2) [54].

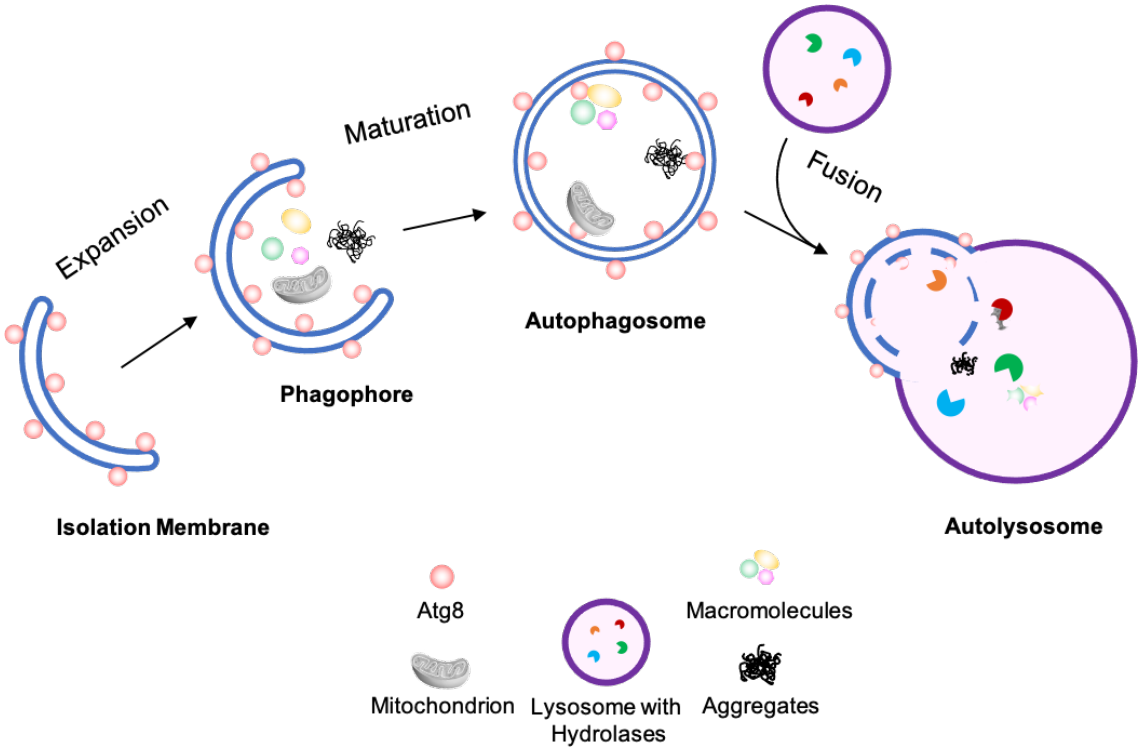

Figure 1.2. ***Simplified Autophagy Pathway Progression***. The process begins with the formation of a double-membrane template, which progressively elongates into a developing phagophore. The phagophore expands and eventually closes and matures to a complete autophagosome. During the entire process, the Atg8-family of proteins functions to expand the membrane and sequester cargo for degradation on the structure. Autophagosomes then fuse with lysosomes (autolysosome) and are degraded along with all their contents by the resident hydrolases in the lysosomal lumen. Leftover salvaged material can then be recycled back to the cell, to fuel subsequent reactions.

Since these initial studies, research on autophagy continued to grow in an accelerated pace, and described the physiological role of the pathway as a survival response and its regulation according to nutrient availability in the extracellular environment [55], [56]. Furthermore, A. Poli [57], and G.E Mortimore [55], [56] independently showed in similar experiments that certain amino-acids in various combinations could inhibit the pathway. In around the same time U. Pfeifer also reported on the downregulatory effect of insulin on autophagy [58].

Up to this point in time, ultrastructural EM investigations and biochemical assays dominated the field of autophagy. Two major limitations however hindered additional progress: the lack of specific markers for autophagosomes and autolysosomes, and a simple enough model organism to monitor autophagy *in-vivo*. These were eventually addressed through the individual efforts from the research teams of Y.Ohsumi [59], [60], D.H Wolf [61] and D.J. Klionsky [62], who employed the common brewer's yeast *Saccharomyces cerevisiae* to study the process under the light microscope [59] and characterize the first core autophagy genes [60]. By inducing random genomic mutations, Y. Ohsumi and M. Tsukada created a library of *S. cerevisiae* mutants, which they screened for and then performed genomic sequencing on those strains that did not form autophagosomes following starvation and died faster compared to controls [60]. The first autophagy-defective yeast mutant characterized in this manner was "*apg1",* and in which the authors later pinpointed the responsible gene, named "***Atg1"*** (**A**u**t**opha**g**y-related **1**) [60]. Using the absence of autophagic bodies and the reduced viability of the *apg1* mutant as the reference phenotype, Y. Ohsumi and M. Tsukada isolated similar autophagy-defective mutants and compiled a list of the initial 15 core *Atg* genes that are conserved in all metazoans [60]. This seminal work opened new avenues in autophagy research to explore and laid the foundation for all subsequent studies that continue to build on an expand this *Atg* list. In acknowledgment of his contributions, Y.Ohsumi was awarded in return the 2016 Nobel Prize in Physiology [63].

2.3 *Autophagy Through the Lens of Evolution*

To highlight the intricate relationship between the innate immune system and autophagy, it would be helpful to take a brief look on the evolutionary history of these two processes as they developed in eukaryotes.

Targeting of cargoes to lysosomes makes up the core mechanism of autophagy, and it remains largely the same from yeast to mammals. This high degree of conservation suggests that the process appeared early during eukaryotes' evolution. It is generally accepted that autophagy along with endocytosis, were both present in the last common eukaryotic ancestor [64]. As autophagy is a major component of the survival response to starvation, according to the most prevalent theory, cells in nutrient-scarce environments may have utilized an early form of self-eating as an alternative way to acquire nutrients [64], [65]. Break-down of own material would provide a surge of essential amino-acids to fuel vital functions long enough for cells to escape harsh conditions for more favourable ones [64]; an acceptable trade-off of functionality for survival, under this context. The same environmental stressors which pushed eukaryotic cells to re-arrange, degrade and recycle cytoplasmic components, may have also provided the evolutionary impetus for differentiation and development to emerge; collectively resulting in cells gaining progressively increased control of their intracellular environment [64], [65]. As both development and differentiation involve large-scale changes of extensive intracellular re-shuflling and turnover, it is conceivable that they would have benefitted by pre-existing trafficking mechanisms that degraded and recycled long-lived, or damaged components [65]. Supporting this view, in some lower eukaryotes the external stimuli that upregulate autophagy also act as signals for their differentiation and development pathways [65].

The ability to selectively sequester portions of the cytoplasm in isolation membranes may have been a key event that accelarated the emergence of the first host-defense mechanisms against invading pathogens. Harmful microbes and hosts have been developing adaptation strategies to each other since early in their shared history. In such a scenario, the host could utilize an autophagy-like process to encapsulate potential invaders in membranous vesicles, isolating them from the rest of the cytoplasm, and perhaps eliminating them later by targeting those vesicles for degradation. As such, autophagy may have been one of the earliest forms of anti-microbial defense in the developing arsenal of the first innate immune response, while pathogens co-evolved in turn to avoid detection by, or even exploit the host autophagic machinery for their replication [66], [67].

2.4 *Different Types of Autophagy*

The pronounced upregulation of autophagy following starvation had prompted the scientific community to regard the process for a time as a solely indiscriminate pathway for the *en-masse* degradation of cytoplasmic material, aptly rereferred to as "bulk-autophagy" [68], [69]. While cells indeed utilize non-selective bulk-autophagy as their primary survival response to starvation, this is only one aspect of an otherwise multi-faceted process. As of yet, there are 3 primary types of autophagy encountered in eukaryotes (Figure 1.4): i) ***c****haperone-****m****ediated* ***a****utophagy* (CMA; so far only in mammals), ii) ***m****icro-****a****utophagy* (mA) and iii) *macro-autophagy*. CMA is solely selective, while mA and macro-autophagy can degrade substrates either selectively, or in-bulk. Given our current understanding, it seems that overall indiscriminate autophagy may be more important for the adaptation of cells to nutrient scarcity, while selective autophagy maintains homeostasis under basal conditions by recycling cytosolic proteins and organelles. However, these two forms are not necessarily exclusive to one another and overlap to varying degrees, which often makes their distinction challenging.

2.4.1 Chaperone-mediated autophagy

CMA has only been observed in mammals so far. It is a form exclusive to proteins; more specifically those that contain the KFERQ motif, or amino-acid sequences which closely mimic the biochemical properties of this penta-peptide [70]. By nature of its function, CMA is strictly selective towards its target substrates, unlike micro- and macro-autophagy, which can also operate in a less-discriminate manner. With regards to its mechanism of action, the **h**eat-**s**hock **c**ognate **70** kDa (HSC70) chaperone (also known as HSP8; **h**eat-**s**hock **p**rotein family A member **8**) recognizes and binds the KFERQ motif, and together with other co-chaperone complexes, bring the protein substrate to the lysosomal surface [71]. Here, resident proteins on either side of the lysosomal membrane act synergistically to form a receptor/translocation complex, which will shuttle the target substrate to the lumen. On the cytosolic side, monomers of **l**ysosome-**a**ssociated **m**embrane **p**rotein **2A** (LAMP2A) sequester the target molecule —acting here as a receptor— with aid from HSC70/HSP8, and are brought to close proximity with each other [72], [73]. In the meantime on the luminal side, the HSP90 chaperone stabilizes those

monomeric LAMP2A subunits further [74], thus contributing in the formation of the multimer receptor/translocation complex. After the substrate has passed through to the lysosome lumen, the complex disassembles and LAMP2A returns to its monomeric state and the cycle can begin anew [74]. LAMP2A's availability to engage in substrate binding is the rate-limiting step for CMA activity, and this appears to be governed more so by degradation and organization of LAMP2A at the lysosomal surface, rather than by *de-novo* synthesis of the protein [75], [76].

CMA participates during protein quality control [77], and is also upregulated by a wide range of stressors including starvation [78], DNA damage [79], hypoxia [80] and lipid challenges [81]. Nutrient-depriving stimuli in particular, seem to be among the strongest upregulators of the pathway [78]. Most cells that undergo starvation activate non-selective autophagy as their first response. Bulk macro-autophagy exhibits an activity window between the first 30 minutes to 8 hours post-induction. Despite generating a source of essential amino-acids to keep vital functions operating, the excessive degradation of cytoplasmic material on the other hand can also be equally life-threatening to the cell. To prevent this, if the starvation-inducing stimulus persists for more than 10 hours, cells can preferentially switch to CMA, with peak activation reached around the 36- hour mark, and maintained for about 3 additional days thereafter [78], [82], [83]. It is still largely unclear when the exact switch from bulk autophagy to CMA happens and which cues aid in this regard. One theory posits that the depletion of target substrate may be one such signal for the degradation of some enzymes by CMA, as is the case for certain glycolytic enzymes [84]. Many glycolytic enzymes harbour KFERQ-like targeting motifs that may be potentially hidden by HSP70/HSP8 when the enzymes are bound on their substrate or protein complex [84], however the lack of substrate or dissociation from active complexes may contribute in these nested motifs becoming more readily accessible to the chaperone HSP70/HSP8 and promote in turn the CMA-mediated degradation of the enzyme [78], [82]–[84].

HSC70/HSP8 and LAMP2A may reportedly also take part in a form of macro-autophagy called chaperone-**assisted** selective autophagy. In this mode of autophagy, chaperones in conjunction with ubiquitination complexes present substrates to autophagy receptors, such as SQSTM1/p62 (**se**q**ue**s**t**oso**m**e **1**/ubiquitin-binding **p**rotein **62**) and NBR1 (**n**eighbour of **BR**CA1 gene **1**) [85]–[87]. This may further facilitate recognition of the target substrate by macro-autophagy and subsequent turnover to the lysosome [85]–[87].

With regards to disease phenotypes, it is difficult to attribute a specific pathology to CMA dysregulation, especially because when CMA is perturbed, other forms of autophagy

will take over to compensate [88]. As perhaps an interesting exception to the above, in the ageing retinal tissue CMA activity seems to increase, despite the overall decline of autophagy function [89].

Even though CMA remains so far exclusive to mammals, certain aspects of the process can be also observed in comparatively lower complexity organisms such as *Drosophila*. Out of the 6 *Hsc70* paralogues encoded in total by the fly genome, *Hsc70-4* shares the largest sequence identity with human *HSC70* (87%), making it the closest to its mammalian counterpart closest in terms of sequence [90]. In addition, despite fruit flies lacking a *Lamp2A* gene, ectopically-expressed human LAMP2A is reportedly still able to recapitulate facets of its functionality in mammals, such as promoting autophagic flux [91]. This was observed in the *Drosophila* brain, where the function of human LAMP2A contributed to a protective net effect in neurons that also ectopically-expressed human synuclein A [91]. This largely prevented the development of Parkinson-like symptoms in these neurons [91] and highlights that the molecular machinery which enables the autophagy-related functions of LAMP2A in mammals, is also retained to a degree in flies.

2.4.2 Micro – autophagy

mA is the least understood type of autophagy. Here, the lysosome directly pinches-off portions of the cytoplasm, through localized re-arrangement/deformation of its limiting membrane. Degradation substrates enter the lumen either via small invaginations of the lysosomal membrane, or via arm-like protrusions that extend and progressively encircle the substrate until it is completely engulfed [92]. A third form of mA termed "*endosomal mA*", involves the endosome; specifically the late endosome, which sequesters degradation material on **m**ulti-**v**esicular **b**odies (MVBs) by small surface invaginations [92]. Members of the ESCRT family of proteins localizing on the surface of late endosomes are central in the formation of MVBs, which are subsequently targeted to the lysosome via chaperone proteins [92]. This mode has been identified in mammalian cells [93], and more recently in *Drosophila* as well [90], [94]. However, most of our current knowledge about mA comes from studies on yeast vacuoles (the functional equivalents of lysosomes). Small-sized cytoplasmic material seems to enter the vacuole through non-selective mA and this process also likely counter-balances the increased membrane influx from other intracellular vesicle

trafficking routes [95], thus contributing in the regulation of the vacuole's size and surface composition [95]. Selective mA has been described for mitochondria (micro-mitophagy), the ER [96], portions of the nucleus (micro-nucleophagy, or piecemeal micro-nucleophagy), lipid droplets [97], and peroxisomes (micro-pexophagy) [98].

To-date, the only process that has been unequivocally attributed to mA is the turnover of peroxisomes to the vacuole under specific conditions in the fungus *Pichia pastoris* [98]. Information on pathologies associated with perturbed mA is equally scarce. mA might be a potential route for glycogen entry into lysosomes of skeletal muscle cells [99]. Pompe disease is a rare autosomal recessive myopathy in the larger group of lysosomal storage disorders, where lysosomes lack the necessary enzyme to metabolise glycogen in their lumen [100]. This leads to build-up of intralysosomal glycogen, with progressive muscle deterioration and breathing difficulties being among the more common symptoms of the disease [100]. The most frequent causes of death among Pompe disease patients are associated with cardiomuscular atrophy and respiratory failure [100]. A fluorescent analogue of glycogen was shown to localize within large lysosomes, into distinct sub-membrane compartments not normally seen under physiological conditions [100]. The localization of these compartments within lysosomes prompted the authors to suggest that glycogen may be entering the organelle through mA via lysosomal invaginations [100].

2.4.3 Macro - autophagy

Macro-autophagy was the first type of autophagy discovered in cells, and despite being the most well-studied form to-date, new data continuously emerge about its physiology, regulation, and mode of operation. This type is distinguished from the others by its signature structure: the ***autophagosome***. Several different protein complexes work in a synergistic fashion throughout the *de-novo* synthesis of this transient organelle, to the anchoring of degradation cargo on its membrane, and its subsequent fusion with lysosomes. The results of the work presented herein stem exclusively from studying this form of the process. Therefore, to demonstrate how autophagy may discriminate between different target substrates, via specific interactions between autophagy receptors and autophagosome-localized proteins, the core principles of its mechanism and selectivity need to be discussed.

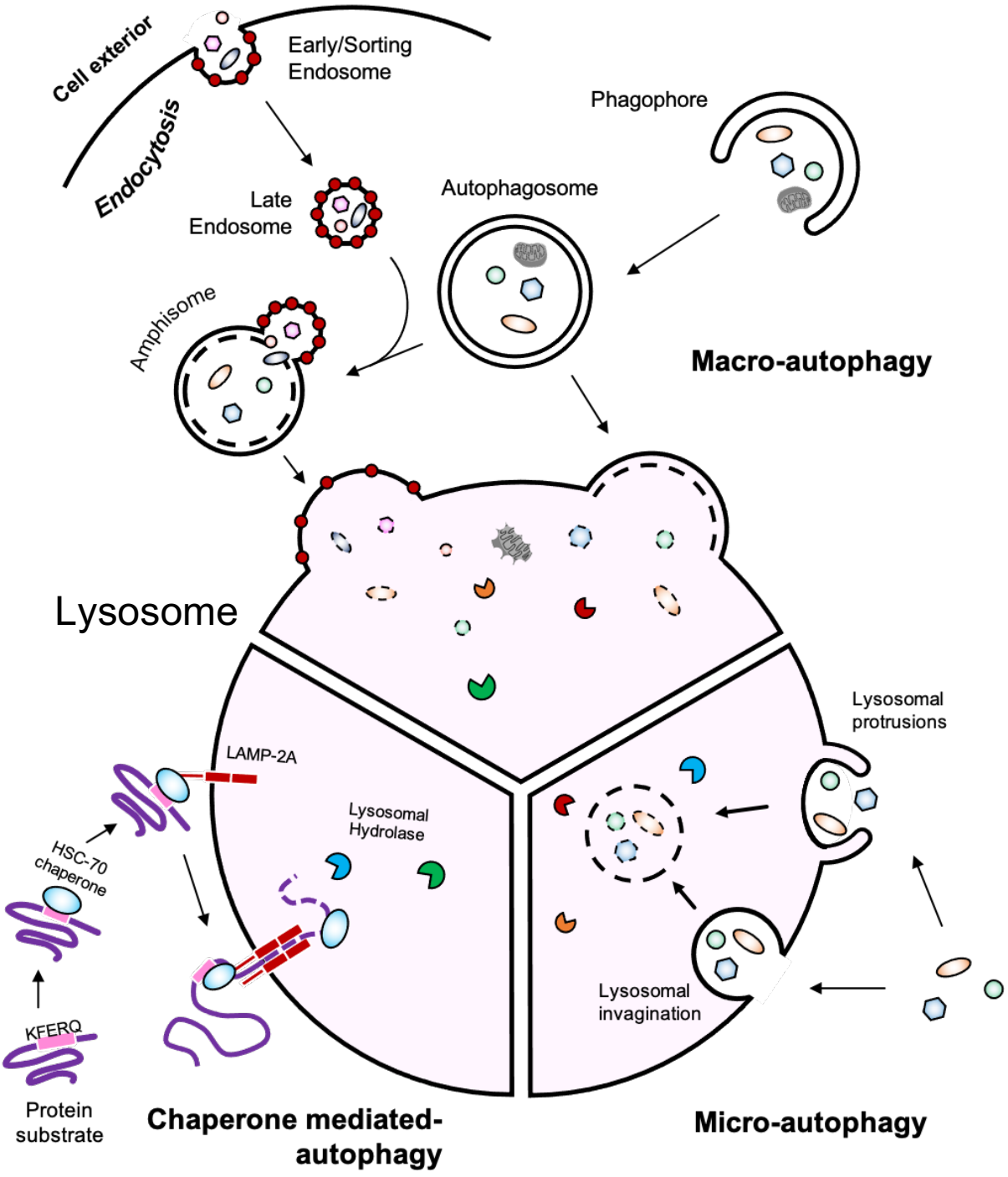

Figure 1.3. ***Different Types of Autophagy***. Three distinct sub-types have been described so far for autophagy, based on the manner by which the cargo reaches the common endpoint of the process: the lysosome. In **chaperone-mediated autophagy** (only in mammals as of yet), no vesicles are formed and the HSC-70 chaperone binds the KFERQ motif if present on target substrates, as well as monomers of LAMP-2A, inducing multimerization and transport of the cargo into the lysosomal lumen via the formed LAMP-2A receptor complex. In **micro-autophagy** the lysosome itself engulfs cargo that is in close proximity, by formation of either lysosomal arm-like protrusions, or invaginations of its surface. These cargo-loaded lysosome-derived vesicles are subsequently degraded by the resident hydrolases. Finally, **macro-autophagy** sequesters cargo on de-novo formed double-membrane organelles called phagophores and upon closure, autophagosomes. Macro-autophagy shares many components with the other major trafficking pathway, endocytosis, and autophagosomes often fuse with endosomes to form an "amphisome". Cargo-loaded autophagosomes, endosomes and amphisomes then merge with the lysosomal membrane and are eventually degraded.

2.5 *Mechanism of Autophagy — Key Proteins & Markers*

As a note, the autophagy stages and key protein complexes presented here relate to the *Drosophila* system, with several parallel comparisons to mammals, where appropriate. Even though a wide range of stimuli upregulate autophagy, the ensuing chain of events and the corresponding core protein complexes which regulate membrane dynamics and dictate autophagosome development and fusion with lysosomes are largely the same and relatively well-conserved across eukaryotes.

Table 1.1 summarizes the main *Drosophila* ATGs and closely related proteins with regards to their importance in autophagy upregulation. Their function and stage they are involved in, as well as their mammalian counterparts are also listed.

Table 1.1. ***Drosophila Autophagy Proteins and Mammalian Homologues.*** Proteins are grouped according to the main stage they participate in the autophagy pathway, with details on their function and mammalian counterparts also shown.

***Drosophila* Gene**	**Mammalian homologue**	**Function**
Insulin-TOR Signalling		
InR	**INSR**	Insulin-like receptor
PI3K	**PI3K**	Kinase of the PI3K class I complex
TOR	**mTOR**	PIK-family Ser/Thr kinase
Autophagy Induction		
Atg1	**ULK-1**	Effector kinase of TOR. Component of the Atg1 complex, upregulated upon dis-inhibition from TOR
Atg13	**ATG13**	Component of the Atg1 complex
Atg17	**FIP-200 / RB1CC1**	Component of the Atg1 complex
Atg101	**ATG101**	Component of the Atg1 complex
Autophagosome Nucleation		
Vps-34	**VPS-34**	PI3 class III kinase, involved in generation of the isolation membrane
Vps-15	**VPS-15**	Component of Vps-34 complex
Atg6	**BECLIN-1**	Component of Vps-34 complex
Atg14	**ATG14L**	Component of Vps-34 complex
Uvrag	**UVRAG**	Component of Vps-34 complex
Rubicon	**RUBCN**	Component of Vps-34 complex
Autophagosome Expansion		
Atg8a/b	**LC3,GABARAP, GATE-16**	Ubiquitin-like protein that conjugates with PE and anchored on autophagosome membranes.

		Recruits membrane expansion complexes and anchors autophagic cargo for degradation
Atg7	**ATG7**	E1-like enzyme. Involved in conjugation of Atg8 and Atg12
Atg3	**ATG3**	E2-like enzyme. Conjugates Atg8
Atg10	**ATG10**	E2-like enzyme. Conjugates Atg12
Atg4a/b	**ATG4A/B/C/D**	Cysteine protease. Cleaves Atg8a to reveal PE conjugation site and removes PE from Atg8a
Atg12	**ATG12**	Ub-like protein. Conjugates with Atg5 during formation of the Atg12-Atg5-Atg16 expansion complex, and participates in Atg8a lipidation
Atg5	**ATG5**	Component of the Atg12-Atg5-Atg16 expansion complex. Interacts with Atg12
Atg16	**ATG16L1/2**	Component of the Atg12-Atg5-Atg16 expansion complex. Participates in Atg8a lipidation
Recycling		
Atg18a/b	**WIPI-1/2/3/4**	Effector and binding partner of PI(3)P
Atg2	**ATG2**	Atg18-interacting partner
Atg9	**ATG9A/B**	Transmembrane protein that shuttles between cytosolic compartments and transports membrane material to the expanding autophagosome

2.5.1 The Atg8 family of proteins and Atg8 lipidation

The Atg8 protein family contains members which are instrumental for autophagosome biogenesis and autophagy progression, and are some of the most commonly used as markers to monitor the different stages of the pathway [101]. Lipidation of Atg8 is the key process which drives autophagosome formation in all eukaryotes. Due to the next sections dealing with each autophagy stage at greater length, I dedicate some space here to present a snapshot of the Atg8 lipidation mechanism, in an effort to make the sequence of autophagy events discussed later on somewhat easier to follow.

The Atg8 family is represented by two paralogues in *Drosophila*, termed *Atg8a* and *Atg8b*. Of the two, only *Atg8a* shows ubiquitous tissue expression and seems to be indispensable for normal autophagy progression [102]. *Atg8b* on the other hand, only exhibits tissue-specific enrichment in the adult male testis [102], [103] and is thought to have originated from an *Atg8a* retro-transposition event during the evolution of flies [104]. As such, most autophagy studies in *Drosophila* use Atg8a as the marker of choice. The ATG8 family in mammals, is considerably more diverse and split between two sub-families: **GATE-16/GABARAP** (***G****olgi-associated* ***AT****Pase* ***e****nhancer of* ***16*** *kDa /* ***g****amma-****a****mino****b****utyric* ***a****cid* ***r****eceptor-****a****ssociated* ***p****rotein*) with three known members, GABARAP, GABARAPL1/GEC1 and GABARAPL2/GATE-16/GEF2); and **MAP-LC3** (***m****icrotubule-****a****ssociated* ***p****rotein-****l****ight* ***c****hain* ***3****;* shortened to **LC3**) with four known members, LC3A, LC3B, LC3B2 and LC3C. Similarly to *Atg8b* in flies, mammalian *LC3B2* is thought to have resulted from an evolutionary retro-transposition event of *LC3B* [104]. With regards to autophagy progression in mammals, it is thought that LC3 members participate mostly during phagophore elongation, while GATE-16/GABARAP proteins are largely involved later, at the autophagosome maturation stage [105]. Compared to its mammalian counterparts, *Drosophila* Atg8a shares most sequence and structural similarities with GABARAP, however it more closely mimics LC3B in terms of function.

The components and their functions, which comprise the pathway of Atg8 lipidation are highly conserved from yeast to mammals. Atg8 proteins share a remarkable structural similarity with ubiquitin (despite differences in sequence) and are activated in a likewise similar fashion, after being synthesized as precursors [104]. The process of Atg8 lipidation is schematically illustrated in Figure 1.4. There are two ubiquitin-like conjugation systems, which together mediate the orderly succession of the E1, E2 and E3 catalytic reactions that result in the fusion of Atg8 to **p**hosphatidyl-**e**thanolamine (PE) at the surface of the developing autophagosome [106]. In the first conjugation complex, the cysteine protease Atg4 processes Atg8 at its C-terminal, exposing a **g**lycine (G) residue [107]. This aids in the recognition of Atg8 by Atg7 (an E1-like enzyme), that binds and subsequently transfers Atg8-G to Atg3 (an E2-ubiquitin ligase) [107], creating the **Atg8**-G-**Atg3** conjugation complex (Atg8 complex for simplicity).

The second complex of the Atg8 lipidation process consists of Atg5, Atg12 and Atg16. Here, Atg7 activates Atg12 and transfers it to Atg10 (E2 enzyme) [107]. Atg10 covalently attaches Atg12 to Atg5, resulting in an Atg12-Atg5 E3-like multimer [107]. Atg16 completes the multimer complex by binding to Atg5, and the newly formed **Atg12-**

Atg5-Atg16 (Atg16 complex, for simplicity) anchors at the membrane of the forming autophagosome [108].

At the surface of the developing vesicle, the Atg8 and Atg16 complexes act in a synergistic manner to transfer Atg8-G from Atg3 and attach it to the membrane-bound PE [109]. Atg4 can also function as a de-conjugation enzyme, releasing Atg8 from PE [110], and this is thought to aid in Atg8 recycling.

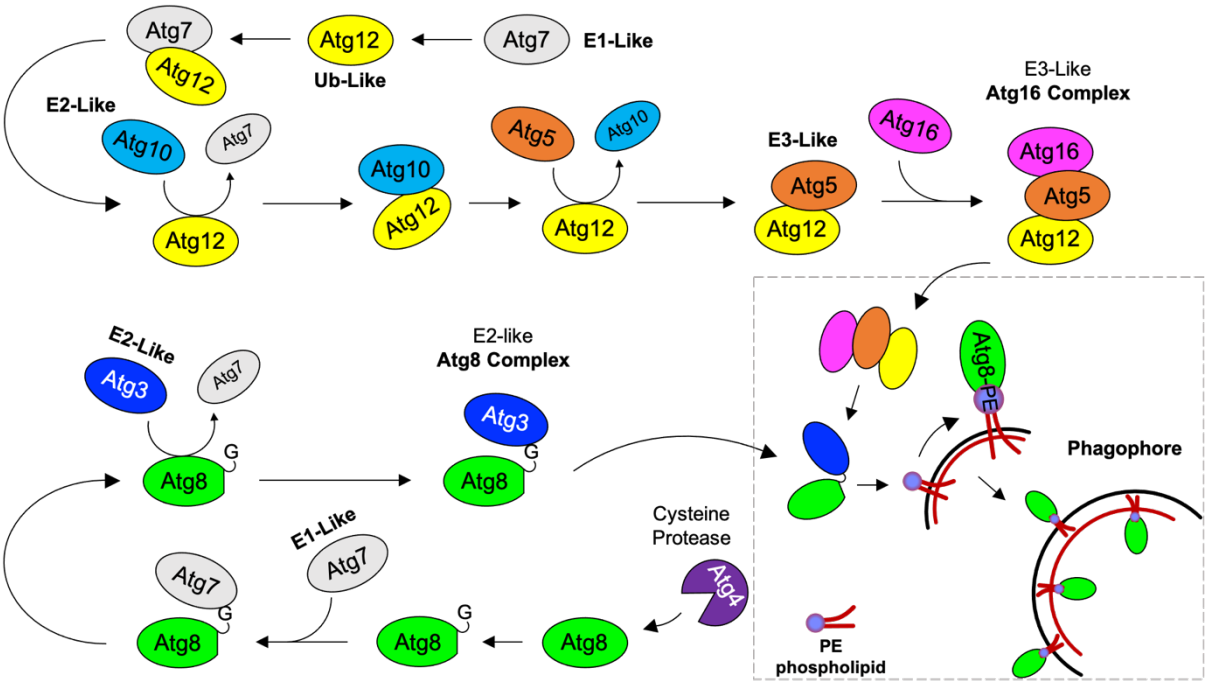

Figure 1.4. ***Process of Atg8 Lipidation.*** The process and its components are highly conserved and function in very similar fashion across eukaryotes. Shown is a simplified depiction of the E1-E2-E3 reactions that lead to the creation of the Atg8 and Atg16 conjugation complexes upon autophagy induction., which catalyze the reversible attachment of Atg8 to. The cysteine protease Atg4 cleaves pro-Atg8 at its C-terminal, creating a Gly (G) overhang that Atg7 binds to. Atg7 then transfers Atg8-G to the E2-like enzyme Atg3, creating an Atg8-G-Atg3 multimer (Atg8 complex). Atg7 also binds to an exposed G residue of processed Atg12 (not shown) and later transfers it to the E2-like enzyme Atg10. The E3-like protein Atg5 then replaces Atg10, creating an Atg12-Atg5 complex, which is further complemented by Atg16, creating the Atg12-Atg5-Atg16 multimer (Atg16 complex). The Atg8 and Atg16 complexes coordinate their functions to conjugate Atg8-G to the phospholipid **p**hosphatidyl-**e**thanolamine (PE) at — mainly — the convex side of the phagophore and detach afterwards.

2.5.2 Autophagy induction — development of the phagophore

Starvation is a simple enough stimulus that induces autophagy and is commonly used in a laboratory setting to activate and monitor the process [111].

Autophagy is under strict control by the insulin-responsive TOR (***t**arget **o**f **r**apamycin*) signalling pathway, which is highly sensitive to nutrient level fluctuations [112]–[114]. TOR is a Ser/Thr kinase that acts downstream of the insulin receptor (only a single receptor in fly) [115]. TOR forms two distinct complexes; TORC1 and TORC2, of which only TORC1 responds to rapamycin treatment and nutrient levels in general, while TORC2 is insensitive to rapamycin and its function is still not fully understood [116]. The autophagy initiation complex in *Drosophila* is a multimer consisting of an Atg1-Atg13 core [114], [117], [118], and complemented by the auxiliary subunits Atg17 [119] and Atg101 [120]. Atg1 is a Ser/Thr kinase that strongly associates with Atg13, regardless of TOR activity [117]. Atg17 and Atg101, are the functional homologues of the mammalian scaffold proteins FIP200 and ATG101 respectively, and are required for the efficient activation of the Atg1-complex during starvation-induced autophagy [119]–[122].

Under normal conditions TORC1 phospho-inhibits Atg1, thus maintaining autophagy at basal levels [117]. Upon nutrient deprivation, the inhibitory effect of TORC1 on Atg1 is lifted. This frees the Atg1 kinase, which phospho-activates itself and also hyper-phosphorylates Atg13, which is crucial for the latter's activation [117]**.** However, the opposite is also reportedly true; i.e hyper-phosphorylated, or overexpressed Atg13 also enhances Atg1 activity [117], [123], [124]. This suggests that Atg1 and Atg13 may engage in a mutually enhancing feedback loop, and potentially exist at the same tier of activation rather than one being downstream of the other. This is also a point of discrepancy regarding autophagy induction between flies and mammals. In fruit flies, overexpression of Atg1 is often sufficient to promote autophagy, whereas hyperactivation of Atg13 inhibits the pathway [117]. In mammals however, overexpression of either ULK1 (mammalian equivalent of Atg1) or ATG13 result in autophagy inhibition instead [117], [118], [125].

The fully activated initiation complex is then able to signal for the recruitment of additional effectors at the phagophore nucleation site, from where the isolation membrane will progressively develop.

Phagophore nucleation is the next important step during autophagy upregulation. It is generally accepted that pre-existing membrane sites serve as cradles for the *de-novo*

synthesis of the phagophore structure. In yeast, phagophores have a single point of origin near the vacuole, termed the ***p**re-**a**utophagosomal **s**ite* (PAS) [126], whereas in higher eukaryotes, phagophore assembly can occur simultaneously at different compartments within the cell [127]. During starvation-induced autophagy, one may identify such intracellular compartments by observing characteristic "**Ω**"-shaped membrane protrusions known as "*omegasomes"* (named after their resemblance of the Greek capital case for the letter omega "Ω" in EM images) [128].

Omegasomes result from the synergistic actions of autophagy initiation and nucleation complexes, and are the precursor platforms from where phagophores will begin to develop [127]. They were originally identified as ER-associated spots [129] and as such the ER has been largely accredited as the primary donor of membrane material to the nascent phagophore. However, the subject of membrane origin of the phagophore still remains a matter of controversy [127], [130], [131]. Several membranous compartments such as the ER-exit sites [132], [133], the ER-Golgi intermediate compartment [134], the Golgi apparatus [135], [136], mitochondria [137], the plasma membrane [138] and recycling endosomes [139], [140], have all been proposed as scaffolds for phagophore assembly. One of the most plausible arguments put forth is that the ER may act as the initial platform for the omegasome cradle to form. This is jointly supported by ultrastructural studies demonstrating a physical connection between the phagophore and the ER [141], [142], and by observations of the phagophore-expanding kinase ATG14L (discussed below) co-localizing to specific sub-domains of the ER [129], [143]. Due to the wide range of potential donors, it is unlikely that one site acts as the sole membrane provider; rather, it is becoming increasingly accepted that the phagophore receives phospholipid input from multiple sources and at different stages during autophagy progression [128]. Furthermore, it might also be possible that the sources which contribute membrane material to the phagophore may alternate, depending on the nature of the autophagy-inducing stimulus, as well as the cargo to be sequestered by the isolation membrane.

Because most of the phospholipid bilayers which are donated to the phagophore are enriched in **p**hosphatidyl**i**nositol-**3**-**p**hosphate (PI3P), the developing structure is in turn highly dependent on a steady influx of PI3P. PI3P is generated by **p**hospho**i**nositide-**3** **k**inases (PI3Ks), which form three distinct **PI3K** **c**omplex (PI3KC) classes (I, II and III), with differential effects regarding autophagy progression. Generally, class I PI3KCs are well-studied autophagy inhibitors that act downstream of insulin-signalling and activate

TOR**,** while class III PI3KCs are the quintessential autophagy promoters [144]. Class II PI3KCs are a relatively new discovery in the PI3K family. In the context of autophagy, they are generally regarded to facilitate autophagosome formation by acting as a supplementary source of PI3P [145], [146], although their exact functions still remain under investigation.

The class III PI3KC consists of the PI3K **v**acuolar **p**rotein **s**orting **34** (Vps34), which forms a complex with Vps15, Atg6 and Atg14 [147], [148] (Atg6 is known as Beclin-1 in mammals). This Vps34 complex docks on the omegasome and generates a localized pool of PI3P, which in turn acts as a beacon, signalling the on-site recruitment of additional effectors involved in membrane trafficking and remodelling [127], [147]. Overexpression of Vps34 further boosts autophagy upregulation following starvation but has no effect under normal feeding conditions [147]. This illustrates that influx of PI3P alone is not sufficient to promote autophagy, but rather effective induction of the process depends on the upstream activity of the Atg1 initiation complex and its de-inhibition from TOR [147].

Once again, here is another point of uncertainty regarding the autophagic process as observed in flies and mammals. Mammalian PI3K-III complexes can be distinguished into 3 sub-populations depending on their Beclin-1 and Vps34 activity-modulating binding partners [149], [150]. The first group associates with AMBRA-1, while the second and third groups bind ATG14L, or UVRAG respectively [149], [150]. ATG14L and UVRAG promote autophagy and compete for their binding on Beclin-1, with their respective PI3K complexes functioning at different stages; namely in autophagosome biogenesis, and maturation/fusion with lysosomes accordingly [149]–[151]**.** Furthermore, a number of UVRAG-binding PI3KC-III associates with Rubicon, which is considered an inhibitor of autophagosome maturation [149], [150], that becomes particularly enriched with age [152], [153].

With regards to the fly, it is yet to be confirmed whether or not *Drosophila* class III PI3KCs form distinct sub-complexes that mediate different effects on autophagy [149]–[151].The fruit fly possesses orthologues of the aforementioned ATG14, UVRAG and Rubicon. *Drosophila* UVRAG has been suggested to function in endolysosome maturation, while its downregulation does not affect autophagic flux [154], and Atg14 was shown to be required for autophagy in larval fat body [155]. However, their exact degree of involvement in autophagy and the details of their mechanism still remain unclear.

Among the many other important members involved in autophagy progression, are **v**acuolar **m**embrane **p**rotein 1 (Vmp1) and Atg9. Atg9 remains so far the only

characterized trans-membrane member among the Atg family. It is regarded as the primary membrane-trafficking protein, that transports material from donor sources to the nascent phagophore; as is able to shuttle between different membranous cytosolic compartments [112], [131]. Vmp1 is another highly conserved trans-membrane protein and is thought to aid in phagophore formation by tethering the active Vps34-Vps15-Atg6 complex on the surface of the developing structure [156]–[158].

2.5.3 Expansion and maturation — phagophore to autophagosome

Elongation of the phagophore is largely dependent on the influx and incorporation of donor membrane material, as well as maintenance of correct curvature. Lipidation of Atg8 (Figure 1.4) is essential in this regard, as the phagophore-anchored Atg8 is recognized and bound by many proteins involved in cargo transport and membrane dynamics [107], [159], [160]. The transmembrane Atg9 transporter contributes phospholipid material ferried from various vesicular compartments, such as the Golgi network and recycling endosomes [127], [161]. Interestingly a study in mammals reported that ATG9 is able to traffic between the plasma membrane and recycling endosomes and co-localize with ATG16L1 in a process which is thought to provide ATG9/ATG16L1-positive membrane on the growing phagophore [139]. This mechanism might be further facilitated by sorting nexin SNX18, which possesses membrane remodelling capability and also co-localizes to forming autophagosomes [140]. SNX18's homologue in *Drosophila*, SH3PX1 (further discussed in Introductory section 2.7.3), has been shown to function in a similar manner during autophagosome assembly by maintaining positive membrane curvature [140]. Cargo-bearing vesicles themselves that bring the degradation material to the phagophore, can also reportedly contribute membrane material to the growing organelle [128].

The correct geometry of the phagophore membrane is equally important for proper autophagosome formation. Atg8-PE which accumulates near the growing edges of both the outer and inner membrane of the phagophore, as well as curvature-sensing protein complexes, may together create a crowding effect that promotes positive membrane bending [128]. The uneven distribution of Atg8-PE between the inner and outer phagophore membrane, coupled to the Atg8-medited sequestration of cargo-receptors at the inner surface, might collectively contribute to the phagophore curving in the correct dimension [128]. *In-vitro* observations described that Atg8-PE can anchor the Atg16 complex on the

outer side of the phagophore through Atg8 binding of Atg12, resulting in the assembly of a "coat-like" structure [162]. Meanwhile, on the concave side, binding of cargo, or cargo-adaptors to Atg8 can outcompete binding of the Atg16 complex, which may provide a partial explanation as to why this ternary ubiquitin-like complex is almost always found on the outer surface of the phagophore [128].

Eventually, upon phagophore closure and maturation to autophagosome, Atg8 molecules on the convex side of the structure are cleaved off by the Atg4 protease and recycled back to the cytosol [110].

2.5.4 Fusion with lysosomes — input from endocytosis

Mature, cargo-loaded autophagosomes, are finally targeted towards lysosomes where they will subsequently fuse and have their contents degraded. In yeast, autophagosome fusion with the vacuole is mediated by the tethering factor complex HOPS (***ho****motypic fusion and vacuole* ***p****rotein* ***s****orting*), with the aid of SNARE proteins Vam3, Vam7 and Vti1 [163]; collectively bridging the membranes of the two organelles. The different HOPS and SNARE protein complexes are equally important in mediating membrane fusion events in higher eukaryotes. The most well-studied SNARE member for promoting autophagosome-lysosome fusion is **s**yn**t**a**x**in **17** (STX17) [164], [165]. HOPS attaches to a ternary SNARE complex formed by Syx17 (naming of STX17 in *Drosophila*), ubisnap and the late endosomal/lysosomal Vamp7, and primes the autophagosome for the fusion event with the lysosome [164], [165].

An characteristic point of crosstalk here between autophagy and endocytosis (further presented in Introduction section 2.7), is the fusion of autophagosomes and late endosomes into single-membrane vesicles called "*amphisomes*" [166]. Amphisomes can subsequently merge with lysosomes for their degradation and interestingly, blocking late endosome formation results in prominent autophagosome accumulation in both *Drosophila* and mammals [147], [167], [168], in a Syx17/STX17-dependent manner [164]. These observations suggest that in fruit fly and mammals components of the endocytic pathway, together with the ability of autophagosome to merge with late endosomes, are both essential for their effective subsequent fusion and degradation by lysosomes. With the exception of yeast, it is yet unclear in higher eukaryotes, if there is a preference of cargo delivery to the lysosome via autophagosomes, or amphisomes [38].

Following fusion with lysosomes, the contents of the autophagosome are degraded by resident acidic proteases such as cathepsins, and leftover material is salvaged and recycled back to the cytosol to fuel other biosynthetic, or energy producing pathways.

2.6 *Selective Autophagy — Principles & Functions*

As already mentioned, cells can utilize the autophagy machinery for either bulk or niche functions. In the first instance, it can often be that intracellular constituents are randomly engulfed by the developing isolation membrane, simply due to them being in close proximity to the site of autophagosome formation at the time autophagy is induced.

On the opposite end of the spectrum, the process can also be highly discriminative towards its target substrates. The common denominator which distinguishes this form, is that an adaptor protein interacts with the cargo (or is itself part of the cargo) and with a scaffold protein on the autophagosome membrane. Such adaptors are known as ***s**elective **a**utophagy **r**eceptors* (SARs) and they typically —but not always— recognize and dock lipidated Atg8-family members via a specific amino-acid sequence in the latter's structure, known as ***A**tg8-**i**nteracting **m**otif* (AIM), or ***L**C3-**i**nteracting **r**egion* (LIR) [169], [170]. Hereafter I will refer to this sequence as "LIR" since this term is commonly used for higher animal eukaryotes, while AIM has mostly been associated with yeast and plants. Finally, **ub**iquitin (Ub) has a cardinal role in selective autophagy as well, since it can label the target cargo to facilitate its uptake by SARs and can also interact with scaffold proteins on the autophagosome membrane; collectively creating an indirect link between the cargo and the autophagic machinery [171].

2.6.1 Selective autophagy receptors and the LIR motif

Despite their variation in size, sequence and structure, all SARs need to fulfil two essential criteria: cargo recognition, and binding of Atg8. As such, certain architectural features that allow SARs to carry out these two functions seem to appear more frequently — yet not universally — among the known autophagy receptors characterized so far. These are: *a)* the presence of a multimerization domain or domains, *b)* a ***U**b-**b**inding*

d*omain* (UBD) that facilitates docking of ubiquitinated substrates, and *c)* a LIR peptide that aids in the tethering of Atg8-family members.

SQSTM1/p62 was the first mammalian SAR to be identified [172]–[174], and remains the most comprehensively studied to date, in terms of structure and function. It is known for its involvement in NF-κB-dependent signalling pathways where it acts as a scaffold [175] and co-localizes with Ub into protein inclusions observed in several aggregate-forming neuropathies such as Alzheimer's, Parkinson's, Lewy-body dementia, and Pick's disease [176], [177]. It is itself a substrate for autophagic degradation and contains a LIR motif for binding the autophagy marker LC3 [172], [174]. However the LIR alone is not sufficient to mediate strong tethering to the phagophore and polymerization of p62 is also required for its effective anchoring to the isolation membrane and subsequent clearance by autophagy [178]. Other notable p62/SQSTM1-like mammalian autophagy receptors that interact with ATG8-family members via a LIR motif include NBR1 [179], NDP52 [180] and OPTN [181].

The *Drosophila* genome encodes a single p62-homologue called ***ref****ractory* ***to*** *Sigma* ***P*** [Ref(2)P)], pertaining to its initial identification in a screen for modifiers of sigma virus multiplication [182]. Ref(2)P retains some of the functional domains of p62 and similar to its mammalian counterpart, is also prone to aggregation as seen in the brain of certain *Drosophila* models for neurodegenerative diseases [183]. The remaining *Drosophila* SARs identified so far in addition to Ref(2)P, is *bluecheese*; the fly homologue to the mammalian autophagy adaptor ALFY (***A****utophagy-****l****inked* ***FYVE***) [184], and Kenny; the regulatory subunit of the *Drosophila* IKK complex that mediates signalling of the IMD innate immune response [33].

With their discovery of the LIR motif in 2007, the group of T. Johansen demonstrated that autophagy can be selective towards its substrates [174], [185]. The peptide was originally mapped within a 22 amino-acid region on p62, in a sequence containing an evolutionarily conserved repeat of three consecutive Asp (D) residues followed by Trp (W); the electrostatic interactions of which were indispensable for binding LC3B [174]. Further structural analysis of the crystalized murine p62-LC3 complex narrowed down the region of interest to 11 amino-acids [178] and shortly thereafter, similar structural data from the human p62-LC3 and yeast Atg8-Atg19 complexes, further assigned the LIR to just 4 residues [186]. These studies served to identify the core of what is now known as a "canonical LIR motif". The LIR peptide core is represented as "**Θ-x-x-Γ**", where ***Θ*** (*theta*) is any hydrophobic aromatic amino-acid (W/F/Y), ***x*** is any amino-acid, and ***Γ*** (*gamma*) is

any of the hydrophobic L, I, or V amino-acids [170], [178], [186]. The LIR core is also frequently displayed as "**X_0-x_1-x_2-X_3**" in literature, since there are also "non-canonical" LIR motifs with different amino-acid composition of their cores, and because several positions to the left and right of the LIR core are also important for LIR motif function [170], [185].

LIR motifs bind to Atg8/LC3 at a cleft called the ***LIR-docking site*** (LDS), which is formed by the N-terminal arm and the Ub-like domain of Atg8/LC3 [170]. The LDS contains two **h**ydrophobic **p**ockets (HPs), HP1 and HP2 where LIR motifs dock through their X_0 and X_3 positions respectively (Figure 1.5A) [170], [178], [186]. As such, the X_0 and X_3 residues in the canonical LIR motif are absolutely conserved and indispensable for interacting with Atg8/LC3 (Figure 1.5B) [187]. Substitutions at these positions with any other amino-acid, for example the neutral Ala (A), can reduce or completely abolish the binding affinity of LIR peptides to LDS and are frequently employed to identify LIR-dependent interactions of novel SARs [187]. Of positions $\mathbf{x_1}$ and $\mathbf{x_2}$ within the functional LIR motif of many known SARs, $\mathbf{x_1}$ is most often occupied by acidic or hydrophobic residues, while $\mathbf{x_2}$ is more relaxed and can welcome a broader range of amino-acid substitutions [170]. N-terminal and C-terminal sequences immediately flanking the core of the peptide have also been shown to modulate specificity of the LIR for its LDS site. The N-terminal positions $\mathbf{X_{-3}}$, $\mathbf{X_{-2}}$, $\mathbf{X_{-1}}$ are frequently occupied by residues susceptible to phosphorylation and can be either acidic (D, or E), or Ser (S) or Tr (T) [188], [189]. Phosphorylation regulates the binding affinity of LIR for its cognate site on Atg8/LC3 [188], [189]. Proline (P), which is often found at positions $\mathbf{X_4}$ and $\mathbf{X_6}$ at the C-terminal side [170], is a hydrophobic amino-acid that is regarded as aiding in tight turns of the protein structure [190] and as such, it is frequently localized at protein surface [190]. This might help in better exposing the X_3 residue of the LIR core, for being recognized and binding the LDS HP2 site on Atg8/LC3. In *Drosophila*, Atg8a has been shown to rely on residues K48 and Y49 of its LDS region, in order to effectively dock LIR motifs [191]. Mutations resulting in substitution of both amino-acids at these positions with Ala (A), prohibits Atg8a from participating in LIR-dependent interactions [191].

Finally, it is important to emphasize that: *a*) several SARs interact with Atg8/LC3 in a LIR-independent manner, *b*) not all LIR-containing proteins are SARs, and *c*) not all autophagy-related proteins have a LIR motif [170].

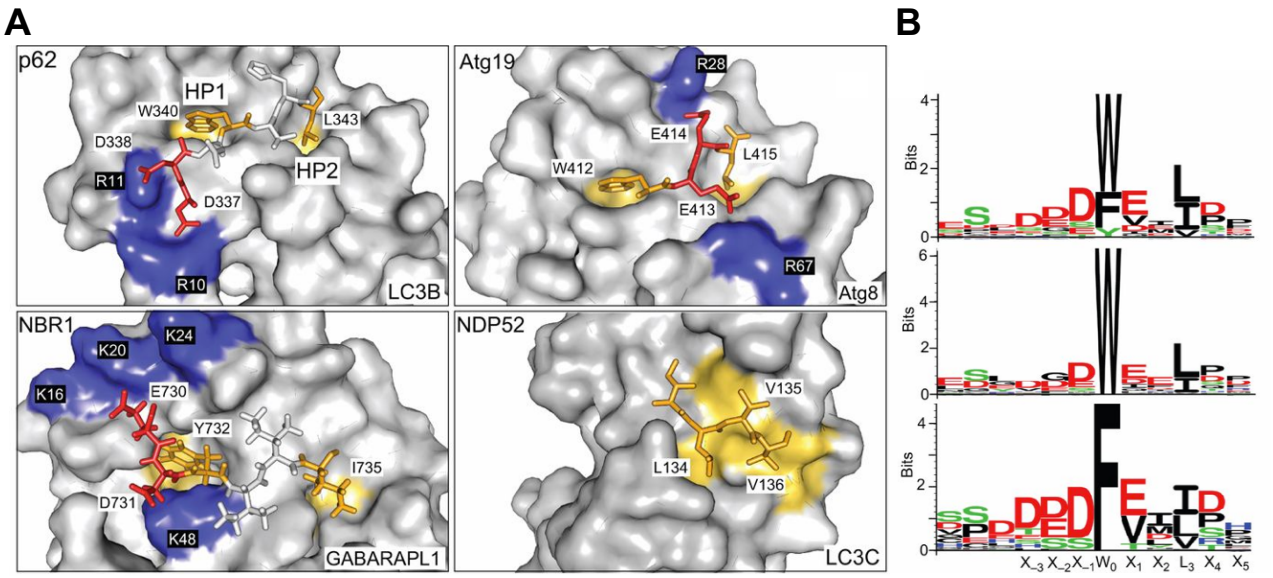

Figure 1.5. ***Structural Properties of LIR-LDS Interactions and LIR Motif Consensus.*** (**A**) 3D-rendered representation of the LIR-LDS binding between known SARs and different Atg8-famliy proteins. (top left) p62-LC3B interaction, (top right) yeast Atg19-Atg8 interaction, (bottom left) NBR1-GABARAPL1 binding and (bottom right) NDP52-LC3C binding as example of non-canonical LIR-motif interaction. Shown in yellow are the hydrophobic pockets (HP1 and HP2) of LC3B, Atg8 and GABARAP-L1 as well as the hydrophobic patch of LC3C. The corresponding amino acids of each LIR peptide that anchor the pockets are also shown in yellow, while red indicates the amino acids that interact with basic residues of these ATG8 ubiquitin-like modifiers (blue). (**B**) The core LIR residues as sequence logos that represent the frequency by which they are encountered in each of the X_{-3} X_{-2} X_{-1} **W**$_0$ X_1 X_2 **L**$_3$ X_4 X_5 positions. Sequence logos were created based on multiple alignments of a total 42 verified LIR motifs (upper panel). These 42 LIR motifs are further sub-divided into three groups: 22 **W**-type LIRs (middle panel), 15 **F**-type LIRs (lower panel), and 5 **Y**-type LIRs (not shown) with respect to the amino-acids found at position 0 of the LIR core. Height of each stack represents the sequence conservation at that position, whereas the height of symbols within the stack indicates the frequency by which each residue is encountered at that position. Tyr (Y) is the least common amino acid for position 0 which anchors the HP1 pocket. Figure adapted with permission from T.Johansen (Full figure available at [185]).

2.6.2 Role of ubiquitin

Discovered in the 70s, Ub is a small (8.5 kDa), universally conserved regulatory protein, which can be covalently attached to proteins [192]. While predominantly associated with degradation by the 26S proteasome, protein ubiquitination has been established to be a multi-faceted modification that regulates a wide range of different pathways, including endocytosis and intracellular sorting and cell signalling cascades [193]. Ubiquitination utilizes E1, E2, and E3 enzymes is an elaborate process, which culminates in the formation of an iso-peptide bond between the C-terminal G residue of Ub and the ε-amino-group of lysine (K) on the target protein [194]. Ub molecules can interlock with one another primarily via K residues at specific positions within their sequence, creating poly-Ub chains of various lengths and conformations, which mediate different outcomes for their substrates [195], [196]. Two of the most studied modifications on Ub-chains are K48 and K63 linkage. Poly-Ub chains cross-linked by K48 primarily target substrates for proteasomal degradation, while K63-linked poly-Ub chains are frequently associated with functions in signal transduction, DNA repair and transcription pathways [195]. chains on substrates are also used as recognition signals that recruit the selective autophagy machinery [86], [196]. The prototypic SAR, p62, recognizes both Ub^{K48}- and Ub^{K63}-linked chains, but binds the latter with higher affinity [197], [198]. This is an example that showcases how nodal components such as p62 may be shared by different pathways (e.g autophagy and the proteasome) that can in turn function in parallel, or in a context-dependent manner [199]. Certain forms of selective autophagy rely on these Ub signals at the surface of their target cargoes for the latter to be effectively recognized by the respective SARs [200]. Some of the most notable instances include autophagic clearance of mitochondria (mitophagy), protein aggregates (aggrephagy), invading pathogens (xenophagy), peroxisomes (pexophagy), zymogens (zymophagy), and the proteasome itself (proteaphagy) [200].

Single Ub moieties on cargoes (mono-ubiquitination) are also reportedly able to recruit p62, however the UBD of p62 does not bind mono-Ub as efficiently compared to poly-Ub [86]. This has prompted researchers such as Dikic and colleagues to suggest that additional factors e.g. substrate/receptor oligomerization are perhaps equally required for the efficient uptake of mono-ubiquitinated cargo by selective autophagy [86].

Ub may also drive certain SAR and adaptor interactions with Atg8/LC3. Recently, Vierstra and colleagues identified a subset of Atg8-interacting proteins in yeast and *Arabidopsis*, that possess what is likely to be a ***U**b-**i**nteracting **m**otif* (UIM), via which they

anchor to the UDS (***U**b-**d**ocking **s**ite*) of Atg8 [201], [202]. They demonstrated that UIM-UDS interactions take place independent of LIR-LDS ones, illustrating that a single Atg8 molecule can participate in both types of interaction at the same time, binding cargoes from two distinct routes [201], [202].

Components of the core Atg1/ULK and PI3K complexes of the autophagy machinery undergo cycles of ubiquitination/de-ubiquitination and as such, Ub may also regulate the rate of autophagosome biosynthesis [86].

2.6.3 Regulation of other pathways by autophagy

The selective labelling and targeting of material to the autophagosome membrane can also serve as a mode of regulation for other intracellular processes. A number of prominent examples mentioned here include regulation of cell differentiation, apoptosis, immune system responses, as well as overall cell maintenance.

Delineating the mechanisms that control late stage oogenesis in *Drosophila*, Nezis and colleagues demonstrated that autophagy is an important factor for the upregulation of programmed cell death during maturation of the egg chamber [203] They observed that the apoptosis inhibitor dBruce in nurse cells, is degraded by autophagy; an essential event, which subsequently facilitates upregulation of apoptosis in these cells [203].

Caspases themselves; the signature agents of apoptosis, are also able to influence and be influenced in turn by elements of the autophagic apparatus [204]. Caspases are synthesized as inactive zymogens, whose switch to an active state is dependent on oligomerization and reciprocal cross-cleavage of regulatory domains [204]. Evidence from mammalian cell studies suggest that autophagy may have a role in activating the apical caspase-8 during apoptosis under certain contexts. The autophagosome surface was shown to act as a platform, where inactive caspase-8 precursor molecules are brought to close proximity with each other, enabling their oligomerization and self-activation [205]–[207]. In these studies, procaspase-8 co-localized with ATG5/ATG12-positive complexes on the convex side of autophagosome; facilitated by the abilities of the apoptosis adaptor FADD to anchor both procaspase-8 and ATG5 on the ATG16L-complex [206], and of p62 to bring poly-Ub procaspase-8 cargo to the surface of the autophagosome [206], [207]. Conversely, excessive retention of caspase-8 on the autophagosome can also lead to its lysosomal degradation; a way by which, it has been proposed, certain cancer cells can escape

apoptosis [208]. The above contradictory examples illustrate how "time" and "place" in the crosstalk of pathways can be crucial determining factors of cell fate.

With regards to the immune response, recent findings from the I. Nezis group in collaboration with T. Johansen indicate that autophagy is responsible for the degradation of the *Drosophila* IKK signalling complex; the major effector kinase hub of the ***im****mune* ***d****eficiency* (IMD) pathway [33]. The relevant work identified that the regulatory subunit of the IKK complex, Kenny, can function as a SAR by interacting with Atg8a through is harboured LIR motif [33]. In doing so, the entire IKK complex is sequestered on the autophagosome through the Kenny-Atg8a interaction and subsequently degraded in the lysosome [33]. This is regarded as leaving fewer IKK complexes available to participate in signal propagation, and is therefore considered to be part of the downregulatory mechanism of the IMD pathway [33]. This study showcased how autophagy may contribute in the regulation of the IMD signalling cascade. The IMD signalling pathway is further expanded upon in introductory section 3.1.

Remaining within the context of immunity, inhibition of autophagy results in failure of human and murine monocytes to differentiate into macrophages [209], [210]. The differentiation signal upregulates autophagy through the combinatory actions of c-**J**un **N**-terminal **k**inase (JNK) on Beclin-1 which releases it from its inhibitory binding with BCL-2; and on ATG5, which prevents its cleavage and enables the formation of the ATG5/ATG12 complex [209], [210]. Inflammasome activation of monocytes/macrophages is also, at least partly, under control of autophagy. Inflammasome upregulation and subsequent enhancement of interleukin (IL) -1β and -18 cytokine production, was shown to correspond with loss of either ATG16L1 [211], or ATG7 [212]. Similarly, a link between dysfunctional autophagy and increased levels of inflammatory cytokines has been proposed for chronic inflammatory diseases, such as Gaucher's disease; an inherited lysosomal storage disorder [213].

For organisms with an adaptive immune system such as mammals, the activity of the MHC-II complex in presenting antigens at the surface of $CD4^+$ T cells, is largely dependent on the autophagic pathway [214]–[216]. Timely regulation of autophagy in this case is key, as exacerbated antigen presentation on the other hand, may contribute to auto-immune responses [217]. The CTLA4 receptor on the surface of peripheral $Foxp3^+$ regulatory T cells, was shown to mediate suppression of autophagy in dendritic cells, thus decreasing MHC-II-dependent antigen presentation and consequently keeping auto-immune responses within tolerance levels [217].

With regards to ageing, functional autophagy positively affects lifespan and delays functional deterioration [218], with a common method employed for its upregulation being caloric restriction and control of nutrient intake in general, as already mentioned [36], [219]. The autophagy-stimulatory effects of dietary restriction are suggested to be mediated at least partially by sirtuins; a family of protein de-acetylases, that contains several members which enhance transcription of ATG genes [220]. Several sirtuin members are upregulated during starvation and inhibit mTOR, thereby allowing the autophagy response to initialize in turn [221]. Sirtuin activity is also required to dampen NF-κB signalling, which controls among others the bulk of pro-inflammatory responses that are exacerbated during ageing [220].

2.7 *Endocytic Vesicle Trafficking & Autophagy*

As both endocytosis and autophagy are conserved intracellular vesicle trafficking processes with similar characteristics, they share many components which operate in both pathways like the SNX9-family of sorting nexins. *Drosophila* has a single SNX9-family homologue called SH3PX1. Of note, the terms "endocytic trafficking", "endosomal" and "endocytosis" mentioned throughout, are used interchangeably to refer to the intracellular trafficking of material by endosomes; the signature transport vesicles of endocytosis. In order to retain focus on the main investigative theme being on autophagy, the complexity of endocytosis presented below is vastly simplified, with only cursory mentions of few signature proteins and structures that denote the process.

2.7.1 A snapshot of endocytosis

"Endocytosis" is an umbrella term proposed by Christian de Duve [52], to collectively refer to the network of inter-linking routes which sort internalized material into membrane-coated vesicles and transport these across multiple destinations within a cell [38]. Clathrin-mediated endocytosis (CME) is arguably the most well-known form of the process, where a vast array of adaptor and accessory proteins coordinate their functions at the plasma membrane to eventually produce a vesicle containing the material internalized from the cell surface. At the nucleation site, heterologous protein complexes along with components of the cytoskeleton machinery synergize to create a localized membrane invagination that

begins to be coated by polymerized clathrin in a lattice-like fashion [222]. The cargo itself is covalently attached to clathrin with the aid of **a**daptor **p**rotein-**2** (AP-2), which recognizes particular dileucine- and tyrosine-based motifs present at internalized cargoes [223], [224], similar to LIR motifs for selective autophagy. The inwards-facing membrane deformation continues to grow as clathrin is added at the bud, while a vesicle neck develops behind, which becomes increasingly constricted by the localized funtions of the recruited membrane-deforming complexes [222]. Finally, the membrane scission GTPase dynamin, catalyzes the fission reaction and the fully clathrin-coated vesicle is released in the cytosol [225]. The clathrin lattice is subsequently removed and the bare vesicle is then trafficked towards he appropriate intracellular compartment [222]. The contributing functions of accessory proteins are equally important to those of clathrin, AP-2 and dynamin during endocytosis, as they facilitate membrane deformation and budding of the vesicle. BAR-domain containing proteins such as amphipsysin and the SNX9-family of sorting nexins (further presented in Introductory section 2.7.3) can sense, induce and maintain membrane curvature as they bind clathrin and AP-2 and recruit dynamin at clathrin nucleation sites [226]–[230].

Much like autophagy, endocytosis is characterized by formation of a specific cargo-bearing vesicle known as the "*endosome*". Endosomes are single-membrane vesicles —as opposed to double-membrane autophagosomes — and can be grouped to early/sorting, late, and recycling endosomes (EE/SE, LE, and RE respectively) depending primarily on four factors: a) protein and lipid composition of their membranes, b) intraluminal pH, c) morphology, and d) sub-cellular localization [231].

Membrane phosphatidyl-inositol lipids are essential in endocytosis as well. They can serve as markers of different endocytic compartments since they can be phosphorylated into various phospho-inositide forms [231]. Vesicles formed by clathrin-dependent, or clathrin-independent routes near the plasma membrane merge into EEs [38]. These EEs create a hub from where cargoes are sorted and targeted towards their final destinations [38]. Ultimately, endocytic transport can recycle material back to the plasma-membrane via REs, target substrates to the trans-Golgi network via retrograde trafficking, or sort them for lysosomal degradation through LEs [232]. EEs may further sequester material into intra-luminal vesicles created by invaginations of their own membrane, in which case they develop into MVBs [231], [232]. Such MVBs can be seen throughout all stages of the endocytic pathway [231], however they are more often associated with a commitment of endosomal cargoes towards degradation [38], [231]–[233].

EEs/MVBs that are destined for degradation mature into LEs (or fuse with pre-existing ones) in an elaborate process which includes acquirement of several lysosomal markers and acidification of their intra-luminal space [231]–[233]. As such, LEs are capable of degrading a number of cargoes on their own and are in fact regarded as morphologically and functionally closer to lysosomes than endosomes [231], [232].

As already mentioned one of the major cross-roads between endocytosis and autophagy is with their frequent merging of their respective vesicles into amphisomes (Figure 1.6), that continue *en route* to fuse with a lysosome [38]. The fusion organelle between an amphisome and a lysosome is still referred to as an “autolysosome”.

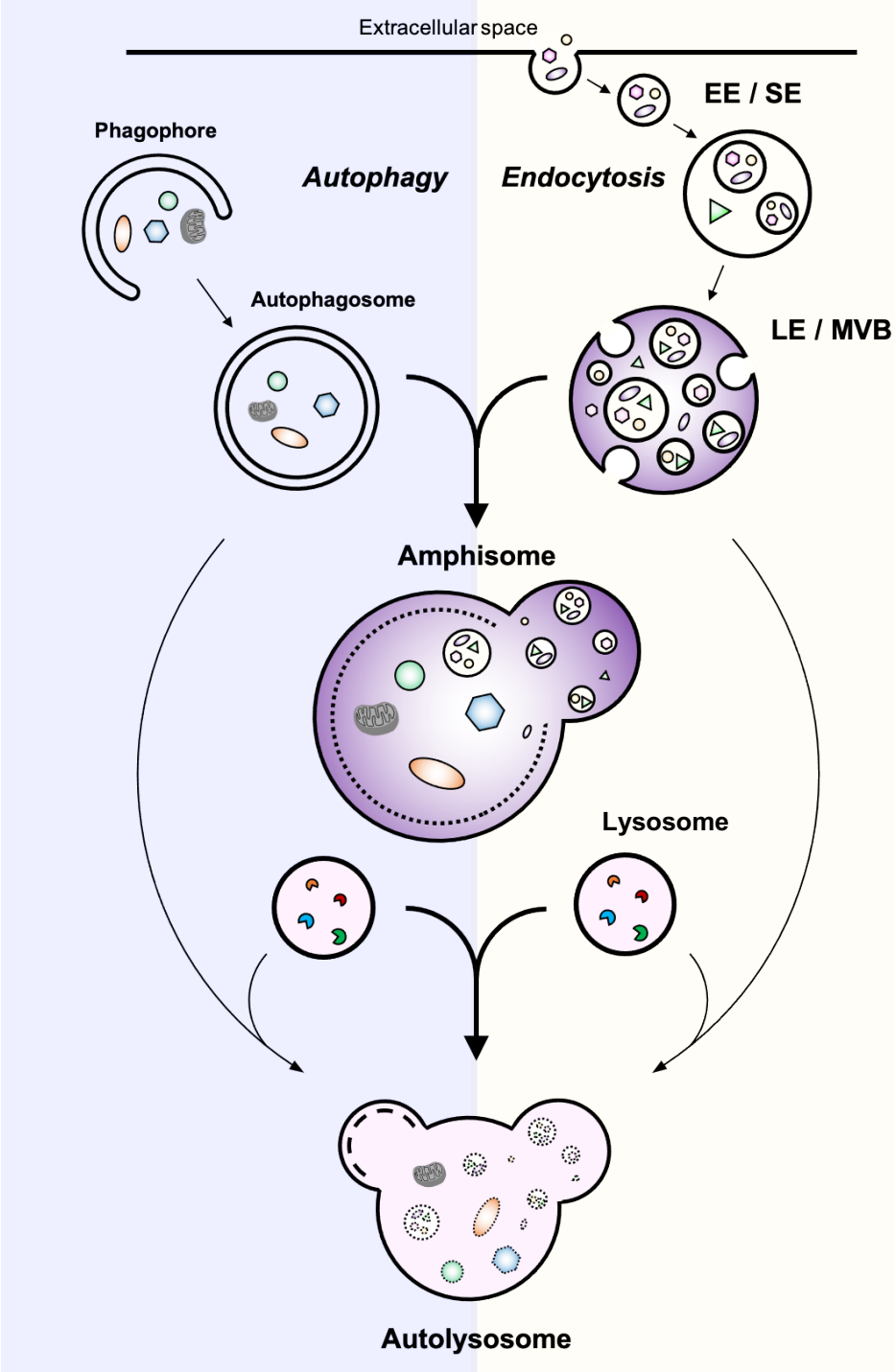

Figure 1.6. ***Synergy of Autophagy and Endocytosis.*** Depicted are the simplified views of autophagy and endocytosis as stand-alone pathways towards the lysosome, and in a co-operative manner. Autophagy and endocytosis share many similarities and components as they are both responsible for intracellular vesicle trafficking, with one main difference being that endocytosis is more heavily involved as well in internalization and sorting of material from the cell surface, or extracellular space. Internalized material is sorted into single-membrane **e**arly/**s**orting **e**ndosomes (EE/SE). Multiple EEs can subsequently fuse together into **m**ulti-**v**esicular **b**odies (MVBs). Individual EEs/SEs, or MVBs later mature into **l**ate **e**ndosomes (LE) whereupon their lumen is acidified (shown in dark purple). Arguably the most characteristic point of cross-talk between autophagy and endocytosis, is the frequent merging of autophagosomes and endosomes (shown here with LEs/MVBs for ease of depiction purposes) into a single-membrane acidified vesicle called “amphisome". Despite the combined origin of the vesicle, the end result of the subsequent amphisome-lysosome fusion is still referred to as “autolysosome”.

2.7.2 Classification of sorting nexins

SNXs comprise a super-family of proteins, mostly involved in endocytic trafficking, and grouped together based on the presence of a unique ***Phox**-homology* (PX) domain, through which they bind to PI(3)P [234]. Therefore, SNXs are recruited at PI(3)P-enriched compartments such as the aforementioned autophagy and endocytosis nucleation sites. The presence of specific domains on their structure, rather than their function, is used to further split SNXs into distinct families [234]. Of the different SNX clusters, the one most relevant to this work is the SNX-**B**in-**a**mphiphysin-**R**vs (BAR) family, whose members contain a BAR domain, with which they are able to participate in membrane deformation events as they can sense, generate, and stabilize membrane curvature [228], [234], [235]. The SNX-BAR family consists of approximately 12 members, of which the most relevant for this current work is the SNX9-group.

2.7.3 Overview of the mammalian and *Drosophila* SNX9-group

The mammalian SNX9 sub-family comprises of SNX9 and its paralogues, SNX18 and SNX33 [234]. In contrast, the *Drosophila* genome encodes for a single representative of the mammalian SNX9-group, **SH3PX1** (***Sh3**-homology and **Phox**-**1** domain-containing*); an alternative nomenclature that used to describe SNX9 [39]. They all share a conserved domain structure; an N-terminal SH3 (***S**rc-**h**omology-**3***) domain involved in protein-protein interaction and signalling events [236], followed by a low-complexity region (LC) and a C-terminal BAR domain (Figure 1.7) [234]. They are all able to promote membrane tubulation events as well as binding to partners such as dynamin and components of the cytoskeleton machinery [234].

Despite these similarities, the SNX9-group only shares limited sequence homology between its members. As such, it may be reasonable to expect a certain degree of functional overlap between SNX9 members in some areas, while displaying distinct functions in others.

Of the three mammalian members of the group SNX9 is the best characterized, with a well-established role in CME, as a major binding partner of dynamin, clathrin and AP-2 [227], [229], [237]. In addition it has also been reported to function during dorsal-ruffle formation and clathrin-independent, actin-dependent fluid-phase endocytosis [237]. Either SNX9, or

SNX18 are partially dispensable for CME progression, showcasing an example of functional redundancy shared between the two proteins [238].

On the other hand, SNX18 specifically, was shown to be involved in clathrin-independent endosomal trafficking, mediated via AP-1 and the retrograde transport protein PACS1, in contrast to SNX9 [239]. As an example of oppositely distinct functions within the same pathway, SNX18 promotes extracellular matrix degradation; a membrane remodelling event required for invadopodia formation of cancer cells during metastasis, whereas SNX9 inhibits the process [240].

SNX33 is the least-characterized, therefore not much is yet known about the molecular pathways this sorting nexin is involved in. A 2012 study identified all SNX9-family members to be indispensable for cells to successfully undergo mitosis, and have several distinct roles in the process [241]. Depletion of either SNX9, SNX18, or SNX33, attenuated mitosis at different stages, thus identifying a role for SNX33 during cell division, as well as the mitotic stages each SNX9-member is involved in [241].

In a similar fashion to its mammalian SNX9 counterparts, *Drosophila* SH3PX1 seems to be required for the controlled cell division of intestinal stem cells in the gut, through a network involving autophagy and endocytosis [242]. Enhanced - but properly regulated - intestinal stem cell proliferation is a standard anti-inflammatory response of the tissue during the fly's defence against invading pathogens via its food intake route. However, aberrant proliferation is the signature property of cancer cells. In this context, SH3PX1 was shown to keep intestinal stem cell division in check, through an elaborate network involving components of endocytosis and autophagy, which collectively counter-balanced over-proliferation brought about by over-activation of the EGFR-ERK signalling cascade [242]. The membrane-remodelling capabilities of the mammalian SNX9-group members, as well as the interactions with the cytoskeleton machinery are also retained in SH3PX1, as the sorting nexin is required at optimal levels for effective lamellipodia formation in cultures of *Drosophila* Schneider-2 cells [243]. Furthermore, both the mammalian SNX9-members and the fly SH3PX1, positively regulate synaptic vesicle ultra-structure, and neuro-transmitter release during synapse development [244].

With regards to autophagy, only SNX18 has been shown beyond doubt to positively regulate autophagosome biogenesis in mammalian cells, partially attributed to its membrane tubulation properties [140]. The involvement in autophagosome formation is so far unique to SNX18, as depletion of SNX9 does not inhibit the process in mammalian cell cultures [140]. SNX18 interacts with ATG16L1 and enables targeting of ATG16L1-positive

REs to the site of phagophore formation [140]. REs have been shown to contribute membrane material from the Golgi network to the nascent autophagosome and promote starvation-induced autophagy [140], [245]. Furthermore, SNX18 is a SAR, which interacts in a LIR-dependent manner with both lipidated and non-lipidated LC3/GABARAP, but via a "non-canonical" LIR motif [140]. The same motif is reportedly required also for SNX18's interaction with AP-1, which too is important for autophagosome formation [246]. Based on tandem observations from the fat bodies of *Drosophila* larvae, SH3PX1 is also necessary for induction of autophagy following nutrient-deprivation, however it is not sufficient on its own to drive the process upon over-expression [140].

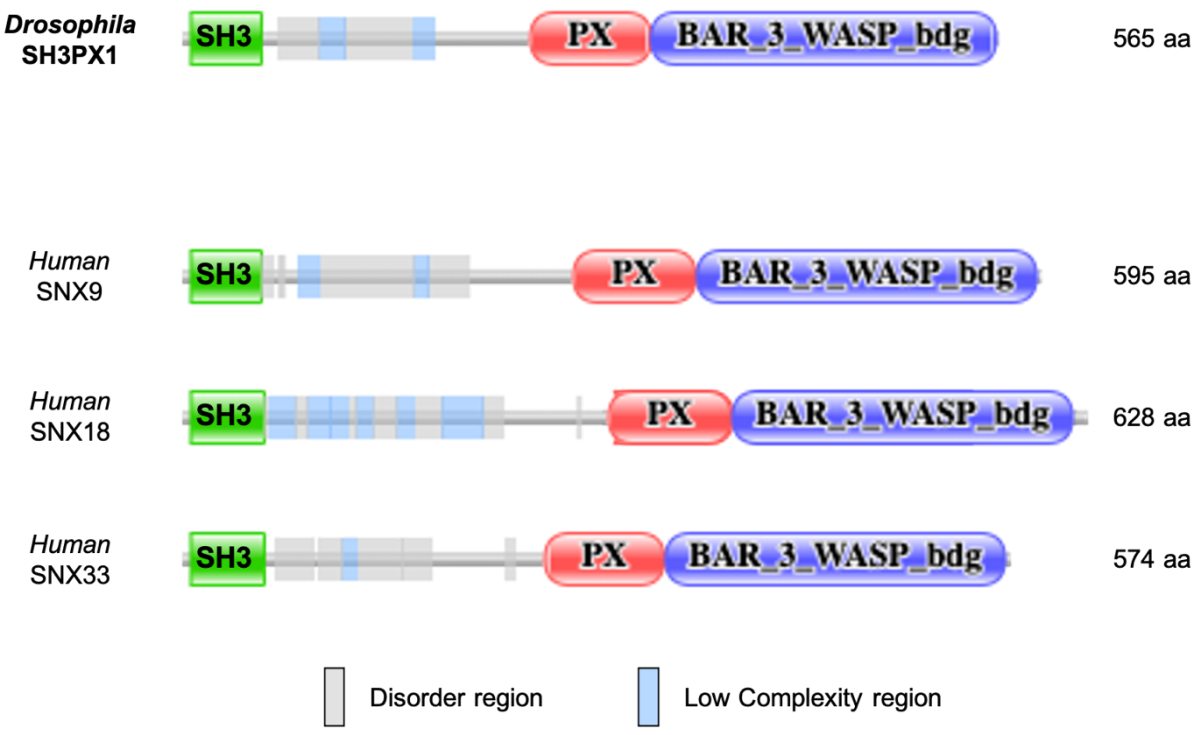

Figure 1.7. ***Domain Conservation between human SNX9-family and Drosophila* SH3PX1**. Domain architecture and function is largely shared between all human SNX9 members (SNX9, SNX18, and SNX33), and these features are also mimicked in the sole representative in Drosophila, SH3PX1. Protein domains were visualized by Pfam.

Abbreviations used in figure; *aa: amino-acids*; *SH3: Src-homology 3*; *PX: Phox-homology*; *BAR-3-WASP-bdg*: *Bin-Amphiphysin-Rvs 3 and Wiskott–Aldrich syndrome protein-binding*

Chapter 3

The Innate Immune Defence of the Fruit Fly

The innate immune response is a host's first line of defence against invading pathogens and the ancestral basis in the evolution of the immune system. As such, it is the most conserved across all eukaryotes compared to the mammalian adaptive immune response and although not as refined as the latter, its range of action covers a broader spectrum of harmful microbes [247].

With regards to the humoral aspect of innate immunity, in both insects and mammals part of it involves the production and subsequent release in the circulation of soluble peptides with anti-microbial properties, that trigger a system-wide defence response of the organism [248]. The best known examples of such proteins are the ***a**nti-**m**icrobial **p**eptides* (AMPs) and for the insect systemic response, these are predominantly manufactured and secreted by the fat body (functional equivalent of mammalian liver) [249]. Barrier epithelial tissues which come into frequent contact with extracellular microbes, such as the gut, trachea, Malpighian tubules and respiratory tract, also produce tissue-specific patterns of AMP cocktails to control localized microbial load [250]–[252]. In mammals, the NF-κB-mediated branch of humoral innate immune responses, is carried out by the multi-faceted Toll-like and TNFα pathways [248]. These pathways are conserved in *Drosophila* as Toll and IMD respectively (although fruit flies utilize a more integrated signalling cascade of these two pathways), which fend-off pathogens remarkably well, despite fruit flies lacking the sophisticated arsenal of the mammalian adaptive immune system [248]. The research focus of this study is at the regulatory interactions which take place at the level of the IMD apical kinase complex; dTAK1/dTAB2, and collectively shape the response of the pathway according to the cell's needs.

3.1 *The IMD Pathway*

The IMD immune response has a two-pronged role in maintaining homeostasis by: a) protecting against potentially harmful microbial invaders, and b) controlling commensal microbiota populations, such as the gut microbiome [253]. It was initially characterized by the "*immune deficiency"* recessive mutation, which impaired production of several anti-bacterial peptides causing flies to succumb by extent to bacterial, but not fungal challenges [254], [255]. Furthermore, *imd* flies were reported to be more vulnerable to infections from Gram^{-ve} strains, rather than Gram^{+ve} bacteria or fungi, in contrast to Toll-mutant flies [256]. Such observations helped in identifying that the IMD pathway is predominantly involved in host defence against Gram^{-ve} bacteria —and certain Gram^{+ve} bacilli— and accordingly, the activities of most IMD-regulated AMPs are tailored primarily against these types of invaders [257]. Following its upregulation, the signalling cascade activates the transcription factor Relish (*Drosophila* NF-κB homologue). Relish in turn mobilizes the humoral branch of the innate immune response, by translocating to the nucleus to promote expression of specific AMPs, which will be subsequently secreted in the haemolymph to drive the fly systemic immune response [255], [258], [259].

3.1.1 Intruder alert: Fly PGRPs in pathogen recognition and signalling

Conserved macromolecules found on the outer surface layers of most pathogens can serve as markers that are recognised by specific pattern-recognition receptors of the host [260]. This constitutes the first step in the successful detection of microbial intruders. For the majority of bacteria that activate the IMD pathway, this signature macromolecule is **p**eptido-**g**lyca**n** (PGN) (also known as murein); a polymer of long sugar chains cross-linked by short stem peptides, and forming a characteristic mesh-like structure that defines the bacterial wall [261]. Based on the amino-acid composition of the stem peptide links, PGN chains are grouped into K-type and **d**i-**a**mino-**p**imelic acid (DAP)-type PGNs, which are predominantly associated with Gram^{+ve} and Gram^{-ve} bacteria respectively [262].

PGN is recognized by a family of receptor molecules known as **PG**N-**r**ecognition **p**roteins (PGRPs). All PGRP members share a conserved 160aa-long PGRP domain [263], but have different binding affinities for either K-type, or DAP-type PGNs, and are therefore preferentially activated by Gram^{+ve} or Gram^{-ve} bacteria respectively [264]. The

PGRP family is represented in mammals by 4 members, whereas the *Drosophila* genome contains 13 genes that encode for a total of 19 different splice variants [264]. Moreover, the functions between mammalian and fruit fly PGRPs seem to have diverged throughout evolution. *Drosophila* PGRPs can be PGN-lytic enzymes as well as regulators of immune response and proteolytic cascades, while mammalian PGRPs retain their PGN-degrading functions but have since lost their signalling capabilities [265], [266].

Two groupings exist for PGRPs based on their transcript size: short (S) or long (L). All identified short PGRPs (SA, SB1, SB2, SC1a, SC1b, SC2, SD) are primarily extracellular scavenger proteins with limited signalling capacity, that sense PGN and act as antibacterial amidases, while some can activate the Toll pathway [263], [264]. Long PGRPs can be found on either side of the cell or at the plasma-membrane, and generally act as PGN receptors that primarily activate the IMD pathway [263], [264]. The *Drosophila* IMD pathway is regulated by the synchronized functions of most long and several short PGRPs.

The fruit fly PGRP-L group is made up by five members (LA, LB, LC, LE and LF). The principal activator of the IMD pathway is PGRP-LC; a transmembrane receptor located at the cell surface, where it binds DAP–type PGN [267]–[269]. This receptor exists as three isoforms (-LCα, -LCx, -LCy) that share the same intracellular signalling domain, but distinct extracellular PGN-sensing domains and homo- or hetero-dimerize with each other to mediate their signalling effects [270], [271]. PGRP-LCx binds polymeric DAP-PGN with higher affinity [270], whereas PGRP-LCα recognizes the more immunogenic monomers of DAP-PGN called **t**racheal **c**yto**t**oxin (TCT) [272]. PGRP-LCα likely acts as a co-receptor in a hetero-dimeric complex of PGRP-LCx/LCα that binds TCT [271], [272]. The third isoform PGRP-LCy is expressed at low levels, and seems to be functionally redundant [270], or a minor antagonist of IMD activation [273].

The PGRP-LE receptor, is produced as two variants: a short and a full-length isoform [273], [274]. Short PGRP-LE is secreted in the haemolymph where it surveys and binds DAP-PGN and is thought to assist in activation of the IMD cascade by presenting PGN moieties to PGRP-LC [275]. The full-length PGRP-LE is intracellular and monitors the cytosol, where it binds TCT fragments that may pass freely through the plasma membrane, due to their small size [274]. This makes PGRP-LE the only PGRP member so far with an intracellular variant. PGRP-LC mutant flies still mount an immune response after challenge with TCT, due to the cytoplasmic PGRP-LE receptor recruiting the Imd adaptor, which propagates the immune response signal further downstream (see below in 3.1.2)

[273]–[275]. In addition, intracellular PGRP-LE is also capable of activating autophagy in response to bacterial infection [276].

PGRP-LF is a transmembrane protein with neither PGN-binding ability nor an intracellular signalling domain. It acts as an inhibitor of the IMD pathway by binding PGRP-LCx in the presence or absence of TCT, and prevents its dimerization with itself or with PGRP-LCa [277], [278].

Not much is known about PGRP-LA. It is predicted to lack PGN-binding properties and be dispensable for the IMD response upon systemic infection [279]. It may likely function as a positive IMD pathway regulator in a tissue-specific manner, as it is expressed at high levels in barrier epithelia such as the respiratory tract [279].

Finally, PGRP-LB, as well as PGRP-SC-1A/B and PGRP-SC-2, display PGN-lytic activity and downregulate IMD by virtue of degrading PGN to non-immunogenic fragments [280]–[283]. This is thought to also serve as a way of protecting commensal bacteria populations by preventing overactivation of IMD from excessive release of immunogenic PGN fragments in the haemolymph [282], [283]. PGRP-LB is the major negative regulator of the IMD pathway in the insect gut [280].

3.1.2 Activation and signal transduction

While sharing elements with the mammalian Toll-like cascade at the receptor level, the *Drosophila* IMD pathway mostly resembles the TNF cascade of mammals, concerning the downstream events that take place following its induction (Figure 1.8) [284]. Both TNF and IMD signalling result in the activation of the cytoplasmic transcription factors NF-κB and Relish respectively, which translocate to the nucleus to drive expression of their target sites, such as AMP genes [285].

Under IMD upregulation conditions, the various PGRP-L receptors at, or near the cell surface, are mobilized and brought in close proximity by binding PGN and forming multimer complexes which facilitate assembly of the downstream Imd-signalling complex [270], [286]. The Imd-complex consists of the pathway's namesake death-domain adaptor Imd (*Drosophila* orthologue of RIP-1) [287], the scaffold protein Fadd [288], and the fly caspase Dredd (homologue of caspase-8) [289]. An E3-ligase called ***i**nhibitor of **ap**optosis-**2*** (Iap-2) activates Dredd by ubiquitination [290], [291], with help from three additional E2-conjugating enzymes, Uev-1a, Bendless (UBC13 homologue) [292], and Effete (UBC5 homologue) [293].

Dredd cleaves a 30aa N-terminal fragment from Imd, to reveal a site that Iap-2 recognizes and docks to, so it can in turn promote K63-ubiquitination of this adaptor protein [291], [293].

The Ub^{K63} signal on Imd facilitates the assembly of the dTAK1/dTAB2 complex on-site. dTAK1 is the apical kinase for both the IMD and JNK pathways, and dTAB2 is an adaptor protein, important for co-activating the kinase [294], [295]. In contrast to the single TAB2 isoform in *Drosophila*, there are three different TAB adaptors in mammals (TAB1, TAB2, TAB3) that regulate TAK1 activation in a context-dependent manner [296], [297]. Once activated, dTAK1 propagates the signal to its downstream effector, the *Drosophila* IKK complex; comprised of the catalytic subunit, IKKβ and its regulatory subunit IKKγ/Kenny, which is phosphorylated by dTAK1 [298], [299].

IMD signalling then converges on the cytosolic transcription factor Relish. Full-length Relish undergoes two major post-translational modifications: phosphorylation and proteolytic cleavage [299]. The IKK complex phosphorylates Relish at multiple site near its N-terminus, while Dredd cleaves the transcription factor into an N-terminal (Rel-68) and a C-terminal (Rel-49) fragment [259], [299]. Rel-68 contains the nuclear localisation signal and upon processing, Rel-68 translocates to the nucleus, while Rel-49 remains in the cytoplasm [259]. Interestingly, the IKK-mediated phosphorylation of Relish is not necessary for its proteolytic cleavage by Dredd. Rather, it is essential for the subsequent recruitment of RNA polymerase II by Rel-68 following its nuclear translocation, and induction of the AMP genes controlled by the transcription factor [300].

Upregulation of the IMD pathway eventually leads to the expression of AMP gene products predominantly optimized against pathogenic $Gram^{-ve}$ bacteria, and therefore considered largely under the influence of IMD. Such AMPs include *Drosocin* (*Dro*), several *Cecropin* (*Cec*) and *Attacin* (*Att*) members; with *Diptericin* (*Dpt*) being the most characteristically IMD-specific gene [301]–[305].

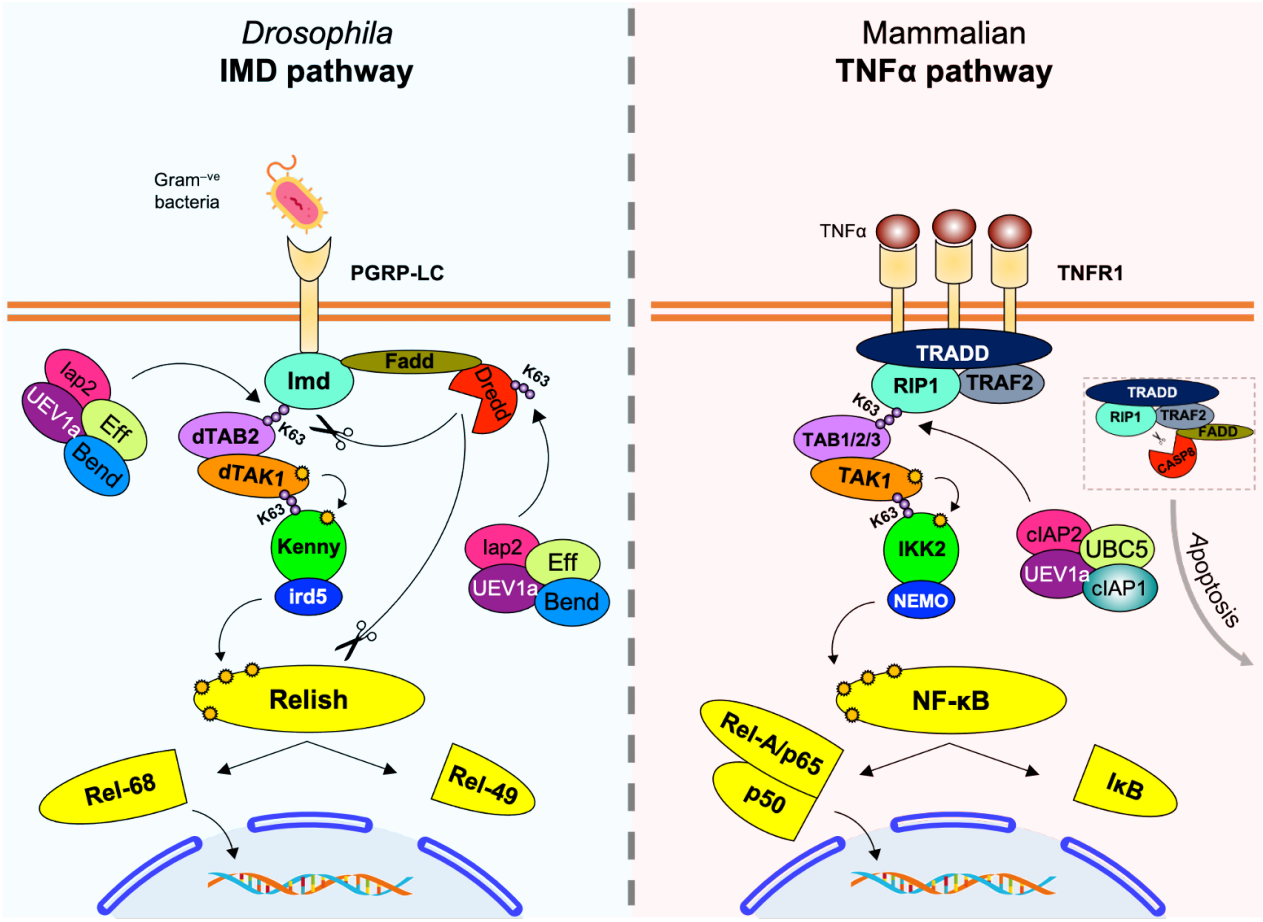

Figure 1.8. ***Induction Cascade of Drosophila IMD and Mammalian TNFα Pathways***. Graphical comparison of the *Drosophila* IMD and mammalian TNFα signalling cascades, showcasing the large degree of component conservation between the two pathways. Functionally similar proteins are depicted with the same colour. For simplicity of comparison, only a limited detail of events and components is shown. The Ub-ligase complex of Iap2-Effete-UEV1a-Bendless promotes the K63 ubiquitination of Dredd during its activation, which allows it to cleave the Imd adaptor exposing its Iap2-binding site. The members of the core TAK1 and ird5/NEMO kinase complexes are retained between the two pathways, except for the TAB-family in mammals which is more extended. Activation of the TAK1 and Kenny/NEMO complexes by successive K63-Ub and phosphorylation events lead to the subsequent phospho-activation of Relish/NF-κB respectively (in IMD pathway Dredd cleaves Relish in addition to phosphorylation). The corresponding Rel-68 fragment and p65-p50 subunits translocate to the nucleus to drive transcription of associated genes such as AMPs, cytokines and interleukins. Notable differences from IMD include the additional requirement of the scaffold and adaptor proteins TRADD and TRAF2 respectively in TNFα signalling, the substitution of Bendless (in IMD) with cIAP1 in the mammalian Ub-ligase complex, and that the primary functions of CASP8 are more targeted towards apoptosis following activation of the caspase, despite contributing to the cleavage of RIP1 for its K63-ubiquitination.

Abbreviations used in figure; *Bend: Bendless; Eff: Effete; CASP8: Caspase 8; TRADD: TNFR1-associated death domain protein; IκB: Inhibitor of NF-κB*

3.1.3 Pathway regulation

Due to its fundamental importance in cell survival, it is imperative that the IMD pathway transiently activates for just the necessary amount of time and falls back to baseline shortly after the source of the initial stimulus has been eliminated. As such, cells employ a wide and elaborate network of regulators in order to fine-tune IMD signalling on every level and ensure homeostasis is quickly re-established. It is therefore not within this dissertation's capabilities and space limitations to describe each known aspect of such modulatory interactions, but rather present here a few relevant examples for several IMD components in a top-to-bottom manner, according to their perceived activation hierarchy in the cascade.

Since ubiquitination events are pivotal in upregulating the IMD pathway, it is reasonable to expect that de-ubiquitination is oppositely critical for its downregulation. At the level of the Imd protein, the de-ubiquitinating enzyme dUSP36/Scny can uncouple K63-polyUb chains from the adaptor; which consequently allows K48-ubiquitination to occur and target Imd for proteasomal degradation [306].

Further downstream, Trabid has been shown to interact with the dTAK1/dTAB2 complex and de-ubiquitinate dTAK1 by removing Ub^{K63} chains from the kinase, thus reducing its signalling capabilities [307]. This is evidently an IMD-specific function of Trabid, since dTAK1 can still induce the JNK pathway irrespective of the de-ubiquitinase's activity [307]. Conversely, it is the K48-ubiquitination of dTAK1 by the E3-ligase POSH that attenuates dTAK1-dependent JNK signalling, which marks the kinase for proteasomal degradation [308]. In addition the *Drosophila* de-ubiquitinating enzyme Cylindromatosis is another strong negative regulator of IMD signalling, as it interacts with IKKγ/Kenny and prohibits activation of the IKK complex[309], [310].

Several downregulatory mechanisms have been identified for the transcription factor Relish with regards to suppressing its nuclear translocation and expression of IMD-regulated AMP genes. Dnr-1 and Caspar can inhibit the caspase Dredd from proteolytically processing Relish into its active N-terminal Rel fragment (Rel-68) [311], [312]. The SCF complex can target post-translationally modified Relish for proteasomal elimination [313]. Furthermore, transglutaminase (single fly representative of mammalian family of transglutaminases) can cross-link multiple Rel-68 fragments into Rel-68 clusters that cannot easily pass through the nuclear envelope, and this in turn can suppress

expression of IMD-regulated AMP genes [314]. The functions of transglutaminase are particularly important in the fly midgut [314], where a fine balance needs to be maintained between commensal microbiota populations and activation of the host's innate anti-microbial defences, as discussed below.

At the transcriptional level, the IMD pathway also regulates expression of one of its own negative regulators; Pirk (***p**oor **I**MD **r**esponse upon **k**nock-in*, also known as Pims; ***P**GRP-LC-interacting **i**nhibitor of IMD signalling*) [315]–[317]. Interestingly, peak transcriptional expression of Pirk precedes that of many IMD-controlled AMP genes, and the most plausible model of its function is that it interferes with the formation of the PGRP-L/Imd-signalling complex, by being able to directly interact with PGRP-LC, PGRP-LE, as well as Imd; prohibiting them from the required proximity to assemble active-receptor multimers, and thus dampening downstream signalling [315]–[317]. Finally, Pirk has also been reported to promote internalization of PGRP-LC receptors from the cell surface and their targeting towards the lysosome for degradation [315]–[317]. A collective overview of the IMD downregulators at the different tiers of the pathway is shown in Figure 1.9.

3.2 *Role of IMD in Maintenance of Homeostasis*

Apart from its role as an alert-and-elimination mechanism of foreign intruders, the IMD pathway also carries out house-keeping functions. Observations from the *Drosophila* trachea argue that epithelial damage caused by localized infection, can trigger expression of IMD-mediated tissue re-modelling genes; the products of which will work in conjunction with other repair pathways to restore functionality to the affected area [251], [252]. The IMD's balancing act between protection and maintenance is however better exemplified in the fly gut. The intestine is a major entry route for pathogens that gain access via food intake, but also provides a habitat for a number of beneficial microbial populations [253]. Similar to mammals, the *Drosophila* gut is an extensively compartmentalized organ, where morphologically distinct regions perform equally diverse functions, and characterized by their native gene expression profiles [318]. The organ is divided into three main regions (each with further sub-domains): the foregut, midgut, and hindgut. IMD is activated throughout the entire tissue [253], but a combination of anatomical and functional features in each region, ensure the pathway effectively discriminates between friend or foe and is proportionally induced to match the microbial load.

The first way is by the density of microbial populations themselves and more specifically, the levels of the Gram^{-ve} DAP-PGN ligand that elicits the IMD response. Generally, the outer lipopolysaccharide layer on the bacterial cell wall masks this component, which makes it less accessible by the host PGN sensors and by extent less probable to induce IMD, thereby preventing overactivation of the pathway [253]. However, when bacteria divide, re-structuring of the bacterial wall releases PGN fragments in the extracellular space where they are more easily detected by PGN-scavenging proteins [253]. The population densities of commensal microbiota in the gut are generally much lower compared to those of the bacteria used for infections in experimental settings and in addition, residential microbiota proliferate at slower rates compared to invading pathogens [319]–[321]. Both these aspects mean that only low traces of immunogenic PGN would be present in the extracellular space under normal conditions. These PGN fragments would be quickly cleared by scavenger PGRPs and other negative regulators of the IMD response, thereby keeping the pathway at a baseline activation milieu. It is conceivable that this situation could be reversed when more rapidly-dividing bacteria enter the midgut space, in which case there would be a sudden spike of immunogenic PGN levels, pointing to an acute infection [253]. This surge of DAP-PGN fragments would in turn be sufficient to lift the inhibitory controls on IMD, and therefore mobilize the host innate immune response across its full spectrum.

Another layer of regulation comes from the local enrichment of gut regions and sub-domains in particular PGRP receptors. PGRP-LC, which is the main activator of the systemic IMD response in the fat body; is mostly enriched in the fore- and hind-gut regions, as well as the anterior part of the midgut [249], [318]. By contrast, the intracellular receptor PGRP-LE is the main IMD inducer in the middle and posterior parts of midgut [273], [318]. This most likely reflects the architectural and functional differences between gut regions [318]. The fore- and hind-gut regions are predominantly tasked with food and waste preparation respectively, and not involved as much with nutrient uptake. Together with their additional lining by a somewhat impermeable cuticle, these regions are not favourable habitats to support dense microbial populations that rely on constant nutrient exchange. As such, surface-expressed PGRP-LC in these regions, can more readily sense the presence of DAP-PGN and induce the IMD response to eliminate harmful pathogens from food before ingesting it further to the midgut [253]; and in a potentially similar manner during water-reabsorption from waste in the hindgut. On the other hand, the midgut is covered by a relatively permeable peritrophic matrix [318]. It is conceivable that PGRP-LC expression in

the anterior midgut might be a failsafe mechanism to ensure any potential pathogenic escapees are neutralized by the IMD pathway here, and do not cross over to the middle and posterior parts, where digestion takes place. Commensal microbiota populations instead are particularly enriched in the middle and posterior midgut, where the IMD pathway is activated by the intracellular PGRP-LE, which binds DAP-PGN fragments such as TCT that freely cross the cell membrane [273], [318]. This aids in keeping immune signalling lower than if surface PGRP-LC was also active, and creates a favourable environment in these midgut regions for beneficial bacteria to colonize and proliferate [318]. Furthermore, enrichment of the midgut in scavenger PGRPs (PGRP-LB, and isoforms of PGRP-SB and PGRP-SC), suggests that these amidases survey the gut lumen and process immunogenic PGN into non-immunostimulatory fragments, thus keeping IMD activation at tolerable levels for local microbiota [280], [283], [318].

Other negative regulators of the pathway, such as PGRP-LF, which dimerizes with PGRP-LC, and Pirk which also binds the receptor and disrupts its association with the Imd adaptor, also contribute in shaping the immune signalling in the midgut [253], [277], [315]. In addition, AMP production is also regulated by region-specific expression of transcription factors, so that different AMP patterns are found in different gut areas [251], [253]. Such is the function for the *caudal* intestinal homeobox transcription factor, which is locally expressed in the posterior midgut, and antagonizes Relish to modulate AMP genes expression in the area [320]. Silencing of *caudal* was shown to lead to aberrant expression of AMPs and affect the fitness of the animal in the long term [318], [320].

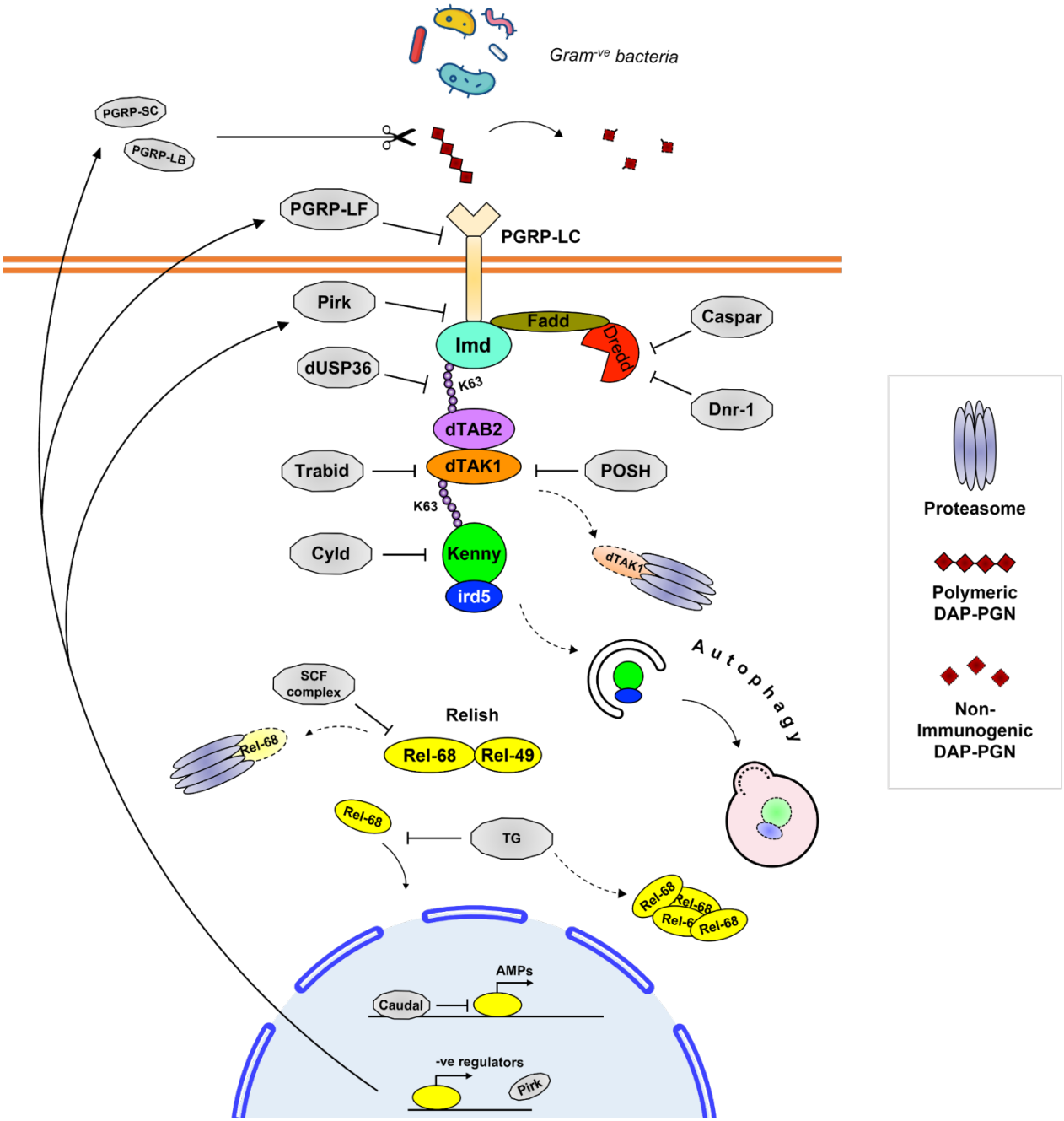

Figure 1.9. ***Downregulation of the IMD Signalling Pathway***. A complex network of proteins comprises the negative feedback loop that attenuates and fine-tunes signalling of the IMD immune response. Some of the negative regulators are tissue-specific. IMD also encodes for its own downregulators following induction. Scavenging PGRPs such as PGRP-SC and PGRP-LB process polymeric DAP-PGN of the bacterial cell wall into non-immunogenic PGN fragments. PGRP-LF and Pirk can inhibit multimerization of the PGRP-LC receptor and formation of the PGRP-LC-Imd signalling complex. Pirk can also target PGRP-LC for lysosomal degradation (not shown). Caspar and Dnr-1 inhibit the activity of the caspase Dredd. dUSP36 and Trabid can uncouple K63 poly-Ub chains from Imd and dTAK1 respectively. POSH labels dTAK1 with K48 Ub and targets it for proteasomal degradation. Cyld prevents activation of the IKK complex consisting of Kenny and ird5. The IKK complex is also removed via selective autophagy. The SCF complex turns over activated Relish to the proteasome and TG catalyzes the aggregation of Rel-68 fragments that reduces the ability of Rel-68 to translocate to the nucleus. Finally, at the transcriptional level, Caudal suppresses AMP genes expression by antagonizing Relish for its AMP promoter sites.

Abbreviations used in figure; *Cyld: Cylindromatosis; SCF: Skp, Cullin, F-box-containing TG: Transglutaminase;*

3.3 *IMD Deregulation & Loss of Homeostasis in Ageing*

As ageing progresses, the innate immune system attains a chronic gain-of-function phenotype, with increased production and secretion of inflammatory cytokines [11], [21], [322], [323]. This sustained activation progressively deteriorates global homeostasis, in a way that not only compromises the innate immune system's pathogen-deterring capability, but also increases susceptibility to infection as well as the risk of the system turning against its own host [34]. In *Drosophila*, a number of IMD pathway components, including Relish, PGRPs and several AMPs, have been found to be upregulated across its lifespan. The response to infections also becomes increasingly persistent and more difficult to terminate in older flies [324]. This has a negative effect on the health of the fly and corresponds with a significant reduction of its lifespan [324].

The intestine of older flies is burdened with increased microbial load, despite the simultaneous increased presence of AMPs and other anti-microbial factors [319], [321], [325], [326]. This may be at least partially attributed to a hypothesized positive —and deleterious— feedback loop created, where the increased presence of anti-microbial factors in the gut lumen pushes for the selection of more resistant microbial strains; which in turn results in increased production of immune agents and so on, and so forth. This loop can cause large-scale alterations of the gut microbiome, and the reciprocal mutualism gradually shifts to dysbiosis [253], [320]. The hyper-activation of the immune response in the ageing fly gut correlates with other characteristic markers, including tissue dysplasia, aberrant ISC proliferation and accumulation of undifferentiated ISCs, which all progressively compromise epithelial integrity, and allow bacteria groups to migrate across the limiting barrier, prompting further activation of systemic immune mechanisms [327]–[329]. In line with the above, the transcription factor **fo**rkhead bo**x** subgroup **O** (Foxo) has been found to be chronically upregulated in the gut of old flies, possibly as a result from persistent oxidative stress [326]. Foxo was shown to attenuate expression of the IMD negative regulator, PGRP-SC2, thus facilitating prolonged activation of the IMD response in the gut of aged flies [326].

In the *Drosophila* brain, localised microbial infection by pricking, results in age-dependent neuro-degeneration at the injection site, accompanied by locomotor defects [330]. Relish overactivation was shown to cause the observed neuron loss, an effect that was mimicked by inducing over-expression of individual Relish-controlled AMPs in neurons, or glial cells [330]. This suggests that AMPs may be directly cytotoxic to brain cells under poor regulation conditions [330]. It is quite interesting to note however that several AMPs

may promote lifespan extension in flies and can have a protective effect against some deleterious aspects of ageing, when overexpressed separately under certain conditions [331], [332].

The complex network of contributing factors to ageing notwithstanding, it becomes apparent that at least with regards to increasing the window of relatively good health well into old age, this may be achieved to a large degree by keeping the fine balance between pro- and anti-inflammatory markers. In this context, the above examples showcase the importance of understanding and preserving the regulatory mechanisms that maintain innate immunity under optimal working conditions across our lifespans.

Part II

MATERIALS & METHODS

Chapter 4

4.1 Chemicals &Reagents

The following list describes chemicals and reagents that were used in experiments, together with the chosen provider. For the reagents used but not included in the list, their supplier details are given in text on the first instance they are mentioned.

Table 4.1. ***List of Chemicals and Reagents Used.***

Reagent Name	Provider Reference
10% Ammonium persulfate [$(NH_4)_2S_2O_8$]	(Sigma, A3678-100G)
16% Formaldehyde	(ThermoFisher, 28908)
Agar	(Formedium)
Bovine serum albumin (BSA)	(Sigma, A7906)
Bromophenol blue sodium	(Sigma, B8026)
EGTA	(Sigma, E4378)
Glycerol	(Sigma, G6279)
Igepal CA 630	(MP, 198596)
Paraquat	(Sigma, 856177)
Ponceau S	(Sigma, P3504)
Propionic acid	(Sigma, P1386)
Sodium fluoride	(Sigma, S1504)
Sodium orthovanadate	(Alfa Aesar, 81104)
Sodium pyrophosphate	(Sigma, P8010)
Sucrose	(Sigma, 16104)
TEMED	(Sigma, T9281)
Triton™ X-100	(Sigma, T8787)
Tween® 20	(Sigma, P9416)

The Running and Transfer Buffers for SDS-PAGE and Western Blot respectively, as well as double-distilled and sterilized H_2O, EDTA, Tris-HCl (of various pH), and TAE solutions, were obtained as ready-made concentrated stocks from the Media Prep Room facility, situated within the School of Life Sciences at the University of Warwick. All solutions were prepared according to standard recipes.

4.2 List of Antibodies and Dilutions Used

4.2.1 Immunoblotting

Primary Antibodies

1. Mouse monoclonal anti-6xHis tag® (Abcam, ab18184, 1:2000 in TBST)

2. Mouse monoclonal anti-GST (clone B-14) (Santa Cruz Biotechnologies, sc-138, 1:2000 in TBST)

3. Mouse monoclonal anti-α Tubulin (Sigma, T5168, 1:53,000 in TBST)

4. Rabbit anti-Kenny/IKKγ [333] (kindly gifted by Dr. Silverman, 1:5000 in TBST)

5. Rabbit monoclonal anti-dTAK1 (Abcam, ab239353, 1:300 1:500 in TBST)

6. Rabbit polyclonal anti- β-Actin (Abcam, ab8227, 1:2000 in TBST)

7. Rabbit polyclonal anti-dTAB2 (Eurogentec, ZGB19056, 1:500-1:1000 in TBST)

8. Rabbit polyclonal anti-Ref(2)P (Abcam, ab178440, 1:1000 in TBST)

9. Rabbit polyclonal anti-SH3PX1 [243] (kindly gifted by G.B Gonsalvez, 1:60,000 in TBST)

Secondary Antibodies

1. HRP-conjugated rabbit polyclonal anti-mouse IgG (H+L) (ThermoFisher # 31450, 1:5000 in 1% blocking solution)

2. HRP-conjugated goat polyclonal anti-rabbit IgG (H+L) (ThermoFisher # 31460, 1:5000 in 1% blocking solution)

4.2.2 Immunofluorescence

Primary Antibodies

1. Rabbit polyclonal anti-SH3PX1 [243] (kindly gifted by Dr. Gonsalvez, 1:60,000 in blocking solution)

2. Mouse monoclonal anti-FLAG® (clone M2) (Sigma, F1804, 1:1000 in blocking solution)

3. Mouse monoclonal anti-Mono/Poly-Ubiquitinylated conjugates (clone FK2) (Enzo® BML-PW8810, 1:1000 in blocking solution)

4. Rabbit polyclonal anti-Ref(2)P (Abcam, ab178440, 1:1000 in blocking solution)

5. Rabbit polyclonal anti-pH3 (Ser10) (Merck Millipore, 06-570, 1:1000 in blocking solution)

6. Rabbit monoclonal anti-dTAK1 (Abcam, ab239353, 1:100 in blocking solution)

Secondary Antibodies and Dyes

1. Goat polyclonal Anti-Mouse IgG (H+L), highly cross-adsorbed, CF™ 488A (Sigma, SAB4600042, 1:1000 in blocking solution)

2. Goat polyclonal Anti-Rabbit IgG (H+L), highly cross-adsorbed, CF™ 488A (Sigma, SAB4600045, 1:1000 in blocking solution)

3. Goat polyclonal Anti-Mouse IgG (H+L), highly cross-adsorbed, CF™ 568 (Sigma, SAB4600082, 1:1000 in blocking solution)

4. Goat polyclonal Anti-Rabbit IgG (H+L), highly cross-adsorbed, CF™ 568 (Sigma, SAB4600085, 1:1000 in blocking solution)

DNA dyes

The Hoechst 3342 DNA staining dye (New England Biolabs, 4082, 1:1000 in PBS) was used to visualise nuclei in all immunofluorescence tissue preparations.

4.3 *Fly Husbandry & Genetics Principles*

4.3.1 Ectopic gene expression — UAS/GAL4 and FLP-out systems

To monitor protein expression and localization in fly tissues, I used the UAS/GAL4 and FLPout systems that allow for ectopic expression of a gene construct either across an entire tissue or in only a sub-population of clonal cells respectively. Both systems are schematically presented in Figure 4.1.

The UAS/GAL4 system

This genetic tool was first described by Brand and Perrimon in 1993 [43], and exploits the high binding affinity of the *Saccharomyces cerevisiae* transcription factor GAL4 for its *cis*-regulatory site (UAS), that promotes expression of any sequence immediately downstream of UAS [43]. With regards to flies, fly lines expressing GAL4 under the control of a tissue-specific promoter are known as "*driver lines*". When a GAL4-driver line is crossed to recombinant flies containing UAS-regulated genetic constructs, the UAS-product will therefore be transcribed in the progeny only in the target tissue where GAL4 is also expressed. As such, one can determine when and where a UAS-construct is expressed in the fly, by selecting specific promoters for GAL4 that may be active during particular stages in the fly's lifespan. For example, a Cg>GAL4 driver will activate UAS only in the fat body and haemocytes, early in development and maintain its transcription in those sites throughout the lifespan of the fly. Similarly, a ubiquitous driver such as actin>GAL4 will instead drive expression of the UAS-regulated construct across all tissues throughout the fly life cycle.

The FLP-out system

The UAS/GAL4 and FLP/FRT system for mitotic recombination have been combined together to form the 'FLP-out system'. The two key components of the FLP-out system, which like UAS/GAL4 derive from yeast, are:

- A **h**eat **s**hock-inducible and site-specific recombinase called "***fl**ip**ase**"* (Hs-FLP)
- A FLP-out cassette

The core FLP-out cassette consists of two **F**LP **r**ecognition **t**arget (FRT) sites, which flank a transcriptional termination signal (Figure 4.1). A marker gene can also be present within the cassette if required, in order to label non-clonal cells. When the FLP recombinase binds to its cognate FRT sites, it induces the "flipping-out" of the termination cassette, allowing the suppressed transgene to be expressed [44], [334]. The FLP-out system can be combined with UAS/GAL4 for additional levels of control.

An example of the above are the FLPout-mCherry:Atg8a transgenic flies that I employed in my work, and which have been created previously in the lab of I.Nezis by A.C Jacomin (Table 4.2). These flies express an mCherry-tagged Atg8a transgene under the control of the UAS promoter (UAS-mCherry:Atg8a), located on the 2nd chromosome. The same flies also contain the GAL4 transcription factor, which is under the transcriptional control of the **Ac**tin (Ac) promoter on the 3rd chromosome. The FRT-CD2 (marker gene; encodes for a rat membrane protein for cell adhesion)-STOP-FRT cassette is interspaced between the Ac promoter and GAL4, thereby dampening transcription of the latter as a result of the STOP signal. Finally, the same flies have on the 1st chromosome the coding sequence for Hs-FLP, which exhibits leaky expression at 25 ºC; a commonly-used temperature for maintaining flies during experiments. Altogether, this means that expressed FLP will bind the FRT sites of the FLPout cassette in a subset of clones, causing the excision of the termination signal and allowing expression of GAL4. GAL4 will in turn activate UAS-mCherry:Atg8a and allow expression of the fluorescent mCherry:Atg8a construct. The neighbouring cells where FLP-recombination was not induced will not express mCherry:Atg8a, but can be visualized by an anti-CD2 Ab, thus acting as negative controls to the mCherry-positive mitotic clones. Combined with another UAS-line, this allows the generation of fly progenies with double (or multiple)-transgene expressing clonal cells, while they can be directly compared to un-manipulated cells in the same environment [44], [334].

An advantage under certain circumstances of the FLP-out over the UAS-GAL4 system, is that the transgene of interest is expressed by a subset of cells in a tissue, instead of the entire tissue. This can allow the monitoring of transgenic constructs without potentially affecting the viability of flies as much as if the construct was expressed in a whole-tissue manner [44], [334].

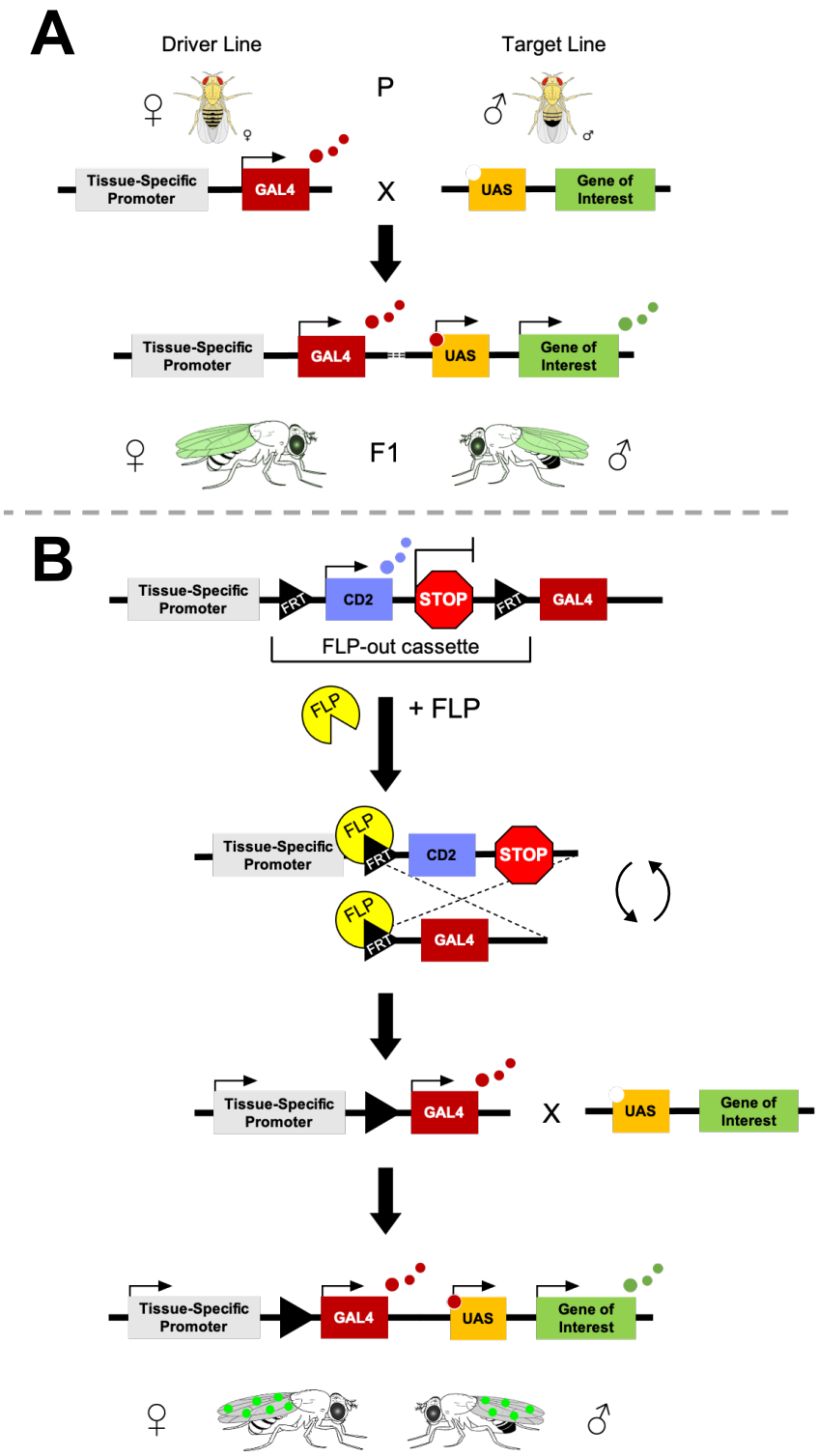

Figure 4.1. ***The UAS/GAL4 and FLP-out Systems for Transgene Expression.*** Graphic depiction of the UAS/GAL4 (**A**) and FLP-out (**B**) systems for ectopic gene expression in Drosophila. The FLP-out system allows for mosaic gene expression in a tissue. In the presence of FLP, the FRT sites induce a retro-transposition event that excises the STOP sequence and allows transcription of GAL4 in the specific tissue. A marker gene (in this example, *CD2*) can be inserted within the FLP-out cassette, that is removed upon successful FLP recombination. Therefore one can identify non-recombined from FLP-recombined cells in the same tissue, if desired. A FLP-out fly line can carry its own UAS-driven transgenes or be combined with another UAS-target line to create progeny that express the gene or construct of interest in only a subset of cells in a specific tissue.

4.3.2 Rearing Conditions

Flies used for experiments or stock passaging, were both kept in either 25(ø) x 95(h) mm transparent polypropylene vials (Dutscher Ltd, 789222), or half-pint heavy glass bottles (Dutscher Ltd. 789040), capped with dense cellulose acetate plugs (Dutscher Ltd, 789036 for vials, 789034 for bottles).

For stock preservation, flies were maintained at 18 ºC, 70% relative humidity, and were transferred into new vials or bottles, with freshly prepared fly food (see 4.3.4 for recipe) once in a generation (roughly every four weeks). During experiments, flies were kept at 25 ºC, 70% relative humidity, unless otherwise explicitly specified for an experiment. In order to enhance reproductive rates of weaker strains, additional yeast paste was applied to one side of the tube walls, as needed.

4.3.3 Fly Stocks Used

Table 4.2. ***List of Fly Lines Used in Experiments of Current Study.***

Obtained from the Bloomington *Drosophila* Stock Centre:

Short Name	***Full Genotype***	***Stock number***
w ^{1118} ǂ	*w[1118]*	# BL 3605
Tak1 $^{[2]}$	*y[1] w[*] Tak1[2]*	# BL 26272
Tak1 $^{[179]}$	*w[*] Tak1[179]*	# BL 26275
Tak1 $^{[2527]}$	*Tak1[2527]*	# BL 58809
Cg>GAL4	*w[1118]; P{w[+mC]=Cg-GAL4.A}2*	# BL 7011

Kindly gifted from other researchers:

Short Name	***Full Genotype***	***Stock Donor***
Atg8a ^{KG07569}	*P{hsFLP} Atg8a[KG07569]*	Dr. Gábor Juhász

Sh3px1 ^{10A}	*yw; Sh3px1 10A CRISPR / TM6*	Dr. Graydon B. Gonsalvez
Sh3px1 ^{C1}	*yw; Sh3px1 C1 CRISPR / TM6*	Dr. Graydon B. Gonsalvez

Created by I Nezis group, or external collaborators. Available in the I.Nezis laboratory:

Short Name	***Full Genotype***	***Stock Creator***
UAS-FLAG:Tak1 ^{WT}	*w[1118]; P{w[+mC]=UASp-3xFLAG-Tak1}/TM6B*	BestGene Inc.
UAS-FLAG:Tak1 ^{LIR1}	*w[1118]; P{w[+mC]=UASp-3xFLAG-Tak1 W669A I672A }/TM6B*	BestGene Inc.
CRISPR Tak1 ^{LIR1}	*w1118, Tak1 W669A I672A CRISPR / FM7A*	WellGenetics Inc.
Flpout-mcherry:Atg8a	*yw, hs-flp; UAS- mCherryAtg8a; Ac>CD2>GAL4/SM66*	Dr. Anne-Claire Jacomin

‡ Unless specified in text, w ^{1118} flies were used as the wild-type (WT) controls in experiments

4.3.4 Fly Food Recipe

Fly food was prepared in liquid form, before distributing in vials, or bottles.

For 1L of fly food, the recipe followed was:

- 1L Water (Super Q)
- 42g Inactive Yeast (Dutscher Ltd, 789126)
- 60g Cornmeal (Quaker®, 00030000570203)
- 130g Sucrose
- 6g Agar (Bacto)
- 30ml 10% w/v Nipagin

The mixture was autoclaved at 121ºC for 20 minutes and then supplemented with the appropriate volume and final concentration of Nipagin once it had cooled to a temperature of ~ 60 ºC, whilst still in liquid form.

4.4 *Lifespan Assays*

Male and female flies were collected within 24 hours from hatching and kept together for 2-3 days at 25 °C, 70% relative humidity, before being separated in single gender cohorts of 20–25 flies per vial. Death events and remaining survivors were recorded daily, and flies were transferred into new vials containing standard fly food on a 2–3 day interval. The lifespan assays progressed until death of the last remaining fly for each genotype tested was observed. I used the Kaplan-Meier method in order to calculate population at risk and survivability percentages.

Subsequent data analysis and survival curve construction used data pulled from multiple repeat experiments where the same assay conditions were met. Statistical comparisons of the survival curves generated for each genotype and gender, were performed using the Log-rank Mantel-Cox test.

4.5 *Immunoblot Assays — Buffer Solutions & Protocols*

4.5.1 Protease Inhibitors

To reduce protein degradation during extraction, all protein extraction buffers were supplemented with protease inhibitors. I also used the Roche Complete™ ULTRA, Mini, EDTA-Free Protease Inhibitor Cocktail tablets (supplied by Sigma, 5892970001). To obtain a 2x stock, 1 tablet was dissolved per 5 ml lysis buffer. The stock was kept at 4 ºC for no more than four weeks and diluted to the final working concentration at the point of use. Aliquots were not frozen.

4.5.2 Phosphatase Inhibitors

To preserve phosphorylation state of proteins, all protein extraction working solutions were supplemented with endogenous phosphatase inhibitors. For this purpose, buffer salts of sodium fluoride (NaF), sodium orthovanadate (Na_3VO_4) and sodium pyrophosphate ($Na_4P_2O_7$) were prepared. These can be dissolved immediately in the working lysis buffer, however due to the very small quantities required in the working solution, for convenience these were made as separate higher concentration buffers, which were diluted to the desired final concentration at the point of use. The NaF, $Na_4P_2O_7$, and Na_3VO_4 stock buffers were prepared and activated as follows:

- NaF did not require activation. For a 50 ml solution, of 0.5 M NaF, 1.05 grams of NaF were dissolved in distilled or sterile water (NaF molecular weight = 41.99 g/mol). Aliquots were stored at 4 ºC, for a maximum period of 2 weeks.

- Stocks of 100 mM $Na_4P_2O_7$ were prepared fresh every 2 weeks, due to reduced shelf life of the compound. For a 50 ml solution, 1.33 grams of $Na_4P_2O_7$ were dissolved in distilled or sterile water ($Na_4P_2O_7$ molecular weight = 265.90 g/mol). Aliquots were kept at 4 ºC.

- For a 100 ml solution of 100 mM Na_3VO_4, 1.84 grams of the compound were dissolved in distilled or sterile water (Na_3VO_4 molecular weight = 183.91 g/mol). Because the initial stock of 100 mM Na_3VO_4 is very alkaline (pH > 10), this was

further adjusted to pH 10 by repeated cycles of adding 1 M HCl and refluxing the solution at 100 ºC until colourless. The now activated 100 mM Na_3VO_4 stock was distributed into 1 ml aliquots, which were stored at -20 ºC and thawed as needed.

For all experiments the lysis buffer was further supplemented with a 1:100 final working dilution of Phosphatase Inhibitor Cocktail 2 (Sigma, P5726) at the point of use.

4.5.3 Lysis Buffers

To enhance protein extraction from fly tissue, I used the RIPA lysis buffer at first for its harsher denaturing properties, that allow for the more efficient lysing of cells and improve solubility of proteins. The final working concentrations for each ingredient used to make up 100 ml of RIPA buffer are provided below:

- 50 mM Tris-HCl pH 7.4
- 150 mM NaCl
- 1 % Igepal (NP-40)
- 0.1 % SDS
- 1 mM Na_3VO_4
- 5 mM $Na_4P_2O_7$
- 50 mM NaF
- Fill up remaining volume to 100 ml with distilled or sterile H_2O

I later switched to using the milder **p**hospho-**l**ysis **b**uffer (PLB) almost exclusively for extracting protein content from fly tissue samples. This was done in order to maintain integrity and phosphorylation state of the proteins of interest in the lysate as intact as possible. The below recipe was used to make 100 ml PLB buffer with the relevant final working concentrations for each of its ingredients:

- 120 mM NaCl
- 50 mM Tris-HCl, pH 6.8
- 1 mM Benzamidine
- 1 mM EDTA

- 6 mM EGTA
- 50 mM NaF
- 1 mM Na_3VO_4
- 15 mM $Na_4P_2O_7$
- 1 % Igepal (NP-40)
- When the volume is ~ 80 mL pH is adjusted to 6.8 with 32% HCl
- Make up remaining volume to 100 mL with distilled or sterile H_2O

Finally, for all *in-vitro* protein purifications, such as during GST-pulldown assays, I prepared the bacterial cell lysate in Classic Lysis Buffer. 100 ml solution was made, consisting of the following working chemical concentrations:

- 25 mM Tris-HCl, pH 7.4
- 100 mM NaCl
- 2 mM EDTA

The buffer was kept at room temperature in the above state. Immediately before each experiment, the desired volume of buffer to be used was further supplemented with a final working concentration of 0.1 ‰ β-mercaptoethanol (β-ME) and 1x protease inhibitor cocktail. In addition to these, the designated buffer volume to be used exclusively for cell lysing, was additionally supplemented with a 1 μg/μL lysozyme (ThermoFisher, 90082) final concentration.

4.5.4 Protein Extraction From Flies and Storage

Age-matched flies were collected at a 1:1 female/male ratio for a total of 10 flies per condition. If not to be used immediately for lysing, collected fly samples were stored at -80 ^{o}C. For experiments looking at phosphorylated proteins flies were flash-frozen in liquid nitrogen after collection and used immediately. 250 µl of supplemented lysis buffer were added in each tube and samples were processed on ice until homogenous. Protein content was extracted by the use of a motorised mortar and pestle. Samples were then centrifuged at 13,000 rcf for 10 minutes at 4 ^{o}C and the supernatant was collected.

4.5.5 Bradford Assay & Gel Loading Sample Preparation

Protein concentration of the centrifuged fly extracts was determined by construction use of the colorimetric Bradford assay [335]. BSA (≥ 98 % purity, Sigma, A7906) was used as the reference protein to construct the standard curve. I generated serial dilutions for the BSA reference (on a 0-20 μg/μl range), as well as all unknown samples, in sterile water, to which the Bio-Rad Protein Assay Dye Reagent was added (Bio-Rad, 5000006) for a final volume of 1ml. Next, the absorbance of each sample was measured at wavelength λ = 595 nm, on a GENESYS™ 10S Vis spectrophotometer. The absorbance values for the BSA serial dilutions of known concentration were used to construct the standard curve, which then served as the reference to match the absorbances of the unknown samples to, and correspondingly estimate the protein amount in the undiluted lysate.

Having calculated the protein concentration in each lysate, I prepared gel loading samples with a final uniform concentration of 1 μg/μl in lysis solution supplemented with homemade Laemmli buffer [336], to a total volume of 100 μl. Samples were finally boiled at 80 °C for 10 minutes to denature proteins, and stored at -20 °C.

4.5.6 Gel Casting

Polyacrylamide gels of the appropriate bis-acrylamide consistency were prepared fresh prior to SDS-PAGE, using the reagent volumes according to the table below:

Table 4.3. ***Resolving & Stacking Gel Volumes Guide***

Resolving Gel	**8%**	**10%**	**12%**
Distilled or Sterile H_2O [ml]	2.262	1.922	1.592
1.5 M Tris-HCl (pH 8.8) [ml]	1.25	1.25	1.25
30 % Acrylamide / 0.8 % bis-acrylamide [ml]	1.33	1.67	2
10 % SDS [μl]	50	50	50
10 % APS [μl]	100	100	100
TEMED [μl]	8	8	8
TOTAL **[ml]**	***5***	***5***	***5***

Stacking Gel, liquid	1 gel	x10
Distilled or Sterile H_2O [ml]	1.97	19.7
0.5 M Tris-HCl (pH 8.8) [ml]	0.875	8.75
30 % Acrylamide / 0.8 % bis-acrylamide [ml]	0.582	5.82
10 % SDS [μl]	35	350

A stock of stacking gel was prepared in liquid form without addition of the polymerising agents and stored long-term at 4 °C. APS and TEMED were added at the point of use.

no. of gels	1	2	3	4
Stacking Gel, liquid [ml]	2	3	5	6
10 % APS [μl]	40	60	100	120
TEMED [μl]	3	4	7	8
***TOTAL* [ml]**	***2.04***	***3.06***	***5.11***	***6.13***

Stacking Gel polymerization

APS and TEMED were added immediately prior to gel casting.

4.5.7 SDS-PAGE and Wet Transfer

After assembling the gel running apparatus, the gel tank was filled with 1x running buffer consisting of:

- 25 mM Tris-HCl, pH 8.6 ± 0.2
- 192 mM Glycine
- 1 % SDS

For 10-well gels, I loaded 10 µg (10 µl) of total protein sample per well and 5 µg (5 µl) for 15-well gels). Stacking was set at 75 V for 10 min so that samples across all lanes would reach the resolving front in a synchronized fashion. Once in the resolution phase, voltage was increased to 120-150 V. Electrophoresis continued until the ~25 kD molecular weight band of the marker lane reached near to the bottom of the gel, after 40 min to 1 hr run for 8-10% polyacrylamide gels that were most frequently used. Gels were then moved into a wet-transfer assembly, for migration onto either nitrocellulose or PVDF membranes. Transferring was set for 90 minutes at 100 V in cold conditions. The Tobin's transfer buffer used, consisted of:

- 25 mM Tris-HCl pH 8.6 ± 0.2
- 192 mM Glycine
- 10 % Ethanol

4.5.8 Blocking, Antibody Stain, and Film Development

Membranes were blocked in 5% BSA diluted in TBST (0.1% Tween®-20 in TBS) for 1 hr, at room temperature. They were then incubated with the appropriate primary antibodies diluted in TBST, either overnight (O/N) at 4 °C, or for 2 hrs at room temperature, with gentle agitation. HRP-coupled secondary antibody incubation was performed at room temperature for 45 minutes in 1% BSA dissolved in TBST. All intermediate washes prior to each incubation were performed in TBST, three times at room temperature. After primary antibody incubation these were for 10 min per wash, while after secondary antibody incubation they were for 15-20 min each. The Amersham ECL Detection Reagent (Amersham, RPN2106) was applied to membranes for 2 minutes at room temperature and in dark conditions. X-Ray sheets were exposed to the membrane in a dark room, and then passed through an AGFA automated developer.

4.6 *Immunofluorescence & Confocal Microscopy*

4.6.1 *Drosophila* Tissue Dissections

Both larvae, and adults, were placed inside droplets of PBS on a dark-coloured silicon pad. Tissues were dissected in room-temperature PBS using a pair of Dumostar #55 tweezers.

Tissue samples were loaded into mesh-bottom baskets, fashioned from the cap of Corning™ Falcon™ 35 μm Cell Strainer Tubes (Corning, 352235). The tissue-loaded baskets were then incubated in Greiner Bio-One CELLSTAR® 48-well culture plates (supplied by Sigma, M8937), and serially transferred from well to well, with each row containing the appropriate wash solution corresponding to each step of the tissue preparation protocol for confocal microscopy (as described in 4.6.2 below). Each well was filled with approximately 250 μl of the corresponding solution so that baskets were half-submerged upon incubation, thus ensuring tissue was sufficiently covered by the solution, while at the same time reducing the risk of tissue spilling over due to overflow.

4.6.2 Tissue Preparation for Confocal Microscopy

All incubation and washing steps were performed with gentle agitation of samples on a table-top rocker platform and at room temperature unless otherwise explicitly specified.

Fly tissue was fixed for 40 minutes with 4% ice-cold formaldehyde in PBS, then washed three times in 0.1% PBX (0.1% Triton™ X-100 in PBS) for 15 minutes per wash, in order to permeabilize cells and remove residual formaldehyde. Following the final wash, baskets were submerged was transferred to 0.3% PBX blocking (B) solution (0.3% BSA in 0.1% PBX), and left to incubate for 1 hr. After blocking, baskets were transferred to the appropriate primary antibody-containing solution (made in 0.3% PBX-B) and incubated either O/N at 4 °C, or for 2 hrs at room temperature. Samples were then washed three times in 0.1% PBT (0.1 % Tween®-20 in PBS) for 10 minutes per wash. From this point on, all subsequent steps were carried out with the sample-containing plate being kept in a dark box, due to the photo-sensitivity of the fluorophore-conjugated secondary antibody and the nuclei-staining dye.

The baskets were incubated with the appropriate secondary antibody (diluted in 0.3% PBX-B), either O/N at 4 ºC, or for 45 minutes at room temperature. I then performed three washes in 0.1% PBT for 20 minutes per wash, and transferred samples to a Hoechst 3342 (ThermoFisher, 62249) solution (1:1000 in PBS), to stain nuclei for 10 minutes at room temperature. Samples were then moved to PBS-only wells, before mounting on microscopy observation slides, using VECTASHIELD® Antifade Mounting Medium (Vector Laboratories, H-1000-10), and sealing cover slips with transparent nail varnish‡.

‡ Alternatively, they can be mounted in 90 % glycerol, containing 1,4´diazabicyclo-octane

4.6.3 Image Acquisition

All images were acquired on a Carl Zeiss LSM-710 and later LSM-880 confocal microscopes, using the built-in ZEN Imaging Software and user interface (https://www.zeiss.com). For all objectives used, oil immersion of the lens is required (used Immersol™ 518F; supplied by Fisher, 10539438).

Fat body and midgut tissue images were captured using Apochromat Å~40 and Å~63 objectives for widefield and zoomed areas respectively. Laser strength and photon-to-electron gain were adjusted accordingly, in order to enhance signal-to-noise ratio, while keeping overexposed pixels below 5% of the total number of pixels in the image.

4.7 *Larvae & Adult Infections*

The phytopathogenic bacteria *Erwinia carotovora carotovora 15* (*Ecc15*) was used to selectively induce activation of the fly IMD pathway [337]. This Gram^{-ve} bacteria infect potato plants and use fruit flies as an intermediate host [337]. As such, *Ecc15* is naturally occurring, mild pathogen of *Drosophila*, that upon infection mobilizes the host systemic immune response for the preferential expression of IMD-controlled AMP genes [254], [268], [305], [337]. The bacterial culture and infection protocol of fly larvae and adults was adapted from Bassett *et.al,* 2000 [337].

4.7.1 *Ecc15* Culture Preparation

Ecc15 pre-cultures were prepared by inoculating 100 μl of bacteria glycerol stock into 5 ml of lysogeny broth (LB) supplemented with 1:1000 final dilution of the antibiotic rifampicin [338]. Pre-cultures were incubated O/N, at 29 ºC in a 200 rpm shaking incubator. They were used the following day to grow large volume cultures in Erlenmeyer flasks, by inoculating 100 ml LB with the pre-culture stock at a 1:100 final dilution, without any antibiotics. Top of the flask was covered with aluminium foil in a loose manner, to allow aeriation of the culture. Large *Ecc15* cultures were incubated O/N at 29 ºC, in a 150 rpm shaking incubator.

Culture absorbance was measured the next day on a spectrophotometer at wavelength λ=600 nm, before spinning down at 3200 rcf in room temperature for 15 minutes. The bacterial pellet was resuspended in a 1:1 mix of LB and 5% filter sterilised sucrose, to a final OD ~150. This concentrated bacterial suspension was used to infect the flies by oral ingestion of the bacteria during normal feeding behaviour.

4.7.2 Natural Infection of Larvae and Adults

Collected larvae samples made up from evenly mixed female and male 3rd instar feeding larvae, were added to Eppendorf tubes containing 200 ml of concentrated bacterial suspension (approximately 16-20 larvae/tube). Bacteria-free LB-5% sucrose medium was used for control. Samples were incubated at room temperature for 30 minutes, before transferring to fresh fly food and incubating at 29 ºC for another 6 hours. Larvae samples

were used on the same for immunofluorescence experiments and were accordingly dissected and fixed, in preparation for confocal microscopy.

Age-matched adult flies were starved and dehydrated for 2 hours in empty tubes at 29 ºC, after which they were transferred to tubes with Whatman® paper discs placed at the bottom and soaked with ~ 300 μl of concentrated *Ecc15* suspension (LB-5% sucrose solution for controls). Medium was added or removed accordingly from tubes so that discs were sufficiently soaked without overflowing, in order to reduce number of flies becoming stuck at the bottom.

Fly-containing tubes were incubated for a further of 6 hours at 29 ºC. Upon completion of the incubation period, flies were separated into cohorts of evenly mixed female/male individuals (approximately 8-12 flies/cohort) per condition, in safe-lock Eppendorf tubes, and were subsequently flash frozen in liquid N_2. They were either used immediately for qPCR (see 4.8 below), or stored at -80 ºC for later use.

4.8 *RT- PCR & Real Time qPCR*

4.8.1 RNA Extraction

RNA was extracted from full-body fly specimens using the Invitrogen™ PureLink™ RNA Mini Kit (supplied by ThermoFisher, 12183025), according to the manufacturer's protocol. Based on the total number of samples to be processed each time, I obtained the desired working volume of the supplied lysis buffer (250 μl per sample), which was further supplemented this further with 1 % β-ME at the point of use. Extracts were obtained from age-matched and evenly mixed female/male flies per condition (8-12 flies per sample). RNA was eluted in nuclease-free H_2O and final concentration was measured on an IMPLEN NanoPhotometer® N60/N50. Subsequent steps were performed using 1 μg of RNA as template. For long-term storage, RNA samples were kept at -80 °C.

4.8.2 Genomic DNA Removal

To degrade genomic DNA, RNA samples were treated with DNAse I (ThermoFisher, EN0521). 1 μl of DNAse I was added for every 1 μg of RNA processed, according to the following table:

Table 4.4. ***Genomic DNA Removal Reaction Volumes.***

Reagent	**Volume**
Template RNA [μl]	Appropriate volume from eluted RNA stock for a final concentration of 1 μg / 10 μl
10x DNAse I Reaction Buffer [μl]	1
DNAse I [μl]	1
Nuclease-free H_2O [μl]	Top Up to 10 μl
TOTAL [μl]	**10**

Samples were then incubated for 30 min at 37 °C to allow the enzyme to digest genomic DNA. The nuclease was deactivated by adding 1 μl of 50 mM EDTA in each tube and

incubating for an additional 10 minutes at 65 ºC, bringing the final volume to 11 μl in each tube.

4.8.3 cDNA Synthesis

The Thermo Scientific™ RevertAid RT Reverse Transcription Kit (ThermoFisher, K1691) was used to reverse synthesise cDNA from the RNA template. The following reagents were added to the 11 μl mixture obtained at the end of the DNAse I treatment step, bringing the final reaction volume to 20 μl:

- 4 μl 5x Revert-Aid Reaction Buffer
- 2 μl 10 mM dNTPs
- 1 μl Random Hexamers
- 1 μl Ribo-Lock RNAse inhibitor
- 1 μl Revert-Aid Reverse Transcriptase

Samples were warmed for 5 minutes at 25 ºC, incubated for 60 minutes at 42 ºC, followed by enzyme inactivation at 70 ºC for 5 minutes. They were then retained at 12 ºC, or at 4 ºC overnight if they were to be used on the next day.

4.8.4 Real-Time qPCR Setup

All qPCR reactions were set up using Promega GoTaq® qPCR Master Mix 2x (Promega, A6002) which contains a pre-mix of dsDNA-binding dye, a low level of carboxy-X-rhodamine reference dye, GoTaq® Hot Start Polymerase, $MgCl_2$, dNTPs and reaction buffer. I used the Fisher Scientific 96-well plates (ThermoFisher, AB0600), where each condition can be represented in triplicate per gene of interest (including the housekeeping reference gene). As such, the total volume needed per qPCR reaction for each gene of interest is:

20 μl * number of conditions * 3 (technical repeats per condition)

The qPCR samples were prepared using the following table as guide according to the number of reactions needed (+1 reaction to account for leftover volume in pipette tip):

Table 4.5. ***qPCR Reagent Volumes per Number of Reactions.***

qPCR mix per reaction	**x1**	x3^{+1}	x6^{+1}	x9^{+1}	x12^{+1}	x15^{+1}
2x Master Mix [μl]	12.5	50	87.5	125	162.5	200
Nuclease-free H_2O [μl]	6.5	26	45.5	65	84.5	104
Forward Primer [μl]	0.5	2	3.5	5	6.5	8
Reverse Primer [μl]	0.5	2	3.5	5	6.5	8
TOTAL **[μl]**	**20**	**80**	**140**	**200**	**260**	**320**

A 1:50 dilution of the reverse transcription product was used as the qPCR template. 5 μl of cDNA were added directly to the plate in technical triplicates, for a total volume of 25 μl in each tube. Finally, wells were sealed with transparent optical strip caps (Agilent Technologies, 401425 or ThermoFisher, AB0866). qPCR was performed on an Agilent Technologies Stratagene MX3005P cycler, using the built-in MxPro software for analysis setup and quantification. The ribosomal protein 49 (rp49) was used as the reference housekeeping gene to carry out within-sample normalization of expression for the remaining genes of interest. This process was repeated across all conditions. The thermal profile setup used for target gene amplification was as follows:

Step 1: Initial Denaturing (x 1 cycle)

- 95 ºC for 5 minutes

Step Duration | 5 minutes

Step 2: Denature / Annealing (x 45 cycles)

- 95 ºC for 15 seconds
- 60 ºC for 40 seconds

Step Duration | 41 minutes, 15 seconds

Step 3: Final Melt Curve (x 1 cycle)

- 95 ºC for 1 minute
- 60 ºC for 30 seconds
- 95 ºC for 30 seconds

Step Duration | 2 minutes

Hold at 10 ºC

Total qPCR Duration | 49 minutes, 15 seconds

4.8.5 PCR Product Electrophoresis and Acquisition

RT-PCR was used to validate successful amplification of the desired gene, or transgenic construct (see 4.9.1). The product acquired by RT-PCR was subsequently visualised on a gel. I mixed 25 μl of amplified cDNA with a 1:100 dilution of GelRed™ , which was then loaded in a 2% agarose gel in 1x TAE gel. Electrophoresis was performed at 75 V for 1-1.30 hrs. Bands were visualised either with the aid of a UV trans-illuminator, or using an ImageQuant™ LAS 4000 CCD camera imaging station, together with the accompanying ImageQuant software.

4.8.6 Primers

All primers used were supplied by IDT. The following primers were used in the RT-PCR, as well as qPCR assay, written here in a 5’ to 3’ direction. For the qPCR experiments in particular, the primers used were all selected after achieving at least a 90% efficiency during a standard fluorescence curve experiment, performed in MxPro.

Attacin A F: 5’-GATGGACGTGCTAATCTCTG-3’
Attacin A R: 5’-GGCTTAGCCGAAATGATGAG-3’

Diptericin B F: 5'-AGTTCACCATTGCCGTCGCC-3'
Diptericin B R: 5'-GTAGGTGTAGGTGCTTCCCA-3'
Drosocin F: 5'-TCCACCACTCCAAGCACAATG-3'
Drosocin R: 5'-ACACATCTTTAGGCGGGCAG-3'
Rp49 F (*housekeeping gene*): 5'- GCTAAGCTGTCGCACAAATG -3
Rp49 R (*housekeeping gene*): 5'- CGATCTCGCCGCAGTAAA -3'
Sh3px1 F: 5'- GACAATGACACGTACTCGGAAA -3'
Sh3px1 R: 5'- GTCACTGGTGGAATGCGACAA -3'

4.8.7 Processing and Statistical Analysis of qPCR data

qPCR data analysis was performed according to the **d**ouble-**d**elta **c**ycle to **t**hreshold (ΔΔCt) method for quantifying gene expression, which uses the Ct values generated during amplification of each gene across the conditions tested. The logic behind the method is that genes with higher representation in the sample will amplify faster than less abundant genes, therefore requiring fewer cycles to reach and surpass threshold dye value.

An internal sample normalization step was carried out, by subtracting the Ct value of the reference gene rp49 from the Ct of each gene of interest. This is to eliminate any potential variation due to unequal loading of qPCR reaction per condition and render the expression of the same gene comparable between conditions. This generates a ΔCt value for each gene and represents the fold-change in expression on a log2 scale for each studied gene.

Each gene's ΔCt/log2 value was subtracted from its corresponding value in the chosen calibrator group, returning the ΔΔCt/log2 fold-change value of that gene compared to the reference condition (the latter's ΔΔCt values are consequently set to 0 as they are subtracted from themselves). Repeating this for each gene tested across conditions, creates the log2 fold-change of each group's genes relative to its calibrator group. As such, upregulation or downregulation for each gene of interest compared to control, is represented in the graph by positive or negative change respectively.

For statistical comparisons of experiment groups to a control condition I employed a one-sample t-test for each studied gene against a “0” value. To compare the differences in gene expression between three or more experiment groups (not control) that were calibrated to the same reference condition, I used a one-way ANOVA with Bonferroni post-hoc correction.

4.9 *Molecular Cloning & In-Vitro Protein Interaction*

For all cloning procedures, and for shipment of samples to external collaborators, isolation of plasmid DNA was performed by either the QIAprep® Spin Miniprep Kit (Qiagen, 27104), or QIAGEN® Plasmid Midi Kit (Qiagen, 12143) when quantities exceeding 20 μg of DNA were required, according to manufacturer's protocol. The following bacterial competent cell lines were used for transformation during the various molecular cloning protocols and general stock keeping of plasmid constructs:

- ***NEB® 5-alpha Competent Cells, Subcloning Efficiency*** (NEB, C2988J)

  Escherichia coli DH5a™ derivative. Used here for all subcloning routines and general plasmid stock keeping.

- ***NEB® 10-Beta Competent Cells, High Efficiency*** (NEB, C3019H)

  Escherichia coli DH10B™ derivative. Used here for all molecular cloning protocols except for subcloning routines and stock keeping.

- ***Rosetta™ (DE3) Competent Cells*** (Novagen Millipore, 70954)

  Escherichia coli B21 strain derivatives. Used here to insert recombinant plasmid vectors isolated from *10-beta* cells, in order to overexpress eukaryotic protein constructs in preparation for GST Pulldown assays.

4.9.1 Plasmid Constructs

3xFLAG:Tak1$^{WT/LIR1}$ construct and transgenic flies

I used the pUASattB (which contains a 5x repeat of the inducible UAS promoter). The vector carries both the sequence of an N-terminal appended 3xFLAG tag, and the fly coding sequence for Tak1. To create the Tak1 LIR1 mutant, an additional mutagenesis step was employed on a prior successfully recombinant pUASattB/3xFLAG:Tak1 clone. Initial screening of successfully recombined plasmids was carried out by PCR and gel electrophoresis (as described in 4.8.5). Samples of candidate recombinant plasmids identified in this manner, were sent to Eurofins Genomics for further sequencing to assess

correct in-frame orientation of the transgene. Finally, after sequencing had been performed, we sent a sample from a selected recombinant vector for each transgene to BestGene Inc, who carried out the fly embryo microinjections to create the transgenic lines.

In-vitro protein interaction by GST-Pulldown

The following plasmid vectors were used:

- **pET28a**
  Contains the 6xHis-tag sequence. Recombined with the fly cDNA for either Tab2, Tab2^{LIR1}, Tab2^{LIR2}, Tak1, Tak1^{LIR1}, Tak1^{LIR2}, or Sh3px1.

- **pGEX**
  Contains the GST-tag sequence. Used as empty vector, as well as recombined with the fly cDNA for Atg8a, or Tab2.

- **pDEST15**
  Contains the GST-tag sequence. The vector is recombined with the fly cDNA for Atg8a, or Atg8a^{LDS}

The pGEX-GST, pGEX-GST:Atg8a, pDEST15-GST:Atg8a, and pDEST15-GST:Atg8a^{LDS} have already been created and validated previously by the lab of I. Nezis. To append either the GST or a 6xHis-tag, to the DNA insert of choice, cDNAs were made from recombinant donor vectors which contain the coding sequence for each fly gene (pMT/V5-His:Tab2 and pMAL-c2T/MBP:Tak1 vectors were kindly gifted by Dr. P. Meier while the pDEST/EGFP:Sh3px1 vector was generously provided by Dr. Simonsen A.). PCR was performed using the Dream-Taq DNA polymerase (ThermoFisher, K1081). Primers were designed to additionally append a 5'- and 3'-prime restriction site flanking the amplicon, according to the presence of the site in the target (oligonucleotide sequence of these primers provided in Table 4).

The QuikChange site-directed mutagenesis kit (Stratagene, 200523), and Pfu Ultra II HS DNA Polymerase (Agilent, 60070) were used according to the manufacturer's protocol, to create the LIR mutant isoforms for Tab2 and Tak1 respectively. For the LIR1 and LIR2

mutants of Tak1 these amino-acid substitutions were on key residues W669A/I672A (full mutant motif sequence: EG**W**VV**I** → EG**A**VV**A**) for LIR1, and Y559A/V562A (full mutant motif sequence: KE**Y**LS**V** → KE**A**LS**A**) for LIR2. Similarly for Tab2, the amino-acid substitutions were on key residues F372A/L375A (full mutant motif sequence: KS**F**TS**L** → KS**A**TS**A**) for LIR1, and F339A/I342A (full mutant motif sequence: RD**F**RS**I** → RD**A**RS**A**) for LIR2.

Samples of all recombined constructs were sent to Eurofins Genomics, who performed sequencing of the products to cross-validate the correct sequence and in-frame alignment of the insert.

Table 4.6. ***Oligonucleotides Used To Generate Tagged, or Mutant Constructs***. Nucleotide point mutations for inducing amino-acid substitutions on the selected LIR motifs of *Tak1* and *Tab2* are shown in red

DNA Insert	Target Vector	5'- Forward primer	3'- Reverse primer
3xFLAG	pUASattB	CCGGAATTCATGGACTACAAAGACC	CCGCTCGAGTCGGTACCGGAT
Tak1	pUASattB/ *3xFLAG*	CCGCTCGAGATGGCCACAGCATC	GCTCTAGACTACGCATTGTGATGCGG
Sh3px1	pET28a	CCGGAATTCATGACCTCGTACGTG	CCCAAGCTTCTACTCAATCTGACGGC
Tab2	pGEX	TCCCCCCGGGTATGGCGGCTACAC	CCGCTCGAGTTATGTATGCAGAGCGTACG
Tak1	pET28a	CCGGAATTCATGGCCACAGCATCG	CCCAAGCTTCTACGCATTGTGATGC
Tak1 LIR1	pET28a/ *Tak1*	GAGTCCGTGGAAGAAGGC**GC**GGT GGTC**GC**CCCACCGCATCACAATG	CATTGTGATGCGGTGGG**GC**GACC ACC**GC**GCCTTCTTCCACGGACTC
Tak1 LIR2	pET28a/ *Tak1*	CACCGACACATGGCCAAGGAG**GC**C CTGAGC**G**CCGACACGAACCTCTAC	GTAGAGGTTCGTGTCGG**C**GCTCAG G**GC**CTCCTTGGCCATGTGTCGGTG
Tab2	pET28a	CCCAAGCTTATATGGCGGCTACACCAC	CCGCTCGAGTTATGTATGCAGAGCGTAC
Tab2 LIR1	pET28a/ *Tab2*	CTGGTGGACGCAAGAGC**GC**CACCTCG **GC**CAATCTCACCCTG	CAGGGTGAGATTG**GC**CGAGGTG**GC**GCTCT TGCGTCCACCAG
Tab2 LIR2	pET28a/ *Tab2*	CGTACGCGCGAC**GC**TCGCAGC**GC**TGA CTTTCCGCCGAC	GTCGGCGGAAAGTCAGCGCTG**CG**AGCGTC G**CG**CGCGTACG

4.9.2 Protein Induction and Extraction Protocol

Successfully transformed competent cells containing either the *GST*-fusion bait, or *His*-tag prey were incubated at 37 ºC in a 200 rpm shaking incubator, as liquid LB cultures (of at least 100 ml) in Erlenmeyer flasks at a 1:4 volume ratio of culture per empty flask space. Each liquid culture was additionally supplemented with the appropriate combination of antibiotics at a 1:1000 final dilution for each. Culture density was assessed by taking samples at regular intervals and measuring the absorbance at a wavelength λ=600 nm. Bacteria reached optimum population density when sample absorbance was within the range of 0.5-0.7 Au. At that point cultures were redirected from growth to expression of the transgenic product, by addition in the culture of the *lac* operon activator IPTG, at a final concentration of 0.5 mM for pGEX- or pDEST15- transformed cultures, and 1 mM for pET28a-transformed cultures. Bacteria were left to further incubate for 16 hours, at 20 ºC, 150 rpm, to allow sufficient expression of the target product. before pelleting and lysing to extract the protein content.

Bacteria were pelleted by centrifugation at 7,000 rpm, for 15 minutes in room temperature. Supernatant was discarded and pellet was either kept at – 20 ºC for short-term storage (maximum 2 weeks), or re-suspended in appropriate volume of Classic Lysis Buffer prepared for lysing (recipe as seen in 4.5.3). 1.5 ml of buffer was used per 40-50 ml of initial culture. Cell integrity was disrupted by sonication using an EpiShear™ Probe Sonicator (in pulses 10sec ON, 5 sec OFF, 30% amplitude) for 1-2 minutes per sample. Lysates were centrifuged at 20,000 rpm, 4 ºC, for 20 minutes, in a Beckman Coulter™ Avanti JXN-26 High Performance Centrifuge. The supernatant was collected to be used for the protein purification step below.

4.9.3 Protein Purification and GST-Pulldown Assay

Both the *GST*-bait and *His*-prey lysates were each incubated using Glutathione Sepharose® 4 Fast Flow affinity resin (Cytiva, supplied by Sigma, GE17-5132-01) for 30 min, at 4ºC. This step was performed to anchor the GST-tagged bait to the resin, and pre-clear the prey lysate from non-specific GST-binders respectively. For all subsequent steps, including washing of the samples, centrifugation was performed at 500 g, 4 ºC, for 0.5 minutes, and supernatant was aspirated before re-suspending the resin in the new solution.

The bait samples were washed once in High Salt (25 mM Tris pH 7.4, 500 mM NaCl, 2 mM EDTA) and once in Low Salt wash buffer (25 mM Tris pH7.4, 50 mM NaCl, 2 mM EDTA). The appropriate pre-cleared prey lysate was then added to each GST-bait, and samples were further incubated for 2 hrs at 4 ^{o}C with gentle rotation. They were subsequently washed once with supplemented classic lysis buffer, and then Imidazole buffer (25 mM Tris pH7.4, 100 mM NaCl, 2 mM EDTA, 10 mM imidazole) to remove non-specific His-binding from GST-anchored baits. Samples were finally re-suspended in matching volume of 2x Laemmli solution and boiled at 80^{o}C for 10 min, in preparation for immunoblot detection.

4.10 *Software Used for Image Analysis, Statistical Testing, Graph & Figure Generation*

All acquired images from the immunoblot and confocal microscopy experiments, were post-processed with the Fiji/ImageJ software (version 2.1.0/1.53c). For confocal microscopy the software was used to merge channels, add scale bars, perform colocalization studies and quantify aggregate formation between control and unknown groups. With regards to the immunoblot assays, the software was used to adjust brightness/contrast of gel images and perform signal intensity calculations for the protein bands of interest.

The Prism software (GraphPad, versions 8-9) was used to conduct all statistical analyses of data and to plot the corresponding graphs. Each dataset was tested for normality, or log-normality (where appropriate) using the built-in Shapiro-Wilk normal distribution test, prior to determining whether a parametric or non-parametric test should be employed to analyze the experiment data.

Finally, multi-experiment compound figures were assembled in Adobe Photoshop 2020 (version 21.2.5).

Part III

RESULTS & DISCUSSION

Chapter 5

Drosophila Tab2 & Tak1 are Novel Atg8-Interacting Proteins

Chapter Introduction: **Identifying the Atg8-interactome**

The I. Nezis group studies the conserved functions of autophagy in *Drosophila*, to gain insight that may also at least partially explain aspects of how the process operates under physiological and pathological conditions in humans as well. This is achieved following a two-pronged approach for delineating the complex mechanism and physiological functions of autophagy. One method is by discovering proteins that interact with *Drosophila* core autophagy machinery components such as Atg8a, and identifying the cellular processes (other than autophagy) they may participate in, before proceeding to investigate the role of autophagy in these processes. Alternatively, the group characterizes the potential function(s) of autophagy in pathways that contain signalling components with a high probability of binding Atg8a. To aid in this search, the I.Nezis lab has previously developed a series of tools for narrowing down the existing proteome to the most promising Atg8a-interacting candidates. These tools consist of i) a software for quickly scanning the amino-acid sequence of a protein in order to predict LIR motifs [339], ii) a list of UBD-containing fly proteins that possess at least one such predicted LIR motif [340], and of the most recent addition; iii) a high-throughput yeast-two-hybrid (Y2H) screen that identified several Atg8a-interacting proteins in *Drosophila*. Utilizing these powerful tools, I was able to characterize that both components of the initiator kinase complex of the IMD pathway, dTAK1, and its co-activator dTAB2, were novel Atg8a-binding proteins. This chapter will present the step-by-step approach and results by which dTAK1 and dTAB2 were verified to associate with Atg8a, along with the manner that each of them binds to this autophagy receptor. Because of their importance in laying the foundations of my PhD work, as well as explaining the rationale for including dTAB2 in my investigation, the UBD list as well as the LIR-predicting software and Y2H screen results are first briefly expanded upon in 5.1 below, with subsection 5.1.3 in addition explaining the thought process for how work with dTAB2 and dTAK1 would proceed.

5.1 *High-Throughput Analyses for Candidate Atg8a-interactors*

5.1.1. A *Drosophila* Ref(2)P-like UBD proteome & *iLIR*

Based from observations in mammalian systems, two very common [although not universal [170]] structural features shared by SARs, are the presence of at least one functional LIR motif and at least one UBD [341]. In mammals there are 20 UBD-family members, which despite their structural diversity and modes of interaction on an individual scale, they all share the unifying ability to non-covalently bind Ub moieties and chains [342].

Former PhD work conducted in the Nezis lab, used the domain structure of *Drosophila* Ref(2)P (only known fly SAR at the time) as a reference to screen the fly proteome for members with similar domain organization [340]. Combining the results by Husnjak *et al*, 2012 [342], with available information from the Pfam, InterPro and SMART online databases [343]–[345], that work returned an exhaustive list of UBD-containing proteins with similar organization to Ref(2)P, which was then subjected to analysis by the iLIR software [340].

The "*iLIR*" is a free-to-use software that was previously developed by the collaboration between the research labs of I. Nezis, V. Promponas and T. Johansen (available online at: http://repeat.biol.ucy.ac.cy/iLIR/) [339]. I would only wish to briefly reiterate here the definitions of "xLIR", "PSSM" and "ANCHOR" (as seen in Figures 5.1, 5.3 and Appendix Table 9.1), since their output data by the software was used as reference to inform decisions about including or excluding predicted LIR sequences for further experimental analysis by this study.

E**x**tended LIR (xLIR) motifs, refer to LIRs for which a certain degree of freedom is allowed in terms of the amino-acids found at the 2 proximal positions to the left of the *W-x-x-L* core [339]. This is because many LIRs do not bear the prototypical "*W-x-x-L*" pattern and even from those that do, the N- and C-terminal peptide sequences adjacent to the core are equally important in regulating the successful docking to Atg8/LC3 [170]

The **p**osition-**s**pecific **s**coring **m**atrix (PSSM) indicates how conserved each predicted LIR motif is according to the software, with higher positive net PSSM values corresponding to increased likelihood of the peptide sequence in question representing a critical function domain [339]. The current consensus shared by the developers of iLIR, is that PSSM values in the range between 10-13, constitute a confident lower cut-off boundary when selecting candidate Atg8-interactors by virtue of their PSSM score alone [339].

iLIR also uses the ANCHOR database to identify whether a predicted LIR sequence lies within a disordered region in the protein (ANCHOR: "Yes"), or not (ANCHOR: "No") [339]. Disordered regions can undergo disorder-to-order transition upon interaction with another substrate [346]. Therefore a "Yes" ANCHOR readout for a predicted LIR motif may indicate that the motif could lie in a region of the protein which is most likely exposed and able to participate in interactions with other substrates [346].

Taking the above into consideration, potential attributes that may define some — but not all — strong candidate Atg8/LC3-interacting proteins are: 1) presence of UBDs and xLIR motifs on the protein query, 2) xLIRs with individual net PSSM scores $\geq$ 10-13 range, and 3) xLIRs nested within ANCHOR regions.

5.1.2. Y2H screen for *Drosophila* Atg8a-interactors— Discovering dTAK1

The final piece of work prior to my own, was a high-throughput Y2H screen, aimed at identifying novel Atg8a-interacting proteins, conducted by Hybrigenics Services (Appendix Figure 9.1 and Appendix Table 9.1). This assay has been established in genetically modified *S.cerevisiae* strains, taking advantage of the properties and versatility of the yeast UAS/GAL4 system and based on a simple enough premise: transcription of a reporter gene which is under the influence of the UAS promoter, following reassembly of its activating cognate ligand, GAL4 [347]. For this purpose, the DNA-binding, and activating region of the GAL4 transcription factor are split between two fusion 'hybrids' that can act as bait and prey [347]. If the bait and prey successfully interact, they can form a protein-protein complex, which brings the two GAL4 domains in close proximity to allow reconstitution and activation of the transcription factor [347]. The newly re-assembled GAL4 can then bind and activate the UAS promoter and subsequently allow transcription of the reporter gene and development of a marker phenotype [347]. In this manner, a hybridized bait protein can be used to screen libraries of protein fragments of an entire organism; with the method having been successfully applied previously in *Drosophila* (I. Nezis lab and [348]). The identity of the interacting partners can be then obtained through sequencing of the corresponding plasmids, selected from yeast colonies harbouring the desirable phenotype.

Using this rationale, the autophagy receptor Atg8a was used as a bait to fish for Atg8a-interacting partners, in a high-throughput Y2H screen against *Drosophila* libraries

from 3rd instar stage larvae, and adult heads. For each protein identified as a candidate Atg8a-interactor in this manner the Y2H analysis also returned a mapped area of interest [termed "selected interaction domain" (SID)], wherein the bait-prey interaction took place. Therefore, the SID represents a region with a high-enough probability of containing at least one Atg8a-recognizing sequence, such as a UIM or LIR motif.

The Y2H screen identified the apical kinase of the IMD pathway; dTAK1 as a high-probability Atg8a-binding protein (Figure 5.1) among other Atg8a-interacting candidates (Appendix Figure 9.1 and Appendix Table 9.1). It should be noted here that Y2H used an automated method to identify protein IDs for all Atg8a-interacting candidates by BLAST-search against protein databases available online. The screen identified a dTAK1 isoform of 258 aa, termed "dTAK1 isoform B". By further searching, I found that this is a computationally predicted fragment of dTAK1, corresponding to the last 258 amino-acids at the C-terminal of the full protein, and devoid of all other domains, including the kinase domain. It is an entry that exists solely in the TrEMBL Protein Directory, which in turn is a heuristic approach in computer-translating the genetic information from the EMBL Nucleotide Sequence Database. Its purpose is to complement experimentally validated entries in SwissProt, however it is expected that computational predictions are not 100% accurate. Since no experimental reports exist for this predicted 258 aa product, and its sequence matches the C-terminal region of the full-length protein, it is unlikely that it represents a true isoform of dTAK1. As such, I opted to proceed with investigating the full-length protein. Nevertheless, this 258 aa-long dTAK1 isoform B is the one shown in Appendix Figure 9.1 and Appendix Table 9.1, as it represents the initial result returned by the Y2H screen. According to the Y2H results, the SID on dTAK1 which mediates the potential interaction was mapped within an area spanning the last 258 amino-acids in the C-terminus of the protein. I analysed the dTAK1 protein FASTA sequence with iLIR and found that this 258 aa-long SID contained two xLIR-type and one "*W-x-x-L*"-type motif, all situated within ANCHOR regions. The PSSM score of the "*W-x-x-L*"-type motif was below 10 (value of 3) and as such, was excluded from further analysis. The PSSM scores of the remaining two xLIRs were within, and above the cut-off threshold range (values of 11 and 20) (Figure 5.1).

The Y2H results, combined with the confident predictions by iLIR, strongly argued in favour of dTAK1 interacting with Atg8a in a LIR-dependent manner. Therefore, I began this project having two promising xLIR candidates to test for their ability to mediate interaction of dTAK1 with Atg8a.

All Y2H screen results were processed through iLIR and assembled into a figure and table, depicting the identified Atg8a-interacting proteins along with information on the predicted LIR motifs of each protein that overlap with its SID region mapped by Y2H (Appendix Figure 9.1 and Appendix Table 9.1).

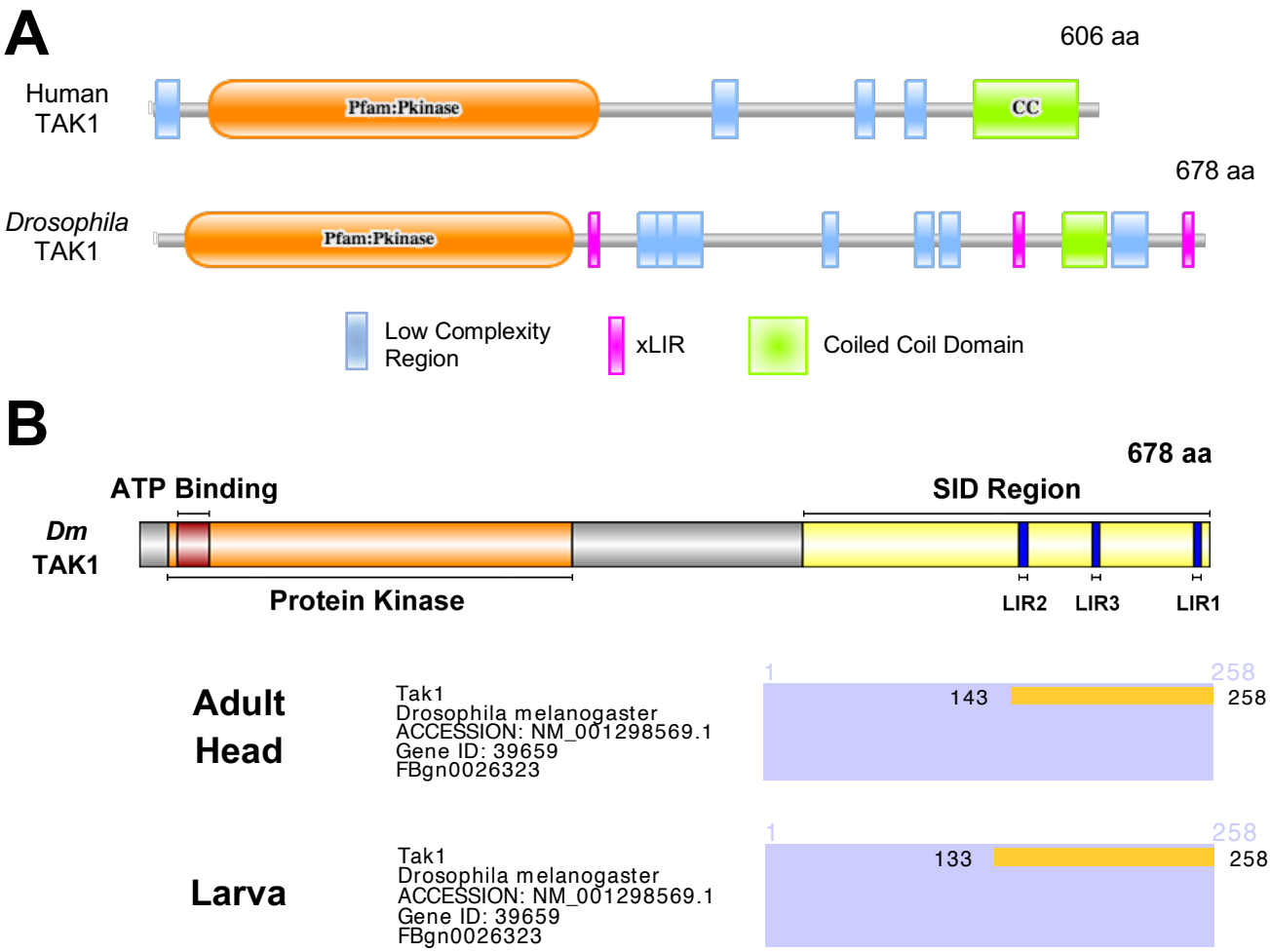

Motif Name	Motif Type	Start	End	Pattern	PSSM Score	LIR in ANCHOR
LIR2	xLIR	557	562	KEYLSV	11	Yes
LIR3	WxxL	603	608	SLYNNL	3	Yes
LIR1	xLIR	667	672	EGWVVI	20	Yes

Figure 5.1. ***Human and Drosophila TAK1 Comparison, LIR Motif Predictions and Y2H Results.*** (**A**) Conserved domain structure between the human and fly TAK1. Protein domain art generated by iLIR (http://repeat.biol.ucy.ac.cy/iLIR/), which also predicted LIR motifs in the respective FASTA sequences. No xLIR motifs were identified on human TAK1. (**B**) Combined *Drosophila* TAK1 (*Dm* TAK1) domain schematic with Y2H result. generated by SID refers to the region where binding of Atg8a was mapped, according to Y2H screen. Middle panel depicts a snippet of the Y2H adult head and 3rd instar larva libraries where dTAK1 was returned as a positive Atg8a-interactor. The lengths shown correspond to the truncated dTAK1 isoform B (258 aa), automatically identified by the screen. Bottom panel shows the details of those LIR motifs predicted by the iLIR software, that fall within the SID region. Motif naming is researcher-generated and was given according to PSSM scores from highest to lowest-scoring.

5.2 *dTAK1 & dTAB2 Independently Bind Atg8a in-vitro*

The dTAK1 co-activator, dTAB2 possesses several LIR motifs located in ANCHOR regions and at least one xLIR-type peptide, according to iLIR. The protein did not come up as an Atg8a-interactor in either of the Y2H libraries, however it was a positive hit for the xLIR/UBD-containing list of Ref(2)P-like proteins created previously in the lab of I. Nezis [340]. Due to the protein also being an essential component of the dTAB2/dTAK1 initiator kinase complex for IMD signalling [295], [297], I altogether opted to include dTAB2 in my investigation.

The first step was to test dTAB2 and dTAK1 independently for their ability to interact with Atg8a as assessed by *in-vitro* GST pulldown assays. For this purpose, I first created recombinant plasmid vectors that contained the coding sequence of the protein of interest, preceded by an N-terminal tag. For the prey proteins (dTAK1 and dTAB2 in this case) the tag was 6xHis, while for the bait proteins this was GST. I used two different isoforms of Atg8a baits, one being WT, and the other a K48A/Y49A LDS mutant (hereafter referred to as "Atg8a LDS") which has been rendered unable to bind LIR motifs. Both Atg8a recombinant proteins have been previously created by the I. Nezis group and maintained in their stocks. A vector containing the GST-tag sequence alone was also used as a control to monitor whether GST affects the binding between prey and bait.

5.2.1 dTAK1 interacts with Atg8a *in-vitro* via a LIR motif

For dTAK1, I tested the two candidate xLIR motifs which lie within the SID region identified by the Y2H screening. These xLIR motifs are at positions 557-562 (LIR2; PSSM score 11; peptide sequence: K E Y L S V) and 667-672 (LIR1; PSSM score 20; peptide sequence: E G W V V I). Naming of the LIR motifs is in descending order according to their respective PSSM score. For each of these two LIR motifs, I created a mutant isoform of dTAK1 carrying amino-acid substitutions at positions 3 and 6 of each LIR peptide sequence, that otherwise code for the acidic and hydrophobic amino-acids respectively, and mediate binding to the HP1 and HP2 pockets of the LDS crevice on Atg8a respectively [185]. These amino-acids were substituted with the neutral amino-acid alanine (A). In particular, the mutations were Y559A/V562A for LIR2 (resulting in KE**Y**LS**V** → KE**A**LS**A**) and W669A/I672A for LIR1 (resulting in EGWVVI → EG**A**VV**A**). The denominations

"dTAK1 LIR2" and "dTAK1 LIR1" are used hereafter to refer to the respective LIR mutant isoforms of dTAK1 created in the aforementioned manner, while "dTAK1 WT" describes the unmutated normal construct.

By co-incubating the prey and bait proteins in the appropriate combinations, I was able to identify that dTAK1^{WT} co-purified with Atg8a^{WT}, but not Atg8a^{LDS} (Figure 5.2 A/B). It should be noted for Figure 5.2B that there was a lower enrichment of GST:Atg8a^{LDS} bait compared to GST:Atg8a^{WT}, which may have at least partially affected the affinity of dTAK1 for Atg8a (Figure 5.2B). Nevertheless, both Atg8a baits are enriched in a directly comparable manner in Figure 5.2A and still dTAK1^{WT} did not co-precipitate with Atg8a^{LDS}, but did with Atg8a^{WT} (Figure 5.2A). This suggests an LDS/LIR-mode of interaction between the two proteins. Furthermore, similar pulldown assays revealed that the dTAK1^{LIR2} isoform was still able to bind Atg8a^{WT} without any noticeable reduction in affinity compared to dTAK1^{WT} (Figure 5.2B), while the dTAK1^{LIR1} mutant was in turn, greatly impaired in interacting with Atg8a^{WT}, with only a detectable trace signal relative to dTAK1^{WT} (Figure 5.2A). Moreover, neither dTAK1^{LIR} mutant was able to sufficiently co-purify with GST:Atg8a^{LDS} (Figure 5.2), serving as a complementary observation, corroborating the LDS/LIR-dependency of the dTAK1-Atg8a interaction.

Taken together, these results indicate that dTAK1 directly binds Atg8a *in-vitro*. The interaction is specific between the two proteins, as no His-signal is detected in the GST-only samples, indicating that the GST-tag does not influence their binding. Moreover, the association between dTAK1 and Atg8a is dependent on an LDS/LIR-manner of interaction, and have proceeded to characterize the functional motif on dTAK1 being LIR1 (667-E G W V V I-672), as the one responsible for tethering dTAK1 to Atg8a.

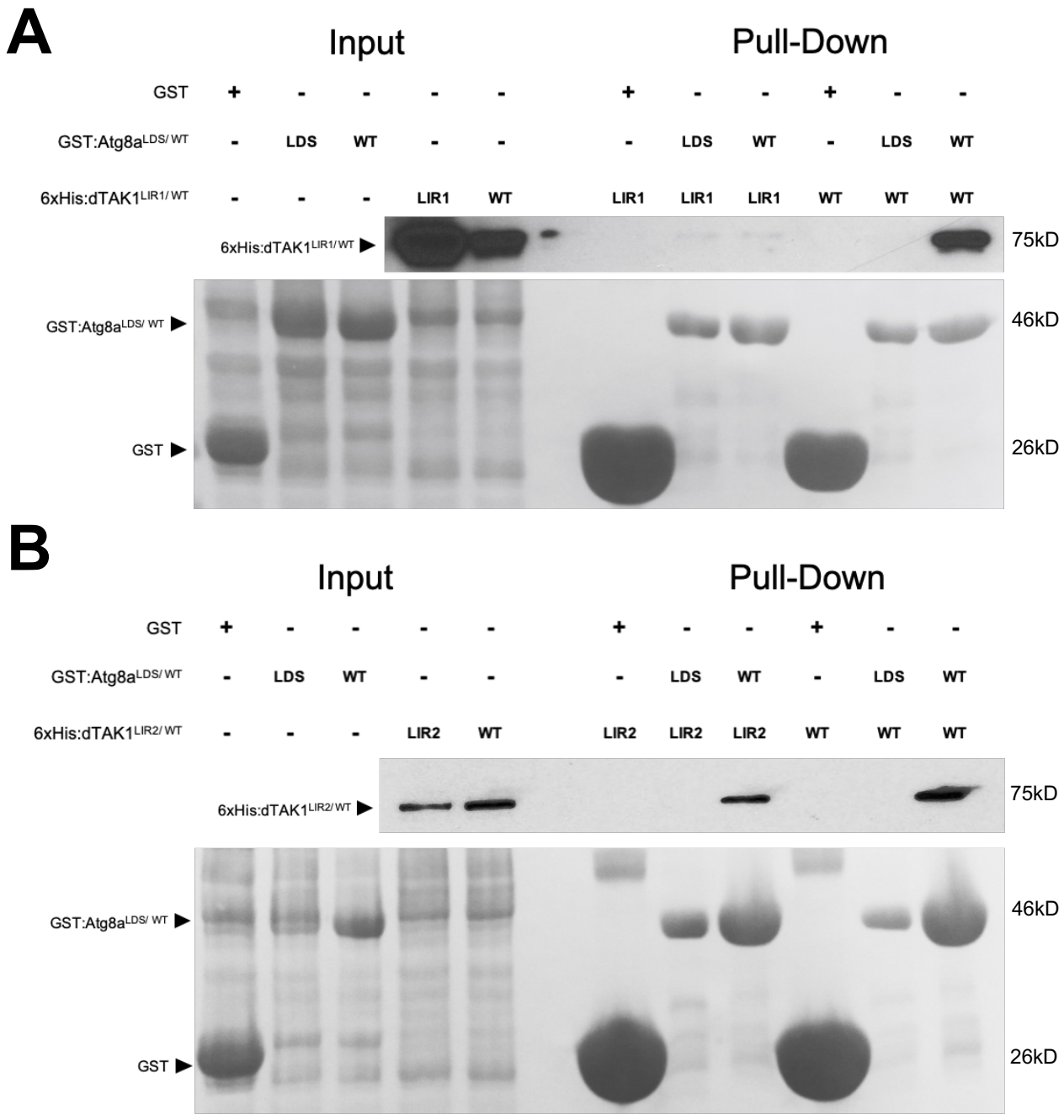

Figure 5.2. ***dTAK1 Interacts Directly with Atg8a in a LIR-Dependent Manner****.* GST Pulldown assays to compare binding affinities of (**A**) dTAK1^{WT} vs. dTAK1$^{W669A/I672A}$ (dTAK1 LIR1), and (**B**) dTAK1^{WT} vs. dTAK1$^{Y559A/V562A}$ (dTAK1 LIR2), each for Atg8a$^{LDS/WT}$. Atg8a used as GST-fused bait and dTAK1 as 6xHis-labelled prey respectively. Bait and prey samples were co-incubated in the combinations shown above each gel image, with LIR1, LIR2 and LDS referring to the presence of the inactive mutant isoform for each protein, while WT indicates presence of the normal protein. Further presence, or absence of proteins in the sample is indicated by (+), or (-) respectively. 6xHis-proteins detected by anti-6xHis antibody, while GST-proteins visualized by Ponceau S total protein stain.

5.2.2 dTAB2 is an Atg8a-interacting protein

As mentioned, the co-activator of dTAK1, dTAB2, had been a positive hit in the xLIR- and UBD-containing list of Ref(2)P-like proteins [340], that was constructed prior to the Y2H screen. Analysis of the sequence by iLIR, revealed a total of 6 candidate LIR motifs, all located within ANCHOR regions of the protein, according to the software. Since I could not omit motifs based on their presence or not in ANCHOR regions, I opted instead for a trade-off balance between high enough PSSM scores (≥ 10) and motif-type. By employing this combinatorial approach, I was able to rule out of the study 3 out of 6 LIR motifs, due to them being "W-x-x-L"-type motifs with PSSM scores below the accepted cut-off threshold (<10). Of the remaining 3 candidates, one was an xLIR-type motif with PSSM score of 10, while the other two were of the "*W-x-x-L*" pattern with PSSM scores of 11 and 12. However, the "*W-x-x-L*"-type motif with a PSSM value of 11, although scoring above the accepted threshold, presented with Tyr (Y) at the HP1 "W" position of the "*W-x-x-L*" core. Tyrosine is not considered a very conserved amino-acid for this position, compared to the much more frequently encountered Trp (W) or Phe (F), with very few experimentally-verified functional LIR motifs known where the HP1 site is occupied by Y [185]. Because of this discrepancy, I opted to exclude this motif from the present study, despite its satisfactory PSSM score. As such, I was finally left with two candidate LIR motifs to test on dTAB2: one xLIR-type motif at position 370-375 (LIR2; PSSM score 10; peptide sequence K S F T S L), and one "*W-x-x-L*"-type motif at position 337-342 (LIR1; PSSM score 12; peptide sequence R D F R S I). The 2D domain architecture of dTAB2 along with the relevant details for the LIR motifs selected to test in this study, is shown in Figure 5.3.

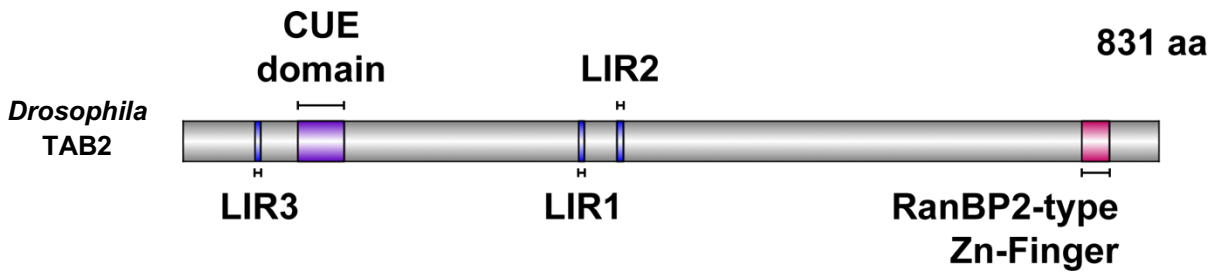

Motif Name	Motif Type	Start	End	Pattern	PSSM Score	LIR in ANCHOR
LIR3	WxxL	62	67	GSYEQL	11	Yes
LIR1	WxxL	337	342	RDFRSI	12	Yes
LIR2	xLIR	370	375	KSFTSL	10	Yes

Figure 5.3. ***2D Domain Architecture of Drosophila TAB2 with Selected LIR Motifs***. The positions of the candidate LIR motifs predicted by the iLIR software with PSSM score ≥ 10 are depicted on the schematic, with their details shown in the accompanying table. Motif naming is researcher-based, according to their PSSM score from highest to lowest. LIR3 was excluded from the investigation due to poor conservation of key residue at position 64. Abbreviations in figure: CUE (**C**oupling of **U**biquitin Conjugation to **E**ndoplasmic Reticulum Degradation); RanBP2 (**Ra**s-related **N**uclear Protein-**B**inding **P**rotein **2**).

Similarly to dTAK1, I employed GST-pulldown assays to test the potential association between dTAB2 and Atg8a, using dTAB2 as prey, as well as whether this was dependent on an LDS/LIR-mode of interaction. For this purpose, I additionally created LIR-mutant isoforms for both motifs, each carrying double amino-acid substitutions for the aromatic and hydrophobic residues at positions 3 and 6 respectively, which were changed to Ala. Specifically, the mutations were F372A/L375A (resulting in KS**F**TS**L** → KS**A**TS**A**) for LIR2, and F339A/I342A (resulting in RD**F**RS**I** → RD**A**RS**A**) for LIR1. The denominations "dTAB2 LIR1" and "dTAB2 LIR2" and "dTAB2 WT" are hereafter used to describe the inactive LIR motif isoforms and wild-type dTAB2 respectively.

I then proceeded to individually co-incubate each of the LIR-mutant and WT preys, in various combinations with the GST-baits in pulldown assays. Following this method, I observed that 6xHis:dTAB2^{WT} (shown as "His:Tab2" in Figure 5.4) co-precipitated with GST:Atg8a^{WT}, and to a lesser extent with GST:Atg8a^{LDS} as well (Figure 5.4A). This interaction was specific between the two proteins, as no His-signal was detected in the GST-only lane, meaning that the GST-tag does not influence the interaction. The reduced binding of dTAB2^{WT} to GST:Atg8a^{LDS}, is attributed to the poorer enrichment of the Atg8a^{LDS} bait

compared to $Atg8^{WT}$, rather than a potential lower affinity of dTAB2 for the Atg8a LDS-mutant. This was corroborated during multiple repeats of this experiment, where the affinity of $dTAB2^{WT}$ for GST:$Atg8a^{LDS}$ fluctuated more than what would normally be expected for LDS/LIR-dependent interactions, and mirrored in the densitometric analysis of these results, where affinity of $dTAB2^{WT}$ for $Atg8a^{LDS}$ was not found to markedly differ compared to $Atg8a^{WT}$ (Figure 5.4B). Finally, neither $dTAB2^{LIR1}$, nor $dTAB2^{LIR2}$ were found to be impaired in their ability to bind $Atg8a^{WT}$ (Figure 5.4A), with their affinities for Atg8a being very similar to that of $dTAB2^{WT}$ (Figure 5.4).

Taking the above into consideration, dTAB2 is indeed a novel Atg8a-interacting protein and capable of associating directly with Atg8a *in-vitro*. Moreover, both the LIR1 and LIR2 motifs tested here seem to be dispensable for the binding of dTAB2 to Atg8a.

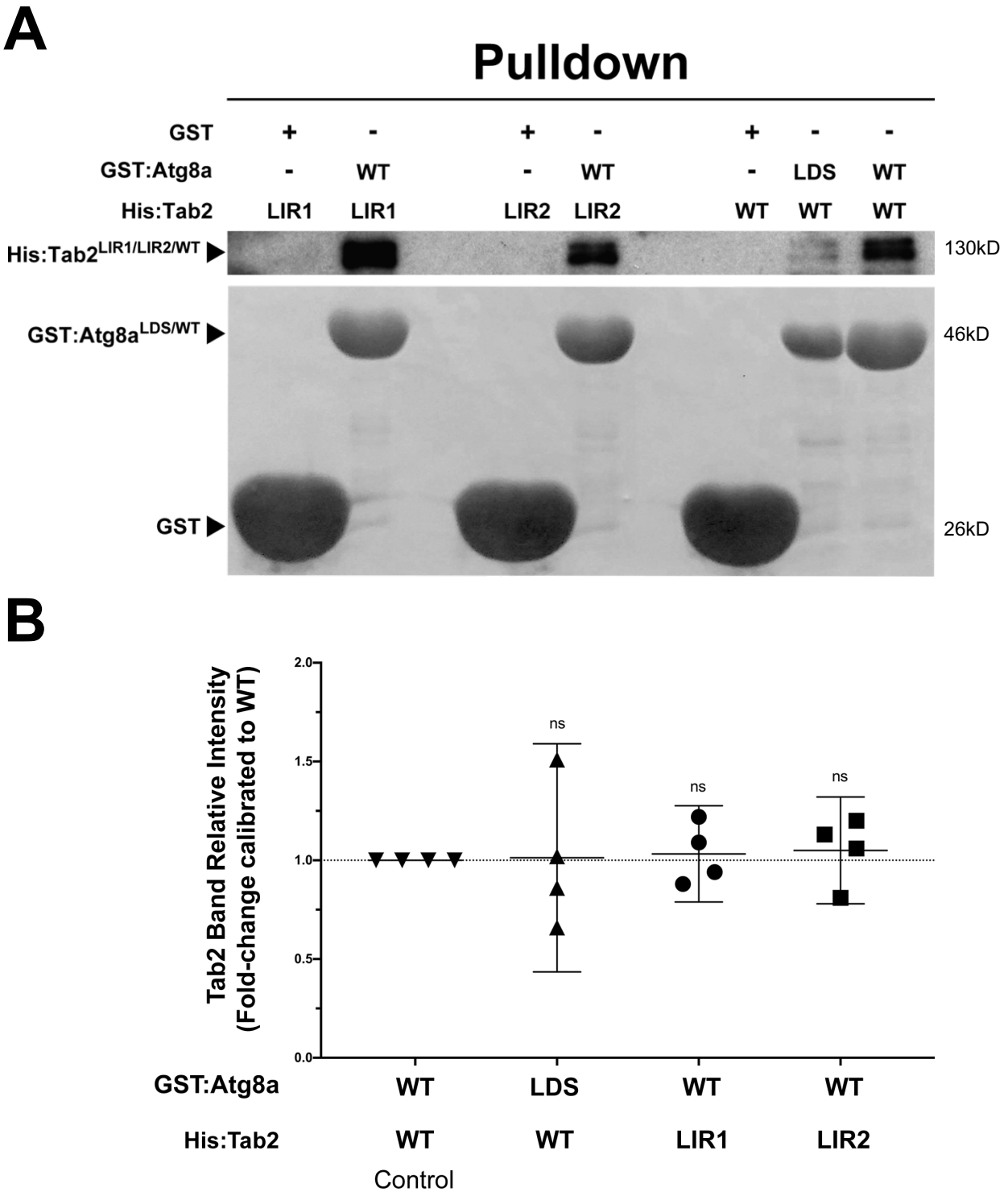

Figure 5.4. ***dTAB2 Binds Directly to Atg8a***. (**A**) GST-Pulldown between dTAB2 and Atg8a. Atg8a and dTAB2 were used as the bait and prey proteins respectively, and co-incubated in the combinations shown above each gel image. LIR1, LIR2 and LDS refer to the presence of the inactive mutant isoform for each protein, while WT indicates presence of the normal protein. Further presence, or absence of proteins is indicated by (+), or (-) respectively. (**B**) Comparative quantification plot for the binding affinity of each dTAB2 isoform for Atg8a. All dTAB2 band intensity values were calibrated to the $dTAB2^{WT}$/$GST:Atg8a^{WT}$ lane (control). Data shown as individual values with mean $\pm$ 95% C.I (n = 4 independent GST pulldown experiments; ns = not significant, $p > 0.05$; one sample t-test).

5.3 *The Functionality of the dTAK1 LIR1 Motif In-Vivo*

5.3.1 Generation of transgenic *FLAG:Tak1 WT/ LIR1 flies*

The discovery of the LDS/LIR-dependent interaction between dTAK1 and Atg8a, coupled to the characterization of the functional LIR motif for promoting the binding *in-vitro*, called for investigating whether this functionality is retained *in-vivo*. For this purpose, in collaboration with the transgenic model services provided by BestGene Inc., we opted to create fly strains, carrying a 3xFLAG-labelled *Tak1* construct under the influence of the inducible *UAS* promoter. Generation of these transgenic fly lines took advantage of the *attB/P* site-specific recombination facilitated by the integrase of the *Streptomyces* phage phi(φ)C31, which is a versatile genetic toolset for targeted genome modifications in *Drosophila* [349]. The system utilizes the unidirectional sequence exchange between an *attB*-donor vector, and an *attP* site-containing recipient, in the presence of the integrase φC31 [349]. The recipient stock is pre-constructed with *attP* landing sites via genetic modification, as the *attB*-donor/*attP*-recipient combination results in higher integration rates in the genome than the alternative [349].

I proceeded to create the recombinant *3xFLAG:Tak1*$^{WT/LIR1}$ plasmids, which would be used by BestGene Inc. as the donors in a series of microinjections to *attP*-containing larvae. I selected an empty p*UASTattB* vector, which apart from the *attB* site, also carries a 5x repeat of the *UAS* promoter, as well as the *white*$^{+mC}$ selectable marker, among other useful sites [350]. I followed a three-step approach in generating the p*UASTattB*/*3xFLAG:Tak1*^{WT} and p*UASTattB*/*3xFLAG:Tak1*^{LIR1} constructs. First, I made the recombinant p*UASTattB*/*3xFLAG* vector following conventional restriction enzyme-based cloning. In the same vein, I also inserted the coding sequence of *Tak1*^{WT} to the newly recombined vector, so that its expression would result in a translated construct with an N-terminal-appended 3xFLAG-tag. Finally, I used a successfully recombined *3xFLAG:Tak1*^{WT} vector, which had been validated for the correct orientation and reading frame of the entire construct and free from any random point mutations in the sequence, to generate the W669A/I672A LIR1 mutant, employing a routine mutagenesis protocol (as described in Materials & Methods section 4.9.1). The p*UASTattB*/*3xFLAG:Tak1*$^{WT/LIR1}$ vectors were subsequently purified in sufficient quantity and shipped to BestGene Inc., who performed the larvae microinjections. We ensured the selected *attP*-target site (*attP40* here)

was the same for both fly lines that would be created in this manner, so that both transgenes would be expressed at similar levels to allow for comparisons to be drawn. The created transgenic *UAS-3xFLAG:Tak1*$^{WT/LIR1}$ fly lines are both maintained in the I. Nezis lab.

5.3.2 The LIR1 motif on dTAK1 facilitates binding to Atg8a *in-vivo*

The lab group of I. Nezis has previously created (A.C Jacomin) and maintains a stock of "FLPout-mCherry:Atg8a" flies (see Materials & Methods Section 4.3.1 "The FLP-out system"; referred to hereafter as "mCherry:Atg8a"), that constitutively express mCherry-tagged Atg8a in subsets of cells across different tissues. The system can in addition, be subjected to varying periods of heat-shock which increase the rates of transgene expression, depending on the heat-shock length, however it also increases the risk of introducing artefact expression patterns as well as resulting in lethality due to construct over-expression. Under normal conditions, roughly 10% of somatic cells express the transgene, which is sufficient for most confocal investigations the I. Nezis research group focuses on. Therefore, as a cautionary rule, no heat-shock is applied to crosses with mCherry:Atg8a, unless a there is a need for a particularly weak strain. I used male flies from each of the newly created *UAS-3xFLAG:Tak1*^{WT} and *UAS-3xFLAG:Tak1*^{LIR1} lines (referred to hereafter as FLAG:dTAK1$^{WT/LIR1}$ respectively), to cross to virgin female mCherry:Atg8a flies, which would enable co-expression of the two proteins in double-transgenic clonal cells of the F1 progeny (Figure 5.5), and therefore allowing me to evaluate co-localization events between dTAK1 and Atg8a following upregulation of autophagy. After performing successful crosses and obtaining viable progeny, I selected double transgenic 3rd instar larvae which were still in the feeding stage, so as to avoid induction of developmental autophagy, which occurs in larvae entering their pre-pupal wandering stage and presents with slightly different features than regular autophagy, more akin to developmental cell death (I.Nezis [203] and personal communication). I subjected larvae to amino-acid deprivation by incubating them in tubes containing 20% sucrose solution (made in water), for 4 hours at 25 ^{o}C, so as to induce upregulation of autophagy [114]. The benefit of 20% sucrose instead of just water is that it allows larvae to float on the surface so they do not drown and suffocate during the incubation period [351]. Autophagy induction was visualized by punctate formations of mCherry:Atg8a^{+ve} autophagosomes. After the 4hr mark, I dissected and fixed the fat bodies

in preparation of the tissue for confocal microscopy, while also staining with an anti-FLAG Ab to visualize dTAK1.

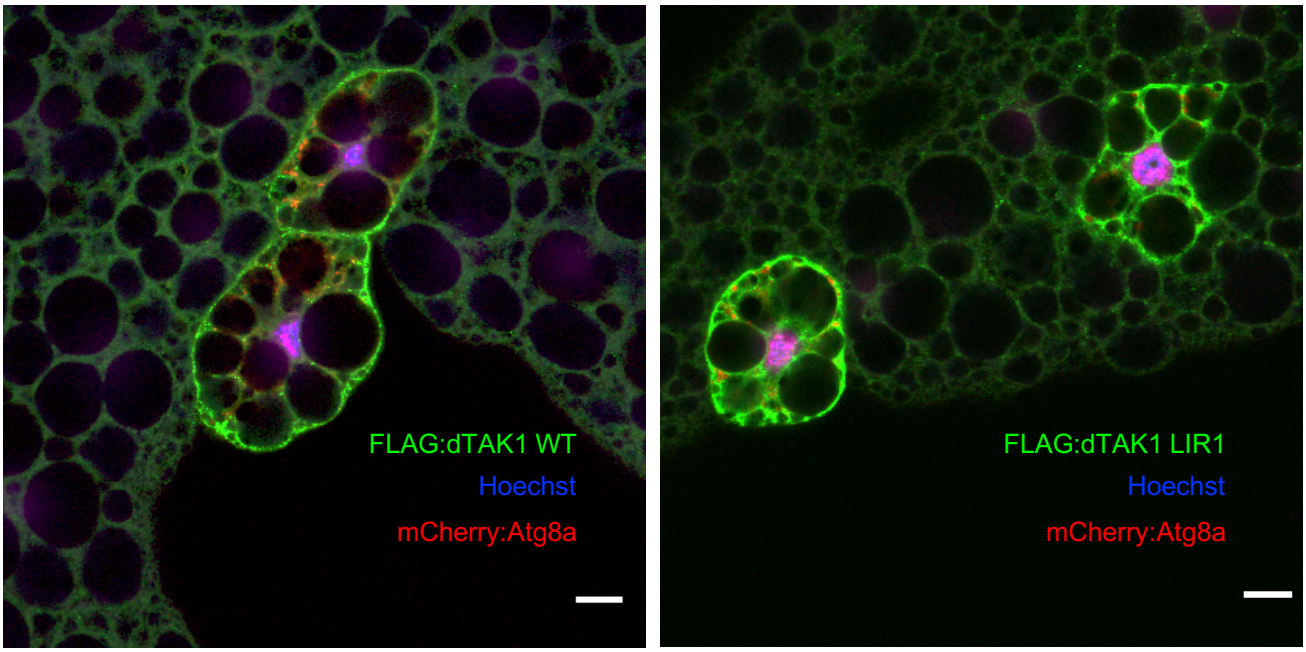

Figure 5.5. ***Mosaic Expression of Double-Transgenic Fat Body Clones.*** Images depicting characteristic examples of fat body clones that co-express mCherry-Atg8a (red) and either the FLAG:dTAK1^{WT} (green; left) or FLAG:dTAK1^{LIR1} (green; right) construct, among neighbouring non-recombinant cells which serve as control of the transgenes' expression. The Hoechst dye (blue) is used to stain and visualize nuclei. Scale bar: 10 μm

Upregulation of autophagy was evident in double-transgenic clones as distinct red puncta for both dTAK1^{WT} and dTAK1^{LIR1} conditions. The distributions of FLAG:dTAK1^{WT} and FLAG:dTAK1^{LIR1} were much more diffuse across the cytoplasm yet still easily distinguishable despite background fluorescence and non-specific staining, as seen in neighbouring control cells (Figure 5.6). Signal overlap between the FLAG:dTAK1 and mCherry:Atg8a channels was more frequently observed for dTAK1^{WT} than dTAK1^{LIR1}, regardless of the relative expression levels of the two proteins (Figure 5.6). To corroborate this observation, co-occurrence events were measured by Pearson's corelation efficient (PCC), while statistical comparison was carried out by two-tailed unpaired t-test with equal variances (Figure 5.6). PCC was preferred in this case, instead of the more commonly used Mander's coefficient due to limitations when observing whole tissues. Mander's coefficient relies on signal strength over area when calculating overlap and is consequently highly

susceptible to background noise. While in single-layer cell cultures this can be easily corrected for and maintained with consistency, it is not as feasible when imaging multi-layer tissue samples, such as *Drosophila* fat bodies. During such sessions, the parameters of the imaging system, such as laser output and photomultiplier settings need to be constantly adjusted to account for change in tissue thickness, orientation and natural variation of protein expression. PCC is much more robust and focuses on signal overlap in terms of area, which is less sensitive to changes in acquisition settings. Nevertheless, to minimise artificial inflation or misrepresentation of PCC values, I performed two background elimination steps, prior to calculating PCC. First, all images were post-processed in Fiji (ImageJ) by subtracting noise signal using a 50-point "rolling ball" setting. Furthermore, I used a semi-automated method for selecting only punctate mCherry:Atg8a^{+ve} regions representing autophagosomes in each image, developed previously by A.C Jacomin [352]. The FLAG and mCherry signal overlap was subsequently calculated only within these regions of interest i.e autophagosomes, and not across the entire cell section. These two corrections allowed for the final PCC values to more faithfully represent the true overlap of the FLAG and mCherry signals. After calculating the PCC value for each condition following the above method, and performing statistical analysis of the data it was corroborated that upon autophagy induction, FLAG:dTAK1^{WT} is encountered more frequently within the vicinity of mCherry:Atg8a autophagosomes compared to FLAG:dTAK1^{LIR1}, with the observed difference assessed as statistically significant (Figure 5.6).

While it is not possible to evaluate by this experiment whether the two proteins truly co-localize by direct interaction, given the physical limitations of light microscopy on the resolution of captured images, it nevertheless suggests that the LIR1 motif on dTAK1 does facilitate to a degree the association between dTAK1 with Atg8a *in-vivo*. Taking its requirement for the efficient binding of dTAK1 to Atg8a already observed *in-vitro*, collectively these results highlight that the dTAK1 LIR1 motif retains some of its functional relevance also *in-vivo*.

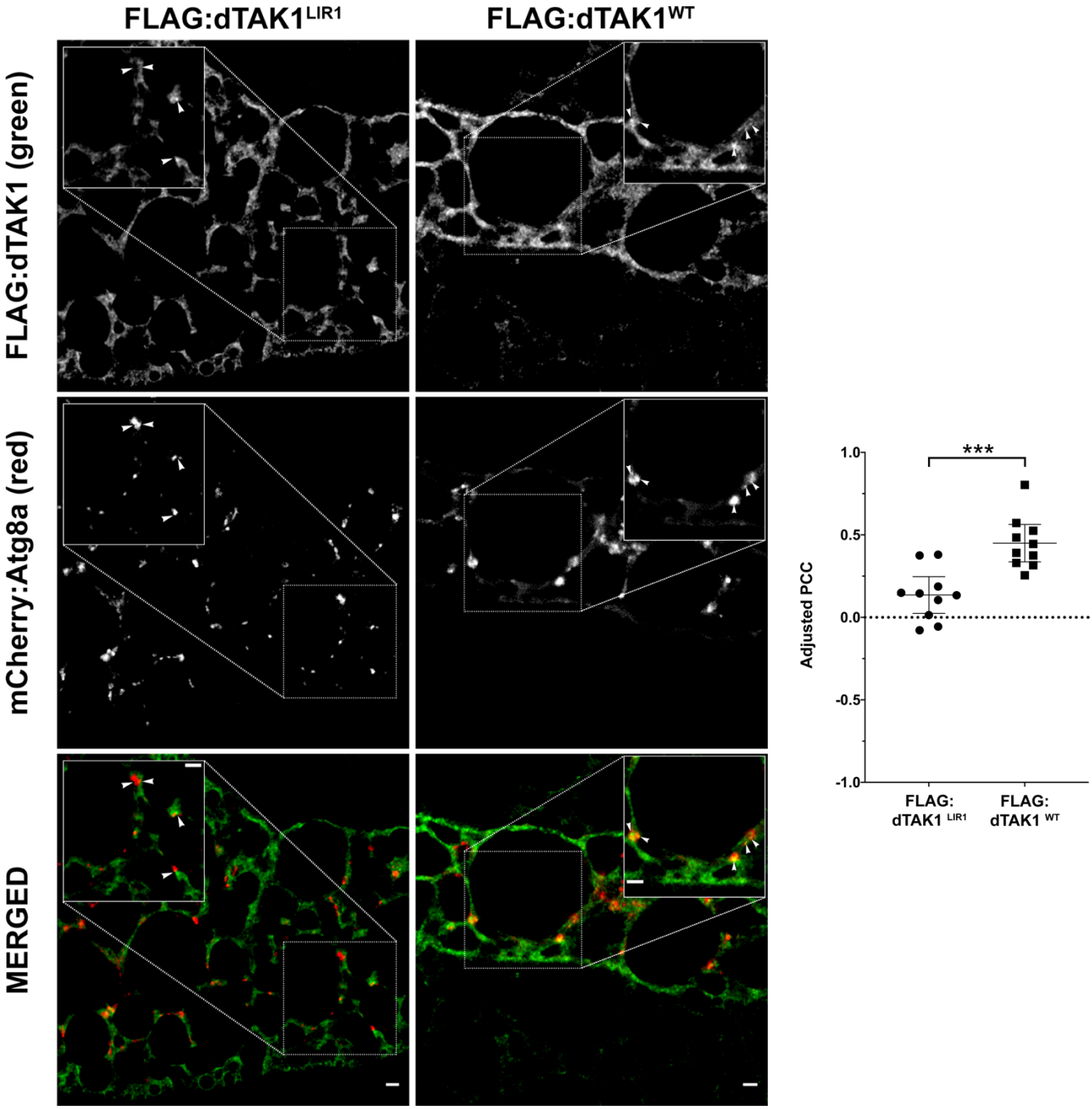

Figure 5.6. ***The EGWVVI LIR Motif Facilitates Association of dTAK1 with Atg8a In-Vivo, Following Autophagy Induction***. ***(A)*** Representative images of double-transgenic *Drosophila* larvae fat body cells, co-expressing FLAG:dTAK1 (either WT, or LIR1 mutant) and mCherry:Atg8a. Punctate regions in the mCherry:Atg8a channel, represent autophagosomes. The snippet image on each channel depicts a representative area of the sample and the arrowheads within, point to autophagosomes with FLAG:dTAK1 also in proximity. Regions of overlap as well as mutual exclusion were encountered in both conditions, however overlap was more frequent in dTAK1^{WT} samples. Scale bar for widefield images and snippets, 5 μm (**B**) Colocalization between Atg8a and dTAK1 within autophagosome regions, assessed by Pearson's correlation coefficient (PCC). Data shown as individual values with mean ± 95% C.I (n = 10; n represents the number of confocal images analyzed from independent samples for each condition, obtaining an average correlation coefficient R value for each image; ***, $p < 0.001$, unpaired t-test with equal variances).

Chapter Conclusions

In our effort to delineate how selective autophagy can participate in the regulation of other cellular pathways, we search for proteins that fulfil the criteria to be considered candidate SARs. For this purpose I.Nezis group has previously constructed a list of UBD- and xLIR-containing proteins, using as structural reference the domain architecture of the *Drosophila* SAR, Ref(2)P [340]. In addition, it has developed the iLIR software for predicting LIR motifs on proteins [339], based solely on *in-silico* sequence analysis, and finally has conducted a high-throughput Y2H screening against *Drosophila* libraries, with the purpose of identifying novel Atg8a-interacting proteins.

By utilizing these available resources, I was able to identify that both components of the IMD initiator kinase complex, dTAK1 and dTAB2, were candidate Atg8a-interacting proteins, with several predicted LIR motifs nested in their sequence. While dTAK1 was identified as an Atg8a-interactor by the Y2H screen, dTAB2 was among the predicted Atg8a-interactors of the previously composed list of UBD/xLIR-containing proteins [340]. This serves as an appropriate example showcasing how high-throughput computer-based and lab-based analyses best serve researchers' interests when utilized in a complementary manner

Following a methodical approach in selecting candidate LIR motifs on dTAK1 and dTAB2 to test experimentally, I employed GST-Pulldown assays to assess each protein's ability to bind Atg8a, and whether it does so in a LIR-dependent fashion. By generating inactive LIR mutant isoforms for each protein and also using an LDS-mutant Atg8a bait, I was able to show here that dTAK1, as well as dTAB2 are capable of interacting directly with Atg8a *in-vitro* (Figures 5.2 and 5.4). In addition for dTAK1, its association with Atg8a is dependent on a LIR motif, which docks to the LDS site of Atg8a. Based on the LIR motifs tested, this interaction is mediated by the 667-EGWVVI-672 LIR motif of dTAK1, which is required for efficient binding of the kinase to Atg8a (Figure 5.2A). Moreover, by creating transgenic flies for dTAK1^{WT} and dTAK1^{LIR1}, I was able to assert that the LIR1 motif retains some of its functionality in mediating association of dTAK1 with Atg8a *in-vivo* (Figure 5.6). The apparent reduction in requirement of the LIR motif for dTAK1 to dock Atg8a within cells as opposed to an *in-vitro* system is expected, since other trafficking and adaptor proteins, such as Ref(2)P can aid in targeting autophagy substrates to autophagosomes. *Drosophila* TAB2 is also a novel Atg8a-interacting protein, that directly binds the autophagy adaptor *in-vitro*, and based on current observation does so in an LDS/LIR-independent manner (Figure 5.4). Collectively, these results aided in establishing dTAK1 and dTAB2 as novel Atg8a-interacting proteins.

Chapter 6

Selective Autophagy Degrades the dTAK1/dTAB2 Complex

Chapter Introduction: **IMD regulation and implications on physiology**

Chapter 5 focused at the molecular level, identifying that both components of the dTAK1/dTAB2 complex are capable of interacting with Atg8a. Moreover, it characterized the nature of the interaction for each component, which for dTAK1 was found to rely on its functional EGWVVI LIR motif, while dTAB2 anchored Atg8a in a LIR-independent fashion. Irrespective of how each of these two IMD signalling components bind Atg8a, these findings provided compelling evidence that autophagy is involved in the regulation of the IMD pathway at the initiator kinase level. As a logical extension of these observations, the aim for the set of results presented in this chapter, is to interpret the meaning of these Atg8a interactions in terms of their physiological implication at a whole-organism level. Since aberrant innate immune signalling is intricately connected with the progressively debilitating effects of ageing [10], [11], my approach here is to attempt and identify themes linked by chronicity. As such, in the following sections I will present my findings regarding how endogenous levels of dTAB2 and dTAK1 behave when autophagy is genetically and chronically impaired, as well as my observations on the degree that selective autophagy is involved in the regulation of the IMD pathway from the perspective of dTAK1, particularly when its LIR motif is rendered inactive.

6.1 *Creation of Antibodies For Endogenous dTAB2 & dTAK1*

To characterize the degree of autophagy's involvement in the regulation the IMD pathway at the tier of the dTAK1/dTAB2 complex, it was important to be able to monitor endogenous levels of these two components and how these may fluctuate under defective autophagy conditions. At the start of this work there were no commercially available antibodies specifically against either dTAK1 or dTAB2. Of the available ones, these were predominantly raised against the mammalian orthologues and were not predicted to work with the *Drosophila* proteins (personal communication with suppliers). Our concerns were corroborated when we opted to test one such mammalian TAK1 antibody (Abcam, ab196955), that was raised against an epitope within a conserved region between the *Drosophila* and mammalian protein (details on the specific position of the epitope are proprietary to the supplier and were not disclosed in our communication). The antibody could not detect the *Drosophila* protein in WB application using whole-fly lysates from wild-type and dTAK1-overexpressing flies. Similarly, the issue of non-detection of the endogenous protein in crude fly extracts persisted, even for an anti-dTAK1 antibody specifically designed against *Drosophila* and kindly provided by Dr. Silverman. While that antibody detects dTAK1 when purified in high yields from large scale bacterial cell cultures, it is not sensitive enough to detect the endogenous levels of the kinase from fly total protein extracts (data not shown and Silverman N. personal communication).

To circumvent this setback, we opted to develop our own antibodies against endogenous dTAK1 and dTAB2, in collaboration with the companies Abcam (dTAK1 antibody), and Eurogentec (dTAB2 antibody). I prepared samples that contained the protein of interest either in total protein fly extracts (dTAK1) or purified from large scale bacterial cultures (dTAB2). These were subsequently shipped to the respective companies and used to immunize rabbit hosts with the appropriate immunogen each time.

For the dTAK1 antibody, in collaboration with Abcam we decided to raise a rabbit monoclonal IgG-type antibody (RabMAb® technology by Abcam) against a conserved epitope that encompasses the phosphorylation site of dTAK1 (Region 1-270aa of full-length dTAK1). This epitope is mutated or largely absent in several commercially available fly lines, which express inactive and truncated dTAK1 of various lengths in place of the full-length kinase. One of which, $Tak1^{2}$, produces a 53aa kinase-dead mutant that is missing this epitope region almost in its entirety and was used here as a negative control to test Ab

specificity (Figure 6.1). The final antibody would ideally be able to recognize the phosphorylated, as well as the unphosphorylated portion of endogenous dTAK1 in fly extracts.

In total I examined 9 candidate immunosera samples in WB and IF applications, following immunization of rabbit hosts by Abcam and shipment of samples to the I. Nezis lab group. I also included autophagy-deficient *Atg8a*^{KG07569} (hereafter "Atg8a" or "Atg8a^{KG}") flies alongside the WT and *Tak1*^{2} mutants, as a positive control for the potential accumulation — and therefore enrichment — of the protein when autophagy is impaired (Figure 6.1). Following this approach, together with Abcam we identified one candidate clone which is seemingly able to detect the protein in both WB and IF applications, albeit with reduced signal strength for IF (Figure 6.2). That clone was further purified by the company to produce a final rabbit monoclonal antibody against *Drosophila* Tak1. The antibody detects the total protein amount of dTAK1 and perhaps the phosphorylated form of the kinase as well in WB applications (Figure 6.1).

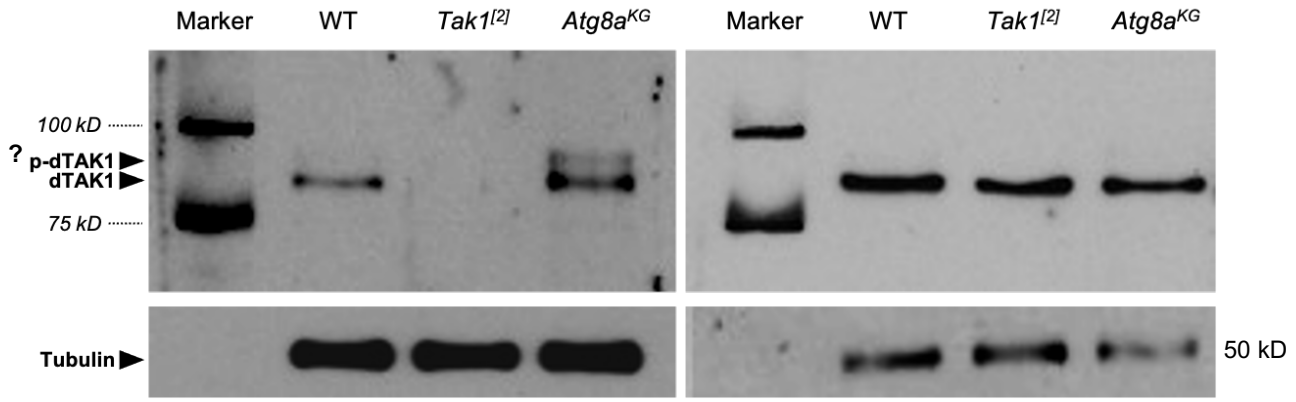

Figure 6.1. ***Testing of Candidate Anti-dTAK1 Antibody Clones in Western Blot***. Panels show representative WB images from the testing of candidate anti-dTAK1 antibodies that took place in collaboration with Abcam. Controls for antibody specificity were lysates from *Tak1* [2] flies (negative control), which encode for a 6 kD truncated and inactive kinase product, that the antibody should not be able to efficiently recognize, and from autophagy-deficient *Atg8a*^{KG07569} (*Atg8a*^{KG} in figure) flies (positive control), where dTAK1 is expected to be enriched. Left panel shows an example of a successful anti-dTAK1 clone, and right panel depicts a clone that did not meet the specificity requirements. A faint upper band can also be seen above the main dTAK1 protein, that is pronounced in the *Atg8a*^{KG} sample of the successful clone in the left panel. Perhaps that band might represent phosphorylated dTAK1 (p-dTAK1), that accumulates upon autophagy impairment. Tubulin used as loading control.

Results from the I. Nezis group suggest the antibody also works in IF (Figure 6.2) and as of submission of this work (May 2021), the corresponding research team in Abcam are performing complementary IF experiments to corroborate our observations. This dTAK1 antibody has since been made commercially available by Abcam (antibody ID: ab239353).

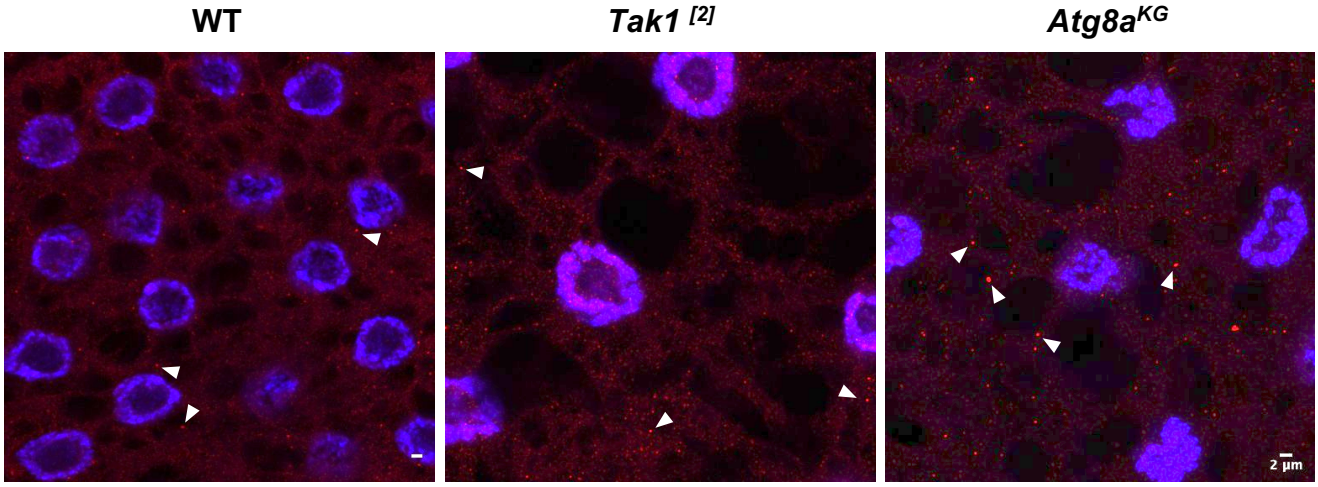

Figure 6.2. ***Anti-dTAK1 Antibody Test in Immunofluorescence Microscopy****.* IF images from working anti-dTAK1 antibody tested in IF application. Tissue is fat body from fed 3rd instar larvae. Controls for antibody specificity were tissue from *Tak1 [2]* flies (negative control), which encode for a 53aa-long inactive isoform that misses most — but not all — of the epitope region that the dTAK1 Ab was raised against. Therefore the anti-dTAK1 antibody is expected to have highly reduced to zero affinity for this 53aa-long dTAK1 mutant isoform. Fat bodies from autophagy-deficient *Atg8a*^{KG07569} (*Atg8a*^{KG}) flies were included as positive control, where dTAK1 is expected to be enriched compared to WT. Ab staining was largely excluded from the nucleus, which indicates reduced non-specific binding. Distinct bright puncta (white arrowheads) indicate dTAK1 aggregates, which were present in all conditions, but much more prominent in fat bodies of *Atg8a*^{KG} larvae. Scale bar in images: 2 µm.

For the dTAB2 antibody we opted for the Speedy 28-Day™ Program by Eurogentec S.A, that can generate rabbit polyclonal antibodies in around 1 month, according to the company. Following the company's guidelines, I prepared a high concentration sample (>1mg) of His:dTAB2 purified from bacterial cultures. This was deemed the most preferable option by the company, to start their immunization protocol with a sample enriched in the fly protein of interest, rather than a mixture of the fly proteome as obtained by crude fly extracts. I purified His:dTAB2 via affinity chromatography by passing the bacterial lysate through a Ni-NTA (**Ni**ckel-**N**itrilo**t**riacetic **A**cid) gravity flow column that binds His-tag. The bound dTAB2 protein was then eluted from the resin and a 1.5 mg of His:dTAB2-containing sample was sent to Eurogentec.

Following the creation and shipment of the final anti-dTAB2 product (Eurogentec, ZGB19056) by the company, I have tested this antibody in GST-Pulldown and WB applications (Figures 6.3 and 6.5), as of submitting this current work. For WB, I used whole-fly lysates from WT and Atg8a flies, while for the PD application test, I utilized previously stored membranes of His:dTAB2 – GST:Atg8a PD. The antibody seemingly works in both applications, however it should be noted that it produces increased background staining when the antigen source is whole-fly protein extract, compared to lysates from bacterial cultures expressing the recombinant fly protein (Figure 6.3). While observations can still be made regarding fluctuation of endogenous levels of dTAB2 in different conditions, future rounds of optimization in order to reduce background stain might be warranted.

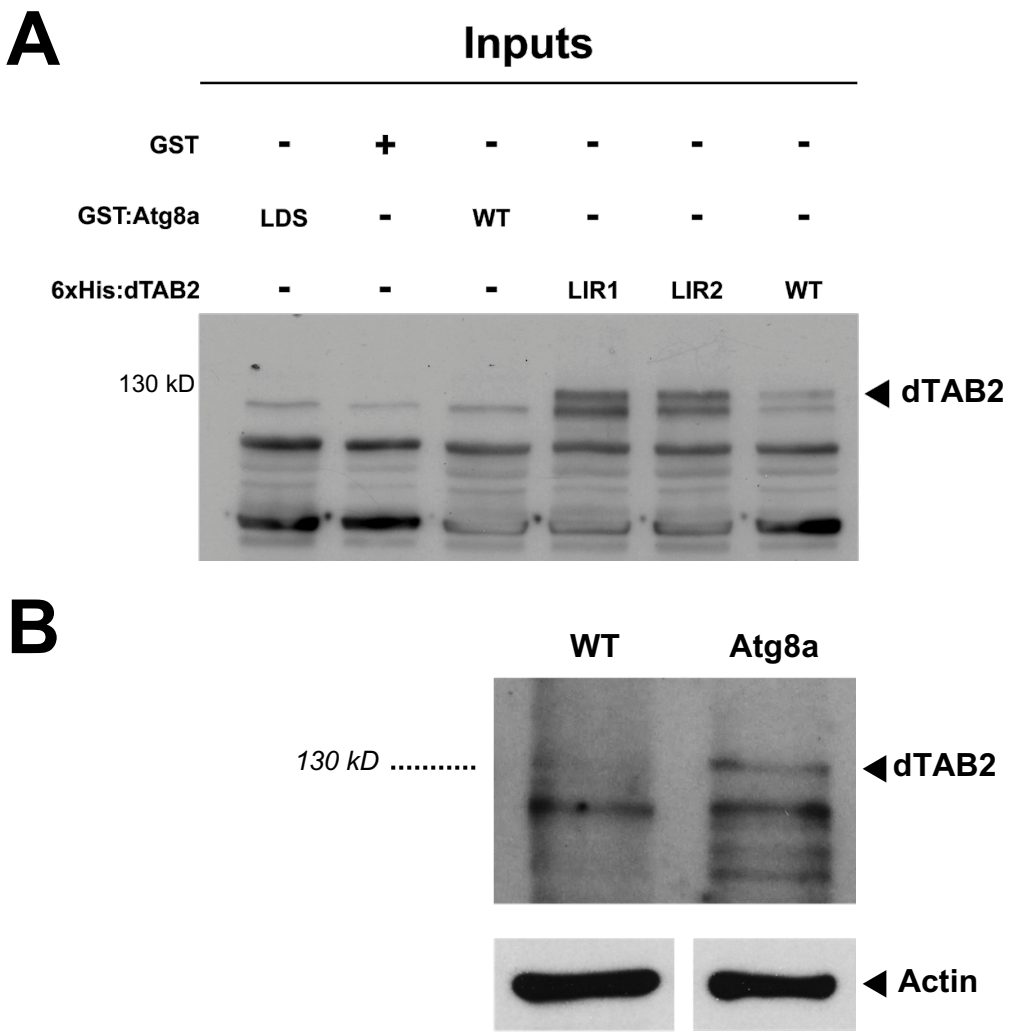

Figure 6.3. ***Anti-dTAB2 Antibody Testing in Biochemical Assays****.* Anti-dTAB2 Ab developed by Eurogentec from purified recombinant dTAB2 protein. (**A**) GST-bait and 6xHis-dTAB2 prey samples from a previous PD assay testing interaction between Atg8a and wild-type as well as dTAB2 LIR mutants (LIR1 and LIR2), loaded as inputs in new gel, and transferred on new membrane which was subsequently blotted with Eurogentec anti-dTAB2 Ab. (**B**) WB of samples made from whole-fly lysates of 3-week adult WT and autophagy-mutant ($Atg8a^{KG}$; "Atg8a" in figure) flies. Membrane was blocked and developed with Eurogentec anti-dTAB2 Ab.Actin used as loading control.

6.2 *Autophagy-Deficient Flies Accumulate dTAB2 & dTAK1*

Several key signalling components of innate immune cascades in *Drosophila*, are selectively picked up by autophagy and targeted for degradation [24], [33], [353]. In this manner autophagy acts as part of the off-switch mechanism, which keeps immune signalling under strict and controlled activation. On the other hand, impairment of autophagic flux, as is the case with progressive waning of the process during ageing, can lead to accumulation of immune signalling components and aberrant activation of these cascades [34].

Since dTAK1 and dTAB2 interact with Atg8a and having antibodies that can detect the endogenous proteins in WB, I was interested to investigate whether autophagy impairment and age play a role in the accumulation of each protein. As a note here; while *Drosophila* normal lifespan in laboratory conditions is approximately 2 months, the autophagy-impaired Atg8a mutant flies live for only about 1 month [340]. In order therefore to obtain Atg8a fly samples that more faithfully represented the whole population, I opted to select flies that were 3-week old adults, instead of selecting at the 1-month mark, where by that time only a handful of the rather more resilient flies have survived. Towards this aim, I prepared samples from conventionally reared 1-week, and 3-week adult Atg8a flies, with their respective age-matched WT used for control. I observed that dTAK1 accumulated in both young and old Atg8a flies, which was found to be significantly higher than their age-matched control groups (Figure 6.4). In a similar manner, dTAB2 levels were markedly increased only in old Atg8a flies compared to their corresponding control group (Figure 6.5).

Collectively, these results show that both dTAK1 and dTAB2 constitute substrates that are degraded by autophagy.

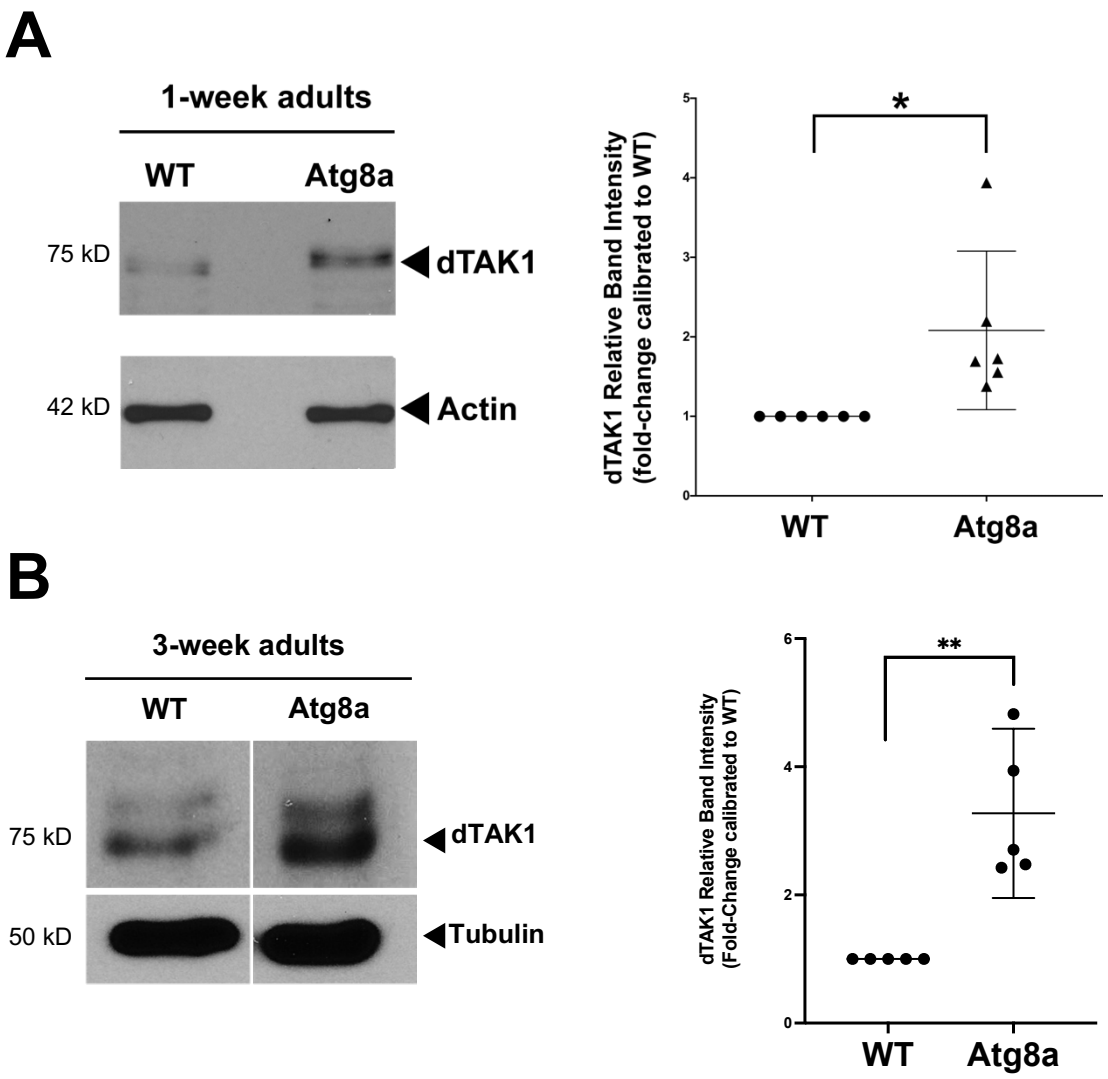

Figure 6.4. ***Chronic Accumulation of dTAK1 in Autophagy-Deficient Flies.*** Whole-fly protein extracts were obtained from conventionally reared 1-week (**A**) and 3-week (**B**) adult WT and autophagy-deficient ($Atg8a^{KG}$; "Atg8a" in figure) flies and run in WB. Staining performed for endogenous dTAK1 with actin (panel A) and tubulin (panel B) used as loading controls. Shown on the right of each panel is the quantification plot for the change of dTAK1 band intensity in Atg8a flies relative to their age-matched WT controls (expressed as fold-change, unitless). Data shown as individual values with mean $\pm$ 95% C.I [data obtained from n = 6 (1-week); n = 5 (3-week) individual experiments, using samples from different fly populations per repeat; *, $p < 0.05$; **, $p < 0.01$; statistical analysis performed by one-sample t-test].

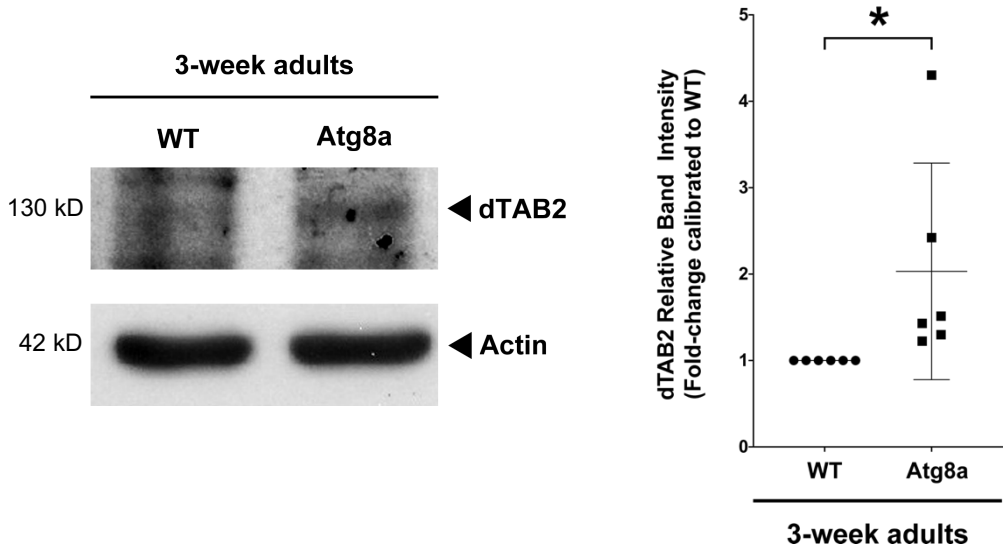

Figure 6.5. ***Old Autophagy-Impaired Flies Accumulate dTAB2****.* Western blot of whole fly extracts from 3-week adult autophagy-deficient ($Atg8a^{KG}$; "Atg8a" in figure) flies and their age-matched WT controls. A newly created anti-dTAB2 Ab (Eurogentec, ZGB19056) was used to detect endogenous dTAB2 and actin served as loading control. Quantification plot shows the change of dTAB2 band intensity in Atg8a flies relative to WT (expressed as fold-change, unitless). Data shown as individual values with mean $\pm$ 95% C.I (data obtained from n = 6 individual experiments, using samples from different fly populations per repeat; *, $p < 0.05$, analyzed by one-sample t-test).

6.3 *dTAK1 Co-localizes with Ub-Aggregates in Autophagy-Deficient Flies*

A characteristic feature of autophagy impairment is the formation of visible protein inclusions in IF applications, that are often also enriched in Ub [183], [354].

I examined whether dTAK1 co-aggregates with Ub in tissues of autophagy-mutant flies, after having previously validated the dTAK1 antibody's specificity in WB and IF (Figures 6.1 and 6.2). I dissected the fat bodies of normally fed 3rd instar WT and Atg8a fly larvae and prepared these for observation in confocal microscopy, using anti-dTAK1 in tandem with an antibody that detects mono- or poly-Ub chains on proteins. Following this approach, I observed distinct accumulation of dTAK1 and Ub in fat body tissue samples of Atg8a larvae relative to WT (Figure 6.6). Atg8a fat bodies formed characteristic Ub as well as dTAK1-containing aggregates across the whole fat body tissue, whereas in WT some disperse puncta formations could be seen in certain fat body cells, but not to a comparable density with Atg8a mutants (Figure 6.6). Interestingly, there were many instances in the fat bodies of Atg8a larvae, that dTAK1 seemed to co-localize within the vicinity of the same puncta formations as Ub, as observed by their respective signals overlapping in each channel (Figure 6.6).

Taken together these findings provide compelling evidence that dTAK1 is cleared by autophagy and accumulates in aggregate formations once the process is impaired, which in many instances can also be positive for other ubiquitinated substrates.

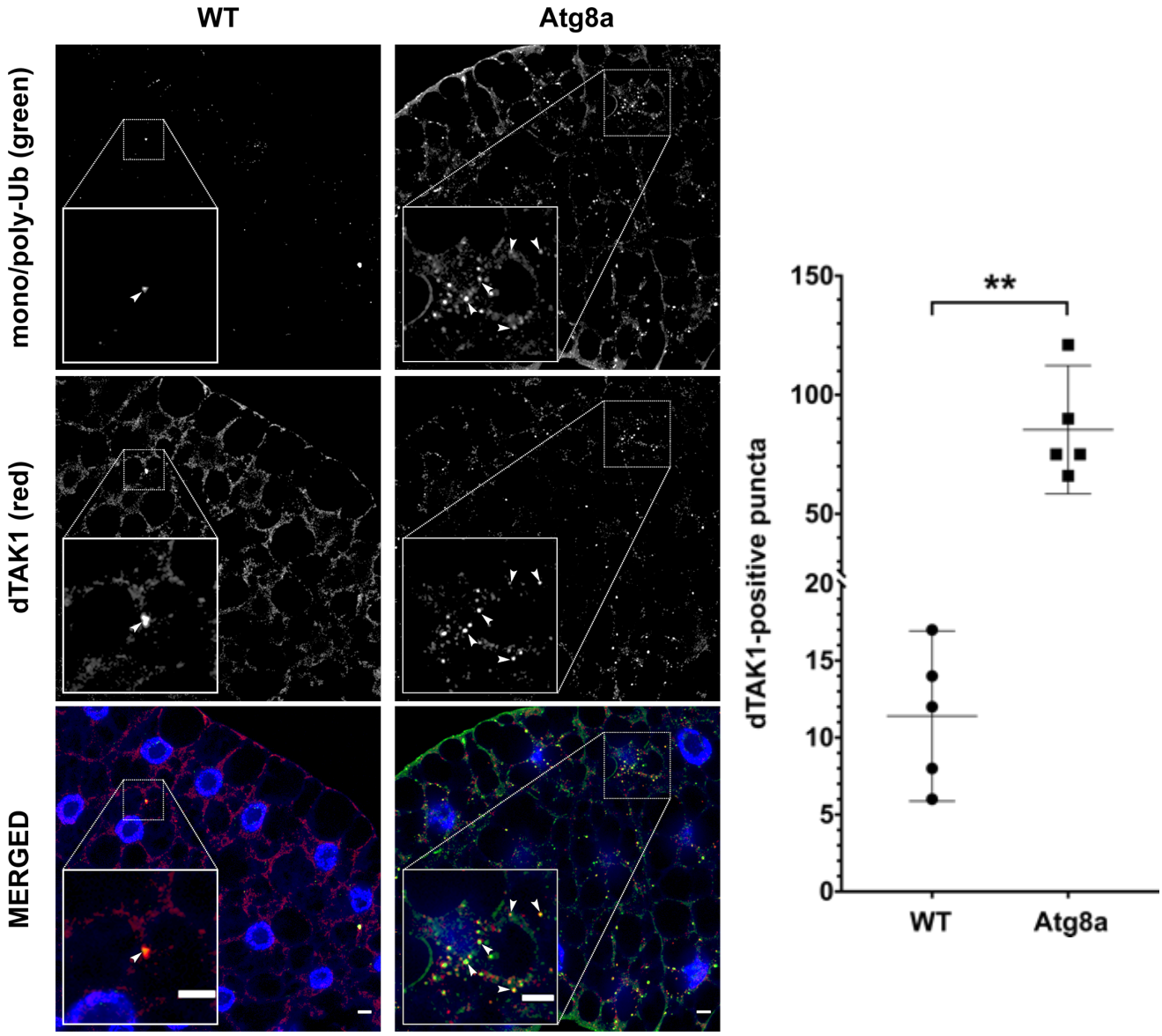

Figure 6.6. ***dTAK1 Forms Aggregates in Autophagy-Deficient Flies In-Vivo***. Representative confocal images of *Drosophila* fat body cells from WT and Atg8a 3rd instar larvae, following induction of autophagy by starvation. Staining performed against endogenous mono/poly-Ub, and dTAK1. Punctate regions in both Ub, and dTAK1 channels represent aggregates of each protein respectively. Snippet showcase representative areas of the widefield images and arrowheads point towards instances where Ub and dTAK1 associate together in the same aggregate formations. Scale bar for widefield images and snippets, 5 μm. Quantification plot shows the number of dTAK1-positive puncta counted in fat body images from WT and Atg8a flies. Data shown as individual values with mean ± 95% C.I (*n* = 5; n represents the number of representative confocal images analyzed from independent samples for each condition; **, $p < 0.01$, unpaired t-test with unequal variances).

6.4 *Generation of CRISPR-Mutant Tak1 LIR1 Flies*

Having established the requirement of the dTAK1 LIR1 motif (EGWVVI for the efficient interaction of the kinase with Atg8a *in-vitro* and *in-vivo*, I was interested in examining how this might translate in terms of the IMD pathway activation, and health of flies on an organism-wide level. We decided that the most direct approach, which would provide the more accurate answers for these types of questions, would be to monitor expression levels of IMD-regulated AMP genes by RT-qPCR, as well as measure the lifespan of flies that have been genetically modified to express only the dTAK1 inactive LIR-motif isoform (dTAK1 LIR1) as the endogenous protein.

Since no such fly strain existed at the time, we opted to have one commissioned as we did for the *UAS-FLAG:Tak1*$^{WT/LIR1}$ lines. The difference with the previous flies would be that in contrast to overexpressing a labelled transgenic construct in a controlled induction manner, this line would have the normal *Tak1* gene replaced with a *Tak1 LIR1* mutant isoform instead. As such, the mutant gene would be the only isoform of *Tak1* present in these flies, and expressed in the otherwise normal pattern for *Tak1* as dictated by its genetic programme. Therefore, we contacted WellGenetics in order to create mutant dTAK1 LIR$^{W669A/I672A}$ (*Tak1*^{LIR1})flies, using site-directed mutagenesis and genome editing via CRISPR/Cas9 homology-dependent repair [47]. The creation of the CRISPR *Tak1*^{LIR1} flies was performed in 4 steps. First, the target gene was mutated at the desired precise locations by site-directed mutagenesis. Then an excisable fluorescent reporter was introduced within the target gene by P element transposition (PBac-DsRed). This disrupts the gene at first, but serves as a screening tool to validate those fly strains, where the construct has successfully integrated within the genome at the desired site, following injections of embryos. Then micro-injections were performed on *Drosophila* embryos to replace endogenous *Tak1* with the transgenic construct in the germline, using CRISPR/Cas9-mediated homology-dependent repair. The PBacDsRed element is excised afterwards in a process that reconstitutes the functional gene — now the *Tak1*^{LIR1} mutant isoform — to be expressed in the germline.

6.5 *Tak1 LIR1 Flies Have a Chronically Activated IMD pathway*

Ageing is characterized by the chronic low-grade activation of the innate immune system in the absence of external stimuli [10], [11]. After obtaining the CRISPR *Tak1^{LIR1}* mutants, I investigated if the IMD response is chronically overactivated in these flies compared to WT controls. Activation of the pathway would be used as a readout to assess the requirement of the dTAK1 LIR1 motif and consequently, the extent to which selective autophagy regulates IMD signalling at the level of dTAK1.

For this purpose, I employed RT-qPCR assays to monitor the relative expression levels of *Drosophila* AMP genes from the *Attacin*, *Diptericin* and *Drosocin* families, whose members are predominantly active against Gram^{-ve} bacteria and as such, their upregulation is almost exclusively under the control of the IMD pathway [305], [355], [356]. Namely, I measured the systemic levels of the AMPs *AttA*, *DptB* and *Dro*, and used these as a gauge for the pathway's degree of activation (Figure 6.7). Expression was measured as total mRNA from whole-fly samples of evenly mixed male/female *Tak1^{LIR1}* young adult (1-week) as well as older adult flies (3-week), and expressed as a log2 fold-change of each gene relative to WT controls (whose log2 fold values are subsequently set as a threshold value of 0). In addition to these conventionally reared flies, I also used transient (6hr) natural infection of WT flies with the mild Gram^{-ve} pathogenic bacteria *Ecc15* as a positive control for the upregulation of the IMD in response to acute microbial challenge [337] (shown as WT$^{inf.}$ in Figure 6.7).

Following analysis of the data obtained in this manner, I observed that AMP levels for all genes tested were significantly elevated in both age groups and across conditions, compared to 1-week WT controls (Figure 6.7), indicative of the IMD pathway activation. This is expected for WT$^{inf.}$ flies, since they were the positive controls for IMD activation. Interestingly, systemic AMP levels were found to be noticeably upregulated in young adult (1-week) *Tak1^{LIR1}* flies as well, which while less than their microbially challenged WT counterparts, they were nonetheless 1-2 times higher relative to their age-matched WT unchallenged controls (Figure 6.7). Another interesting observation was that AMP levels were higher in the older WT flies and comparable to the younger *Tak1^{LIR1}* mutants, which is consistent with the chronic overactivation of the immune response in ageing flies [324]. It is interesting to note that within the older group, expression levels of AMPs were found higher across all conditions, with respect to their younger counterparts (Figure 6.7). This may be perhaps due to the underlying inflammation in older flies, favouring overexpression

of the AMP genes studied, compared to young controls. As such, despite the expression of *AttA*, *DptB* and *Dro* not varying by a large extent between $WT^{inf.}$ flies of both age groups, it was nevertheless observed to be slightly higher in the 3-week adult $Tak1^{LIR1}$ flies compared to their younger age group (Figure 6.7). The AMP expression levels of these older mutant flies were nearly identical to their age-matched $WT^{inf.}$ group. Statistical analysis of variance to compare each gene's expression across conditions within the older fly group revealed that the elevated expression values of *AttA*, *DptB*, and *Dro* observed in the $Tak1^{LIR1}$ flies were significantly higher than those of their age-matched WT (p(*AttA*) ** < 0.01; p(*DptB*) ** < 0.01; p(*Dro*) **** < 0.0001; analysis by equal variance one-way ANOVA with Bonferonni correction, two-tailed p value).

These results revealed that the LIR1 motif of dTAK1 appears to be required for the efficient downregulation of the IMD pathway across the lifespan of the fly, and underscores a major role of selective autophagy in regulating this immune signalling cascade even from a single component, such as dTAK1.

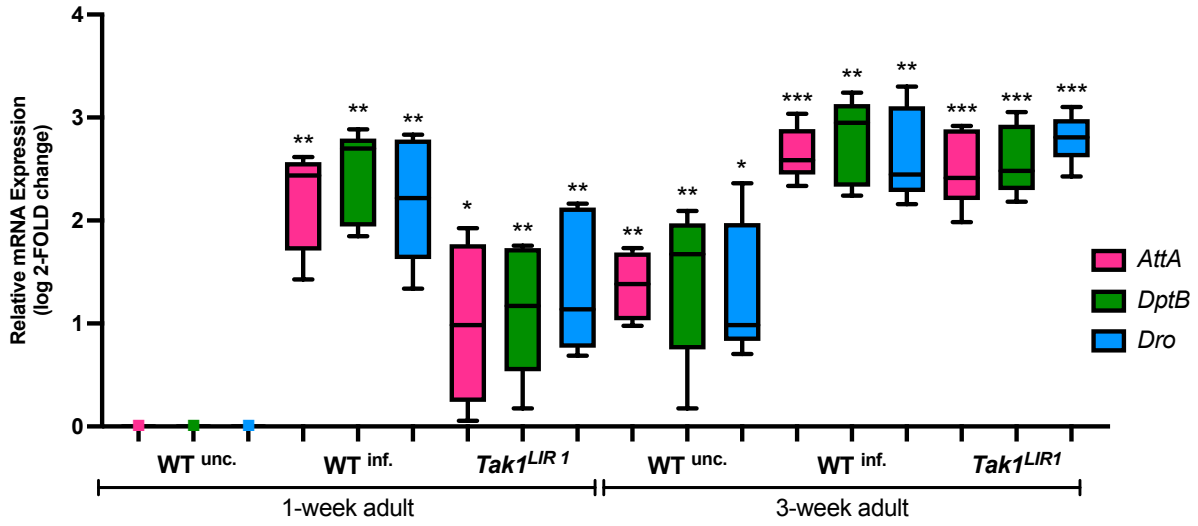

Figure 6.7. ***The dTAK1 Functional LIR Motif Is Required for Regulation of the IMD Pathway by Selective Autophagy***. dTAK1 LIR1 mutant flies have chronically elevated levels of IMD-regulated AMPs. Total mRNA expression levels for *AttaA, DptB* and *Dro*, were measured by qPCR of whole-fly extracts from normally raised 1-week and 3-week adult WT unchallenged (WT^{unc}) and $dTAK1^{W669A/I672A}$ ($Tak1^{LIR1}$) flies. WT flies naturally fed with the $Gram^{-ve}$ bacteria *Ecc15* for 6 hrs, were used as a positive control for the transient activation of the IMD pathway following bacterial infection (WT^{inf}). Data shown as whiskers boxplot log2-fold change with mean ± 95% C.I (data obtained from n = 5 individual experiments, using samples from different fly populations per repeat; *, $p < 0.05$; **, $p < 0.01$; ***, $p < 0.001$; statistical significance assessed by one-sample t-test). All conditions are calibrated to conventionally reared, 1-week adult WT controls, which is subsequently set as the threshold 0 in the log2 fold-change scale.

6.5.1 *Tak1 LIR1* flies tolerate IMD overactivation in terms of longevity

Consistent with mammalian ageing, observations in *Drosophila* generally agree that chronic activation of the IMD immune pathway, either by overexpression of signalling components, or loss of its negative regulators, often results in reduced lifespan of these flies [13], [307], [357]. Since *dTAK1*^{LIR1} flies were found to present with chronically elevated levels of IMD-induced AMPs, indicating constitutive immune signalling of the IMD pathway, I proceeded to monitor if these flies show signs of reduced lifespan compared to WT. For both genotypes, flies were collected on the first day of hatching as adults, with males and females kept together at a ratio of 1 male : 3 females, for three days before distributed into separate vials, and kept under normal rearing conditions (25 ºC, 70% relative humidity). I ensured that at no point vials were overpopulated, and as such individuals did not exceed 30 per vial. Total starting populations per gender for each group were between 500-580 flies.

I followed the Kaplan-Meier method for constructing the survival curve, which estimates the probability of survival of each group's individuals from day to day, based on recorded death events, and returns the result as a fraction, or percentage of population that survives until the next time-point. I opted for this method, because it also takes into account censored data, such as fly escapees or stuck in food —which happens quite often especially at earlier time points— when estimating survival probability of the group. I recorded death events on a daily basis within a fixed time window and monitored the flies until the last survivor of each group had died. Survival curve comparisons were performed using the logrank (Mantel-Cox) test for statistical significance, which treats deaths at every time point with equal weight and as such is not easily influenced by multiple deaths recorded on the same day, which is also often seen in flies that die in batches.

By choosing the above parameters and after constructing and comparing the survival curves for each group and gender, I did not find in the analysis any distinct difference regarding the maximum lifespan, or rate of death between WT and *dTAK1*^{LIR1} individuals (Figure 6.8). Both groups live for around 60-70 days which is the normal expected lifespan of *Drosophila* in controlled laboratory conditions. While not pronounced, male *dTak1*^{LIR1} flies seem to experience better survival rates compared to WT between days 20 to 54, however not to any significantly different extent. In the same vain, slightly more deaths were recorded among *dTak1*^{LIR1} populations for each gender at early time points compared to controls.

Overall, my interpretation of these results is that despite the IMD pathway overactivation, this appears to be within tolerable levels for the fly as a whole, without impairing the individual in any noticeable manner with regards to survival, compared to controls. Given the tight regulation of major immune pathways such as IMD, at multiple levels along their cascade, and by correspondingly numerous sources, these results seem to corroborate that it is unlikely a single mutation in an otherwise functional component would affect the organism as a whole in a profound manner.

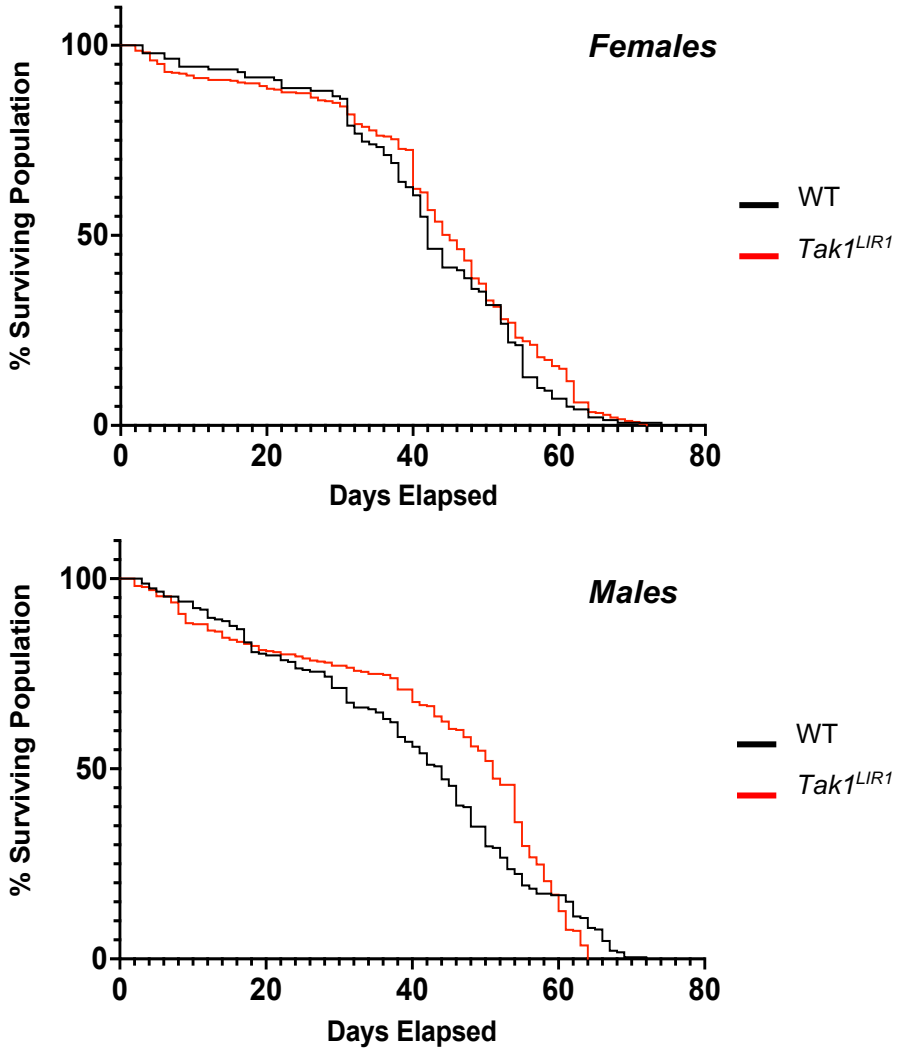

Figure 6.8. ***Longevity of dTAK1^{LIR1} Is Not Affected by IMD pathway Overactivation.*** Survival assays for conventionally raised female (top) and male (bottom) Tak1^{LIR1} flies compared to WT controls. Curves were constructed using the Kaplan-Meier method. Both male and female Tak1^{LIR1} populations do not show any significantly different survivability rate compared to WT controls. Data shown as % population survival percentages (n = 3, where n is the number of independent survival assays repeated per genotype; curve comparison performed by Mantel-Cox logrank test).

Chapter Conclusions

Using two custom-made antibodies for both dTAK1 (Abcam, ab239353) and dTAB2 (Eurogentec, ZGB19056) respectively, I observed that each of the two proteins evidently accumulates in autophagy-deficient (*Atg8a*^{KG07569}) flies in an age-dependent manner (Figures 6.4 – 6.5). This suggests a role of autophagy in the clearance of these proteins. Of the two, dTAK1 displayed evidence of accumulation in both young and old Atg8a flies (Figure 6.4). whereas dTAB2 accumulation seemed to occur only for old autophagy-deficient flies, albeit marginally more so compared to age-matched controls (Figure 6.5). The weak accumulation of dTAB2 compared to dTAK1 and the increased non-specific binding of the anti-dTAB2 Ab provide reasonable grounds to challenge this statement however and perhaps, dTAB2 may be preferentially degraded by other routes under basal conditions (e.g proteasome, endocytosis). Evidence of dTAK1 puncta formations in the fat bodies of otherwise normally feeding *Atg8a*-mutant larvae (Figure 6.6) suggests that autophagy plays a role in the removal of the kinase since early in development.

The qPCR assays measuring total mRNA levels of the largely IMD-regulated genes *AttA*, *DptB*, and *Dro* in CRISPR-generated *Tak1*^{LIR1} mutant flies, revealed that IMD is chronically overactivated in both young and old fly groups and this effect becomes more pronounced as flies grow older (Figure 6.7). Even within the 3-week old adult group, the studied AMP gene levels were significantly elevated in *Tak1*^{LIR1} mutant flies compared to age-matched unchallenged controls (Results Chapter section 6.5). This showcases the dependence of dTAK1 on its LIR motif for its effective uptake by selective autophagy and the consequent downregulation of the IMD pathway.

In survival assays, *Tak1*^{LIR1} mutant flies seemingly tolerate this observed IMD overactivation as their lifespan is directly comparable to WT controls (Figure 6.8). This is at least partially expected, since in contrast to larger genetic manipulations that can inactivate the entire gene, the dTAK1 LIR1 mutant likely retains its functionality with only its efficient turnover to autophagy being affected due to its inactive LIR motif. Since this is a dTAK1-centric mutation that affects the kinase in a specific manner, it may therefore be reasonable to assume that all other homeostasis-maintaining mechanisms of a cell remain largely intact. As such, their functions may counter-balance IMD over-activation to a similar degree as WT flies.

Altogether, the results discussed here suggest that selective autophagy can regulate the IMD pathway at the level of the dTAK1/dTAB2 complex. Moreover, association with Atg8a is important for the downregulation of dTAK1, and to a lesser extent dTAB2.

Chapter 7

SH3PX1 Regulates IMD Signalling at the Level of dTAK1/ dTAB2

Chapter Introduction: **Modulation of IMD activity by SH3PX1**

The fruit fly sorting nexin SH3PX1 is a homologue of mammalian SNX18 and SNX9. These sorting nexins are described as endocytic trafficking components but more generally, participate in various events that involve membrane deformation [237]–[240], with described roles in endocytic trafficking. With regards to autophagy, both SNX18 and SH3PX1 have been shown to participate in autophagosome biogenesis by interacting with LC3/Atg8a and help in maintaining membrane curvature of the expanding phagophore [140]. Moreover, SH3PX1 may associate with dTAB2 (P. Meier personal communication, and [358]). As such, I examined this potential interaction further since it could point to a previously uncharacterized role for SH3PX1 in regulation of the immune response in *Drosophila*. While this work was ongoing, Zhang *et. al*. reported a link between SH3PX1 and chronic inflammation [242]. They observed that loss of *Sh3px1* correlates with increased inflammation in the midgut and reduced lifespan of these flies through an as of yet undefined mechanism [242]. Despite their findings overlapping to a large extent with my own with respect to the work presented in this chapter, I nevertheless discuss my collective results which together with the observations from our collaboration with the team of P. Meier, highlight a plausible mechanistic manner by which SH3PX1 can regulate the IMD immune response in flies.

7.1 *SH3PX1 Directly Binds dTAB2 In-Vitro*

Apart from its function in autophagy [140], SH3PX1 is also a speculative binding partner of dTAB2 according to a *Drosophila* simulated interactome map [358]. This work has so far shown that selective autophagy is involved in the removal of the dTAK1/dTAB2 complex (Figures 6.4 - 6.5), and both dTAK1 and dTAB2 can anchor to Atg8a (Figures 5.2 and 5.4). Therefore, the potential association of SH3PX1 with dTAB2 could add further insight into the mechanistic interactions that altogether facilitate removal of the dTAK1/dTAB2 complex by selective autophagy and characterize the exact manner by which SH3PX1 contributes to regulation of the IMD pathway.

In this particular aspect of the project, we exchanged correspondence with the research group of P. Meier who, in their efforts to discern between artefact and true protein-protein interactions during high throughput analyses, have previously developed a probability-based model termed "***s****ignificance* ***a****nalysis of* ***int****eractome*" (SAINT) [359]. This tool is tailored to mass-spectrometry data and assigns confidence scores to identified interactions, by utilizing the total spectra counted for each protein (spectral counts) during a mass spectrometry assay, as a label-free quantification method to measure protein abundance in proteomic studies [359]. In one such approach to isolate dTAB2-interacting proteins from *Drosophila* S2 cell extracts, P. Meier and colleagues observed that SH3PX1 selectively co-purified with dTAB2 (P. Meier, unpublished results). This interaction was returned with a high confidence SAINT score of 1 (Figure 7.1A). Under the same conditions, SH3PX1 was not co-purified by other components of the IMD signalling cascade used in their study; namely, Imd, Fadd, Dredd, Ird5, Kenny or Relish (SAINT score of 0; P. Meier, personal communication; data not shown).

I tested for the interaction between SH3PX1 and dTAB2 as I have performed already before for dTAK1 and dTAB2 with Atg8a; by employing GST-pulldown assays. In this instance the prey was SH3PX1, labelled with a 6xHis N-terminal tag (His:SH3PX1) and the bait was the GST-fused dTAB2 protein (GST:dTAB2). Both recombinant fly proteins were expressed and purified from bacterial lysates. Upon co-incubation of the bait and prey proteins and after staining for the 6xHis tag, I observed a clear signal of SH3PX1 from the sample where GST:dTAB2 was also present, but not in the GST-tag alone sample (Figure 7.1B). This indicates that SH3PX1 specifically co-precipitates with dTAB2 and is not influenced by the presence of the GST-tag on the recombinant protein. It is important to note here that the signal from His:SH3PX1 was oversaturating the membrane in all

pulldown assays performed, leading to a noticeable "bleaching" effect of the SH3PX1 band upon film development (Figure 7.1B). This oversaturation occurred even with poor enrichment of the GST:dTAB2 bait, which is why in this experiment GST:dTAB2 was visualized using an anti-GST antibody instead of the usual Ponceau S total protein stain used for all other pulldown assays in this work. GST was still visualized by regular Ponceau S staining. This served as an additional observation which further strengthened the argument about SH3PX1 binding GST:dTAB2 with very high affinity, despite the poor enrichment of the bait protein upon co-precipitation.

Taken together, these results suggest that the sorting nexin SH3PX1, strongly associates with dTAB2 in a highly specific manner, as evidenced by mass spectrometry (P. Meier, unpublished data) and GST protein-protein interaction assays (Figure 7.1).

A

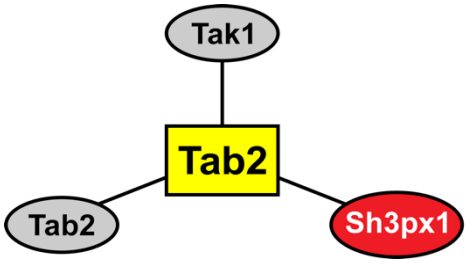

Gene Symbol	Tab2
Sh3px1	44
Tab2	60
Tak1	10

B

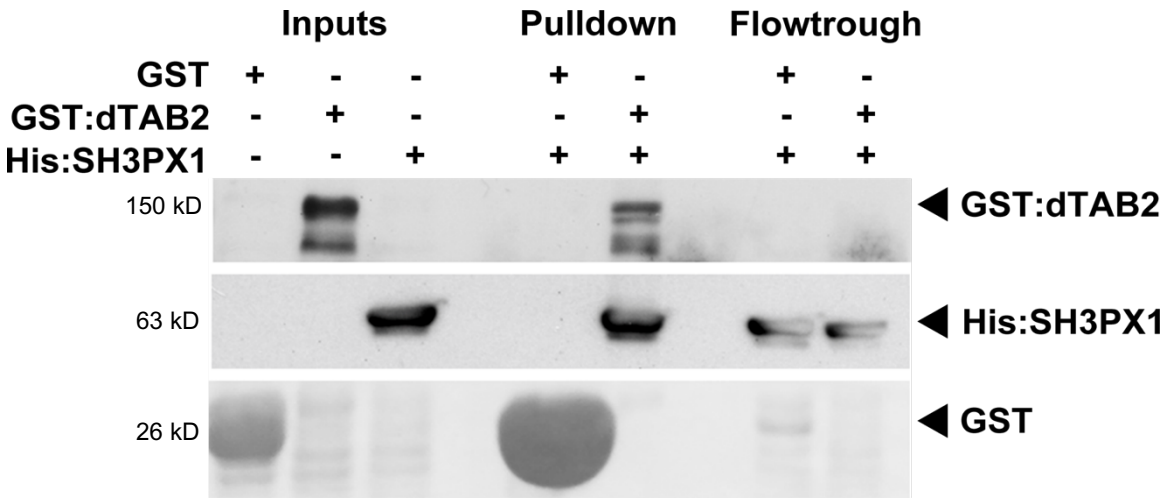

Figure 7.1. ***SH3PX1 Strongly Associates with dTAB2 In-Vitro****. (**A**)* Schematic representation of the dTAB2-bound target proteins that were identified by mass spectrometry analysis of *Drosophila* S2 cells, performed by the P. Meier research team. The table specifies the sum of spectral counts with a SAINT score probability of 1 (as explained in [359]). (**B**) GST Pulldown assay to investigate the interaction between dTAB2 and SH3PX1. dTAB2 and SH3PX1 were used as the bait and prey proteins respectively. Bait and prey were co-incubated in the combinations indicated by the table above each gel, with (+) referring to presence, while (-) denoting the absence of the specific protein from the gel-loading sample. SH3PX1 strongly binds dTAB2 directly *in-vitro.*

7.2 *SH3PX1 Facilitates Progression Of but Is Not Degraded by Autophagy*

The tier at which both the *Drosophila* SH3PX1, and its mammalian counterpart SNX18, mediate their function with regards to autophagy is evolutionarily retained, as they are both mobilized downstream of the PI3K-III complex during development of autophagosomes, to maintain positive curvature of the expanding structure [140]. Moreover, their role in the process is evidently a central one, since loss of either SH3PX1 or SNX18, leads to significantly fewer autophagosome formations *in-vivo* compared to WT controls [140]. By extension then, loss of SH3PX1 should also cause accumulation of the autophagy adaptor Ref(2)P. Moreover, it is unclear though, whether the sorting nexin itself is degraded by autophagy.

Here, I was able to examine these scientific queries by looking at accumulation levels of Ref(2)P and SH3PX1 in different age groups. The rationale behind was a simple, yet straightforward one: If SH3PX1 is required for autophagy progression, then I should be able to observe a significant accumulation of Ref(2)P in the absence of the sorting nexin. Likewise, if autophagy is a major route of degradation for SH3PX1, then accumulation of the protein would be evident when autophagy is extensively blocked by targeting crucial components, such as Atg8a. For this purpose I employed WB assays, where I independently assessed whether endogenous Ref(2)P accumulates in *Sh3px1* CRISPR-null ($Sh3px1^{10A/C1}$, see Materials & Methods section 4.3.3; hereafter "Sh3px1") flies, and if SH3PX1 accumulates in autophagy-deficient $Atg8a^{KG07569}$ ("Atg8a") flies, after autophagy is induced. Validation of CRISPR knockout for the *Sh3px1* gene and protein in full Sh3px1-mutant flies was confirmed by qPCR and WB (Appendix Figure 9.2). Moreover, I was interested in the effect that age may also have in accumulation of the protein; expecting that the natural decline in autophagy function, coupled to its blockage, would collectively lead to an exacerbated aggregation of Ref(2)P and SH3PX1 in older autophagy-mutant flies. It should be noted here that as will be discussed in section 7.3.3, Sh3px1 flies have a considerably shorter lifespan compared to WT and very similar to Atg8a flies. Therefore, in the same manner as with Atg8a flies, in order to obtain samples that more faithfully represented the entire population of old adult Sh3px1 flies, I collected individuals at the 2.5-week old adult mark, as after that time only a very limited number of flies survived. As

such, to assess Ref(2)P accumulation upon loss of *Sh3px1*, I opted for 1-week adult and 2.5-week adult flies.

To assess how basal autophagy is impaired when the *Sh3px1* gene is missing, all WT and Sh3px1 flies were conventionally raised and fed. Samples were made from whole-fly extracts of evenly mixed male/female 10-12 flies per condition. Following staining for Ref(2)P and quantification of results, I observed that accumulation of the autophagy adaptor increased with age, and this was significantly higher in older flies compared to their age-matched controls (Figure 7.2).

To investigate if autophagy constitutes the main route for the degradation of SH3PX1, and if accumulation of SH3PX1 becomes more pronounced with age, I compared WT and Atg8a flies as 3rd instar larvae, 1-week adults and 2-week adults. Autophagy was induced by starvation of flies for 2 (larvae) to 4 hours (1-week/2-week adults) at 25^{o}C. After collecting samples to run in WB, staining for endogenous SH3PX1, and analysing the collective results, I noted that SH3PX1 does not accumulate in Atg8a flies of each age group to a level that would constitute a significant difference compared to their age-matched controls (Figure 7.3).

The results from the accumulation of Ref(2)P in young, and older Sh3px1 adult flies indicate that SH3PX1 might become more necessary as a component with age, that retains a baseline functionality of autophagy as the process progressively wanes (Figure 7.2). However, the sorting nexin itself, does not appear to rely heavily on the autophagy pathway for its degradation (Figure 7.3). This is not unexpected, considering that SH3PX1's functional mammalian homologue, SNX18 is primarily a component of the endocytic trafficking network [238], and the same should be at least partly true for the sole SNX9-family representative in *Drosophila* as well [242]. As already mentioned, endocytosis is the other major route — apart from autophagy — whereby cargo-loaded vesicles are targeted for lysosomal degradation within cells, and the process can take over to some extent, should autophagy become dysfunctional [38]. In addition, based on the existing reports, the sorting nexin's function in autophagy seems to be focused more towards the architectural aspect of autophagosome formation, by sensing curvature and maintaining correct orientation of the phagophore membrane to ensure vesicle closure [128], [140]. Without excluding potential adaptor functions of SH3PX1, it may be the case that the sorting nexin only transiently associates with the phagophore membrane and may not be often found within the concave side of the structure, so as to be otherwise enclosed within the completed autophagosome. This, in conjunction with the endo-lysosomal pathway being arguably the main route of

SH3PX1 degradation, may at least partially explain why the sorting nexin does not exhibit a pronounced accumulation phenotype in autophagy-deficient flies relative to WT controls.

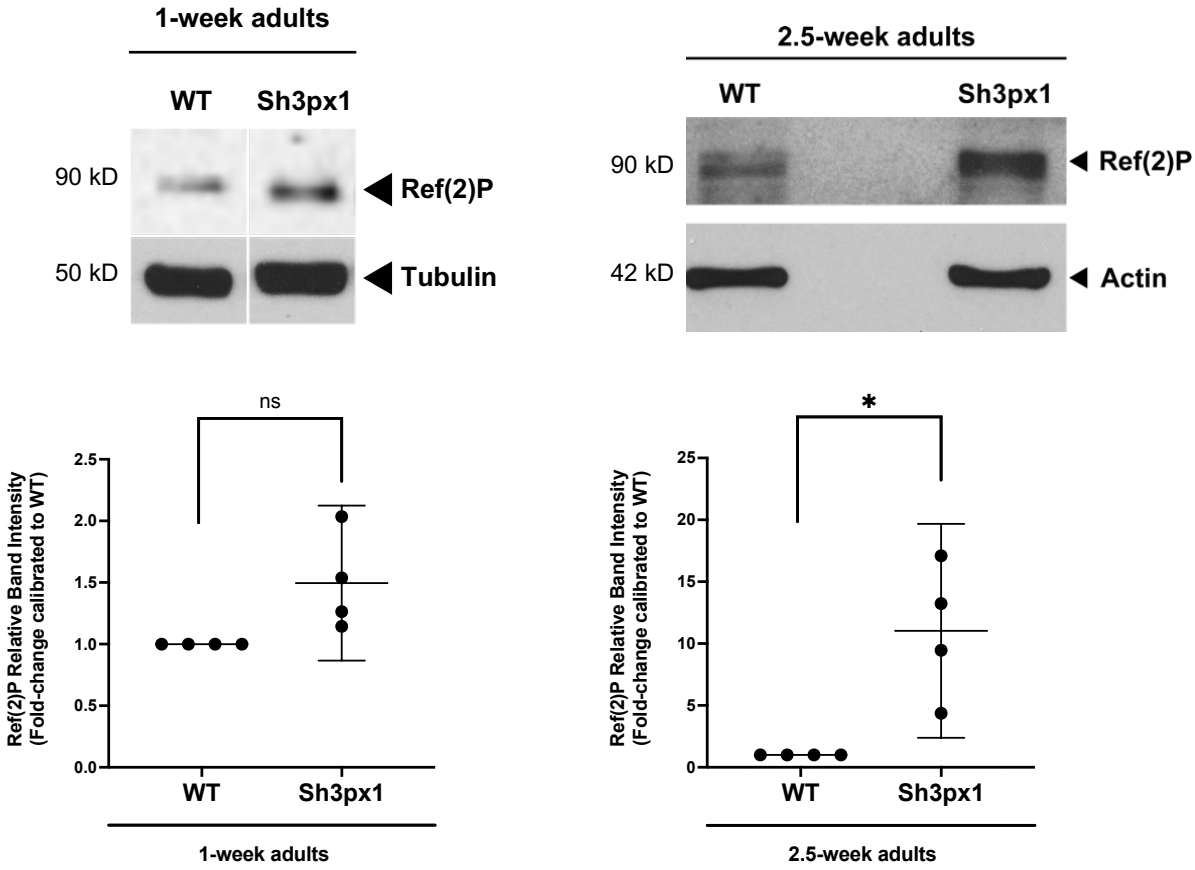

Figure 7.2. ***SH3PX1 Is Required for Basal Autophagy Progression in Older Flies***. WB assays (Top Panel) and corresponding quantification plots (Bottom Panel) of Ref(2)P accumulation in conventionally reared 1-week and 2.5-week WT and autophagy-deficient *Sh3px1*$^{10A/C1}$ ("Sh3px1" in figure) flies. Staining performed for endogenous Ref(2)P. Ref(2)P accumulation was returned as statistically significant in the older fly group, but a noticeable -albeit not significant- increase was also observed in younger flies as well compared to their age-matched controls. For quantification plots, data shown as mean $\pm$ C.I (data obtained from n = 4, individual experiments per age group, using 10-12 flies per sample; ns, "not significant"; * , $p < 0.05$; data analyzed by one-sample t-test).

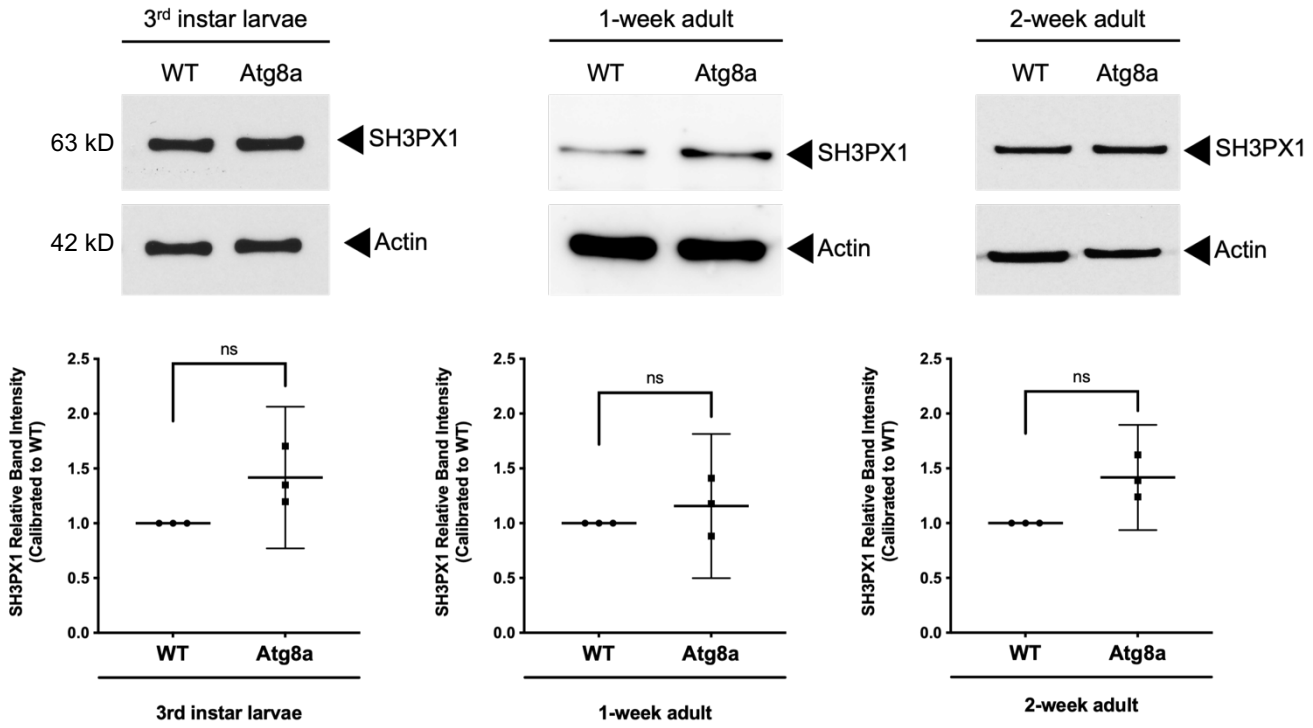

Figure 7.3. ***SH3PX1 Is Not Degraded By Autophagy****.* WB assays (Top Panel) and corresponding quantification plots (Bottom Panel) of SH3PX1 accumulation in WT and autophagy-deficient *Atg8a*^{KG07569} ("Atg8a" in figure) flies. 3rd instar larvae, 1-week and 2-week adult flies used as the selected reference age groups. Following autophagy induction by starvation, and staining for endogenous SH3PX1, the sorting nexin was not observed to accumulate in significantly higher levels in Atg8a flies of either age group, compared to their age-matched controls. For quantification plots, data shown as mean ± C.I (data obtained from n = 3, individual experiments per age group, using 10-12 flies per sample; ns, "not significant"; data analyzed by one-sample t-test).

7.3 *Sh3px1-Mutant Flies Have a Chronically Upregulated IMD Response*

7.3.1. Chronic inflammation in midgut of *Sh3px1*-mutant flies

Similarly to Zhang *et al*, who reported of SH3PX1's involvement in the regulation of the innate immune response in the fly intestine [242], I studied the midguts of *Sh3px1*-null ("Sh3px1") flies in order to corroborate their observations regarding the inflammation phenotype experienced by these flies. For this purpose, I proceeded to count the number of hyperproliferative pH3^{+ve} ISCs (**i**ntestinal **s**tem **c**ells) in the posterior midguts of young (1-week), as well as old (2.5-week) adult WT and Sh3px1 flies. Exposure to pathogens ingested by food intake, leads to acute inflammatory challenges in the midgut epithelium, which subsequently calls for the rapid replacement of damaged cells by new ones, mediated by the increased proliferation rates of the resident ISC pool and accumulation of the mitotic marker pH3 [253], [321]. This phenotype is also mimicked by aberrant inflammatory signalling during chronic overactivation of immune pathways [253], [321]. I collected and fixed midgut samples from normally raised and fed WT and Sh3px1 flies of each age group, in preparation for confocal microscopy. Following analysis of the pH3^{+ve}-ISC counts obtained for each condition, I observed a markedly higher number of hyperproliferative cells in the midguts of otherwise normally fed and unchallenged Sh3px1 flies compared to their respective WT controls for each age group (Figure 7.4). This points to an elevated basal inflammatory signaling, more so than what is expected against common microbes that are frequently present in the fly food.

These observations were in line with Zhang *et al*'s findings regarding the chronic aberrant immune signalling and corresponding midgut inflammation exhibited by loss of *Sh3px1* in flies [242].

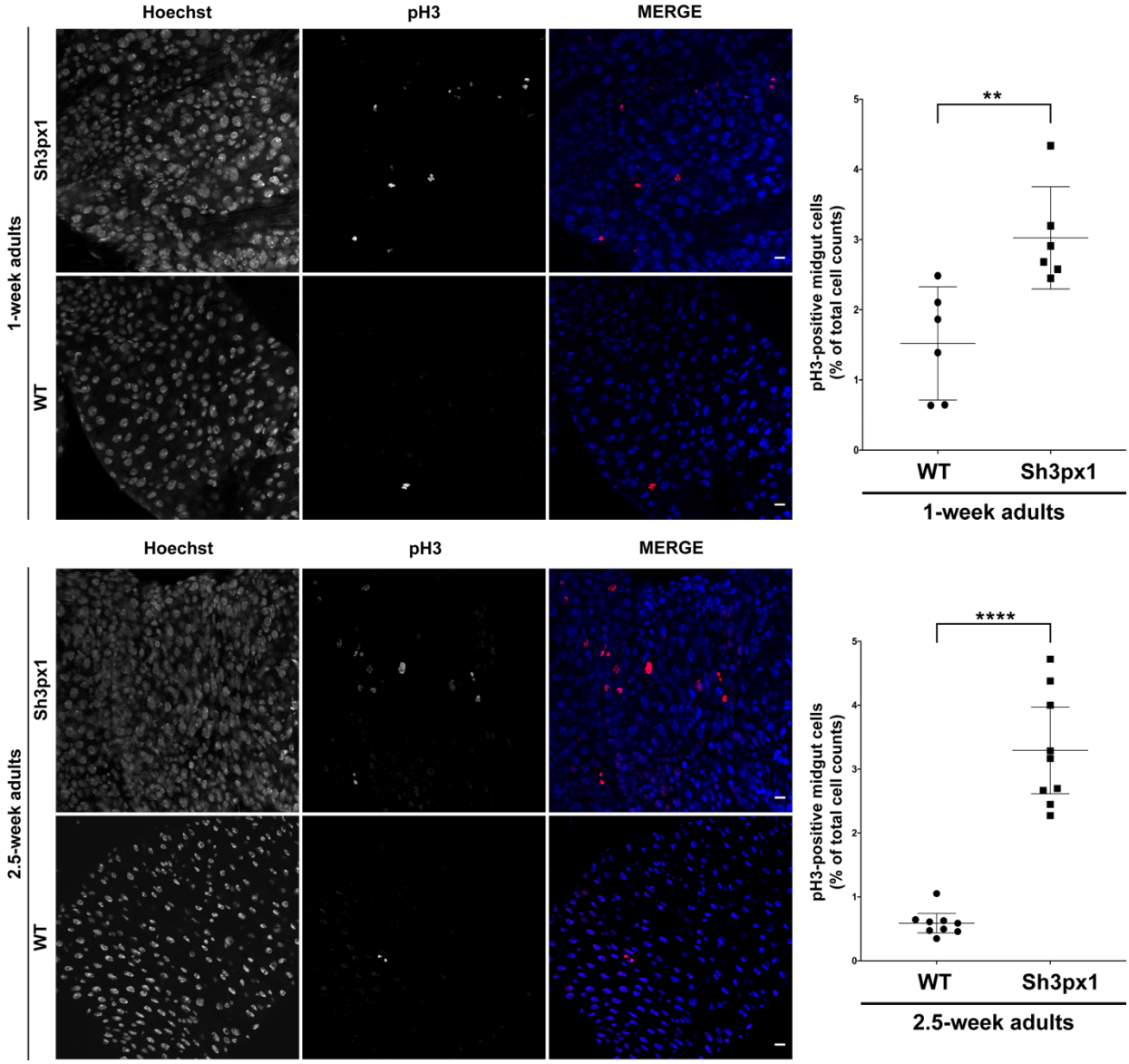

Figure 7.4. ***Chronic Inflammation Phenotype In Midguts of Sh3px1-Mutant Flies***. Representative confocal images of midgut sections from normally fed 1-week (Top panel), and 2.5-week (Bottom panel) adult female Sh3px1-mutant (*Sh3px1*$^{10A/C1}$, "Sh3px1" in figure) and WT flies. Hyper-proliferative ISCs were identified as bright red spots, following staining for the endogenous mitotic marker pH3. Scale bar: 10μm. Quantification plots on the right of confocal images for each panel for 1-week (B) and 2.5-week (D) adult, displaying the percentage (%) of hyper-proliferative pH3+ve ISCs calculated for WT and Sh3px1 flies within each age group. Data shown as individual values with mean + 95% C.I [n = 6 (1-week), n = 9 (2.5-week); n represents the number of images analyzed per condition, each image being from a different midgut; **, $p < 0.05$; ****, $p < 0.0001$; unpaired t-test, equal variances (1-week)/unequal variances (2.5-week)].

7.3.2. IMD pathway is chronically overactivated in *Sh3px1*-mutant flies

I further proceeded to examine whether the IMD pathway in particular displays this chronic gain-of-function phenotype in a systemic manner in Sh3px1 flies. For this purpose and similar to what I previously performed for $dTak1^{LIR1}$ flies, I employed qPCR assays to investigate systemic mRNA levels of the *AttA*, *DptB* and *Dro* AMP genes [305], [355], [356], in order to assess the degree to which the IMD pathway is activated in the absence of *Sh3px1* compared to when it is normally present. I collected samples and extracted mRNA from conventionally reared WT and Sh3px1 whole-fly lysates of evenly mixed male/female young adults (1-week) as well as older adult flies (2.5-week). In addition, I also used transient (6hr) natural infection of WT flies with *Ecc15*, as a positive control for the upregulation of the IMD pathway in response to acute microbial challenge [337] (shown as $WT^{inf.}$ in Figure 7.5). All values were expressed as a log2 fold-change of each gene relative to WT unchallenged ($WT^{unc.}$) controls (whose log2 fold values are subsequently set as a threshold value of 0).

Following analysis of data, I observed that mRNA levels for the AMPs tested are elevated in the $WT^{inf.}$ sample, indicating successful activation of the IMD immune response, as expected after acute microbial infection (Figure 7.5). The increased AMP levels, especially for *AttA* and *DptB*, are directly comparable between transiently infected flies, and their older but normally fed 2.5-week adult WT^{unc} counterparts (Figure 7.5). *Dro* in the older WT sample seems at first glance to exhibit lower expression compared to *AttA* and *DptB*, however displaying a notable upwards distribution (Figure 7.5). More interestingly, all AMP levels in Sh3px1 flies of both age groups, are persistently increased in a very similar fashion to $WT^{inf.}$ positive controls (Figure 7.5). Of note, the AMP expression levels of Sh3px1 flies in each age group, are directly comparable to those of the age-corresponding $dTak1^{LIR1}$ flies observed prior (Results Chapter 6, Figure 6.7).

This observation further corroborates the initial report that the sorting nexin SH3PX1 is a component of the regulatory network that modulates activation dynamics of the IMD immune cascade [242], and is evidently required for the efficient control of signalling from this immune pathway.

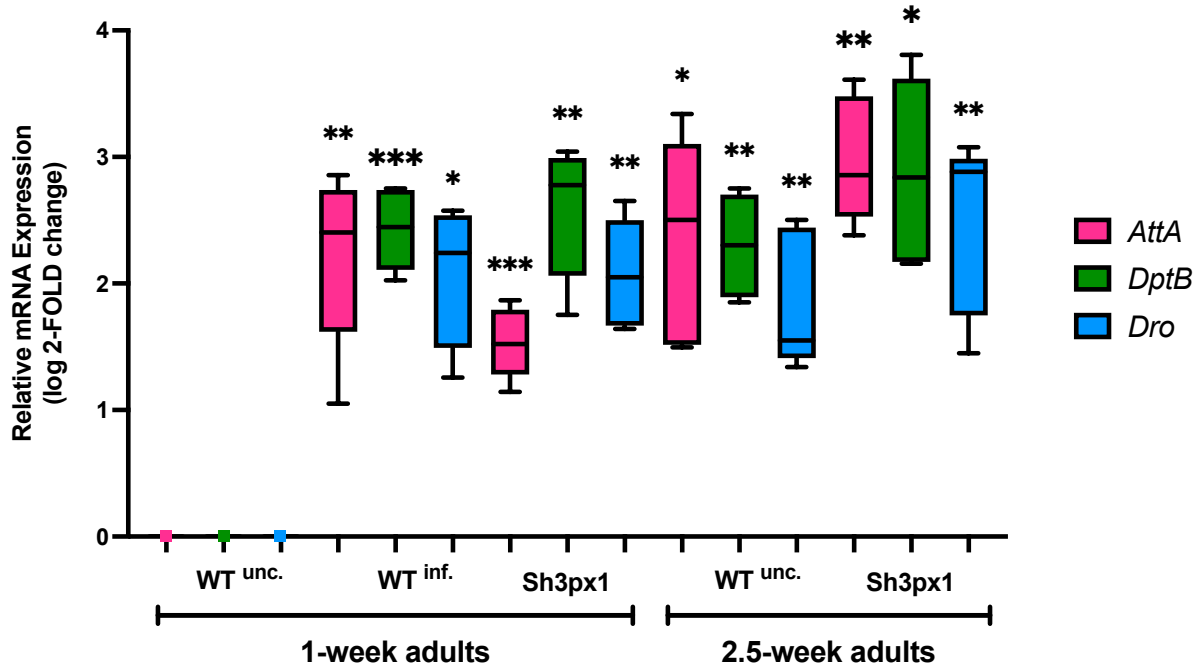

Figure 7.5. ***SH3PX1 Is Required for Regulation of the IMD pathway.*** Sh3px1-mutant (*Sh3px1*$^{10A/C1}$; "Sh3px1" in figure) flies display chronically elevated levels of IMD-regulated AMPs. Total mRNA expression levels for *AttA, DptB* and *Dro*, were measured by qPCR of whole-fly extracts from normally raised 1-week and 2.5-week adult WT unchallenged (WT$^{unc.}$) and Sh3px1 flies. WT flies naturally fed with the Gram^{-ve} bacteria *Ecc15* for 6 hrs, were used as a positive control for the transient activation of the IMD pathway following bacterial infection (WT^{inf}). Data shown as a whiskers boxplot log2-fold change with mean ± 95% C.I (data obtained from n = 5 individual experiments, using samples from different fly populations per repeat; *, $p < 0.05$; **, $p < 0.01$; ***, $p < 0.001$; statistical significance assessed by one-sample t-test). The expression values of the housekeeping gene rp49 were used as reference for the internal normalization of expression for the genes-of-interest within the same condition. All conditions are calibrated to conventionally reared, 1-week adult WT$^{unc.}$ controls, which is subsequently set as the threshold 0 in the log2 fold-change scale.

7.3.3. Longevity of *Sh3px1*-null flies is reduced compared to controls

As a final cross-validation of Zhang *et al*.'s report regarding the negative impact of *Sh3px1*'s loss on fly longevity and deregulation of the IMD immune response [242], I used Sh3px1 flies in lifespan assays to monitor their survival rates alongside WT, as well as autophagy-deficient $Atg8a^{KG07569}$ ("Atg8a") flies. The later would be used as an additional reference group with regards to the impact of dysfunctional autophagy on the fly maximum lifespan, since they have been previously described to experience widely reduced survival rates compared to WT flies [33]. All flies were collected on the first day of hatching as adults, with males and females kept together at a ratio of 1 male : 3 females, for three days before distributed into separate vials, and kept under normal conditions (25 ºC, 70% relative humidity). I avoided over-crowding in vials by having at maximum 30 individuals per tube. Death events were recorded daily and flies were transferred onto fresh fly food-containing vials every 2-3 days. All lifespan assays were completed at the point of death of the last remaining individual per genotype and gender.

Here I report the graphical depiction of the survival curves to mirror the statistical analysis of the data, with respect to the significantly reduced lifespan of both male and female Sh3px1 flies, compared to WT controls (Figure 7.6). Their survival rates were found directly comparable to those of Atg8a flies (Figure 7.6), which have a largely-impaired autophagic pathway. As an added note, despite Sh3px1 and $dTak1^{LIR1}$ flies exhibiting a comparably over-activated IMD immune response based on their respective *AttA*, *DptB*, and *Dro* mRNA levels in qPCR assays (Figure 6.7 and Figure 7.5), $dTak1^{LIR1}$ flies seem to tolerate this elevated inflammatory response much better compared to Sh3px1 individuals, represented in the similar survival rates between WT and $dTak1^{LIR1}$ flies, in contrast to the significantly shortened lifespans of *Sh3px1*-mutants relative to the same WT controls. This may be indicative of the larger impact the complete loss of a component such as SH3PX1 has on the overall cell-maintenance machinery, as opposed to the presence of a mutated, yet otherwise functional isoform, such as $dTAK1^{LIR1}$.

In conjunction with the previous experiments, this set of assays served to establish that absence of SH3PX1 accounts to some extent for the chronic activation of the IMD pathway, and is at least partly responsible for the severely impaired lifespan of Sh3px1 flies compared to WT.

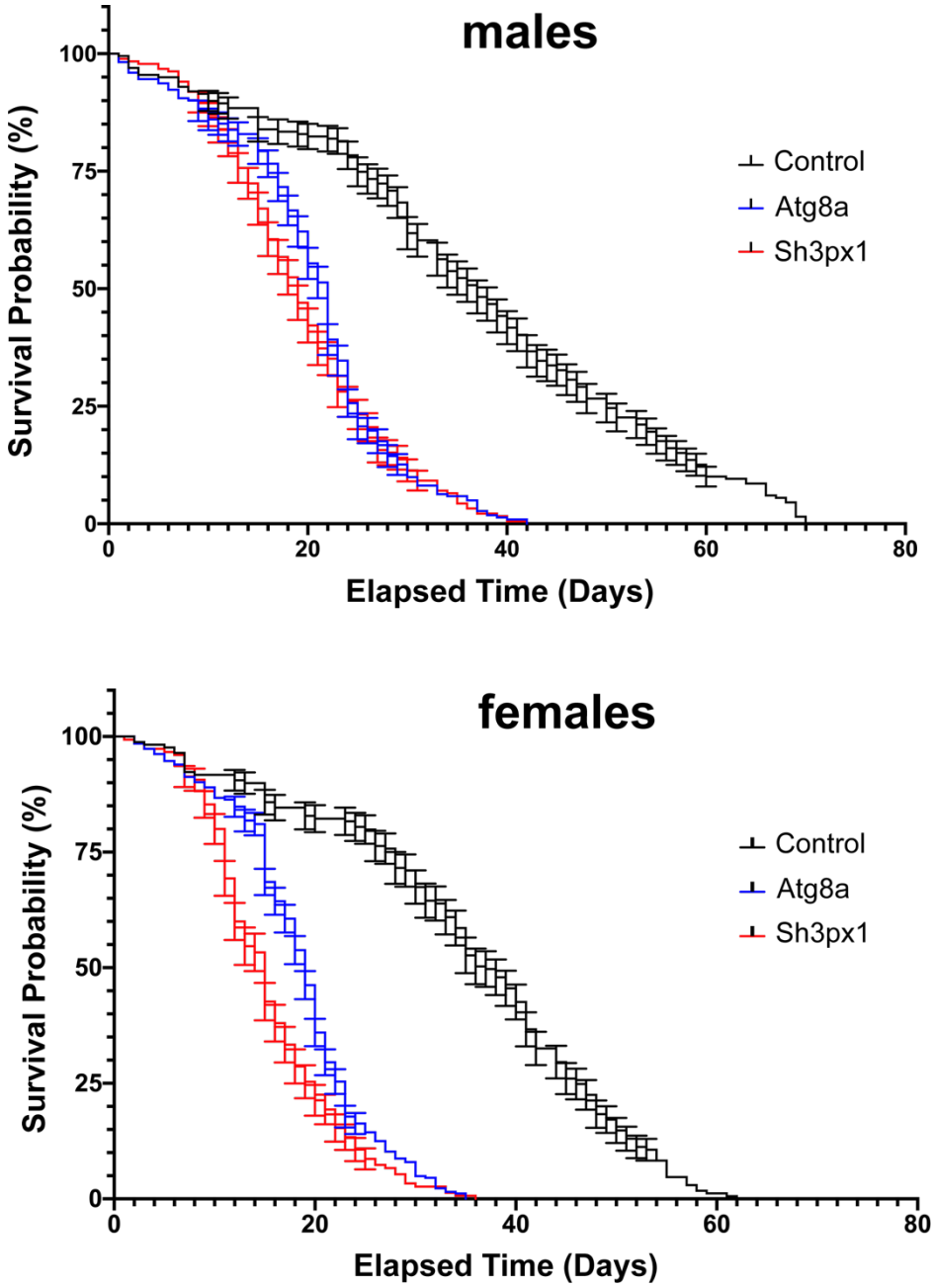

Figure 7.6. ***Loss of Sh3px1 Negatively Affects Survivability of Flies.*** Survival assays of conventionally raised male (top) and female (bottom) Sh3px1-mutant (*Sh3px1*$^{10A/C1}$; "Sh3px1" in figure) flies compared to WT and autophagy-deficient (*Atg8a*^{KG07569}; "Atg8a" in figure) controls. Curves were constructed using the Kaplan-Meier method. Both male and female Sh3px1 flies live for a considerably shorter period compared to WT, but very similar to Atg8a flies. Data shown as percentage (%) survival probability (n = 6, where n is the number of independent survival assays repeated per genotype; curve comparison performed by Mantel-Cox log-rank test).

7.3.4. dTAK1 displays chronic accumulation in *Sh3px1*-mutant flies

As it had been previously mentioned, loss of SH3PX1 impairs autophagic flux to an extent (Figure 7.2 and [140]). In addition I have demonstrated earlier in this current work how dTAK1 is a substrate for degradation by autophagy (Results Chapter section 6.2), by showing evidence of accumulation in autophagy-deficient Atg8a flies (Figures 6.4 and 6.6). I was therefore interested in investigating whether the reduction in autophagic flux by loss of SH3PX1 leads to a similar accumulation phenotype of dTAK1, which would further showcase the role of selective autophagy in regulating the IMD pathway by degrading the dTAK1/dTAB2 complex.

Towards this aim, I examined dTAK1 levels in Sh3px1 flies. I collected whole-fly protein extract samples from normally fed and raised 1-week and 2.5-week old adult WT and Sh3px1 flies, to run in WB and stained for endogenous dTAK1. After collection and analysis of the results I observed that dTAK1 accumulated in both young and old Sh3px1 flies, compared to their age-matched controls (Figure 7.7). While that accumulation was not immediately distinct upon comparison within each age group, the difference was nevertheless persistent across repeat experiments for both young and old adult flies, and represented in the statistical analysis of the data (Figure 7.7).

These results further support selective autophagy as the major route of degradation for dTAK1. Furthermore, when considered together with the identified interaction between SH3PX1 and dTAB2 (Figure 7.1), they highlight the sorting nexin as an evidently necessary component for the efficient degradation of the dTAK1/dTAB2 complex by autophagy, despite dTAK1's interaction with Atg8a remaining intact (Results Chapter section 5.2.1)

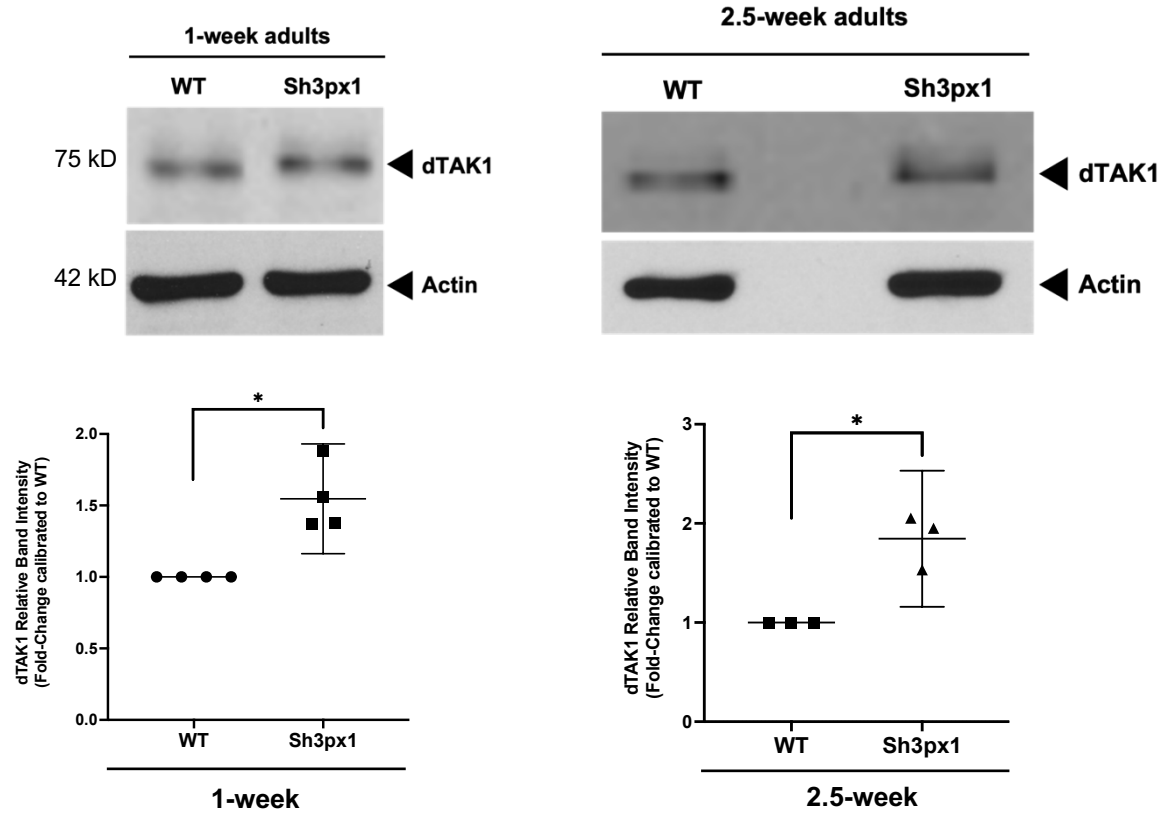

Figure 7.7. ***Loss of SH3PX1 Correlates With Increased Levels of dTAK1 In Autophagy-Mutant Flies.*** WB assays (Top Panel) and corresponding quantification plots (Bottom Panel) of dTAK1 accumulation in conventionally reared 1-week and 2.5-week WT and autophagy-deficient *Sh3px1*$^{10A/C1}$ ("Sh3px1" in figure) flies. Staining performed for endogenous dTAK1. dTAK1 accumulation was found to be statistically significant for both young and old Sh3px1 flies compared to their respective age-matched controls For quantification plots, data shown as mean $\pm$ C.I [data obtained from $n = 4$ (1-week); $n = 3$ (2.5-week), individual experiments per age group, using 10-12 flies per sample; * , $p < 0.05$; data analyzed by one-sample t-test].

Chapter Conclusions

In an attempt to further delineate the mechanism by which selective autophagy may regulate the IMD pathway at the level of the dTAK1/dTAB2 complex, I examined the previously proposed interaction of dTAB2 with the *Drosophila* sorting nexin SH3PX1 (P. Meier, personal communication and [358]). In collaboration with the research team of P. Meier, we corroborated that SH3PX1 co-precipitates with dTAB2, via mass spectrometry and GST Pulldown assays respectively (Figure7.1). Furthermore, SH3PX1 has already been described to interact with Atg8a and participate in autophagosome biogenesis [140].

The experimentally observed association of SH3PX1 with a known component of the IMD pathway prompted for investigating the impact that loss of the sorting nexin may have on IMD activation. I observed that *Sh3px1*-null flies presented with characteristic chronic inflammation markers; namely increased numbers of $pH3^{+ve}$ hyper-proliferative ISCs in the fly midgut [253], [321] (Figure 7.4) and elevated levels of IMD-regulated AMP genes (Figure 7.5). Moreover, the lifespan of *Sh3px1*-null flies was characteristically shortened compared to controls (Figure 7.6). These findings corroborated previous similar observations by Zhang *et. al* [242], whose work was published as this current study was ongoing. The authors of that work reported that loss of SH3PX1 correlates with increased inflammation and reduced longevity of flies [242].

Collectively, these findings highlight the sorting nexin SH3PX1 as an important regulator of the IMD pathway at the level of the dTAK1/dTAB2 kinase complex. Moreover, they further support the working hypothesis of selective autophagy's role in degrading this complex, since dTAK1 displayed evidence of chronic accumulation upon autophagy impairment by loss of *Sh3px1* (Figure 7.7). Based on the protein-protein interaction assays performed in this work, a mechanistic interaction network begins to emerge with regards to how the dTAK1/dTAB2 complex might be targeted to the autophagosome. More specifically, I posit that dTAK1 and dTAB2, each interact with Atg8a (Results Chapter 5), while SH3PX1 binds dTAB2 (Results Chapter section 7.1) and Atg8a [140], seemingly acting as a necessary adaptor that ensures the dTAK1/dTAB2 complex is tethered on the autophagosome membrane, and subsequently degraded by autophagy.

DISCUSSION

Chapter 8

Discussion & Conclusions

The NF-κB-mediated innate immune response is a host's most primordial anti-inflammatory system and the first line of defence against invading pathogens [247]. It is also mainly responsible for the chronic low-grade inflammatory signalling that characterizes ageing, and associated with its most deleterious side-effects [11]. As such, in the interest of maintaining homeostasis, cells keep activation of immune signalling pathways under strict control by their inherent housekeeping mechanisms. One such regulatory housekeeping mechanism is selective autophagy, which contributes in the termination of innate immune defence responses such as STING and IMD [33], [353]. This work expands the current knowledge regarding how exactly selective autophagy can modulate the IMD innate immune response in *Drosophila* models for ageing, by identifying the mechanistic link between the autophagy core machinery component, Atg8a and the apical kinase complex of IMD, dTAK1/dTAB2. Moreover, it sheds additional light on the previous report about the sorting nexin SH3PX1's involvement in regulation of IMD signalling [242], by characterizing the association of SH3PX1 with dTAB2. Autophagy and the innate immune system are ancestral processes, and therefore conserved to an extensive degree from yeast to humans in terms of components and functions [64], [247]. It is therefore plausible that the regulatory interactions between dTAK1, dTAB2, SH3PX1 and Atg8a, as well as their physiological importance discussed herein, may also at least partially translate to mammalian systems as well. In such a case, they may provide additional support to investigations aimed at discovering novel drug targets to reduce chronic inflammation during ageing and extend the window of overall good health.

8.1 *Pros, Cons & Markers in High-Throughput Search for the Fly Atg8a-Interactome*

Part of the basis for this work was the large Y2H screen of *Drosophila* larvae and adult head libraries, conducted previously by Hybrigenics using Atg8a bait samples provided by the I. Nezis group. The aim of the screen was to identify candidate Atg8a-interacting proteins within the fly proteome represented by the two libraries. To our knowledge, this is the first large scale analysis with the specific purpose of delineating the Atg8a-interactome in *Drosophila*.

Previous high-throughput approaches by the group of I. Nezis aimed at identifying Atg8a-binding proteins, were largely restricted to *in-silico* methods (*iLIR* software [339], UBD/xLIR motif-containing protein list [340]). An obvious advantage of such methods is that they can be quickly developed compared to conventional hands-on approaches and provide in turn a refined information for selecting candidate interactors to proceed with testing experimentally. Nevertheless, an opposing caveat is that both, *iLIR* and the UBD/xLIR-containing list are inherently structured around the assumption that Atg8/LC3-interacting proteins bind Atg8a via a typical "W/F/Y-x-x-L/V/I" LIR motif. While this is often true, canonical "*W-x-x-L*" LIR motifs and LIR-dependent interactions are not universally shared attributes among members of the Atg8/LC3-interacting family [170]. For instance, despite the greatly conserved aromatic and hydrophobic residues occupying positions $\mathbf{X_0}$ and $\mathbf{X_3}$ respectively of the "$\mathbf{X_0\text{-}x_1\text{-}x_2\text{-}X_3}$" core in canonical LIR motifs, there are examples of proteins containing "atypical" LIR motifs (e.g mammalian NDP52/CALCOCO-2, Bcl-2, TRIM5α, UBA5) which lack either the aromatic W/F/Y or hydrophobic L/V/I amino-acids found in these positions [170]. As such, even though "atypical" LIR motif-containing proteins can bind Atg8/LC3 [170], these would most likely be either missed, or returned as false negative results, using the UBD/xLIR-containing protein list, or *iLIR* software respectively.

In a similar manner, the recent discovery of the UDS site on ATG8 [202] and consequently, of the UIM/UDS-dependent mode of interaction [201], represents an alternative way that proteins and Atg8/LC3 can interact without the need of LIR motifs. This creates a subset of Atg8/LC3-interactors which neither the *iLIR* software, nor the UBD/xLIR motif-containing protein list can predict/identify, since both these tools were developed with prototypical LIR/LDS-interactions in mind.

In contrast, the relevant Y2H screen was designed by default to focus on "**If**" a protein binds Atg8a, without discriminating between the mode by which it may do so. Furthermore, since it was developed as an assay for direct protein-protein interactions, it simultaneously identifies only those proteins that are capable of directly binding to Atg8a, at least *in-vitro*. Therefore, the protein list of the Y2H screen (Appendix Figure 9.1) altogether represents: a) experimentally observed Atg8a-interactions rather than predicted ones, b) Atg8a-binding proteins able to associate directly with Atg8a, and c) an expanded list of proteins without distinguishing the nature by which they bind Atg8a.

Confidence in the results of the Y2H screen representing rather true interactions than artefact findings was increased since it contained both: a) Fly proteins that have been previously shown to bind Atg8a, and b) proteins for which their mammalian homologues have been known to interact with LC3/GABARAP. Among those hits was the apical kinase of the *Drosophila* IMD immune response pathway, dTAK1. Of note, the findings of this current project in collaboration with the team of P. Meier confirmed that the co-activator of dTAK1, dTAB2 can interact directly with Atg8a at least *in-vitro* (Results Chapter section 5.2.2). This dTAB2-Atg8a interaction was evidently missed by the Y2H screen. dTAB2 however was a positive hit in the UBD/xLIR motif-containing protein list constructed prior by the I. Nezis group with the aid of the iLIR software and using the domain architecture of the *Drosophila* SAR Ref(2)P as a reference [340].

The different origin stories of dTAK1 and dTAB2 with respect to how they were initially observed and confirmed to anchor Atg8a, are prominent examples that showcase how neither computational, nor experimental techniques are without their flaws. It is however their combinatorial use, rather than mutual exclusion that creates an integrative approach, which can in turn better serve researchers' interests.

In this regard and with the hope of aiding future investigations, I used the *iLIR* software to construct a list of the LIR motifs predicted for each of the Y2H screen results (Appendix Table 9.1). In addition, I used an online illustrator software [360] to create a 2-D schematic figure depicting together the protein domains predicted by BLAST for each Y2H result, and those LIR motifs that overlap with the SID region of each protein where interaction with Atg8a was mapped by the Y2H screen (Appendix Figure 9.1).

Interestingly, by looking at the 2D-representation of this Atg8a-interacting protein list, a subtle pattern seems to emerge, where certain domains such as coiled coils and trans-membrane regions are encountered more frequently than others (Appendix Figure 9.1). This can be a coincidental event restricted to the source material used for the screen (*Drosophila*

larvae and adult head libraries), or it may alternatively comprise a selection criterion for identifying potential Atg8/LC3-interacting candidates under certain conditions. For instance, trans-membrane domains are traditionally found in proteins that anchor onto, or span membrane structures. An example of a well-known Atg8/LC3-interacting autophagy protein is ATG9, which is the only characterized transmembrane member of the core ATG protein family [126]. It is thought that it is this feature of ATG9 that allow it to traffic and dock between different cellular compartments and transfer membranous material to the developing autophagosome. Therefore, the presence of transmembrane domain/s on candidate Atg8/LC3-interactors might indicate proteins that could perhaps be easier to move around the cell, or have higher chances of being found spanning membranes such as the surface of autophagosomes.

Concerning coiled coil domains, these structures are more commonly associated with the ability of a protein to oligomerize [361], and several well-known mammalian autophagy receptors such as NBR1, NDP52, and OPTN, as well as the characterized *Drosophila* SARs, Blue-cheese [184], Ref(2)P ([183], and Appendix Figure 9.1), and Kenny ([33], and Appendix Figure 9.1), all possess at least one, or several coiled coil regions across their structure. Of note, it has been reported that coiled coil domains may increase the binding affinity of otherwise weak Atg8/LC3-interactors for their cognate autophagy substrate, as it was recently shown for the "atypical" LIR-containing protein TRIM5α [362]. While monomeric TRIM5α may display reduced affinity for LC3B or GABARAPL1 [362], its ability to dimerize through via coiled coil-mediated interactions allows multimeric TRIM5α to bind two ATG8 moieties, which overall leads to the more secure anchoring of the protein multimer on the autophagosome membrane [170]. As such, it is interesting to consider whether coiled-coil domains and other regions that might favour multimerization of proteins could be used as additional properties of candidate Atg8/LC3-binding proteins under specific contexts.

It may therefore be interesting to examine whether similar structural features can be used as selection criteria alongside computational and experimental approaches, to render the ongoing search for novel Atg8/LC3-interacting proteins more rapid, precise and accurate.

8.2 *Selective Autophagy in the Regulation of the IMD Pathway*

The findings of this current project seem to corroborate the initial hypothesis that dTAK1 and dTAB2 represent novel autophagy substrates that can each interact with Atg8a (Results Chapter 5). Moreover they suggest that selective autophagy removes the apical dTAK1/dTAB2 complex (Results Chapter 6), which in turn favours attenuation of the IMD signal. In this regard, the present work characterized an additional layer for the regulatory controls that fine-tune the IMD immune response at the tier of dTAK1/dTAB2, highlighting autophagy as even more heavily implicated in the downregulation of IMD than previously reported for Kenny/ird5 [33]. Ubiquitin-modifiers are important modulators of dTAK1's status, since they are required for activating (via K63-ubiquitination) [363], as well as de-activating the kinase as assessed by the diverse functions of its characterized negative regulators Trabid and POSH [307], [308]. Whereas Trabid removes K63 Ub-chains from dTAK1 [307], POSH marks the kinase instead with K48 poly-Ub that facilitate its uptake by the proteasome [308]. Moreover, Trabid's role is IMD-specific with regards to dTAK1 [307]. As such, based on its Ub post-translational modifications alone, dTAK1 has at least two proposed routes for its apparent de-activation, via Trabid and POSH. The characterizations in this work that dTAK1 is also degraded by autophagy only adds to the complexity of its downregulation and begs the question whether the above mechanisms are remnants of evolution and perhaps redundant to an extent. This work did not address this question and while such an explanation is certainly possible, it is the opinion of this author that the different de-activation methods for dTAK1 may not necessarily be interchangeable or mutually exclusive. TAK1 is a multi-faceted kinase that has diverse functions, ranging from inflammatory and stress responses to cell proliferation, differentiation and modes of cell death [364]–[370]. It is therefore possible that a nodal component such as TAK1 would in turn have multiple downregulatory mechanisms that could act in parallel or utilized under different contexts, so that the kinase mediates the desired outcomes in a finely-controlled manner. It is conceivable that at least some downregulatory mechanisms that are also closely related to each other (e.g Ub-editing and autophagy targeting) could have co-developed to ensure effective attenuation of TAK1 signalling in pathways that can directly impact cell viability. For example, despite their protective role against pathogens, AMPs can also have cytotoxic side-effects to tissues if overexpressed and as such activation of dTAK1 in IMD signalling is a tightly controlled process [330], [371]. Whether one TAK1-uncoupling method could be favoured over the other within the same pathway is presently unknown.

By further investigating the LIR-LDS interaction of dTAK1 and Atg8a, the dTAK1 LIR motif seems to be functionally relevant also *in-vivo*, as I found that in $dTak1^{LIR1}$ mutant flies, the kinase and the core autophagy component did not co-localize together as frequently compared to the $dTak1^{WT}$ condition (Figure 5.6). Despite the complete dependency of dTAK1 on its LIR motif to bind Atg8a *in-vitro*, a clear exclusion of mutant $dTAK1^{LIR1}$ from $Atg8a^{+ve}$ autophagosomes was never expected *in-vivo*, only reduced at best. This is at least partially due to the presence of selective autophagy transporter proteins such as Ref(2)P, as well as the dTAK1 co-activator dTAB2 which itself interacts with Atg8a (Figure 5.4), and may still target dTAK1 to the autophagosome. Mammalian TAK1 has not yet been reported to associate with LC3/GABARAP directly, but can interact with the selective autophagy receptor p62/SQTSM1 [372]. According to that study, active TAK1/TAB2 kinase complexes associate with p62 in degradation-resistant p62-bodies, via TAK1 binding to the autophagy receptor [372]. These p62-TAK1/TAB2 aggregates can function in turn as signalling platforms and compete with the population of p62 molecules that deliver cargo to autophagosomes for degradation [372]. While some TAK1 and TAB2 can be also be targeted for degradation in this manner, the authors posit that this could be an adaptation of mammalian cells, to exclude certain key components from excessive degradation as the observed TAK1-mediated shift of p62 from an autophagy receptor to a signalling platform [372].

It is tempting to speculate that dTAK1/dTAB2 kinase complexes may also form degradation-resistant inclusion bodies with the *Drosophila* selective autophagy receptors, Ref(2)P, Blue Cheese, and Kenny, similar to the mammalian condition. Ref(2)P and Blue Cheese can bind Ub-moieties on labelled substrates such as dTAK1, which becomes ubiquitinylated during its activation [292]. In my work, I identified a direct LIR-dependent interaction between dTAK1 and Atg8a (Figure 5.2), but the possibility of dTAK1 associating with other SARs and forming distinct signalling hubs that may or may not involve the autophagosome membrane is interesting to explore further. This might also provide further insight regarding the apparent duality of $dTak1^{LIR1}$ flies having an overactive IMD pathway (Figure 6.7), but normal lifespan (Figure 6.8). With the above hypothesis in mind, a sub-population of dTAK1/dTAB2 complexes could theoretically continue to signal from degradation-resistant inclusion bodies or the autophagosome surface, while another portion is still removed and targeted for degradation by selective autophagy.

Mammalian TAK1 is also predicted to possess several canonical — albeit not promising — LIR motifs (sequence analysis by iLIR, data not shown), but an interaction

between the kinase and LC3/GABARAP similar to the dTAK1-Atg8a binding observed here, has not yet been reported in mammals. While this might simply be a matter of a missed research topic, it may also reflect a difference in the regulation of TAK1 activation between fly and mammals, following microbial infection. This is the case for the IKK effector kinase complex, as illustrated in the work of Tusco *et. al*. [33]. The authors suggest, that contrary to the LIR-dependent interaction of Kenny and Atg8a, the mammalian counterpart IKKγ, has secondarily lost the ability for LIR-mediated interactions and relies instead on recognition by selective autophagy receptors via Ub-tagging for its degradation [33]. This arguably represents the evolution history and adaptations between mammalian-specific pathogens and their hosts. Some key signalling components might have foregone the need for LIR motifs, as a means to prevent motif-mimicking microbes from hijacking the host cellular machinery for the latter's benefit [33]. With regards to TAK1, the perceived loss of functional LIR motifs may aid towards leaving the kinase to signal for longer periods. In the context of an acute microbial infection, this could mean the innate immune response remains sufficiently active against LIR motif-mimicking invaders, which could otherwise trick the degradation mechanisms into removing TAK1 and thus weakening the innate immune defences of the host. It is possible that co-evolution of the host-pathogen adaptations in *Drosophila* regarding the manner that IMD signalling components interact with the selective autophagy machinery, have either followed a different path, or the conditions that would favour a similar switch as mammals have not been encountered yet.

8.3 *The Role of SH3PX1 in Modulation of IMD Activity*

SH3PX1 is the single *Drosophila* representative of the mammalian SNX9-group of sorting nexins that contains SNX9, SNX18 and SNX33 [234]. Their domain architecture allows them to function as inducers of membrane curvature [140], [238], [239], [243]. As such, even though these sorting nexins are related with endocytosis and endosomal sorting in particular, they can participate in a wider range of membrane deformation events that also often require a constant supply of phosphoinositides [140], [234], [241], [243], [373]. One prominent example is the formation of the phagophore membrane during autophagy induction. SNX18 and its fly homologue, SH3PX1, are both considered essential for proper autophagosome biogenesis, since they can interact with LC3B/GABARAP and Atg8a respectively, and promote phagophore membrane curvature into the correct conformation [140].

When this work was still at an early stage, the only observation hinting that SH3PX1 may have a role in the IMD pathway came from a Y2H screen that listed SH3PX1 as a potential binding partner of dTAB2, among numerous other interactions identified by the assay [358]. In collaboration with the research team of P. Meier we showed that SH3PX1 does indeed interact with dTAB2 (Figure 7.1). This is the first observation of association of the sorting nexin with an IMD component. Moreover, both this work, as well as that by Zhang *et. al*, have independently shown that SH3PX1 is required for the efficient downregulation of the IMD immune response (Results Chapter Section 7.3 and [242] respectively). In further support of this observation, *Sh3px1*-deficient flies were found by this study to present with chronically elevated systemic levels of IMD-regulated AMPs (Figure 7.5), which suggest an overactive IMD pathway.

An interesting note to add here, is that the dTAK1 band in young and old adult Sh3px1 flies as seen in Figure 7.7 (Results Chapter section 7.3.4), seems to be shifted slightly upwards compared to their respective age-matched WT counterparts. Because this was observed across WB repeats of fly extracts in both 1-week and 2.5-week adult samples, it does not seem very likely that this was due to either gel setting and sample loading inconsistencies, or differences in sample migration due to running buffer and voltage discrepancies. It may therefore be worth considering, whether this dTAK1 band shift can perhaps represent a post-translational modification of dTAK1 that becomes more prominent upon loss of *Sh3px1*. Given the known functions of dTAK1 so far, and the current study's framework, I speculate that at least two of the most probable modifications to expect on the kinase that could in theory result in a slight molecular weight increase and altered migration

dynamics, are phosphorylation and ubiquitination. The conserved *modus operandi* of dTAK1 requires both K63-polyubiquitination and auto-phosphorylation to occur, in order to facilitate activation of dTAK1 and propagate the IMD signal further downstream [294], [363], [374]. Unfortunately, time restraints of the present study did not allow me to investigate the post-translational regulation of dTAK1 via de-ubiquitination and de-phosphorylation assays. dTAK1 evidently accumulates when autophagy is mildly, or more severely impaired by comparison in *Sh3px1*- (Figure 7.7), or *Atg8a*- mutant flies respectively (Figure 6.4). Considering also the observed overactivation of the IMD pathway in both autophagy mutants (for Sh3px1: Figure 7.5; for Atg8a: [340]), as well as dTAK1's regulation by cycles of (de-)/ubiquitination and (de-)/phosphorylation [292], [307], [308], [363], it may reasonable to assume that phosphorylation and ubiquitination of dTAK1 are two of the most probable modifications that could account for the observed band shift of the kinase in autophagy-mutant flies.

There is an extensive interplay between autophagy proteins and key IMD pathway components such as dTAK1, dTAB2, and Kenny/ird5 [33], [340]. This cross-talk unravels the fundamental importance of housekeeping mechanisms such as selective autophagy, that altogether regulate innate immune signalling, so as to maintain the homeostatic balance in cells. As characterization of this regulatory network progresses, new members like SH3PX1 continue to emerge, and the functions they mediate serve to better delineate the elaborate mesh of interactions between different pathways. A collective overview of the regulatory interactions between the IMD components discussed here and the autophagy apparatus, are shown in Figure 8.1 that depicts a top-to-bottom schematic of the IMD signalling pathway.

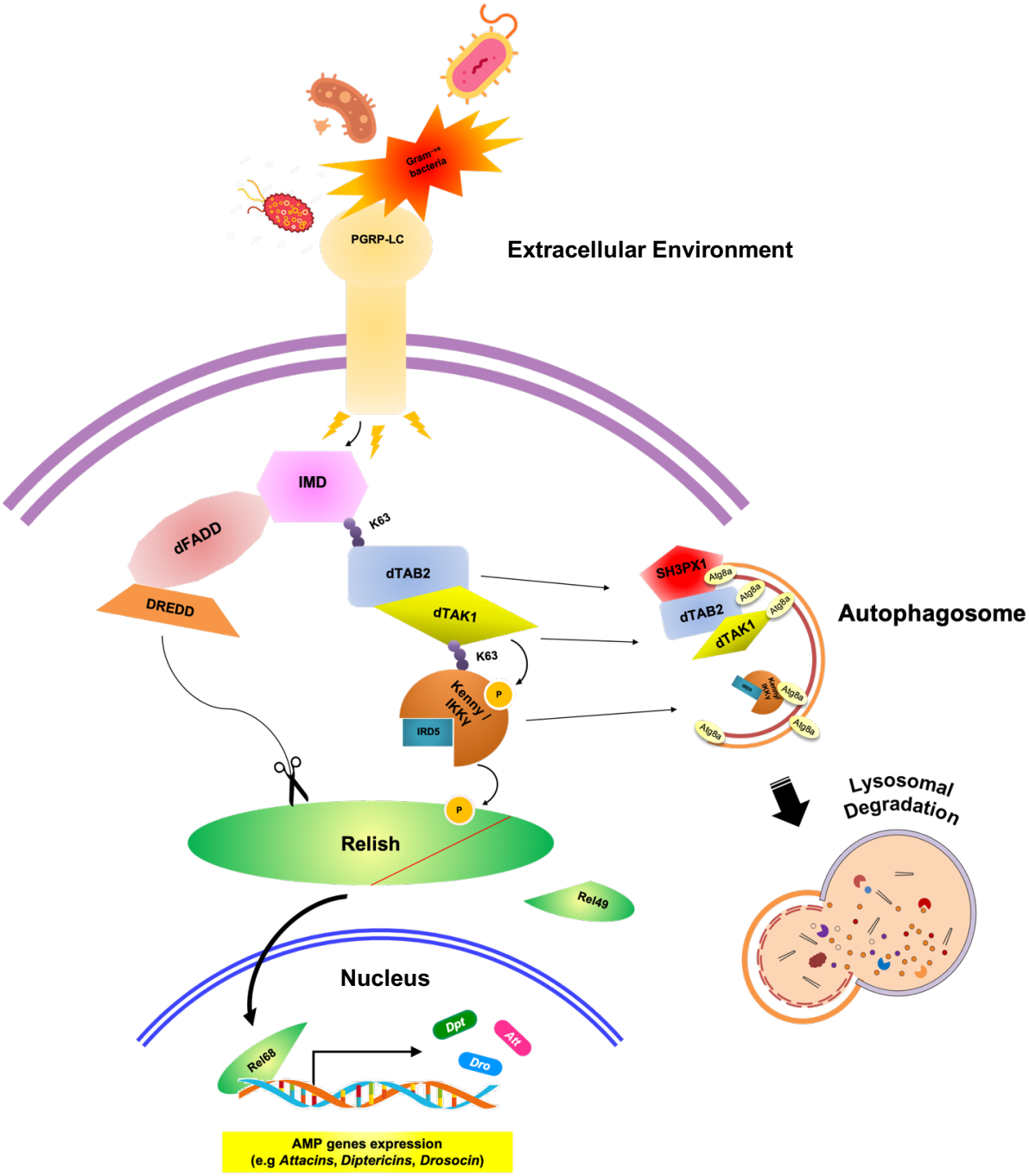

*Figure 8.1. .**An Overview of the IMD pathway Regulation by Selective Autophagy**.* Induction of the IMD pathway leads to receptor-proximal recruitment of adaptor protein complexes, which promote the downstream activation of the dTAK1/dTAB2 initiator kinase complex. dTAK1 further promotes upregulation its effector kinase complex Kenny/ird5, which together with the caspase DREDD phospho-cleave the transcription factor Relish. Rel-68 translocates to the nucleus and drives expression of IMD-regulated AMP-family members mainly from the *Attacin* (*Att*), *Diptericin* (*Dpt*) and *Drosocin* (*Dro*) families. Earlier work from the I. Nezis laboratory identified that selective autophagy downregulates the IMD pathway by degrading the Kenny/ird5 complex ([33]), and the results of this work show that it also degrades the apical dTAK1/dTAB2 complex, with the combined aid from the fly sorting nexin SH3PX1.

8.4 *A Working Model for the Regulation of the IMD pathway by Autophagy*

In an attempt to compile the findings of this current work with existing information from literature, I present here an integrative working model for the proposed interactions between dTAK1, dTAB2, SH3PX1 and Atg8a (Figure 8.2). These interactions may collectively serve to target the dTAK1/dTAB2 complex for autophagic degradation and in turn contribute in the downregulation of the IMD pathway, together with the existing modulatory mechanisms. I also discuss the perceived impact of these interactions with regards to the efficient uptake of the dTAK1/dTAB2 complex by autophagy.

The observations that dTAK1 interacts directly with Atg8a via a LIR motif *in-vitro* (Figure 5.2), and inactivation of the LIR motif reduces co-localization of dTAK1 with Atg8a *in-vivo* (Figure 5.6), together suggest that the kinase is evidently capable of associating with Atg8a directly. The functional LIR motif of dTAK1 seems to be required for the efficient uptake of the kinase complex by selective autophagy, since its inactivation, inversely correlates with a corresponding overactivation of the IMD pathway in flies, despite all other co-interactors and an otherwise working autophagy pathway being in place (Figure 6.7). dTAK1's co-activator, dTAB2 while also able to associate with Atg8a directly *in-vitro* (Figure 5.4), was not found by this study to require a LIR motif in order to do so. It is plausible that if dTAB2 interacts with Atg8a directly *in-vivo* while in a complex with dTAK1, it may be binding to a different site on the same Atg8a moiety, or to neighbouring Atg8a molecules. It has been known that ATG8 proteins can participate simultaneously in LIR-LDS as well as the more recently discovered UIM-UDS interactions [201], [202], since the LDS and UDS crevices are on opposite sides on the autophagy protein, and as such they do not readily obstruct one another [170]. It is presently unclear whether *Drosophila* Atg8a can participate in UIM-UDS interactions, but since this property seems conserved between yeast, plants and human ATG8 [201], it is not unreasonable to expect its conservation in *Drosophila* Atg8a as well. Therefore, it might be argued that dTAB2 and Atg8a interact either in a UIM-UDS manner, or via a non-canonical LIR motif, or finally by a different type of interaction altogether. In the spirit of self-critique, it is still possible that dTAB2 could interact with Atg8a in a LIR-dependent fashion, albeit with one of the identified LIR motifs (e.g LIR3 as seen in Figure 5.3) which were not selected for testing in the present study (for the reasons explained in Results Chapter section 5.2.2).

Because the autophagy machinery is thought to be recruited on-site after induction of IMD signalling, the most probable state of dTAB2 (or at least for a considerable portion of the dTAB2 population) would be expected to be in a multimer complex with dTAK1. Therefore, in the current model, dTAK1 and dTAB2 are depicted as a complex, and for ease of schematic representation, are shown bound to different Atg8a molecules (Figure 8.2). This study was hindered by a lack of proper detection tools to monitor the dTAB2-Atg8a interaction *in-vivo*. These were only made available during the final stages of the project and as such there was not enough time to address this pressing question by the work, but rather make this — as well as similar scientific queries — a priority of future investigations.

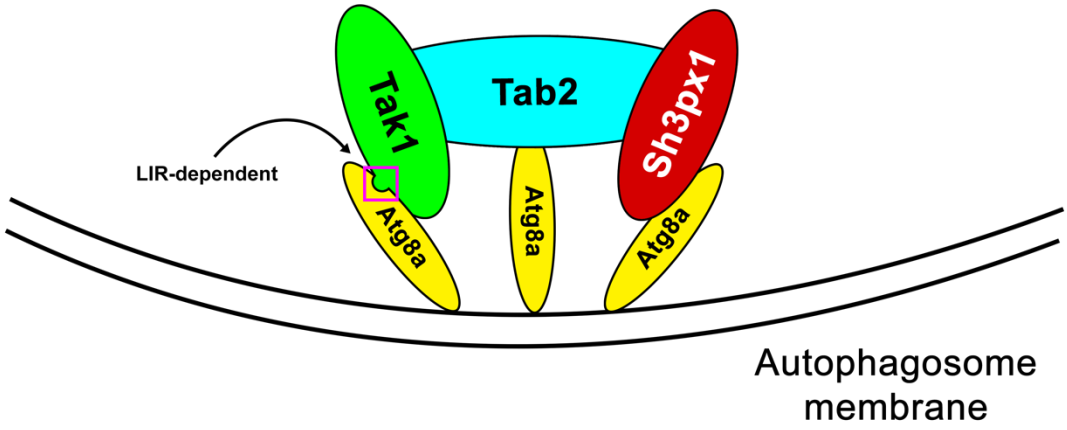

Figure 8.2. ***A Working dTAK1-dTAB2-SH3PX1 Interaction Model with Atg8a***. The 2D schematic reflects a speculative interpretation based on the results from this current study regarding how selective autophagy may regulate the Drosophila IMD pathway at the level of dTAK1/dTAB2/SH3PX1. I posit that both components of the dTAB2/dTAK1 complex interact with Atg8a. dTAK1 binds Atg8a via its functional LIR motif, whereas dTAB2 does not rely on a LIR motif to interact with Atg8a. It is unclear whether dTAB2 and dTAK1 anchor to the same Atg8a molecule, or each associates with a different Atg8a moiety. SH3PX1 binds dTAB2 and Atg8a and likely further stabilizes the dTAB2/dTAK1 complex on the autophagosome membrane. Both the LIR motif of dTAK1 as well as SH3PX1 seem to be individually required for the degradation of the dTAK1/dTAB2 kinase complex by autophagy, as in each's absence the IMD pathway is overactivated.

SH3PX1's interaction with Atg8a was shown before [140], but it is unclear whether the sorting nexin associates with the autophagy protein in a LIR-dependent manner. The analysis of its sequence by the iLIR software predicts several "*W-x-x-L*"-type motifs with

only one having an above-threshold PSSM score, while also being in an ANCHOR region. However, it possesses a Y residue in its HP1-binding site, which as already mentioned, is the least-conserved amino-acid for this particular position [185]. Coupled to the reported caveats of predicting "*W-x-x-L*"-type LIR motifs [339], it is possible that SH3PX1 binds Atg8a in a LIR-independent manner. The sorting nexin however, was found here to associate directly with dTAB2 (Figure 7.1 and P. Meier personal communication).

In the current interaction model, SH3PX1 may serve as a necessary mediator, which ensures the dTAB2/dTAK1 complex is brought in close proximity to the autophagosomal membrane by simultaneously sequestering both dTAB2 and Atg8a. It is conceivable, that loss of *Sh3px1* apart from impairing — without completely abrogating — autophagic flux to a degree [140], may also reduce efficient targeting of the dTAB2/dTAK1 complex to the autophagosome, thus leaving more dTAB2/dTAK1 complexes available for signalling through IMD, as evidenced by the chronically elevated levels of IMD-controlled AMP genes (Figure 7.5).

Several interpretations can be made using the above proposed model in conjunction with the findings of this study. First, it is becoming evident that the LIR motif of dTAK1, as well as the presence of SH3PX1 are both required for the efficient targeting of the dTAK1/dTAB2 complex for autophagic degradation. It would be interesting to characterize the responsible regions on dTAB2 and Atg8a that allow their association. This may in turn help to investigate if impairment of the dTAB2-Atg8a binding leads to similar over-activation of the IMD pathway, or if that interaction is dispensable for the degradation of the kinase complex by selective autophagy.

Secondly, a recognized caveat of the current model is that it does not take into account any possible interactions of dTAK1, dTAB2 and SH3PX1 with the *Drosophila* selective autophagy receptors Ref(2)P, Blue Cheese, and Kenny, as well as any potential interactions with other Atg proteins. Undoubtedly, such interactions can influence the targeting dynamics of the dTAK1/dTAB2 complex, as it was recently described for mammalian TAK1 and p62, which form degradation-resistant signalling aggregates [372].

A final observation that can be made is based on the fact that all three proteins (dTAK1, dTAB2, SH3PX1) are capable *in-vitro* of binding directly to Atg8a. This may perhaps allude to a failsafe mechanism, which increases the likelihood of the dTAK1/dTAB2 complex being efficiently recognized and degraded by autophagy. Taking into account the overall emphasis that cells place on the tight regulation of immune

signalling with regards to maintaining homeostasis, the “failsafe mechanism” explanation does not seem implausible.

Overall, this model provides further mechanistic insight on the manner by which selective autophagy regulates innate immune responses. It also serves as additional evidence for the large, yet still undefined degree that autophagy is involved in modulation of the IMD pathway and the wider extent of innate immune responses.

Concluding Remarks

Efforts into extending our lifespan well past present limits and into unknown territory remain ongoing but a similar rigour for healthspan is often overlooked by comparison. In the context of ageing, autophagy and the innate immune response are two processes that are inversely correlated, where the former progressively declines in function, while the latter becomes increasingly overactivated. These two properties are consequently among the main causes for many deleterious effects associated with late age, such as neurodegeneration, gut dysplasia, frailty, and a shorter lifespan. While it may represent a small contribution to the wider scientific community, this study described a novel mechanistic link between autophagy and innate immunity. This can in part expand our understanding of inflamm-ageing, as well as the molecular mechanisms that progressively widen the gap between autophagy and innate immunity and their homeostatic imbalance. Both these processes are among the most ancestral and therefore, evolutionarily conserved across all eukaryotes. Tissue-specific regulatory interplay between autophagy and innate immunity notwithstanding, it is within reason to expect that the results obtained from *Drosophila* models herein, may offer at least some partial insight into the human mechanics behind chronic inflammation and ageing as well. In conclusion, it is the author's sincere hope for these findings, to provide additional impetus towards the development of more targeted and easily applied strategies, which would tackle the challenge that is the preservation of optimally working homeostatic mechanisms well into old age.

Part IV

APPENDIX &

BIBLIOGRAPHY

Chapter 9

Appendix & Supplementary Information

During my PhD I, together with the generous guidance of my supervisor, Prof. Ioannis Nezis, published a first-author literature review in *Nature: Cell Death & Differentiation*, regarding how the proteolytic enzymes of apoptotic cell death; caspases are involved in the regulation of autophagy:

Panagiotis Tsapras and Ioannis P. Nezis, "**Caspase Involvement In Autophagy**" Nature: *Cell Death & Differentiation*, volume 24, issue number 8, pages 1369–1379 (11 pages), published in print: August 2017. Article doi:10.1038/cdd.2017.43, published online: June 2, 2017.

A print copy of the publication is attached at the end of this PhD Dissertation manuscript.

We have in addition compiled the main findings of this study into a comprehensive manuscript where I sign as the first author and submitted it for publication as original research in the journal *Cell Reports*. At the time of submission of this thesis (30/05/2021), we are expecting a decision from the editor regarding the peer review of this work.

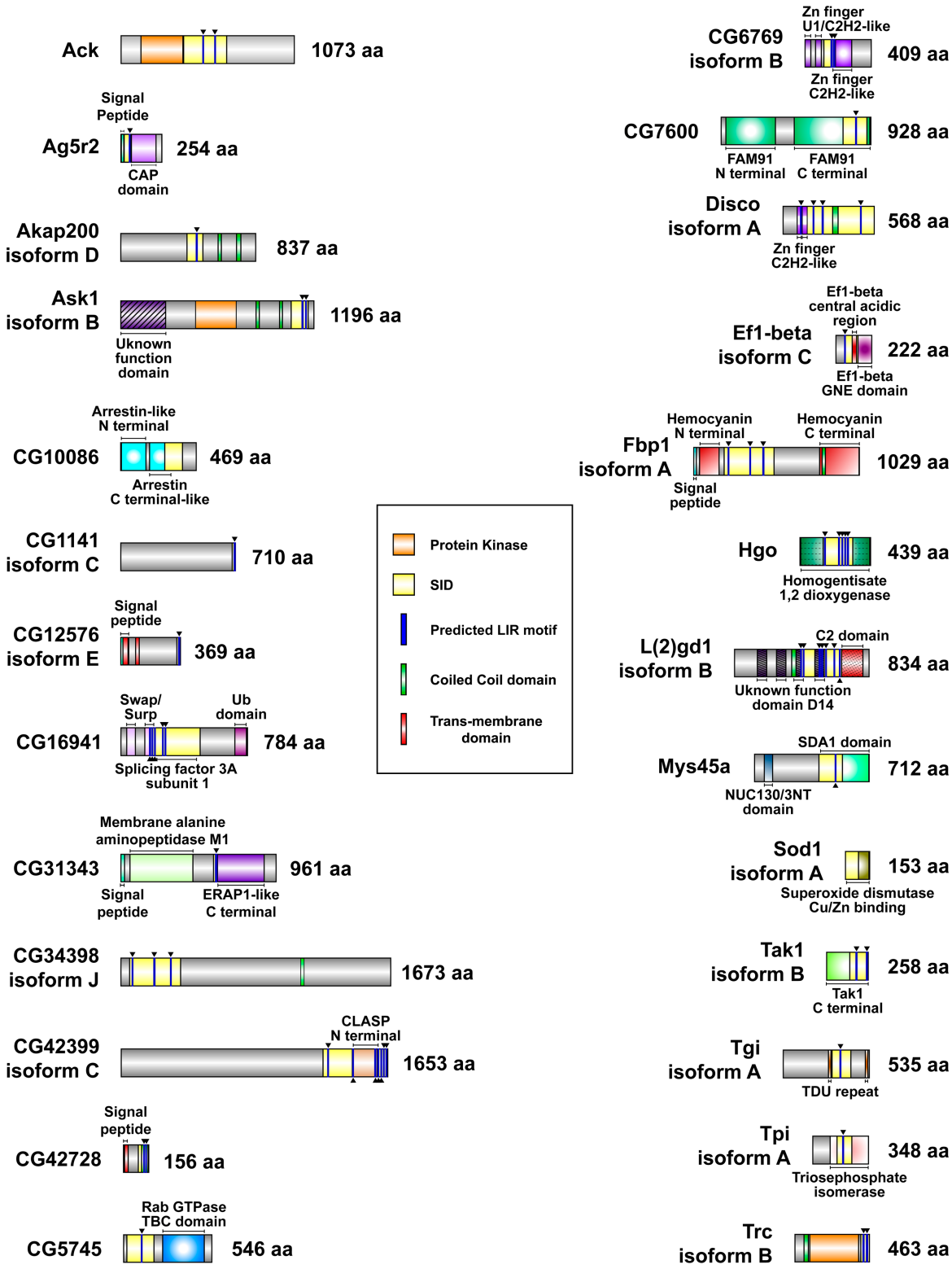

Figure continued on next page…

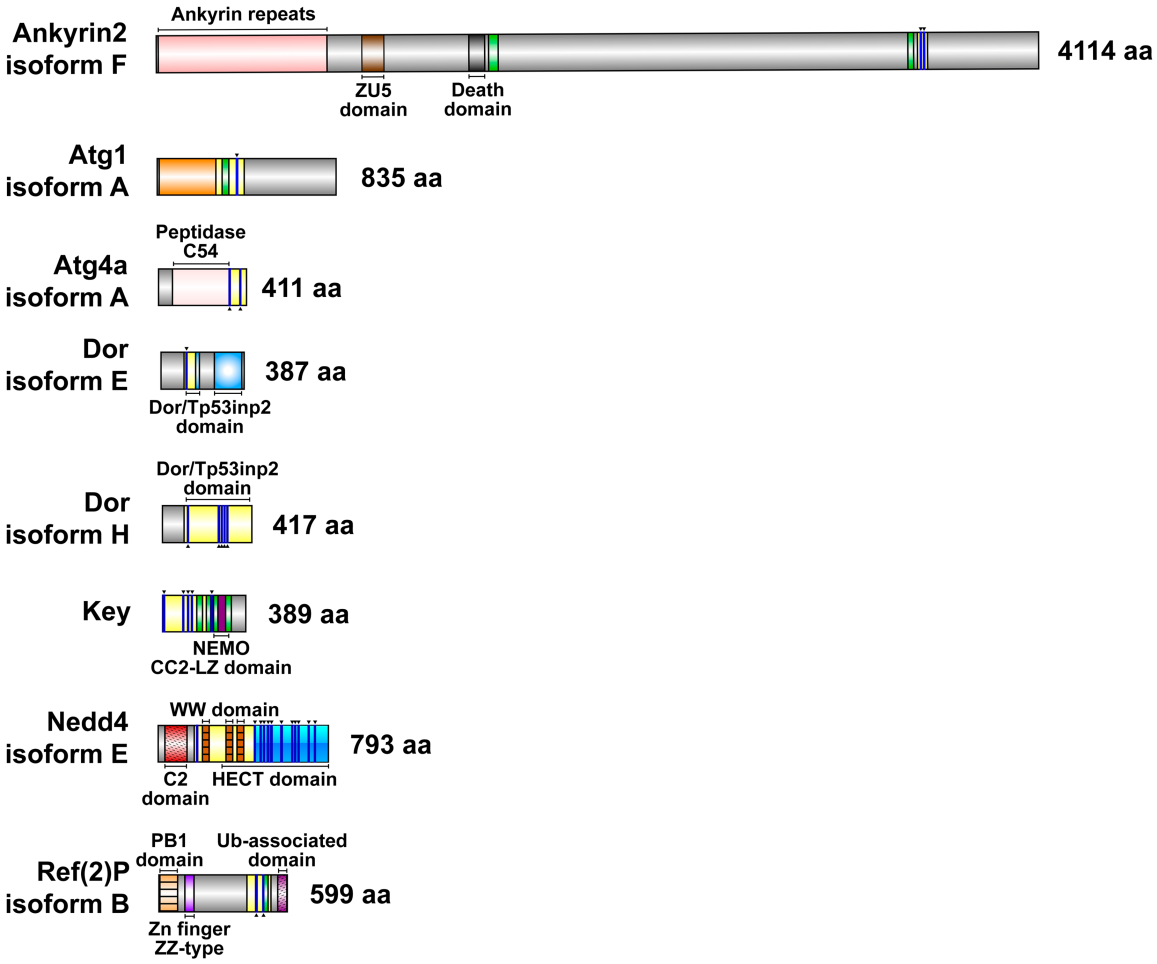

Appendix Figure 9.1. ***Atg8a-Interacting Proteins Identified by Yeast-2-Hybrid Screening***. Amino-acid (aa) length is given for each protein, as well as domain organization, where such domains were identified on the structure. For several proteins the mapped SID region (yellow) is part of, or overlaps with a characterized protein domain (or domains). In such instances, the SID region is depicted at the forefront, while the marker above or below spans the full length of the identified domain. Arrowheads (▼/▲) indicate LIR motifs (blue) predicted within the SID region upon further in-silico analysis. For ease of visualization, the LIR motifs and SID region, as well as Protein Kinase, Coiled Coil and Trans-membrane domains, which occur in multiple proteins, are described in the supplementing legend, and are not mentioned again in name on each protein.

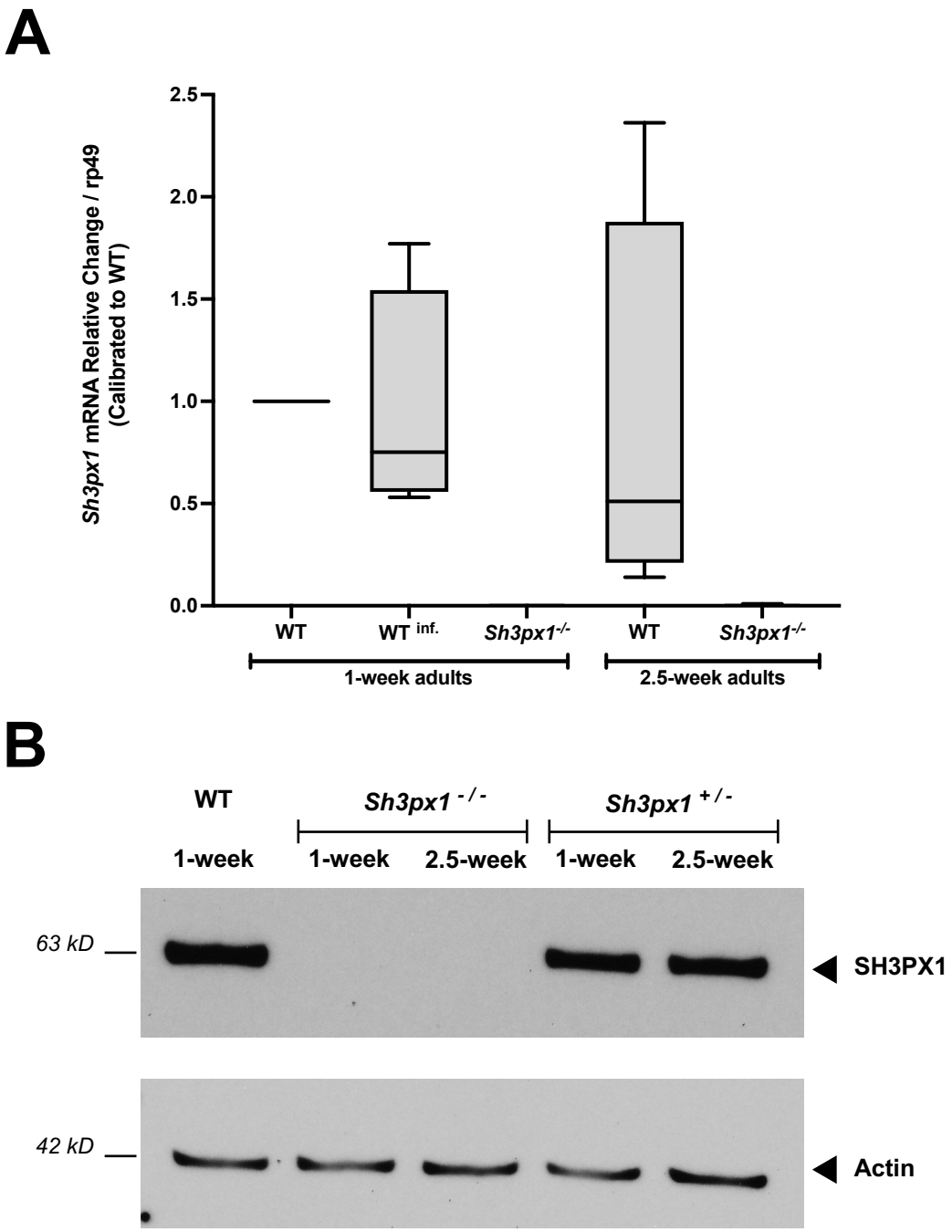

Appendix Figure 9.2. ***Sh3px1 CRISPR Knockout Validation.*** Knockout of *Sh3px1* in the *Sh3px1* CRISPR-mutant flies (provided by G.B. Gonsalvez; Materials section 4.3.3 and [244]) was confirmed by qPCR for the gene (**A**), and WB for the protein (**B**). (**A**) No expression of *Sh3px1* mRNA detected by qPCR in young and old homozygous *Sh3px1* CRISPR-mutant flies (*Sh3px1*$^{-/-}$). *Rp49* was used as internal normalizer and all conditions are calibrated to 1-week WT adults (set as threshold 1). WT infected (WT^{inf}) sample used for additional control of expression. Values are shown as 2^(-ΔΔCt) instead of log-2 fold (ΔΔCt) due to the absence of amplification Ct values from the Sh3px1 samples. (**B**) Absence of SH3PX1 protein in young and old *Sh3px1*$^{-/-}$ flies . Heterozygous Sh3px1 flies, carrying the *Sh3px1* CRISPR construct over the TM6 balancer (*Sh3px1*$^{+/-}$) were used as additional controls for the protein's expression.

Appendix Table 9.1. ***Integrative List of Drosophila Atg8a-Interacting Proteins Identified by Y2H Screen, with LIR Motif Details.*** The accompanying table lists the details of those LIR motifs predicted by the iLIR software that are also within the SID region returned by the Y2H screen for all Atg8a-interacting proteins identified from Drosophila 3rd instar larva and adult head libraries. Predicted motifs outside the SID region are not shown. For each entry in the list, the corresponding NCBI Gene ID number is also given. (Total table length: **15** pages).

Y2H Gene Annotation	NCBI Gene ID	Motif Type	Start Position	End Position	LIR Sequence	PSSM Score	LIR in ANCHOR
>NP_647859.1 activated Cdc42 kinase [Drosophila melanogaster]	38489	WxxL	44	49	AHFDYV	6 (7.4e-01)	No
		WxxL	132	137	GSFGVV	6 (7.4e-01)	No
		WxxL	171	176	DFFREV	5 (1.0e+00)	No
		WxxL	189	194	RLYGVV	4 (1.4e+00)	No
		WxxL	327	332	DPWVGL	16 (3.0e-02)	No
		WxxL	374	379	PTFAAL	7 (5.3e-01)	No
		WxxL	507	512	FAYNKL	6 (7.4e-01)	Yes
		WxxL	580	585	SSFCIL	8 (3.9e-01)	Yes
		WxxL	848	853	IWYEQV	3 (1.9e+00)	Yes
		WxxL	889	894	HSFVAI	9 (2.8e-01)	Yes
		WxxL	911	916	SLYDAV	8 (3.9e-01)	Yes
		WxxL	924	929	TYYGQV	0 (5.0e+00)	Yes
		WxxL	936	941	VLYDEV	6 (7.4e-01)	Yes
		WxxL	985	990	QLYAPV	2 (2.6e+00)	Yes
>NP_524689.2 antigen 5-related 2 [Drosophila melanogaster]	44079	WxxL	56	61	DDYKWV	12 (1.1e-01)	No
		WxxL	149	154	MWFDEV	4 (1.4e+00)	No
		WxxL	199	204	DGWNQV	15 (4.2e-02)	No
		WxxL	237	242	GEFGNL	5 (1.0e+00)	No
		WxxL	246	251	SEWYDV	15 (4.2e-02)	No

Y2H Gene Annotation	NCBI Gene ID	Motif Type	Start Position	End Position	LIR Sequence	PSSM Score	LIR in ANCHOR
>NP_787998.1 A kinase anchor protein 200, isoform D [Drosophila melanogaster]	34170	WxxL	131	136	WSFRSI	4 (1.4e+00)	Yes
		xLIR	469	474	EGFVLV	11 (1.5e-01)	Yes
		WxxL	539	544	IEFESV	9 (2.8e-01)	Yes
>NP_001097535.1 ankyrin 2, isoform F [Drosophila melanogaster]	38863	WxxL	109	114	NGFTPL	9 (2.8e-01)	No
		xLIR	142	147	DGFTPL	13 (7.9e-02)	No
		xLIR	204	209	SGFTPL	11 (1.5e-01)	No
		WxxL	369	374	NGFTPL	9 (2.8e-01)	No
		xLIR	501	506	DMYTAL	14 (5.7e-02)	No
		xLIR	534	539	KGFTPL	10 (2.0e-01)	No
		WxxL	543	548	AKYGHI	5 (1.0e+00)	No
		WxxL	621	626	LEYGAL	7 (5.3e-01)	Yes
		xLIR	633	638	AGFTPL	10 (2.0e-01)	No
		xLIR	699	704	AGYTPL	11 (1.5e-01)	No
		WxxL	732	737	IGYTPL	9 (2.8e-01)	No
		xLIR	776	781	LGYISV	9 (2.8e-01)	Yes
		WxxL	803	808	EKYRVV	7 (5.3e-01)	No
		WxxL	838	843	YGFGPI	4 (1.4e+00)	Yes
		WxxL	865	870	QPYRYL	3 (1.9e+00)	Yes
		WxxL	1040	1045	PHFASL	4 (1.4e+00)	No
		WxxL	1108	1113	PQYFAV	5 (1.0e+00)	No
		WxxL	1231	1236	AQWEDV	15 (4.2e-02)	No
		WxxL	1276	1281	ELYKEV	6 (7.4e-01)	No
		WxxL	1322	1327	ELYTEV	8 (3.9e-01)	No
		WxxL	1463	1468	KDWIQL	20 (8.4e-03)	No

Y2H Gene Annotation	NCBI Gene ID	Motif Type	Start Position	End Position	LIR Sequence	PSSM Score	LIR in ANCHOR
		WxxL	1505	1510	PNYDIL	12 (1.1e-01)	No
		WxxL	1727	1732	VTFSRV	4 (1.4e+00)	No
		xLIR	1745	1750	EDFLEI	16 (3.0e-02)	Yes
		WxxL	2040	2045	DTFHKI	10 (2.0e-01)	No
		WxxL	2092	2097	ETFHKI	8 (3.9e-01)	Yes
		WxxL	2552	2557	EPFENL	7 (5.3e-01)	Yes
		WxxL	2884	2889	SSFIGI	9 (2.8e-01)	Yes
		xLIR	3010	3015	STFEEL	13 (7.9e-02)	No
		WxxL	3177	3182	AGYPSI	7 (5.3e-01)	Yes
		WxxL	3290	3295	ENFDDI	11 (1.5e-01)	Yes
		WxxL	3467	3472	QDYSNI	10 (2.0e-01)	Yes
		xLIR	3562	3567	DSFEMV	15 (4.2e-02)	No
		xLIR	3574	3579	DEFVII	16 (3.0e-02)	Yes
		WxxL	3741	3746	QEFESL	11 (1.5e-01)	Yes
		WxxL	3795	3800	KDFEGL	13 (7.9e-02)	Yes
		WxxL	4073	4078	DSFPGV	6 (7.4e-01)	Yes
>NP_996240.1 apoptotic signal-regulating kinase 1, isoform B [Drosophila melanogaster]	42366	WxxL	127	132	RIYKDI	6 (7.4e-01)	No
		WxxL	160	165	NEYAGI	6 (7.4e-01)	No
		WxxL	205	210	SEYWDV	8 (3.9e-01)	No
		WxxL	211	216	ATFFEI	8 (3.9e-01)	No
		WxxL	292	297	IRFPIL	2 (2.6e+00)	No
		xLIR	307	312	PSYVTI	13 (7.9e-02)	No
		WxxL	339	344	HDFLFV	12 (1.1e-01)	No
		WxxL	360	365	CAYLYV	3 (1.9e+00)	No
		WxxL	384	389	KFYDMI	9 (2.8e-01)	No
		WxxL	397	402	VVFVNL	3 (1.9e+00)	No

Y2H Gene Annotation	NCBI Gene ID	Motif Type	Start Position	End Position	LIR Sequence	PSSM Score	LIR in ANCHOR
		WxxL	427	432	GTYGTV	7 (5.3e-01)	No
		WxxL	485	490	NGFFKI	6 (7.4e-01)	No
		WxxL	506	511	TKWGPL	10 (2.0e-01)	No
		WxxL	550	555	NTYSGV	5 (1.0e+00)	No
		WxxL	617	622	PPFIEL	8 (3.9e-01)	No
		WxxL	778	783	DGFYRL	9 (2.8e-01)	No
		WxxL	881	886	LRYHCI	2 (2.6e+00)	No
		WxxL	1124	1129	RLWKLI	12 (1.1e-01)	No
		WxxL	1156	1161	SSFALI	8 (3.9e-01)	No
>NP_648601.1 Autophagy-related 1, isoform A [Drosophila melanogaster]	39454	WxxL	18	23	GAFAVV	4 (1.4e+00)	No
		xLIR	96	101	ADYLSV	14 (5.7e-02)	No
		WxxL	206	211	IVYQCL	3 (1.9e+00)	No
		xLIR	369	374	DDFVLV	17 (2.2e-02)	Yes
>NP_608563.1 Autophagy-related 4a, isoform A [Drosophila melanogaster]	33283	WxxL	55	60	KKYNAI	6 (7.4e-01)	No
		WxxL	80	85	HGFSPL	6 (7.4e-01)	No
		xLIR	129	134	ATYLKI	11 (1.5e-01)	No
		WxxL	136	141	NRFEDV	6 (7.4e-01)	No
		WxxL	143	148	NSFYSI	6 (7.4e-01)	No
		WxxL	182	187	DDWSSL	22 (4.4e-03)	No
		WxxL	210	215	GSWKPL	15 (4.2e-02)	No
		xLIR	323	328	DSFESL	14 (5.7e-02)	No
		WxxL	379	384	DSFAIV	10 (2.0e-01)	No

Y2H Gene Annotation	NCBI Gene ID	Motif Type	Start Position	End Position	LIR Sequence	PSSM Score	LIR in ANCHOR
>NP_649736.3 uncharacterized protein Dmel_CG10086 [Drosophila melanogaster]	40920	WxxL	121	126	GAYGHI	4 (1.4e+00)	No
		WxxL	146	151	VGFTVL	9 (2.8e-01)	No
		WxxL	197	202	GQFMLI	6 (7.4e-01)	No
>NP_001286159.1 uncharacterized protein Dmel_CG11141, isoform C [Drosophila melanogaster]	35672	WxxL	11	16	REWAPL	16 (3.0e-02)	No
		WxxL	179	184	EAYEIV	10 (2.0e-01)	No
		WxxL	190	195	QSYLLV	9 (2.8e-01)	No
		WxxL	197	202	TLYRCI	1 (3.6e+00)	No
		WxxL	320	325	SNFRQL	6 (7.4e-01)	No
		WxxL	398	403	VIFNPL	1 (3.6e+00)	No
		WxxL	467	472	EIFRRI	3 (1.9e+00)	No
		xLIR	703	708	SEWEFL	21 (6.1e-03)	
>NP_001259775.1 uncharacterized protein Dmel_CG12576, isoform E [Drosophila melanogaster]	33135	WxxL	11	16	STFHCI	6 (7.4e-01)	No
		WxxL	34	39	VLFLGL	2 (2.6e+00)	No
		WxxL	49	54	CSFRVV	4 (1.4e+00)	No
		WxxL	119	124	YTFKLL	6 (7.4e-01)	No
		WxxL	137	142	LNYNNL	4 (1.4e+00)	No
		xLIR	358	363	SDFEIL	17 (2.2e-02)	No

Y2H Gene Annotation	NCBI Gene ID	Motif Type	Start Position	End Position	LIR Sequence	PSSM Score	LIR in ANCHOR
>NP_650583.1 splicing factor 3a subunit 1 [Drosophila melanogaster]	42048	WxxL	65	70	PKFNFL	6 (7.4e-01)	Yes
		xLIR	133	138	PEFEFI	13 (7.9e-02)	No
		WxxL	178	183	FQFDFL	11 (1.5e-01)	No
		WxxL	191	196	QYFTKL	5 (1.0e+00)	No
		WxxL	198	203	EQYTKV	9 (2.8e-01)	No
		WxxL	258	263	VAYAQI	2 (2.6e+00)	Yes
		WxxL	266	271	HDFVVV	13 (7.9e-02)	Yes
		WxxL	761	766	MAFYNL	0 (5.0e+00)	Yes
>NP_732652.1 uncharacterized protein Dmel_CG31343 [Drosophila melanogaster]	326133	WxxL	7	12	NSFSLI	7 (5.3e-01)	No
		WxxL	70	75	ELWTNV	11 (1.5e-01)	No
		xLIR	134	139	REFLVL	13 (7.9e-02)	No
		WxxL	158	163	INYTGI	6 (7.4e-01)	No
		xLIR	220	225	PSYTAI	11 (1.5e-01)	No
		WxxL	287	292	ALWSGL	9 (2.8e-01)	No
		WxxL	299	304	ASYFGV	5 (1.0e+00)	No
		WxxL	363	368	MWFGDL	-1 (6.9e+00)	No
		WxxL	372	377	KWWTYL	11 (1.5e-01)	No
		WxxL	381	386	EGFATL	9 (2.8e-01)	No
		WxxL	514	519	AGYPLL	7 (5.3e-01)	No
		WxxL	548	553	TWYVPL	6 (7.4e-01)	No
		xLIR	588	593	DDWIIV	24 (2.3e-03)	No
		WxxL	599	604	GYYRTL	5 (1.0e+00)	No
		WxxL	608	613	QNYGLI	5 (1.0e+00)	No
		xLIR	635	640	DTYIFV	14 (5.7e-02)	No
		WxxL	699	704	PIFDKI	7 (5.3e-01)	No
		WxxL	716	721	NNYLRI	8 (3.9e-01)	No

Y2H Gene Annotation	NCBI Gene ID	Motif Type	Start Position	End Position	LIR Sequence	PSSM Score	LIR in ANCHOR
		WxxL	772	777	EIYSRV	4 (1.4e+00)	No
		WxxL	807	812	LDFLRL	12 (1.1e-01)	No
		WxxL	852	857	EAYANL	4 (1.4e+00)	No
		WxxL	913	918	SNFAWL	4 (1.4e+00)	No
>NP_001162914.2 uncharacterized protein Dmel_CG34398,isoform J [Drosophila melanogaster]	5740462	WxxL	41	46	REWQRI	18 (1.6e-02)	No
		WxxL	69	74	NSYGKI	6 (7.4e-01)	Yes
		WxxL	205	210	VDFVVI	14 (5.7e-02)	Yes
		WxxL	307	312	DLYGQL	5 (1.0e+00)	Yes
		WxxL	409	414	GEWRRV	13 (7.9e-02)	No
		WxxL	550	555	SAFRPV	4 (1.4e+00)	No
		WxxL	673	678	ETWRDV	14 (5.7e-02)	Yes
		WxxL	1088	1093	ALYDSL	8 (3.9e-01)	Yes
		WxxL	1175	1180	SSWSRL	15 (4.2e-02)	Yes
		WxxL	1280	1285	LSYFGV	4 (1.4e+00)	Yes
		WxxL	1327	1332	TKWQLL	14 (5.7e-02)	Yes
		WxxL	1368	1373	HCYENI	4 (1.4e+00)	Yes
		WxxL	1665	1670	KRFRSL	4 (1.4e+00)	Yes
>NP_001259801.1 uncharacterized protein Dmel_CG42399, isoform C [Drosophila melanogaster]	33176	WxxL	1	6	MFFRRV	-2 (9.5e+00)	Yes
		WxxL	83	88	PLWEHI	14 (5.7e-02)	No
		WxxL	264	269	HEFEEI	11 (1.5e-01)	No
		WxxL	280	285	SRYYQL	5 (1.0e+00)	No
		WxxL	304	309	GAWRAL	11 (1.5e-01)	No
		xLIR	645	650	KSWEDL	18 (1.6e-02)	No

Y2H Gene Annotation	NCBI Gene ID	Motif Type	Start Position	End Position	LIR Sequence	PSSM Score	LIR in ANCHOR
		WxxL	810	815	AVYSLL	5 (1.0e+00)	No
		WxxL	942	947	PSFRQV	5 (1.0e+00)	Yes
		WxxL	1023	1028	DSFIQL	12 (1.1e-01)	Yes
		WxxL	1072	1077	PNYPKV	5 (1.0e+00)	Yes
		xLIR	1096	1101	DSFTKL	13 (7.9e-02)	Yes
		WxxL	1208	1213	EAFGEL	5 (1.0e+00)	Yes
		WxxL	1279	1284	NSFVVV	10 (2.0e-01)	Yes
		WxxL	1435	1440	KTFDQL	10 (2.0e-01)	No
		WxxL	1572	1577	LLFRLV	1 (3.6e+00)	No
		WxxL	1594	1599	DKFFVV	8 (3.9e-01)	No
		WxxL	1617	1622	SLFRAL	4 (1.4e+00)	No
		WxxL	1626	1631	HNYQRL	7 (5.3e-01)	No
		WxxL	1639	1644	RTYRNV	6 (7.4e-01)	No
>NP_001189111.1 uncharacterized protein Dmel_CG42728 [Drosophila melanogaster]	10178859	WxxL	12	17	IVYGLI	1 (3.6e+00)	No
		WxxL	45	50	CNYSLI	5 (1.0e+00)	No
		WxxL	125	130	YFYYCV	-2 (9.5e+00)	No
		xLIR	131	136	DGFLLV	12 (1.1e-01)	No
>NP_650941.3 uncharacterized protein Dmel_CG5745 [Drosophila melanogaster]	42498	WxxL	110	115	DEFCII	11 (1.5e-01)	Yes
		WxxL	223	228	EKFQVV	9 (2.8e-01)	Yes
		WxxL	242	247	ISWSGV	10 (2.0e-01)	No
		WxxL	254	259	VSWRLL	12 (1.1e-01)	No
		WxxL	279	284	QGYQDL	10 (2.0e-01)	No
		WxxL	286	291	HNYFRV	3 (1.9e+00)	No

Y2H Gene Annotation	NCBI Gene ID	Motif Type	Start Position	End Position	LIR Sequence	PSSM Score	LIR in ANCHOR
		WxxL	300	305	DTYRQI	10 (2.0e-01)	No
		WxxL	326	331	EMFERI	11 (1.5e-01)	No
		WxxL	353	358	TPFFIV	3 (1.9e+00)	No
		WxxL	389	394	DSFWCL	7 (5.3e-01)	No
		WxxL	405	410	YIFAQL	0 (5.0e+00)	No
		WxxL	499	504	NDFQGL	11 (1.5e-01)	No
>NP_001259663.1 uncharacterized protein Dmel_CG6769, isoform B [Drosophila melanogaster]	32770	WxxL	2	7	SHFTCL	6 (7.4e-01)	No
		xLIR	163	168	DDFEDI	18 (1.6e-02)	No
		xLIR	176	181	DEWDKI	22 (4.4e-03)	No
		WxxL	238	243	NYFICL	3 (1.9e+00)	No
		WxxL	250	255	KTFYSL	7 (5.3e-01)	No
		xLIR	311	316	DEYQLV	14 (5.7e-02)	No
		WxxL	356	361	SEYRAL	10 (2.0e-01)	No
>NP_648453.1 uncharacterized protein Dmel_CG7600 [Drosophila melanogaster]	39267	WxxL	35	40	VTWELL	16 (3.0e-02)	No
		WxxL	83	88	QRYYEL	5 (1.0e+00)	No
		WxxL	118	123	NYYLDV	5 (1.0e+00)	No
		xLIR	132	137	KSYDTL	13 (7.9e-02)	No
		WxxL	154	159	NEYLAL	11 (1.5e-01)	No
		WxxL	193	198	EPWWRL	10 (2.0e-01)	No
		WxxL	246	251	LIYLDV	5 (1.0e+00)	No
		WxxL	275	280	DYFENL	8 (3.9e-01)	No
		WxxL	401	406	FSFANL	6 (7.4e-01)	Yes
		WxxL	562	567	KKYKFI	8 (3.9e-01)	No

Y2H Gene Annotation	NCBI Gene ID	Motif Type	Start Position	End Position	LIR Sequence	PSSM Score	LIR in ANCHOR
		WxxL	597	602	PMWSKL	15 (4.2e-02)	No
		WxxL	631	636	LGYGKL	6 (7.4e-01)	No
		WxxL	651	656	ENFRSL	7 (5.3e-01)	No
		xLIR	833	838	EEWTLL	19 (1.2e-02)	No
>NP_001097503.1 diabetes and obesity regulated, isoform E [Drosophila melanogaster]	38543	WxxL	116	121	DEWYIV	18 (1.6e-02)	Yes
		WxxL	257	262	SVYHSI	5 (1.0e+00)	Yes
		WxxL	270	275	DSFVNL	12 (1.1e-01)	Yes
>NP_001246625.1 diabetes and obesity regulated, isoform H [Drosophila melanogaster]	38543	WxxL	116	121	DEWYIV	18 (1.6e-02)	Yes
		WxxL	261	266	PCFTSI	6 (7.4e-01)	Yes
		WxxL	274	279	SPFENL	7 (5.3e-01)	Yes
		WxxL	287	292	SVYHSI	5 (1.0e+00)	Yes
		WxxL	300	305	DSFVNL	12 (1.1e-01)	Yes
>NP_001286506.1 eukaryotic translation elongation factor 1 beta, isoform C [Drosophila melanogaster]	45249	WxxL	1	6	MAFGDV	0 (5.0e+00)	No
		xLIR	36	41	SVFDAL	8 (3.9e-01)	No
		WxxL	54	59	RWYRHI	4 (1.4e+00)	Yes
		WxxL	217	222	AAFNKI	4 (1.4e+00)	No

Y2H Gene Annotation	NCBI Gene ID	Motif Type	Start Position	End Position	LIR Sequence	PSSM Score	LIR in ANCHOR
>NP_524065.1 Fat body protein 1, isoform A [Drosophila melanogaster]	39566	WxxL	114	119	GIYRLL	4 (1.4e+00)	No
		WxxL	123	128	QDFDTL	15 (4.2e-02)	No
		WxxL	215	220	MPWREI	10 (2.0e-01)	No
		WxxL	350	355	DRFQRL	9 (2.8e-01)	Yes
		WxxL	431	436	QRFMGL	2 (2.6e+00)	Yes
		xLIR	878	883	RDFVLL	16 (3.0e-02)	No
		WxxL	916	921	EIYRQV	3 (1.9e+00)	No
>AAF58986.2 mystery 45A [Drosophila melanogaster]	35925	WxxL	36	41	QHFLSL	6 (7.4e-01)	No
		WxxL	68	73	QCYPAV	1 (3.6e+00)	No
		WxxL	86	91	KNYATV	7 (5.3e-01)	No
		WxxL	120	125	ELFFQL	3 (1.9e+00)	No
		WxxL	164	169	FMYSML	12 (1.1e-01)	No
		WxxL	206	211	GCFSKV	3 (1.9e+00)	No
		WxxL	282	287	FNFSGI	6 (7.4e-01)	No
		WxxL	299	304	GLFKQL	3 (1.9e+00)	No
		WxxL	334	339	GFYPYI	1 (3.6e+00)	No
		WxxL	502	507	GEWVNV	16 (3.0e-02)	Yes
		WxxL	592	597	EDFKRI	12 (1.1e-01)	Yes
		xLIR	619	624	AEFVKL	12 (1.1e-01)	Yes
		WxxL	677	682	KNFGML	7 (5.3e-01)	Yes
	39251	No LIR detected					

Y2H Gene Annotation	NCBI Gene ID	Motif Type	Start Position	End Position	LIR Sequence	PSSM Score	LIR in ANCHOR
>NP_476735.1 superoxide dismutase 1 [Drosophila melanogaster]							
>AHN59968.1 TGF-beta activated kinase 1, isoform B [Drosophila melanogaster]	39659	xLIR	137	142	KEYLSV	11 (1.5e-01)	Yes
		WxxL	183	188	SLYNNL	3 (1.9e+00)	Yes
		xLIR	247	252	EGWVVI	20 (8.4e-03)	Yes
>NP_729916.1 Tondu-domain-containing growth inhibitor, isoform A [Drosophila melanogaster]	39521	WxxL	5	10	LDYRCL	9 (2.8e-01)	No
		WxxL	100	105	AMFYNV	4 (1.4e+00)	Yes
		WxxL	146	151	QPWRDL	10 (2.0e-01)	Yes
		WxxL	295	300	ENYAAL	8 (3.9e-01)	Yes
		xLIR	353	358	SGWVIL	20 (8.4e-03)	Yes
		WxxL	524	529	ETWKKL	16 (3.0e-02)	Yes
>NP_788764.1 triose phosphate isomerase, isoform A [Drosophila melanogaster]	43582	WxxL	63	68	GKFTAV	7 (5.3e-01)	No
		xLIR	188	193	ADWVIL	23 (3.2e-03)	No
		WxxL	255	260	KDWKNV	16 (3.0e-02)	No
		WxxL	262	267	VAYEPV	6 (7.4e-01)	No
		xLIR	338	343	PEFVDI	12 (1.1e-01)	No

Y2H Gene Annotation	NCBI Gene ID	Motif Type	Start Position	End Position	LIR Sequence	PSSM Score	LIR in ANCHOR
>NP_523362.2 disconnected, isoform A [Drosophila melanogaster]	32579	WxxL	109	114	IHFSAV	2 (2.6e+00)	No
		WxxL	188	193	VAFPGL	-1 (6.9e+00)	Yes
		WxxL	245	250	NDFVYV	12 (1.1e-01)	Yes
		WxxL	482	487	PMWSLL	15 (4.2e-02)	Yes
>sp|Q9VKJ0.3|HGD_DROME RecName: Full=Homogentisate 1,2-dioxygenase	34552	WxxL	2	7	SEYKYL	10 (2.0e-01)	No
		WxxL	60	65	WLYRKL	1 (3.6e+00)	No
		xLIR	153	158	GDFLIV	14 (5.7e-02)	No
		xLIR	241	246	KDFQVI	15 (4.2e-02)	No
		WxxL	261	266	TVFDVV	6 (7.4e-01)	No
		WxxL	280	285	SKFMVI	8 (3.9e-01)	No
		WxxL	296	301	SIFTVL	8 (3.9e-01)	No
		WxxL	340	345	SEFMGL	8 (3.9e-01)	No
		WxxL	425	430	ECWQAL	14 (5.7e-02)	No
>AFH08256.1 kenny, isoform B [Drosophila melanogaster]	37967	xLIR	5	10	ESFVIL	13 (7.9e-02)	Yes
		WxxL	96	101	SQFPSL	5 (1.0e+00)	No
		WxxL	119	124	TEYLAL	11 (1.5e-01)	No
		WxxL	136	141	LNYHNL	4 (1.4e+00)	No
		WxxL	228	233	HSFEFV	9 (2.8e-01)	No
		WxxL	370	375	KSFNAL	7 (5.3e-01)	Yes

Y2H Gene Annotation	NCBI Gene ID	Motif Type	Start Position	End Position	LIR Sequence	PSSM Score	LIR in ANCHOR
>NP_001245976.1 lethal (2) giant discs 1, isoform B [Drosophila melanogaster]	34543	WxxL	287	292	LQFLKV	6 (7.4e-01)	Yes
		WxxL	294	299	KQFDVV	9 (2.8e-01)	Yes
		WxxL	370	375	EKYQSV	9 (2.8e-01)	Yes
		WxxL	389	394	RRFGRI	3 (1.9e+00)	Yes
		WxxL	411	416	VPYDEL	8 (3.9e-01)	Yes
		WxxL	420	425	PGFGPL	6 (7.4e-01)	Yes
		xLIR	526	531	KEYLKI	12 (1.1e-01)	Yes
		xLIR	533	538	KGFDSL	11 (1.5e-01)	Yes
		WxxL	565	570	ASFAIV	7 (5.3e-01)	No
		WxxL	616	621	NRFENL	5 (1.0e+00)	No
		WxxL	650	655	RSFNIV	8 (3.9e-01)	No
		WxxL	685	690	DTYVRV	13 (7.9e-02)	No
		WxxL	728	733	RQFQRI	8 (3.9e-01)	No
		WxxL	827	832	EKWLVL	17 (2.2e-02)	No
>NP_001014491.1 refractory to sigma P, isoform B [Drosophila melanogaster]	35246	WxxL	28	33	QNYTIL	10 (2.0e-01)	No
		WxxL	138	143	FRYKCV	4 (1.4e+00)	No
		WxxL	342	347	EMFSKI	9 (2.8e-01)	Yes
		xLIR	452	457	PEWQLI	18 (1.6e-02)	Yes
		WxxL	485	490	RDFGQL	10 (2.0e-01)	Yes
>NP_001262071.1 tricornered, isoform B [Drosophila melanogaster]	40165	WxxL	33	38	NYYSNL	2 (2.6e+00)	Yes
		WxxL	78	83	TEYLRL	10 (2.0e-01)	No
		xLIR	91	96	EDFEAL	16 (3.0e-02)	No

Y2H Gene Annotation	NCBI Gene ID	Motif Type	Start Position	End Position	LIR Sequence	PSSM Score	LIR in ANCHOR
		WxxL	102	107	GAFGEV	3 (1.9e+00)	No
		WxxL	248	253	DFYRDL	6 (7.4e-01)	No
		WxxL	289	294	LAYSTV	5 (1.0e+00)	No
		WxxL	314	319	CDWWSL	14 (5.7e-02)	No
		WxxL	322	327	IMYEML	12 (1.1e-01)	No
		WxxL	340	345	DTYRKV	10 (2.0e-01)	No
		WxxL	392	397	PFFRGV	-1 (6.9e+00)	No
		WxxL	423	428	DEFPDV	9 (2.8e-01)	No
		xLIR	445	450	KDWVFI	23 (3.2e-03)	No
>NP_996116.1 Nedd4, isoform E [Drosophila melanogaster]	39958	WxxL	54	59	DPYVRI	11 (1.5e-01)	No
		xLIR	179	184	GEWEHV	18 (1.6e-02)	No
		WxxL	448	453	DSYRII	12 (1.1e-01)	No
		WxxL	476	481	LDYGGL	8 (3.9e-01)	No
		WxxL	483	488	REWFYL	15 (4.2e-02)	No
		WxxL	495	500	NPYYGL	2 (2.6e+00)	No
		WxxL	526	531	SYFKFI	6 (7.4e-01)	No
		WxxL	573	578	EYYNSL	5 (1.0e+00)	No
		xLIR	623	628	DEYIKL	15 (4.2e-02)	No
		WxxL	630	635	IEWRFV	13 (7.9e-02)	No
		WxxL	647	652	DGFGSI	9 (2.8e-01)	No
		WxxL	700	705	WFWRAV	5 (1.0e+00)	No
		WxxL	729	734	NGFKEL	8 (3.9e-01)	No
		WxxL	759	764	TCFNRL	1 (3.6e+00)	No
		WxxL	770	775	EGYLQL	11 (1.5e-01)	No
		WxxL	787	792	QGFAGV	3 (1.9e+00)	No

BIBLIOGRAPHY

Chapter 10

REFERENCE LIST

[1] Lawson, C., "The Ubiquity of the Tithonus Error," *Fight Aging*. https://www.fightaging.org/archives/2004/03/the-ubiquity-of-the-tithonus-error/ (accessed Feb. 14, 2021).

[2] Vaiserman, A. M., Lushchak, O. V., & Koliada, A. K., "Anti-aging pharmacology: Promises and pitfalls," *Ageing Res. Rev.*, vol. 31, pp. 9–35, Nov. 2016, doi: 10.1016/j.arr.2016.08.004.

[3] Holliday, R., "Understanding ageing," *Philos. Trans. R. Soc. London. Ser. B Biol. Sci.*, vol. 352, no. 1363, pp. 1793–1797, Dec. 1997, doi: 10.1098/rstb.1997.0163.

[4] Fried, L. P. … McBurnie, M. A., "Frailty in Older Adults: Evidence for a Phenotype," *Journals Gerontol. Ser. A Biol. Sci. Med. Sci.*, vol. 56, no. 3, pp. M146–M157, Mar. 2001, doi: 10.1093/gerona/56.3.M146.

[5] Balcombe, N. R. & Sinclair, A., "Ageing: definitions, mechanisms and the magnitude of the problem," *Best Pract. Res. Clin. Gastroenterol.*, vol. 15, no. 6, pp. 835–849, Dec. 2001, doi: 10.1053/bega.2001.0244.

[6] da Costa, J. P., Vitorino, R., Silva, G. M., Vogel, C., Duarte, A. C., & Rocha-Santos, T., "A synopsis on aging—Theories, mechanisms and future prospects," *Ageing Research Reviews*, vol. 29. Elsevier Ireland Ltd, pp. 90–112, Aug. 01, 2016. doi: 10.1016/j.arr.2016.06.005.

[7] Rattan, S. I. S., "Theories of biological aging: Genes, proteins, and free radicals," *Free Radic. Res.*, vol. 40, no. 12, pp. 1230–1238, Jan. 2006, doi: 10.1080/10715760600911303.

[8] Ruggeri, A., "Do we really live longer than our ancestors?," *BBC Future*, Oct. 03, 2018. https://www.bbc.com/future/article/20181002-how-long-did-ancient-people-live-life-span-versus-longevity (accessed Feb. 13, 2020).

[9] Roser, M., Ortiz-Ospina, E., & Ritchie, H., "Life Expectancy - Our World in Data," *Our World in Data*, 2020. https://ourworldindata.org/life-expectancy (accessed May 18, 2020).

[10] Franceschi, C., Bonafè, M., Valensin, S., Olivieri, F., De Luca, M., Ottaviani, E., & De Benedictis, G., "Inflamm-aging: An Evolutionary Perspective on Immunosenescence," *Ann. N. Y. Acad. Sci.*, vol. 908, no. 1, pp. 244–254, Jan. 2006, doi: 10.1111/j.1749-6632.2000.tb06651.x.

[11] Salminen, A., Huuskonen, J., Ojala, J., Kauppinen, A., Kaarniranta, K., & Suuronen, T., "Activation of innate immunity system during aging: NF-kB signaling is the molecular culprit of inflamm-aging," *Ageing Res. Rev.*, vol. 7, no. 2, pp. 83–105, Apr. 2008, doi: 10.1016/j.arr.2007.09.002.

[12] Clark, R. I. & Walker, D. W., "Role of gut microbiota in aging-related health decline: insights from invertebrate models," *Cell. Mol. Life Sci.*, vol. 75, no. 1, pp. 93–101, Jan. 2018, doi: 10.1007/s00018-017-2671-1.

[13] DeVeale, B., Brummel, T., & Seroude, L., "Immunity and aging: the enemy within?," *Aging Cell*, vol. 3, no. 4, pp. 195–208, Aug. 2004, doi: 10.1111/j.1474-9728.2004.00106.x.

[14] Collado, M., Blasco, M. A., & Serrano, M., "Cellular Senescence in Cancer and Aging," *Cell*, vol. 130, no. 2. Cell, pp. 223–233, Jul. 27, 2007. doi: 10.1016/j.cell.2007.07.003.

[15] Claesson, M. J. … O'toole, P. W., "Gut microbiota composition correlates with diet and health in the elderly," *Nature*, vol. 488, no. 7410, pp. 178–184, Aug. 2012, doi: 10.1038/nature11319.

[16] Kim, S. & Jazwinski, S. M., "The Gut Microbiota and Healthy Aging: A Mini-Review," *Gerontology*, vol. 64, no. 6, pp. 513–520, Oct. 2018, doi: 10.1159/000490615.

[17] López-Otín, C., Blasco, M. A., Partridge, L., Serrano, M., & Kroemer, G., "The Hallmarks of Aging," *Cell*, vol. 153, no. 6. Cell Press, p. 1194, Jun. 06, 2013. doi: 10.1016/j.cell.2013.05.039.

[18] Kuilman, T., Michaloglou, C., Mooi, W. J., & Peeper, D. S., "The essence of senescence," *Genes and Development*, vol. 24, no. 22. Cold Spring Harbor Laboratory Press, pp. 2463–2479, Nov. 15, 2010. doi: 10.1101/gad.1971610.

[19] Rodier, F. & Campisi, J., "Four faces of cellular senescence," *Journal of Cell Biology*, vol. 192, no. 4. The Rockefeller University Press, pp. 547–556, Feb. 21, 2011. doi: 10.1083/jcb.201009094.

[20] Ottaviani, E., Ventura, N., Mandrioli, M., Candela, M., Franchini, A., & Franceschi, C., "Gut microbiota as a candidate for lifespan extension: An ecological/evolutionary perspective targeted on living organisms as metaorganisms," *Biogerontology*, vol. 12, no. 6. Biogerontology, pp. 599–609, Dec. 2011. doi: 10.1007/s10522-011-9352-5.

[21] Larbi, A., Franceschi, C., Mazzatti, D., Solana, R., Wikby, A., & Pawelec, G., "Aging of the Immune System as a Prognostic Factor for Human Longevity," *Physiology*, vol. 23, no. 2, pp. 64–74, Apr. 2008, doi: 10.1152/physiol.00040.2007.

[22] Dev, A., Iyer, S., Razani, B., & Cheng, G., "NF-κB and Innate Immunity," in *NF-kB in Health and Disease*, M. Karin, Ed. Berlin, Heidelberg: Springer Berlin Heidelberg, 2010, pp. 115–143.

[23] Zhou, R., Yazdi, A. S., Menu, P., & Tschopp, J., "A role for mitochondria in NLRP3 inflammasome activation," *Nature*, vol. 469, no. 7329, pp. 221–226, Jan. 2011, doi:

10.1038/nature09663.

[24] Nakahira, K. … Choi, A. M. K. K., "Autophagy proteins regulate innate immune responses by inhibiting the release of mitochondrial DNA mediated by the NALP3 inflammasome.," *Nat. Immunol.*, vol. 12, no. 3, pp. 222–30, Mar. 2011, doi: 10.1038/ni.1980.

[25] Latz, E., Xiao, T. S., & Stutz, A., "Activation and regulation of the inflammasomes," *Nature Reviews Immunology*, vol. 13, no. 6. NIH Public Access, pp. 397–411, Jun. 2013. doi: 10.1038/nri3452.

[26] Martinon, F., Burns, K., & Tschopp, J., "The Inflammasome: A molecular platform triggering activation of inflammatory caspases and processing of proIL-β," *Mol. Cell*, vol. 10, no. 2, pp. 417–426, 2002, doi: 10.1016/S1097-2765(02)00599-3.

[27] Mishto, M. … Franceschi, C., "Immunoproteasome and LMP2 polymorphism in aged and Alzheimer's disease brains," *Neurobiol. Aging*, vol. 27, no. 1, pp. 54–66, Jan. 2006, doi: 10.1016/j.neurobiolaging.2004.12.004.

[28] Zhang, G., Li, J., Purkayastha, S., Tang, Y., Zhang, H., Yin, Y., Li, B., Liu, G., & Cai, D., "Hypothalamic programming of systemic ageing involving IKK-β, NF-κB and GnRH," *Nature*, vol. 497, no. 7448, pp. 211–216, 2013, doi: 10.1038/nature12143.

[29] Meng, Q. & Cai, D., "Defective hypothalamic autophagy directs the central pathogenesis of obesity via the IκB kinase β(IKKβ)/NF-κB pathway," *J. Biol. Chem.*, vol. 286, no. 37, pp. 32324–32332, Sep. 2011, doi: 10.1074/jbc.M111.254417.

[30] Qing, G., Yan, P., Qu, Z., Liu, H., & Xiao, G., "Hsp90 regulates processing of NF-kB2 p100 involving protection of NF-kB-inducing kinase (NIK) from autophagy-mediated degradation," *Cell Research*, vol. 17, no. 6. Cell Res, pp. 520–530, Jun. 2007. doi: 10.1038/cr.2007.47.

[31] Niida, M., Tanaka, M., & Kamitani, T., "Downregulation of active IKKβ by Ro52-mediated autophagy," *Mol. Immunol.*, vol. 47, no. 14, pp. 2378–2387, Aug. 2010, doi: 10.1016/j.molimm.2010.05.004.

[32] Qing, G., Yan, P., & Xiao, G., "Hsp90 inhibition results in autophagy-mediated proteasome-independent degradation of IκB kinase (IKK)," *Cell Res.*, vol. 16, no. 11, pp. 895–901, Nov. 2006, doi: 10.1038/sj.cr.7310109.

[33] Tusco, R., Jacomin, A. C., Jain, A., Penman, B. S., Larsen, K. B., Johansen, T., & Nezis, I. P., "Kenny mediates selective autophagic degradation of the IKK complex to control innate immune responses," *Nat. Commun.*, vol. 8, no. 1, p. 1264, Dec. 2017, doi: 10.1038/s41467-017-01287-9.

[34] Franceschi, C., Garagnani, P., Vitale, G., Capri, M., & Salvioli, S., "Inflammaging and 'Garb-aging,'" *Trends Endocrinol. Metab.*, vol. 28, no. 3, pp. 199–212, Mar. 2017, doi: 10.1016/j.tem.2016.09.005.

[35] Salminen, A., Kaarniranta, K., & Kauppinen, A., "Inflammaging: Disturbed interplay between autophagy and inflammasomes," *Aging (Albany. NY).*, vol. 4, no. 3, pp. 166–175, 2012, doi: 10.18632/aging.100444.

[36] Jia, K. & Levine, B., "Autophagy is required for dietary restriction-mediated life span extension in C. elegans," *Autophagy*, vol. 3, no. 6, pp. 597–599, 2007, doi: 10.4161/auto.4989.

[37] Fontana, L., Partridge, L., & Longo, V. D., "Extending Healthy Life Span--From Yeast to Humans," *Science (80-.).*, vol. 328, no. 5976, pp. 321–326, Apr. 2010, doi: 10.1126/science.1172539.

[38] Tooze, S. A., Abada, A., & Elazar, Z., "Endocytosis and autophagy: Exploitation or cooperation?," *Cold Spring Harb. Perspect. Biol.*, vol. 6, no. 5, p. a018358, May 2014, doi: 10.1101/cshperspect.a018358.

[39] Worby, C. A. & Dixon, J. E., "Sorting out the cellular functions of sorting nexins," *Nature Reviews Molecular Cell Biology*, vol. 3, no. 12. Nature Publishing Group, pp. 919–931, Dec. 01, 2002. doi: 10.1038/nrm974.

[40] Siegel, V., "I kid you not," *DMM Disease Models and Mechanisms*, vol. 2, no. 1–2. Company of Biologists, pp. 5–6, Jan. 2009. doi: 10.1242/dmm.002352.

[41] Adams, M. D., "The Genome Sequence of Drosophila melanogaster," *Science (80-.).*, vol. 287, no. 5461, pp. 2185–2195, Mar. 2000, doi: 10.1126/science.287.5461.2185.

[42] Ugur, B., Chen, K., & Bellen, H. J., "Drosophila tools and assays for the study of human diseases," *Dis. Model. Mech.*, vol. 9, no. 3, pp. 235–244, Mar. 2016, doi: 10.1242/dmm.023762.

[43] Brand, A. H. & Perrimon, N., "Targeted gene expression as a means of altering cell fates and generating dominant phenotypes," *Development*, vol. 118, no. 2, pp. 401–415, 1993.

[44] Golic, K. G. & Lindquist, S., "The FLP recombinase of yeast catalyzes site-specific recombination in the drosophila genome," *Cell*, vol. 59, no. 3, pp. 499–509, Nov. 1989, doi: 10.1016/0092-8674(89)90033-0.

[45] Muller, H. J., "Genetic Variability, Twin Hybrids and Constant Hybrids, in a Case of Balanced Lethal Factors.," *Genetics*, vol. 3, no. 5, pp. 422–99, Sep. 1918.

[46] Fire, A., Xu, S., Montgomery, M. K., Kostas, S. A., Driver, S. E., & Mello, C. C., "Potent and specific genetic interference by double-stranded RNA in caenorhabditis elegans," *Nature*, vol. 391, no. 6669, pp. 806–811, Feb. 1998, doi: 10.1038/35888.

[47] Jinek, M., Chylinski, K., Fonfara, I., Hauer, M., Doudna, J. A., & Charpentier, E., "A programmable dual-RNA-guided DNA endonuclease in adaptive bacterial immunity," *Science (80-.).*, vol. 337, no. 6096, pp. 816–821, Aug. 2012, doi: 10.1126/science.1225829.

[48] De Duve, C., Pressman, B. C., Gianetto, R., Wattiaux, R., & Appelmans, F., "Tissue fractionation studies. 6. Intracellular distribution patterns of enzymes in rat-liver tissue.," *Biochem. J.*, vol. 60, no. 4, pp. 604–617, 1955, doi: 10.1042/bj0600604.

[49] Novikoff, A. B., Beaufay, H., & De Duve, C., "Electron microscopy of lysosome-rich fractions from rat liver," *J. Cell Biol.*, vol. 2, no. 4, pp. 179–184, Jul. 1956, doi:

10.1083/jcb.2.4.179.

[50] Clark, S. L., "Cellular differentiation in the kidneys of newborn mice studies with the electron microscope.," *J. Biophys. Biochem. Cytol.*, vol. 3, no. 3, pp. 349–362, May 1957, doi: 10.1083/jcb.3.3.349.

[51] Ashford, T. P. & Porter, K. R., "Cytoplasmic components in hepatic cell lysosomes.," *J. Cell Biol.*, vol. 12, no. 1, pp. 198–202, 1962, doi: 10.1083/jcb.12.1.198.

[52] Klionsky, D. J., "Autophagy revisited: a conversation with Christian de Duve.," *Autophagy*, vol. 4, no. 6, pp. 740–3, Aug. 2008, doi: 10.4161/auto.6398.

[53] Arstila, A. U. & Trump, B. F., "Studies on cellular autophagocytosis. The formation of autophagic vacuoles in the liver after glucagon administration.," *Am. J. Pathol.*, vol. 53, no. 5, pp. 687–733, Nov. 1968.

[54] Parzych, K. R. & Klionsky, D. J., "An overview of autophagy: morphology, mechanism, and regulation.," *Antioxid. Redox Signal.*, vol. 20, no. 3, pp. 460–73, Jan. 2014, doi: 10.1089/ars.2013.5371.

[55] Mortimore, G. E., Hutson, N. J., & Surmacz, C. A., "Quantitative correlation between proteolysis and macro- and microautophagy in mouse hepatocytes during starvation and refeeding," *Proc. Natl. Acad. Sci. U. S. A.*, vol. 80, no. 8 I, pp. 2179–2183, Apr. 1983, doi: 10.1073/pnas.80.8.2179.

[56] Mortimore, G. E. & Schworer, C. M., "Induction of autophagy by amino-acid deprivation in perfused rat liver," *Nature*, vol. 270, no. 5633, pp. 174–176, 1977, doi: 10.1038/270174a0.

[57] Seglen, P. O., Gordon, P. B., & Poli, A., "Amino acid inhibition of the autophagic/lysosomal pathway of protein degradation in isolated rat hepatocytes," *BBA - Gen. Subj.*, vol. 630, no. 1, pp. 103–118, Jun. 1980, doi: 10.1016/0304-4165(80)90141-5.

[58] Pfeifer, U. & Warmuth-Metz, M., "Inhibition by insulin of cellular autophagy in proximal tubular cells of rat kidney.," *Am. J. Physiol.*, vol. 244, no. 2, pp. E109-14, Feb. 1983, doi: 10.1152/ajpendo.1983.244.2.E109.

[59] Takeshige, K., Baba, M., Tsuboi, S., Noda, T., & Ohsumi, Y., "Autophagy in yeast demonstrated with proteinase-deficient mutants and conditions for its induction," *J. Cell Biol.*, vol. 119, no. 2, pp. 301–311, Oct. 1992, doi: 10.1083/jcb.119.2.301.

[60] Tsukada, M. & Ohsumi, Y., "Isolation and characterization of autophagy-defective mutants of Saccharomyces cerevisiae," *FEBS Lett.*, vol. 333, no. 1–2, pp. 169–174, Oct. 1993, doi: 10.1016/0014-5793(93)80398-E.

[61] Thumm, M., Egner, R., Koch, B., Schlumpberger, M., Straub, M., Veenhuis, M., & Wolf, D. H., "Isolation of autophagocytosis mutants of Saccharomyces cerevisiae," *FEBS Lett.*, vol. 349, no. 2, pp. 275–280, Aug. 1994, doi: 10.1016/0014-5793(94)00672-5.

[62] Harding, T. M., Morano, K. A., Scott, S. V., & Klionsky, D. J., "Isolation and

characterization of yeast mutants in the cytoplasm to vacuole protein targeting pathway," *J. Cell Biol.*, vol. 131, no. 3, pp. 591–602, Nov. 1995, doi: 10.1083/jcb.131.3.591.

[63] Nobel Media AB, "The 2016 Nobel Prize in Physiology or Medicine - Press release," *Nobelprize.org*, 2014. http://www.nobelprize.org/nobel_prizes/medicine/laureates/2007/press.html (accessed Apr. 09, 2020).

[64] Hughes, T. & Rusten, T. E., "Origin and evolution of self-consumption: Autophagy," *Advances in Experimental Medicine and Biology*, vol. 607. Springer New York, pp. 111–118, 2007. doi: 10.1007/978-0-387-74021-8_9.

[65] Levine, B. & Klionsky, D. J., "Development by self-digestion: Molecular mechanisms and biological functions of autophagy," *Developmental Cell*, vol. 6, no. 4. Elsevier, pp. 463–477, Apr. 01, 2004. doi: 10.1016/S1534-5807(04)00099-1.

[66] Nakagawa, I. … Yoshimori, T., "Autophagy defends cells against invading group A Streptococcus," *Science (80-.).*, vol. 306, no. 5698, pp. 1037–1040, Nov. 2004, doi: 10.1126/science.1103966.

[67] Ogawa, M., Yoshimori, T., Suzuki, T., Sagara, H., Mizushima, N., & Sasakawa, C., "Escape of intracellular Shigella from autophagy," *Science (80-.).*, vol. 307, no. 5710, pp. 727–731, Feb. 2005, doi: 10.1126/science.1106036.

[68] Kuma, A., Hatano, M., Matsui, M., Yamamoto, A., Nakaya, H., Yoshimori, T., Ohsumi, Y., Tokuhisa, T., & Mizushima, N., "The role of autophagy during the early neonatal starvation period," *Nature*, vol. 432, no. 7020, pp. 1032–1036, Dec. 2004, doi: 10.1038/nature03029.

[69] Kopitz, J., Kisen, G., Gordon, P. B., Bohley, P., & Seglen, P. O., "Nonselective autophagy of cytosolic enzymes by isolated rat hepatocytes," *J. Cell Biol.*, vol. 111, no. 3, pp. 941–953, 1990, doi: 10.1083/jcb.111.3.941.

[70] Chiang, H. L. & Dice, J. F., "Peptide sequences that target proteins for enhanced degradation during serum withdrawal," *J. Biol. Chem.*, vol. 263, no. 14, pp. 6797–6805, 1988.

[71] Chiang, H. L., Terlecky, S. R., Plant, C. P., & Dice, J. F., "A role for a 70-kilodaton heat shock protein in lysosomal degradation of intracellular proteins," *Science (80-.).*, vol. 246, no. 4928, pp. 382–385, 1989, doi: 10.1126/science.2799391.

[72] Cuervo, A. M. & Dice, J. F., "A receptor for the selective uptake and degradation of proteins by lysosomes," *Science (80-.).*, vol. 273, no. 5274, pp. 501–503, Jul. 1996, doi: 10.1126/science.273.5274.501.

[73] Agarraberes, F. A. & Dice, J. F., "A molecular chaperone complex at the lysosomal membrane is required for protein translocation," *J. Cell Sci.*, vol. 114, no. 13, pp. 2491–2499, 2001.

[74] Bandyopadhyay, U., Kaushik, S., Varticovski, L., & Cuervo, A. M., "The chaperone-mediated autophagy receptor organizes in dynamic protein complexes at the lysosomal

membrane.," *Mol. Cell. Biol.*, vol. 28, no. 18, pp. 5747–63, Sep. 2008, doi: 10.1128/MCB.02070-07.

[75] Cuervo, A. M. & Dice, J. F., "Regulation of Lamp2a levels in the lysosomal membrane," *Traffic*, vol. 1, no. 7, pp. 570–583, 2000, doi: 10.1034/j.1600-0854.2000.010707.x.

[76] Cuervo, A. M. & Dice, J. F., "Unique properties of lamp2a compared to other lamp2 isoforms," *J. Cell Sci.*, vol. 113, no. 24, pp. 4441–4450, 2000.

[77] Arias, E. & Cuervo, A. M., "Chaperone-mediated autophagy in protein quality control," *Current Opinion in Cell Biology*, vol. 23, no. 2. pp. 184–189, Apr. 2011. doi: 10.1016/j.ceb.2010.10.009.

[78] Cuervo, A. M., Knecht, E., Terlecky, S. R., & Dice, J. F., "Activation of a selective pathway of lysosomal proteolysis in rat liver by prolonged starvation," *Am. J. Physiol. - Cell Physiol.*, vol. 269, no. 5 38-5, 1995, doi: 10.1152/ajpcell.1995.269.5.c1200.

[79] Park, C., Suh, Y., & Cuervo, A. M., "Regulated degradation of Chk1 by chaperone-mediated autophagy in response to DNA damage," *Nat. Commun.*, vol. 6, p. 6823, Apr. 2015, doi: 10.1038/ncomms7823.

[80] Dohi, E., Tanaka, S., Seki, T., Miyagi, T., Hide, I., Takahashi, T., Matsumoto, M., & Sakai, N., "Hypoxic stress activates chaperone-mediated autophagy and modulates neuronal cell survival," *Neurochem. Int.*, vol. 60, no. 4, pp. 431–442, Mar. 2012, doi: 10.1016/j.neuint.2012.01.020.

[81] Finn, P. F., Dice, J. F., Finn, P. F., Mesires, N. T., Vine, M., & Dice, J. F., "Ketone bodies stimulate chaperone-mediated autophagyEffects of small molecules on chaperone-mediated autophagy," *J Biol Chem*, vol. 280, no. 27, pp. 25864–25870, 2005, doi: 10.1074/jbc.M50245620010.4161/auto.1.3.2000.

[82] Schneider, J. L., Suh, Y., & Cuervo, A. M., "Deficient chaperone-mediated autophagy in liver leads to metabolic dysregulation," *Cell Metab.*, vol. 20, no. 3, pp. 417–432, Sep. 2014, doi: 10.1016/j.cmet.2014.06.009.

[83] Aniento, F., Roche, E., Cuervo, A. M., & Knecht, E., "Uptake and degradation of glyceraldehyde-3-phosphate dehydrogenase by rat liver lysosomes," *J. Biol. Chem.*, vol. 268, no. 14, pp. 10463–10470, 1993.

[84] Orenstein, S. J. & Cuervo, A. M., "Chaperone-mediated autophagy: molecular mechanisms and physiological relevance," *Semin. Cell Dev. Biol.*, vol. 21, no. 7, pp. 719–726, Sep. 2010, doi: 10.1016/j.semcdb.2010.02.005.

[85] Kirkin, V., Lamark, T., Johansen, T., & Dikic, I., "NBR1 cooperates with p62 in selective autophagy of ubiquitinated targets," *Autophagy*, vol. 5, no. 5. Taylor and Francis Inc., pp. 732–733, Jul. 01, 2009. doi: 10.4161/auto.5.5.8566.

[86] Kirkin, V., McEwan, D. G., Novak, I., & Dikic, I., "A Role for Ubiquitin in Selective Autophagy," *Molecular Cell*, vol. 34, no. 3. pp. 259–269, May 15, 2009. doi: 10.1016/j.molcel.2009.04.026.

[87] Lamark, T., Kirkin, V., Dikic, I., & Johansen, T., "NBR1 and p62 as cargo receptors for selective autophagy of ubiquitinated targets," *Cell Cycle*, vol. 8, no. 13. Taylor and Francis Inc., pp. 1986–1990, Jul. 01, 2009. doi: 10.4161/cc.8.13.8892.

[88] Kaushik, S. & Cuervo, A. M., "The coming of age of chaperone-mediated autophagy," *Nature Reviews Molecular Cell Biology*, vol. 19, no. 6. Nature Publishing Group, pp. 365–381, Jun. 01, 2018. doi: 10.1038/s41580-018-0001-6.

[89] Rodríguez-Muela, N., Koga, H., García-Ledo, L., de la Villa, P., de la Rosa, E. J., Cuervo, A. M., & Boya, P., "Balance between autophagic pathways preserves retinal homeostasis," *Aging Cell*, vol. 12, no. 3, pp. 478–488, Jun. 2013, doi: 10.1111/acel.12072.

[90] Mukherjee, A., Patel, B., Koga, H., Cuervo, A. M., & Jenny, A., "Selective endosomal microautophagy is starvation-inducible in Drosophila," *Autophagy*, vol. 12, no. 11, pp. 1984–1999, Nov. 2016, doi: 10.1080/15548627.2016.1208887.

[91] Issa, A. R. … Birman, S., "The lysosomal membrane protein LAMP2A promotes autophagic flux and prevents SNCA-induced Parkinson disease-like symptoms in the Drosophila brain," *Autophagy*, vol. 14, no. 11, pp. 1898–1910, Nov. 2018, doi: 10.1080/15548627.2018.1491489.

[92] Oku, M. & Sakai, Y., "Three Distinct Types of Microautophagy Based on Membrane Dynamics and Molecular Machineries," *BioEssays*, vol. 40, no. 6, p. 1800008, Jun. 2018, doi: 10.1002/bies.201800008.

[93] Sahu, R. … Santambrogio, L., "Microautophagy of Cytosolic Proteins by Late Endosomes," *Dev. Cell*, vol. 20, no. 1, pp. 131–139, Jan. 2011, doi: 10.1016/j.devcel.2010.12.003.

[94] Uytterhoeven, V. … Verstreken, P., "Hsc70-4 Deforms Membranes to Promote Synaptic Protein Turnover by Endosomal Microautophagy," *Neuron*, vol. 88, no. 4, pp. 735–748, Nov. 2015, doi: 10.1016/j.neuron.2015.10.012.

[95] Müller, O., Sattler, T., Flötenmeyer, M., Schwarz, H., Plattner, H., & Mayer, A., "Autophagic Tubes: Vacuolar Invaginations Involved in Lateral Membrane Sorting and Inverse Vesicle Budding," 2000.

[96] Schuck, S., Gallagher, C. M., & Walter, P., "ER-phagy mediates selective degradation of endoplasmic reticulum independently of the core autophagy machinery," *J. Cell Sci.*, vol. 127, no. 18, pp. 4078–4088, Sep. 2014, doi: 10.1242/jcs.154716.

[97] Van Zutphen, T., Todde, V., De Boer, R., Kreim, M., Hofbauer, H. F., Wolinski, H., Veenhuis, M., Van Der Klei, I. J., & Kohlwein, S. D., "Lipid droplet autophagy in the yeast Saccharomyces cerevisiae," *Mol. Biol. Cell*, vol. 25, no. 2, pp. 290–301, Jan. 2014, doi: 10.1091/mbc.E13-08-0448.

[98] Fry, M. R., Thomson, J. M., Tomasini, A. J., & Dunn, W. A., "Early and late molecular events of glucose-induced pexophagy in Pichia pastoris require Vac8," *Autophagy*, vol. 2, no. 4, pp. 280–288, 2006, doi: 10.4161/auto.3164.

[99] Takikita, S., Myerowitz, R., Schreiner, C., Baum, R., Raben, N., & Plotz, P. H., "The

values and limits of an in vitro model of Pompe disease: The best laid schemes o' mice an' men...," *Autophagy*, vol. 5, no. 5. Taylor and Francis Inc., pp. 729–731, Jul. 01, 2009. doi: 10.4161/auto.5.5.8525.

[100] Takikita, S., Myerowitz, R., Zaal, K., Raben, N., & Plotz, P. H., "Murine muscle cell models for Pompe disease and their use in studying therapeutic approaches," *Mol. Genet. Metab.*, vol. 96, no. 4, pp. 208–217, Apr. 2009, doi: 10.1016/j.ymgme.2008.12.012.

[101] Klionsky DJ, Abdelmohsen K, Abe A, Abedin MJ, Abeliovich H, Acevedo Arozena A, Adachi H, Adams CM, Adams PD, Adeli K, Adhihetty PJ, Adler SG, Agam G, Agarwal R, Aghi MK, Agnello M, Agostinis P, Aguilar PV, Aguirre-Ghiso J, Airoldi EM, Ait-Si-Ali S, Akemat, Z. S., "Guidelines for use and interpretation of assays for monitoring autophagy (3rd edition)," *Autophagy*, vol. 12, no. 1, pp. 1–222, 2016, doi: 10.1080/15548627.2015.1100356.

[102] Érdi, B., Nagy, P., Zvara, Á., Varga, Á., Pircs, K., Ménesi, D., Puskás, L. G., & Juhász, G., "Loss of the starvation-induced gene Rack1 leads to glycogen deficiency and impaired autophagic responses in Drosophila," *Autophagy*, vol. 8, no. 7, pp. 1124–1135, Jul. 2012, doi: 10.4161/auto.20069.

[103] "FlyAtlas 2." http://flyatlas.gla.ac.uk/FlyAtlas2/index.html?search=gene&gene=Atg8b&idtype=symbol#mobileTargetG (accessed Apr. 13, 2020).

[104] Shpilka, T., Weidberg, H., Pietrokovski, S., & Elazar, Z., "Atg8: an autophagy-related ubiquitin-like protein family.," *Genome Biol.*, vol. 12, no. 7, p. 226, Jul. 2011, doi: 10.1186/gb-2011-12-7-226.

[105] Weidberg, H., Shvets, E., Shpilka, T., Shimron, F., Shinder, V., & Elazar, Z., "LC3 and GATE-16/GABARAP subfamilies are both essential yet act differently in autophagosome biogenesis," *EMBO J.*, vol. 29, no. 11, pp. 1792–1802, Jun. 2010, doi: 10.1038/emboj.2010.74.

[106] Geng, J. & Klionsky, D. J., "The Atg8 and Atg12 ubiquitin-like conjugation systems in macroautophagy. 'Protein modifications: beyond the usual suspects' review series.," *EMBO Rep.*, vol. 9, no. 9, pp. 859–64, Sep. 2008, doi: 10.1038/embor.2008.163.

[107] Nakatogawa, H., Ichimura, Y., & Ohsumi, Y., "Atg8, a Ubiquitin-like Protein Required for Autophagosome Formation, Mediates Membrane Tethering and Hemifusion," *Cell*, vol. 130, no. 1, pp. 165–178, Jul. 2007, doi: 10.1016/j.cell.2007.05.021.

[108] Mizushima, N., Noda, T., & Ohsumi, Y., "Apg16p is required for the function of the Apg12p-Apg5p conjugate in the yeast autophagy pathway.," *EMBO J.*, vol. 18, no. 14, pp. 3888–96, Jul. 1999, doi: 10.1093/emboj/18.14.3888.

[109] Ichimura, Y. … Ohsumi, Y., "A ubiquitin-like system mediates protein lipidation," *Nature*, vol. 408, no. 6811, pp. 488–492, Nov. 2000, doi: 10.1038/35044114.

[110] Kirisako, T. … Ohsumi, Y., "The reversible modification regulates the membrane-binding state of Apg8/Aut7 essential for autophagy and the cytoplasm to vacuole

targeting pathway," *J. Cell Biol.*, vol. 151, no. 2, pp. 263–275, Oct. 2000, doi: 10.1083/jcb.151.2.263.

[111] Shang, L., Chen, S., Du, F., Li, S., Zhao, L., & Wang, X., "Nutrient starvation elicits an acute autophagic response mediated by Ulk1 dephosphorylation and its subsequent dissociation from AMPK," *Proc. Natl. Acad. Sci.*, vol. 108, no. 12, pp. 4788–4793, Mar. 2011, doi: 10.1073/pnas.1100844108.

[112] Mulakkal, N. C., Nagy, P., Takats, S., Tusco, R., Juhász, G., & Nezis, I. P., "Autophagy in drosophila: From historical studies to current knowledge," *Biomed Res. Int.*, vol. 2014, p. 273473, 2014, doi: 10.1155/2014/273473.

[113] Kamada, Y., Funakoshi, T., Shintani, T., Nagano, K., Ohsumi, M., & Ohsumi, Y., "Tor-mediated induction of autophagy via an Apg1 protein kinase complex," *J. Cell Biol.*, vol. 150, no. 6, pp. 1507–1513, Sep. 2000, doi: 10.1083/jcb.150.6.1507.

[114] Scott, R. C., Schuldiner, O., & Neufeld, T. P., "Role and regulation of starvation-induced autophagy in the Drosophila fat body," *Dev. Cell*, vol. 7, no. 2, pp. 167–178, Aug. 2004, doi: 10.1016/j.devcel.2004.07.009.

[115] Grewal, S. S., "Insulin/TOR signaling in growth and homeostasis: A view from the fly world," *International Journal of Biochemistry and Cell Biology*, vol. 41, no. 5. pp. 1006–1010, May 2009. doi: 10.1016/j.biocel.2008.10.010.

[116] Takahara, T. & Maeda, T., "Evolutionarily conserved regulation of TOR signalling," *J. Biochem.*, vol. 154, no. 1, pp. 1–10, May 2013, doi: 10.1093/jb/mvt047.

[117] Chang, Y. Y. & Neufeld, T. P., "An Atg1/Atg13 complex with multiple roles in TOR-mediated autophagy regulation," *Mol. Biol. Cell*, vol. 20, no. 7, pp. 2004–2014, Apr. 2009, doi: 10.1091/mbc.E08-12-1250.

[118] Scott, R. C., Juhász, G., & Neufeld, T. P., "Direct Induction of Autophagy by Atg1 Inhibits Cell Growth and Induces Apoptotic Cell Death," *Curr. Biol.*, vol. 17, no. 1, pp. 1–11, Jan. 2007, doi: 10.1016/j.cub.2006.10.053.

[119] Nagy, P. … Juhász, G., "Atg17/FIP200 localizes to perilysosomal Ref(2)P aggregates and promotes autophagy by activation of Atg1 in Drosophila," *Autophagy*, vol. 10, no. 3, pp. 453–467, 2014, doi: 10.4161/auto.27442.

[120] Hegedűs, K., Nagy, P., Gáspári, Z., & Juhász, G., "The Putative HORMA Domain Protein Atg101 Dimerizes and Is Required for Starvation-Induced and Selective Autophagy in *Drosophila*," *Biomed Res. Int.*, vol. 2014, p. 470482, 2014, doi: 10.1155/2014/470482.

[121] Kim, M., Park, H. L., Park, H. W., Ro, S. H., Nam, S. G., Reed, J. M., Guan, J. L., & Lee, J. H., "Drosophila Fip200 is an essential regulator of autophagy that attenuates both growth and aging," *Autophagy*, vol. 9, no. 8, pp. 1201–1213, Aug. 2013, doi: 10.4161/auto.24811.

[122] Guo, T. … Ge, W., "The autophagy-related gene Atg101 in Drosophila regulates both neuron and midgut homeostasis," *J. Biol. Chem.*, vol. 294, no. 14, pp. 5666–5676, Apr. 2019, doi: 10.1074/jbc.RA118.006069.

[123] Jung, C. H., Jun, C. B., Ro, S.-H. H., Kim, Y.-M. M., Otto, N. M., Cao, J., Kundu, M., & Kim, D.-H. H., "ULK-Atg13-FIP200 complexes mediate mTOR signaling to the autophagy machinery," *Mol. Biol. Cell*, vol. 20, no. 7, pp. 1992–2003, Apr. 2009, doi: 10.1091/mbc.E08-12-1249.

[124] Kamada, Y., Yoshino, K. -i. K., Kondo, C., Kawamata, T., Oshiro, N., Yonezawa, K., & Ohsumi, Y., "Tor Directly Controls the Atg1 Kinase Complex To Regulate Autophagy," *Mol. Cell. Biol.*, vol. 30, no. 4, pp. 1049–1058, Feb. 2010, doi: 10.1128/mcb.01344-09.

[125] Chan, E. Y. W., Kir, S., & Tooze, S. A., "siRNA screening of the kinome identifies ULK1 as a multidomain modulator of autophagy," *J. Biol. Chem.*, vol. 282, no. 35, pp. 25464–25474, Aug. 2007, doi: 10.1074/jbc.M703663200.

[126] Suzuki, K., Kirisako, T., Kamada, Y., Mizushima, N., Noda, T., & Ohsumi, Y., "The pre-autophagosomal structure organized by concerted functions of APG genes is essential for autophagosome formation," *EMBO J.*, vol. 20, no. 21, pp. 5971–5981, Nov. 2001, doi: 10.1093/emboj/20.21.5971.

[127] Lamb, C. A., Yoshimori, T., & Tooze, S. A., "The autophagosome: origins unknown, biogenesis complex," *Nat. Rev. Mol. Cell Biol.*, vol. 14, no. 12, pp. 759–774, Dec. 2013, doi: 10.1038/nrm3696.

[128] Carlsson, S. R. & Simonsen, A., "Membrane dynamics in autophagosome biogenesis," *J. Cell Sci.*, vol. 128, no. 2, pp. 193–205, Jan. 2015, doi: 10.1242/jcs.141036.

[129] Axe, E. L., Walker, S. A., Manifava, M., Chandra, P., Roderick, H. L., Habermann, A., Griffiths, G., & Ktistakis, N. T., "Autophagosome formation from membrane compartments enriched in phosphatidylinositol 3-phosphate and dynamically connected to the endoplasmic reticulum," *J. Cell Biol.*, vol. 182, no. 4, pp. 685–701, Aug. 2008, doi: 10.1083/jcb.200803137.

[130] Juhasz, G. & Neufeld, T. P., "Autophagy: A forty-year search for a missing membrane source," *PLoS Biology*, vol. 4, no. 2. Public Library of Science, pp. 161–164, Feb. 2006. doi: 10.1371/journal.pbio.0040036.

[131] Shibutani, S. T. & Yoshimori, T., "A current perspective of autophagosome biogenesis," *Cell Research*, vol. 24, no. 1. Nature Publishing Group, pp. 58–68, Jan. 2014. doi: 10.1038/cr.2013.159.

[132] Zoppino, F. C. M., Militello, R. D., Slavin, I., Álvarez, C., & Colombo, M. I., "Autophagosome formation depends on the small GTPase rab1 and functional ER exit sites," *Traffic*, vol. 11, no. 9, pp. 1246–1261, Sep. 2010, doi: 10.1111/j.1600-0854.2010.01086.x.

[133] Graef, M., Friedman, J. R., Graham, C., Babu, M., & Nunnari, J., "ER exit sites are physical and functional core autophagosome biogenesis components," *Mol. Biol. Cell*, vol. 24, no. 18, pp. 2918–2931, Sep. 2013, doi: 10.1091/mbc.E13-07-0381.

[134] Ge, L., Melville, D., Zhang, M., & Schekman, R., "The ER-Golgi intermediate compartment is a key membrane source for the LC3 lipidation step of autophagosome biogenesis," *Elife*, vol. 2013, no. 2, Aug. 2013, doi: 10.7554/eLife.00947.001.

[135] Geng, J., Nair, U., Yasumura-Yorimitsu, K., & Klionsky, D. J., "Post-golgi sec proteins are required for autophagy in Saccharomyces cerevisiae," *Mol. Biol. Cell*, vol. 21, no. 13, pp. 2257–2269, Jul. 2010, doi: 10.1091/mbc.E09-11-0969.

[136] Bodemann, B. O. … White, M. A., "RalB and the Exocyst Mediate the Cellular Starvation Response by Direct Activation of Autophagosome Assembly," *Cell*, vol. 144, pp. 253–267, 2011, doi: 10.1016/j.cell.2010.12.018.

[137] Hailey, D. W., Rambold, A. S., Satpute-Krishnan, P., Mitra, K., Sougrat, R., Kim, P. K., & Lippincott-Schwartz, J., "Mitochondria Supply Membranes for Autophagosome Biogenesis during Starvation," *Cell*, vol. 141, no. 4, pp. 656–667, May 2010, doi: 10.1016/j.cell.2010.04.009.

[138] Ravikumar, B., Moreau, K., Jahreiss, L., Puri, C., & Rubinsztein, D. C., "Plasma membrane contributes to the formation of pre-autophagosomal structures," *Nat. Cell Biol.*, vol. 12, no. 8, pp. 747–757, Aug. 2010, doi: 10.1038/ncb2078.

[139] Puri, C., Renna, M., Bento, C. F., Moreau, K., & Rubinsztein, D. C., "Diverse autophagosome membrane sources coalesce in recycling endosomes," *Cell*, vol. 154, no. 6, pp. 1285–1299, Sep. 2013, doi: 10.1016/j.cell.2013.08.044.

[140] Knævelsrud, H. … Simonsen, A., "Membrane remodeling by the PX-BAR protein SNX18 promotes autophagosome formation.," *J. Cell Biol.*, vol. 202, no. 2, pp. 331–49, Jul. 2013, doi: 10.1083/jcb.201205129.

[141] Ylä-Anttila, P., Vihinen, H., Jokitalo, E., & Eskelinen, E. L., "3D tomography reveals connections between the phagophore and endoplasmic reticulum," *Autophagy*, vol. 5, no. 8, pp. 1180–1185, Nov. 2009, doi: 10.4161/auto.5.8.10274.

[142] Hayashi-Nishino, M., Fujita, N., Noda, T., Yamaguchi, A., Yoshimori, T., & Yamamoto, A., "A subdomain of the endoplasmic reticulum forms a cradle for autophagosome formation," *Nat. Cell Biol.*, vol. 11, no. 12, pp. 1433–1437, Dec. 2009, doi: 10.1038/ncb1991.

[143] Matsunaga, K., Morita, E., Saitoh, T., Akira, S., Ktistakis, N. T., Izumi, T., Noda, T., & Yoshimori, T., "Autophagy requires endoplasmic reticulum targeting of the PI3-kinase complex via Atg14L," *J. Cell Biol.*, vol. 190, no. 4, pp. 511–521, Aug. 2010, doi: 10.1083/jcb.200911141.

[144] Jean, S. & Kiger, A. A., "Classes of phosphoinositide 3-kinases at a glance," *J. Cell Sci.*, vol. 127, no. 5, pp. 923–928, Mar. 2014, doi: 10.1242/jcs.093773.

[145] Devereaux, K., Dall'Armi, C., Alcazar-Roman, A., Ogasawara, Y., Zhou, X., Wang, F., Yamamoto, A., de Camilli, P., & Di Paolo, G., "Regulation of Mammalian Autophagy by Class II and III PI 3-Kinases through PI3P Synthesis," *PLoS One*, vol. 8, no. 10, Oct. 2013, doi: 10.1371/journal.pone.0076405.

[146] Yu, X., Long, Y. C., & Shen, H.-M., "Differential regulatory functions of three classes of phosphatidylinositol and phosphoinositide 3-kinases in autophagy.," *Autophagy*, vol. 11, no. 10, pp. 1711–1728, 2015, doi: 10.1080/15548627.2015.1043076.

[147] Juhász, G., Hill, J. H., Yan, Y., Sass, M., Baehrecke, E. H., Backer, J. M., & Neufeld,

T. P., "The class III PI(3)K Vps34 promotes autophagy and endocytosis but not TOR signaling in Drosophila," *J. Cell Biol.*, vol. 181, no. 4, pp. 655–666, May 2008, doi: 10.1083/jcb.200712051.

[148] Chang, Y. Y. & Neufeld, T. P., "Autophagy takes flight in Drosophila," *FEBS Letters*, vol. 584, no. 7. No longer published by Elsevier, pp. 1342–1349, Apr. 02, 2010. doi: 10.1016/j.febslet.2010.01.006.

[149] Matsunaga, K. … Yoshimori, T., "Two Beclin 1-binding proteins, Atg14L and Rubicon, reciprocally regulate autophagy at different stages," *Nat. Cell Biol.*, vol. 11, no. 4, pp. 385–396, Mar. 2009, doi: 10.1038/ncb1846.

[150] Simonsen, A. & Tooze, S. A., "Coordination of membrane events during autophagy by multiple class III PI3-kinase complexes," *J. Cell Biol.*, vol. 186, no. 6, pp. 773–782, Sep. 2009, doi: 10.1083/jcb.200907014.

[151] Liang, C. … Jung, J. U., "Beclin1-binding UVRAG targets the class C Vps complex to coordinate autophagosome maturation and endocytic trafficking," *Nat. Cell Biol.*, vol. 10, no. 7, pp. 776–787, Jul. 2008, doi: 10.1038/ncb1740.

[152] Zhong, Y., Wang, Q. J., Li, X., Yan, Y., Backer, J. M., Chait, B. T., Heintz, N., & Yue, Z., "Distinct regulation of autophagic activity by Atg14L and Rubicon associated with Beclin 1-phosphatidylinositol-3-kinase complex," *Nat. Cell Biol.*, vol. 11, no. 4, pp. 468–476, Mar. 2009, doi: 10.1038/ncb1854.

[153] Nakamura, S. … Yoshimori, T., "Suppression of autophagic activity by Rubicon is a signature of aging," *Nat. Commun.*, vol. 10, no. 1, pp. 1–11, Dec. 2019, doi: 10.1038/s41467-019-08729-6.

[154] Lőrincz, P., Lakatos, Z., Maruzs, T., Szatmári, Z., Kis, V., & Sass, M., "Atg6/UVRAG/Vps34-Containing Lipid Kinase Complex Is Required for Receptor Downregulation through Endolysosomal Degradation and Epithelial Polarity during *Drosophila* Wing Development," *Biomed Res. Int.*, vol. 2014, p. 851349, 2014, doi: 10.1155/2014/851349.

[155] Bánréti, Á., Lukácsovich, T., Csikós, G., Erdélyi, M., & Sass, M., "PP2A regulates autophagy in two alternative ways in Drosophila," *Autophagy*, vol. 8, no. 4, pp. 623–636, Apr. 2012, doi: 10.4161/auto.19081.

[156] Molejon, M. I., Ropolo, A., Re, A. Lo, Boggio, V., & Vaccaro, M. I., "The VMP1-Beclin 1 interaction regulates autophagy induction," *Sci. Rep.*, vol. 3, no. 1, pp. 1–11, Jan. 2013, doi: 10.1038/srep01055.

[157] Tabara, L. C. & Escalante, R., "VMP1 establishes ER-microdomains that regulate membrane contact sites and autophagy," *PLoS One*, vol. 11, no. 11, Nov. 2016, doi: 10.1371/journal.pone.0166499.

[158] Ropolo, A. … Vaccaro, M. I., "The pancreatitis-induced vacuole membrane protein 1 triggers autophagy in mammalian cells," *J. Biol. Chem.*, vol. 282, no. 51, pp. 37124–37133, Dec. 2007, doi: 10.1074/jbc.M706956200.

[159] Alemu, E. A. … Johansen, T., "ATG8 family proteins act as scaffolds for assembly of

the ULK complex: Sequence requirements for LC3-interacting region (LIR) motifs," *J. Biol. Chem.*, vol. 287, no. 47, pp. 39275–39290, Nov. 2012, doi: 10.1074/jbc.M112.378109.

[160] Wirth, M., Zhang, W., Razi, M., Nyoni, L., Joshi, D., O'Reilly, N., Johansen, T., Tooze, S. A., & Mouilleron, S., "Molecular determinants regulating selective binding of autophagy adapters and receptors to ATG8 proteins," *Nat. Commun.*, vol. 10, no. 1, pp. 1–18, Dec. 2019, doi: 10.1038/s41467-019-10059-6.

[161] Mari, M., Griffith, J., Rieter, E., Krishnappa, L., Klionsky, D. J., & Reggiori, F., "An Atg9-containing compartment that functions in the early steps of autophagosome biogenesis," *J. Cell Biol.*, vol. 190, no. 6, pp. 1005–1022, Sep. 2010, doi: 10.1083/jcb.200912089.

[162] Kaufmann, A., Beier, V., Franquelim, H. G., & Wollert, T., "Molecular mechanism of autophagic membrane-scaffold assembly and disassembly," *Cell*, vol. 156, no. 3, pp. 469–481, Jan. 2014, doi: 10.1016/j.cell.2013.12.022.

[163] Wang, C. W., Stromhaug, P. E., Shima, J., & Klionsky, D. J., "The Ccz1-Mon1 protein complex is required for the late step of multiple vacuole delivery pathways," *J. Biol. Chem.*, vol. 277, no. 49, pp. 47917–47927, Dec. 2002, doi: 10.1074/jbc.M208191200.

[164] Takáts, S., Nagy, P., Varga, Á., Pircs, K., Kárpáti, M., Varga, K., Kovács, A. L., Hegedus, K., & Juhász, G., "Autophagosomal Syntaxin17-dependent lysosomal degradation maintains neuronal function in Drosophila," *J. Cell Biol.*, vol. 201, no. 4, pp. 531–539, May 2013, doi: 10.1083/jcb.201211160.

[165] Itakura, E., Kishi-Itakura, C., & Mizushima, N., "The hairpin-type tail-anchored SNARE syntaxin 17 targets to autophagosomes for fusion with endosomes/lysosomes," *Cell*, vol. 151, no. 6, pp. 1256–1269, Dec. 2012, doi: 10.1016/j.cell.2012.11.001.

[166] Gordon, P. B. & Seglen, P. O., "Prelysosomal convergence of autophagic and endocytic pathways," *Biochem. Biophys. Res. Commun.*, vol. 151, no. 1, pp. 40–47, Feb. 1988, doi: 10.1016/0006-291X(88)90556-6.

[167] Filimonenko, M. … Simonsen, A., "Functional multivesicular bodies are required for autophagic clearance of protein aggregates associated with neurodegenerative disease.," *J. Cell Biol.*, vol. 179, no. 3, pp. 485–500, Nov. 2007, doi: 10.1083/jcb.200702115.

[168] Rusten, T. E. … Stenmark, H., "ESCRTs and Fab1 Regulate Distinct Steps of Autophagy," *Curr. Biol.*, vol. 17, no. 20, pp. 1817–1825, Oct. 2007, doi: 10.1016/j.cub.2007.09.032.

[169] Johansen, T. & Lamark, T., "Selective autophagy mediated by autophagic adapter proteins," *Autophagy*, vol. 7, no. 3, pp. 279–296, Mar. 2011, doi: 10.4161/auto.7.3.14487.

[170] Johansen, T. & Lamark, T., "Selective Autophagy: ATG8 Family Proteins, LIR Motifs and Cargo Receptors," *J. Mol. Biol.*, vol. 432, no. 1, pp. 80–103, Jan. 2020, doi: 10.1016/j.jmb.2019.07.016.

[171] Zaffagnini, G. & Martens, S., "Mechanisms of Selective Autophagy," *J. Mol. Biol.*, vol. 428, no. 9, pp. 1714–1724, May 2016, doi: 10.1016/j.jmb.2016.02.004.

[172] Bjørkøy, G., Lamark, T., Brech, A., Outzen, H., Perander, M., Øvervatn, A., Stenmark, H., & Johansen, T., "p62/SQSTM1 forms protein aggregates degraded by autophagy and has a protective effect on huntingtin-induced cell death," *J. Cell Biol.*, vol. 171, no. 4, pp. 603–614, Nov. 2005, doi: 10.1083/jcb.200507002.

[173] Komatsu, M. … Tanaka, K., "Homeostatic Levels of p62 Control Cytoplasmic Inclusion Body Formation in Autophagy-Deficient Mice," *Cell*, vol. 131, no. 6, pp. 1149–1163, Dec. 2007, doi: 10.1016/j.cell.2007.10.035.

[174] Pankiv, S. … Johansen, T., "p62/SQSTM1 Binds Directly to Atg8/LC3 to Facilitate Degradation of Ubiquitinated Protein Aggregates by Autophagy," *J. Biol. Chem.*, vol. 282, no. 33, pp. 24131–24145, Aug. 2007, doi: 10.1074/jbc.M702824200.

[175] Moscat, J., Diaz-Meco, M. T., & Wooten, M. W., "Signal integration and diversification through the p62 scaffold protein," *Trends in Biochemical Sciences*, vol. 32, no. 2. Elsevier, pp. 95–100, Feb. 01, 2007. doi: 10.1016/j.tibs.2006.12.002.

[176] Zatloukal, K. … Denk, H., "p62 is a common component of cytoplasmic inclusions in protein aggregation diseases," *Am. J. Pathol.*, vol. 160, no. 1, pp. 255–263, Jan. 2002, doi: 10.1016/S0002-9440(10)64369-6.

[177] Kuusisto, E., Salminen, A., & Alafuzoff, I., "Ubiquitin-binding protein p62 is present in neuronal and glial inclusions in human tauopathies and synucleinopathies," *Neuroreport*, vol. 12, no. 10, pp. 2085–2090, Jul. 2001, doi: 10.1097/00001756-200107200-00009.

[178] Ichimura, Y. … Komatsu, M., "Structural basis for sorting mechanism of p62 in selective autophagy," *J. Biol. Chem.*, vol. 283, no. 33, pp. 22847–22857, Aug. 2008, doi: 10.1074/jbc.M802182200.

[179] Kirkin, V. … Johansen, T., "A Role for NBR1 in Autophagosomal Degradation of Ubiquitinated Substrates," *Mol. Cell*, vol. 33, no. 4, pp. 505–516, Feb. 2009, doi: 10.1016/j.molcel.2009.01.020.

[180] Thurston, T. L. M., Ryzhakov, G., Bloor, S., von Muhlinen, N., & Randow, F., "The TBK1 adaptor and autophagy receptor NDP52 restricts the proliferation of ubiquitin-coated bacteria," *Nat. Immunol.*, vol. 10, no. 11, pp. 1215–1221, Nov. 2009, doi: 10.1038/ni.1800.

[181] Wild, P. … Dikic, I., "Phosphorylation of the autophagy receptor optineurin restricts Salmonella growth," *Science (80-.).*, vol. 333, no. 6039, pp. 228–233, Jul. 2011, doi: 10.1126/science.1205405.

[182] Carré-Mlouka, A., Gaumer, S., Gay, P., Petitjean, A. M., Coulondre, C., Dru, P., Bras, F., Dezélée, S., & Contamine, D., "Control of sigma virus multiplication by the ref(2)P gene of Drosophila melanogaster: An in vivo study of the PB1 domain of Ref(2)P," *Genetics*, vol. 176, no. 1, pp. 409–419, 2007, doi: 10.1534/genetics.106.063826.

[183] Nezis, I. P., Simonsen, A., Sagona, A. P., Finley, K., Gaumer, S., Contamine, D.,

Rusten, T. E., Stenmark, H., & Brech, A., "Ref(2)P, the Drosophila melanogaster homologue of mammalian p62, is required for the formation of protein aggregates in adult brain," *J. Cell Biol.*, vol. 180, no. 6, pp. 1065–1071, Mar. 2008, doi: 10.1083/jcb.200711108.

[184] Sim, J., Osborne, K. A., Garcia, I. A., Matysik, A. S., & Kraut, R., "Drosophila BEACH domain autophagic adaptor blue cheese shuttles between vesicle populations and is required for an early step in autophagy," *bioRxiv*, p. 084434, Nov. 2016, doi: 10.1101/084434.

[185] Birgisdottir, Å., Lamark, T., & Johansen, T., "The LIR motif - crucial for selective autophagy.," *J. Cell Sci.*, vol. 126, no. Pt 15, pp. 3237–47, Aug. 2013, doi: 10.1242/jcs.126128.

[186] Noda, N. N., Kumeta, H., Nakatogawa, H., Satoo, K., Adachi, W., Ishii, J., Fujioka, Y., Ohsumi, Y., & Inagaki, F., "Structural basis of target recognition by Atg8/LC3 during selective autophagy," *Genes to Cells*, vol. 13, no. 12, pp. 1211–1218, Dec. 2008, doi: 10.1111/j.1365-2443.2008.01238.x.

[187] Noda, N. N., Ohsumi, Y., & Inagaki, F., "Atg8-family interacting motif crucial for selective autophagy," *FEBS Letters*, vol. 584, no. 7. No longer published by Elsevier, pp. 1379–1385, Apr. 02, 2010. doi: 10.1016/j.febslet.2010.01.018.

[188] Rogov, V. V. … Novak, I., "Phosphorylation of the mitochondrial autophagy receptor Nix enhances its interaction with LC3 proteins," *Sci. Rep.*, vol. 7, no. 1, pp. 1–12, Dec. 2017, doi: 10.1038/s41598-017-01258-6.

[189] Tagaya, M. & Arasaki, K., "Regulation of mitochondrial dynamics and autophagy by the mitochondria-associated membrane," in *Advances in Experimental Medicine and Biology*, vol. 997, Springer New York LLC, 2017, pp. 33–47. doi: 10.1007/978-981-10-4567-7_3.

[190] Betts, M. J. & Russell, R. B., "Amino-Acid Properties and Consequences of Substitutions," in *Bioinformatics for Geneticists*, Chichester, UK: John Wiley & Sons, Ltd, 2007, pp. 311–342. doi: 10.1002/9780470059180.ch13.

[191] Jain, A., Rusten, T. E., Katheder, N., Elvenes, J., Bruun, J.-A. A., Sjøttem, E., Lamark, T., & Johansen, T., "P62/sequestosome-1, autophagy-related gene 8, and autophagy in Drosophila are regulated by nuclear factor erythroid 2-related factor 2(NRF2), independent of transcription factor TFEB," *J. Biol. Chem.*, vol. 290, no. 24, pp. 14945–14962, Jun. 2015, doi: 10.1074/jbc.M115.656116.

[192] Goldstein, G., Scheid, M., Hammerling, U., Schlesinger, D. H., Niall, H. D., & Boyse, E. A., "Isolation of a polypeptide that has lymphocyte differentiating properties and is probably represented universally in living cells," *Proc. Natl. Acad. Sci. U. S. A.*, vol. 72, no. 1, pp. 11–15, 1975, doi: 10.1073/pnas.72.1.11.

[193] Welchman, R. L., Gordon, C., & Mayer, R. J., "Ubiquitin and ubiquitin-like proteins as multifunctional signals," *Nature Reviews Molecular Cell Biology*, vol. 6, no. 8. Nature Publishing Group, pp. 599–609, Aug. 2005. doi: 10.1038/nrm1700.

[194] Hershko, A. & Ciechanover, A., "The Ubiquitin System," *Annu. Rev. Biochem.*, vol.

67, no. 1, pp. 425–479, Jun. 1998, doi: 10.1146/annurev.biochem.67.1.425.

[195] Komander, D., "The emerging complexity of protein ubiquitination," *Biochem. Soc. Trans.*, vol. 37, no. 5, pp. 937–953, Sep. 2009, doi: 10.1042/BST0370937.

[196] Kwon, Y. T. & Ciechanover, A., "The Ubiquitin Code in the Ubiquitin-Proteasome System and Autophagy," *Trends Biochem. Sci.*, vol. 42, no. 11, pp. 873–886, Nov. 2017, doi: 10.1016/j.tibs.2017.09.002.

[197] Long, J., Gallagher, T. R. A., Cavey, J. R., Sheppard, P. W., Ralston, S. H., Layfield, R., & Searle, M. S., "Ubiquitin recognition by the ubiquitin-associated domain of p62 involves a novel conformational switch," *J. Biol. Chem.*, vol. 283, no. 9, pp. 5427–5440, Feb. 2008, doi: 10.1074/jbc.M704973200.

[198] Seibenhener, M. L., Babu, J. R., Geetha, T., Wong, H. C., Krishna, N. R., & Wooten, M. W., "Sequestosome 1/p62 Is a Polyubiquitin Chain Binding Protein Involved in Ubiquitin Proteasome Degradation," *Mol. Cell. Biol.*, vol. 24, no. 18, pp. 8055–8068, Sep. 2004, doi: 10.1128/mcb.24.18.8055-8068.2004.

[199] Liu, W. J., Ye, L., Huang, W. F., Guo, L. J., Xu, Z. G., Wu, H. L., Yang, C., & Liu, H. F., "p62 links the autophagy pathway and the ubiqutin–proteasome system upon ubiquitinated protein degradation," *Cell. Mol. Biol. Lett.*, vol. 21, no. 1, p. 29, 2016, doi: 10.1186/s11658-016-0031-z.

[200] Khaminets, A., Behl, C., & Dikic, I., "Ubiquitin-Dependent And Independent Signals In Selective Autophagy," *Trends in Cell Biology*, vol. 26, no. 1. Elsevier Ltd, pp. 6–16, Jan. 01, 2016. doi: 10.1016/j.tcb.2015.08.010.

[201] Marshall, R. S., Hua, Z., Mali, S., McLoughlin, F., & Vierstra, R. D., "ATG8-Binding UIM Proteins Define a New Class of Autophagy Adaptors and Receptors," *Cell*, vol. 177, no. 3, pp. 766-781.e24, Apr. 2019, doi: 10.1016/j.cell.2019.02.009.

[202] Marshall, R. S., Li, F., Gemperline, D. C., Book, A. J., & Vierstra, R. D., "Autophagic Degradation of the 26S Proteasome Is Mediated by the Dual ATG8/Ubiquitin Receptor RPN10 in Arabidopsis," *Mol. Cell*, vol. 58, no. 6, pp. 1053–1066, Jun. 2015, doi: 10.1016/j.molcel.2015.04.023.

[203] Nezis, I. P. … Stenmark, H., "Autophagic degradation of dBruce controls DNA fragmentation in nurse cells during late Drosophila melanogaster oogenesis," *J. Cell Biol.*, vol. 190, no. 4, pp. 523–531, Aug. 2010, doi: 10.1083/jcb.201002035.

[204] Tsapras, P. & Nezis, I. P., "Caspase involvement in autophagy," *Cell Death Differ.*, vol. 24, no. 8, pp. 1369–1379, Aug. 2017, doi: 10.1038/cdd.2017.43.

[205] Laussmann, M. a, Passante, E., Düssmann, H., Rauen, J. a, Würstle, M. L., Delgado, M. E., Devocelle, M., Prehn, J. H. M., & Rehm, M., "Proteasome inhibition can induce an autophagy-dependent apical activation of caspase-8.," *Cell Death Differ.*, vol. 18, no. 10, pp. 1584–1597, Oct. 2011, doi: 10.1038/cdd.2011.27.

[206] Young, M. M. … Wang, H.-G., "Autophagosomal membrane serves as platform for intracellular death-inducing signaling complex (iDISC)-mediated caspase-8 activation and apoptosis.," *J. Biol. Chem.*, vol. 287, no. 15, pp. 12455–68, Apr. 2012, doi:

10.1074/jbc.M111.309104.

[207] Huang, S., Okamoto, K., Yu, C., & Sinicrope, F. A., "P62/sequestosome-1 Up-regulation promotes ABT-263-induced caspase-8 aggregation/activation on the autophagosome," *J. Biol. Chem.*, vol. 288, no. 47, pp. 33654–33666, Nov. 2013, doi: 10.1074/jbc.M113.518134.

[208] Hou, W., Han, J., Lu, C., Goldstein, L. A., & Rabinowich, H., "Autophagic degradation of active caspase-8: A crosstalk mechanism between autophagy and apoptosis," *Autophagy*, vol. 6, no. 7, pp. 891–900, Oct. 2010, doi: 10.4161/auto.6.7.13038.

[209] Jacquel, A. … Auberger, P., "Autophagy is required for CSF-1-induced macrophagic differentiation and acquisition of phagocytic functions," *Blood*, vol. 119, no. 19, pp. 4527–4531, May 2012, doi: 10.1182/blood-2011-11-392167.

[210] Zhang, Y., Morgan, M. J., Chen, K., Choksi, S., & Liu, Z. G., "Induction of autophagy is essential for monocyte-macrophage differentiation," *Blood*, vol. 119, no. 12, pp. 2895–2905, Mar. 2012, doi: 10.1182/blood-2011-08-372383.

[211] Saitoh, T. … Akira, S., "Loss of the autophagy protein Atg16L1 enhances endotoxin-induced IL-1β production," *Nature*, vol. 456, no. 7219, pp. 264–268, Nov. 2008, doi: 10.1038/nature07383.

[212] Pu, Q. … Wu, M., " Atg7 Deficiency Intensifies Inflammasome Activation and Pyroptosis in Pseudomonas Sepsis ," *J. Immunol.*, vol. 198, no. 8, pp. 3205–3213, Apr. 2017, doi: 10.4049/jimmunol.1601196.

[213] Aflaki, E. … Sidransky, E., "Lysosomal storage and impaired autophagy lead to inflammasome activation in Gaucher macrophages," *Aging Cell*, vol. 15, no. 1, pp. 77–88, Feb. 2016, doi: 10.1111/acel.12409.

[214] Nimmerjahn, F., Milosevic, S., Behrends, U., Jaffee, E. M., Pardoll, D. M., Bornkamm, G. W., & Mautner, J., "Major histocompatibility complex class II-restricted presentation of a cytosolic antigen by autophagy," *Eur. J. Immunol.*, vol. 33, no. 5, pp. 1250–1259, May 2003, doi: 10.1002/eji.200323730.

[215] Dengjel, J. … Stevanovic, S., "Autophagy promotes MHC class II presentation of peptides from intracellular source proteins," *Proc. Natl. Acad. Sci. U. S. A.*, vol. 102, no. 22, pp. 7922–7927, May 2005, doi: 10.1073/pnas.0501190102.

[216] Paludan, C., Schmid, D., Landthaler, M., Vockerodt, M., Kube, D., Tuschl, T., & Münz, C., "Endogenous MHC class II processing of a viral nuclear antigen after autophagy," *Science (80-.).*, vol. 307, no. 5709, pp. 593–596, Jan. 2005, doi: 10.1126/science.1104904.

[217] Alissafi, T. … Verginis, P., "Tregs restrain dendritic cell autophagy to ameliorate autoimmunity," *J. Clin. Invest.*, vol. 127, no. 7, pp. 2789–2804, Jun. 2017, doi: 10.1172/JCI92079.

[218] Pyo, J. O., Yoo, S. M., Ahn, H. H., Nah, J., Hong, S. H., Kam, T. I., Jung, S., & Jung, Y. K., "Overexpression of Atg5 in mice activates autophagy and extends lifespan,"

Nat. Commun., vol. 4, 2013, doi: 10.1038/ncomms3300.

[219] McCay, C. M., Crowell, M. F., & Maynard, L. A., "The effect of retarded growth upon the length of life span and upon the ultimate body size. 1935.," *Nutrition*, vol. 5, no. 3, pp. 155–71; discussion 172, 1989.

[220] Salminen, A. & Kaarniranta, K., "Regulation of the aging process by autophagy," *Trends in Molecular Medicine*, vol. 15, no. 5. pp. 217–224, May 2009. doi: 10.1016/j.molmed.2009.03.004.

[221] Barbosa, M. C., Grosso, R. A., & Fader, C. M., "Hallmarks of aging: An autophagic perspective," *Frontiers in Endocrinology*, vol. 10, no. JAN. Frontiers Media S.A., p. 790, Jan. 09, 2019. doi: 10.3389/fendo.2018.00790.

[222] Doherty, G. J. & McMahon, H. T., "Mechanisms of endocytosis.," *Annu. Rev. Biochem.*, vol. 78, pp. 857–902, 2009, doi: 10.1146/annurev.biochem.78.081307.110540.

[223] Marks, M. S., Woodruff, L., Ohno, H., & Bonifacino, J. S., "Protein targeting by tyrosine- and di-leucine-based signals: evidence for distinct saturable components.," *J. Cell Biol.*, vol. 135, no. 2, pp. 341–354, Oct. 1996, doi: 10.1083/jcb.135.2.341.

[224] Sorkin, A., "Cargo recognition during clathrin-mediated endocytosis: a team effort.," *Curr. Opin. Cell Biol.*, vol. 16, no. 4, pp. 392–399, Aug. 2004, doi: 10.1016/j.ceb.2004.06.001.

[225] Praefcke, G. J. K. & McMahon, H. T., "The dynamin superfamily: universal membrane tubulation and fission molecules?," *Nat. Rev. Mol. Cell Biol.*, vol. 5, no. 2, pp. 133–147, 2004, doi: 10.1038/nrm1313.

[226] David, C., McPherson, P. S., Mundigl, O., & de Camilli, P., "A role of amphiphysin in synaptic vesicle endocytosis suggested by its binding to dynamin in nerve terminals," *Proc. Natl. Acad. Sci. U. S. A.*, vol. 93, no. 1, pp. 331–335, Jan. 1996, doi: 10.1073/pnas.93.1.331.

[227] Lundmark, R. & Carlsson, S. R., "Sorting nexin 9 participates in clathrin-mediated endocytosis through interactions with the core components.," *J. Biol. Chem.*, vol. 278, no. 47, pp. 46772–46781, Nov. 2003, doi: 10.1074/jbc.M307334200.

[228] Peter, B. J., Kent, H. M., Mills, I. G., Vallis, Y., Butler, P. J. G., Evans, P. R., & McMahon, H. T., "BAR Domains as Sensors of Membrane Curvature: The Amphiphysin BAR Structure," *Science (80-.).*, vol. 303, no. 5657, pp. 495 LP – 499, Jan. 2004, doi: 10.1126/science.1092586.

[229] Lundmark, R. & Carlsson, S. R., "Regulated membrane recruitment of dynamin-2 mediated by sorting nexin 9.," *J. Biol. Chem.*, vol. 279, no. 41, pp. 42694–42702, Oct. 2004, doi: 10.1074/jbc.M407430200.

[230] Yoshida, Y. … Takei, K., "The stimulatory action of amphiphysin on dynamin function is dependent on lipid bilayer curvature," *EMBO J.*, vol. 23, no. 17, pp. 3483–3491, Sep. 2004, doi: https://doi.org/10.1038/sj.emboj.7600355.

[231] Scott, C. C., Vacca, F., & Gruenberg, J., "Endosome maturation, transport and functions," *Semin. Cell Dev. Biol.*, vol. 31, pp. 2–10, 2014, doi: https://doi.org/10.1016/j.semcdb.2014.03.034.

[232] Naslavsky, N. & Caplan, S., "The enigmatic endosome - Sorting the ins and outs of endocytic trafficking," *Journal of Cell Science*, vol. 131, no. 13. Company of Biologists Ltd, Jul. 01, 2018. doi: 10.1242/jcs.216499.

[233] Elkin, S. R., Lakoduk, A. M., & Schmid, S. L., "Endocytic pathways and endosomal trafficking: a primer," *Wiener Medizinische Wochenschrift*, vol. 166, no. 7–8. Springer-Verlag Wien, pp. 196–204, May 01, 2016. doi: 10.1007/s10354-016-0432-7.

[234] Cullen, P. J., "Endosomal sorting and signalling: an emerging role for sorting nexins," *Nat. Rev. Mol. Cell Biol.*, vol. 9, no. 7, pp. 574–582, Jul. 2008, doi: 10.1038/nrm2427.

[235] Itoh, T. & De Camilli, P., "BAR, F-BAR (EFC) and ENTH/ANTH domains in the regulation of membrane-cytosol interfaces and membrane curvature," *Biochimica et Biophysica Acta - Molecular and Cell Biology of Lipids*, vol. 1761, no. 8. pp. 897–912, Aug. 2006. doi: 10.1016/j.bbalip.2006.06.015.

[236] Kurochkina, N. & Guha, U., "SH3 domains: Modules of protein-protein interactions," *Biophysical Reviews*, vol. 5, no. 1. Springer Verlag, pp. 29–39, 2013. doi: 10.1007/s12551-012-0081-z.

[237] Yarar, D., Waterman-Storer, C. M., & Schmid, S. L., "SNX9 Couples Actin Assembly to Phosphoinositide Signals and Is Required for Membrane Remodeling during Endocytosis," *Dev. Cell*, vol. 13, no. 1, pp. 43–56, Jul. 2007, doi: 10.1016/j.devcel.2007.04.014.

[238] Park, J., Kim, Y., Lee, S., Park, J. J., Park, Z. Y., Sun, W., Kim, H., & Chang, S., "SNX18 shares a redundant role with SNX9 and modulates endocytic trafficking at the plasma membrane," *J. Cell Sci.*, vol. 123, no. 10, pp. 1742–1750, May 2010, doi: 10.1242/jcs.064170.

[239] Håberg, K., Lundmark, R., & Carlsson, S. R., "SNX18 is an SNX9 paralog that acts as a membrane tubulator in AP-1-positive endosomal trafficking," *J. Cell Sci.*, vol. 121, no. 9, pp. 1495–1505, May 2008, doi: 10.1242/jcs.028530.

[240] Bendris, N., Stearns, C. J. S., Reis, C. R., Rodriguez-Canales, J., Liu, H., Witkiewicz, A. W., & Schmid, S. L., "Sorting nexin 9 negatively regulates invadopodia formation and function in cancer cells," *J. Cell Sci.*, vol. 129, no. 14, pp. 2804–2816, Jul. 2016, doi: 10.1242/jcs.188045.

[241] Ma, M. P. C. & Chircop, M., "SNX9, SNX18 and SNX33 are required for progression: Through and completion of mitosis," *J. Cell Sci.*, vol. 125, no. 18, pp. 4372–4382, Sep. 2012, doi: 10.1242/jcs.105981.

[242] Zhang, P., Holowatyj, A. N., Roy, T., Pronovost, S. M., Marchetti, M., Liu, H., Ulrich, C. M., & Edgar, B. A., "An SH3PX1-Dependent Endocytosis-Autophagy Network Restrains Intestinal Stem Cell Proliferation by Counteracting EGFR-ERK Signaling," *Dev. Cell*, vol. 49, no. 4, pp. 574-589.e5, May 2019, doi: 10.1016/J.DEVCEL.2019.03.029.

[243] Hicks, L., Liu, G., Ukken, F. P., Lu, S., Bollinger, K. E., O'Connor-Giles, K., & Gonsalvez, G. B., "Depletion or over-expression of Sh3px1 results in dramatic changes in cell morphology.," *Biol. Open*, vol. 4, no. 11, pp. 1448–61, Oct. 2015, doi: 10.1242/bio.013755.

[244] Ukken, F. P. … O'Connor-Giles, K. M., "BAR-SH3 sorting nexins are conserved interacting proteins of Nervous wreck that organize synapses and promote neurotransmission," *J. Cell Sci.*, vol. 129, no. 1, p. 166, 2016, doi: 10.1242/JCS.178699.

[245] Longatti, A., Lamb, C. A., Razi, M., Yoshimura, S. I., Barr, F. A., & Tooze, S. A., "TBC1D14 regulates autophagosome formation via Rab11- and ULK1-positive recycling endosomes," *J. Cell Biol.*, vol. 197, no. 5, pp. 659–675, May 2012, doi: 10.1083/jcb.201111079.

[246] Guo, Y., Chang, C., Huang, R., Liu, B., Bao, L., & Liu, W., "AP1 is essential for generation of autophagosomes from the trans-Golgi network," *J. Cell Sci.*, vol. 125, no. 7, pp. 1706–1715, Apr. 2012, doi: 10.1242/jcs.093203.

[247] Hoffmann, J. A. & Reichhart, J.-M., "Drosophila innate immunity: an evolutionary perspective," *Nat. Immunol.*, vol. 3, no. 2, pp. 121–126, Feb. 2002, doi: 10.1038/ni0202-121.

[248] Sheehan, G., Garvey, A., Croke, M., & Kavanagh, K., "Innate humoral immune defences in mammals and insects: The same, with differences ?," *Virulence*, vol. 9, no. 1, pp. 1625–1639, Dec. 2018, doi: 10.1080/21505594.2018.1526531.

[249] Buchon, N., Silverman, N., & Cherry, S., "Immunity in Drosophila melanogaster-from microbial recognition to whole-organism physiology," *Nature Reviews Immunology*, vol. 14, no. 12. Nature Publishing Group, pp. 796–810, Dec. 11, 2014. doi: 10.1038/nri3763.

[250] Ferrandon, D., Jung, A. C., Criqui, M., Lemaitre, B., Uttenweiler-Joseph, S., Michaut, L., Reichhart, J., & Hoffmann, J. A., "A drosomycin-GFP reporter transgene reveals a local immune response in Drosophila that is not dependent on the Toll pathway.," *EMBO J.*, vol. 17, no. 5, pp. 1217–1227, Aug. 1998, doi: 10.1093/emboj/17.5.1217.

[251] Tzou, P., Ohresser, S., Ferrandon, D., Capovilla, M., Reichhart, J.-M., Lemaitre, B., Hoffmann, J. A., & Imler, J.-L., "Tissue-Specific Inducible Expression of Antimicrobial Peptide Genes in Drosophila Surface Epithelia," *Immunity*, vol. 13, no. 5, pp. 737–748, Nov. 2000, doi: 10.1016/S1074-7613(00)00072-8.

[252] Önfelt Tingvall, T., Roos, E., & Engström, Y., "The imd gene is required for local Cecropin expression in Drosophila barrier epithelia," *EMBO Rep.*, vol. 2, no. 3, pp. 239–243, Mar. 2001, doi: 10.1093/embo-reports/kve048.

[253] Buchon, N., Broderick, N. A., & Lemaitre, B., "Gut homeostasis in a microbial world: insights from Drosophila melanogaster," *Nat. Rev. Microbiol.*, vol. 11, no. 9, pp. 615–626, Sep. 2013, doi: 10.1038/nrmicro3074.

[254] Lemaitre, B., Kromer-Metzger, E., Michaut, L., Nicolas, E., Meister, M., Georgel, P., Reichhart, J. M., & Hoffmann, J. A., "A recessive mutation, immune deficiency (imd),

defines two distinct control pathways in the Drosophila host defense," *Proc. Natl. Acad. Sci. U. S. A.*, vol. 92, no. 21, pp. 9465–9469, Oct. 1995, doi: 10.1073/pnas.92.21.9465.

[255] Corbo, J. C. & Levine, M., "Characterization of an immunodeficiency mutant in Drosophila," *Mech. Dev.*, vol. 55, no. 2, pp. 211–220, Apr. 1996, doi: 10.1016/0925-4773(96)00506-0.

[256] Lemaitre, B. & Hoffmann, J., " The Host Defense of Drosophila melanogaster ," *Annu. Rev. Immunol.*, vol. 25, no. 1, pp. 697–743, Apr. 2007, doi: 10.1146/annurev.immunol.25.022106.141615.

[257] Hoffmann, J. A., "The immune response of Drosophila.," *Nature*, vol. 426, no. 6962, pp. 33–8, Nov. 2003, doi: 10.1038/nature02021.

[258] Hedengren, M., Åsling, B., Dushay, M. S., Ando, I., Ekengren, S., Wihlborg, M., & Hultmark, D., "Relish, a central factor in the control of humoral but not cellular immunity in Drosophila," *Mol. Cell*, vol. 4, no. 5, pp. 827–837, Nov. 1999, doi: 10.1016/S1097-2765(00)80392-5.

[259] Stöven, S., Ando, I., Kadalayil, L., Engström, Y., & Hultmark, D., "Activation of the Drosophila NF-κB factor Relish by rapid endoproteolytic cleavage," *EMBO Rep.*, vol. 1, no. 4, pp. 347–352, Oct. 2000, doi: 10.1093/embo-reports/kvd072.

[260] Janeway, C. A., "Approaching the asymptote? Evolution and revolution in immunology," in *Cold Spring Harbor Symposia on Quantitative Biology*, Jan. 1989, vol. 54, no. 1, pp. 1–13. doi: 10.1101/sqb.1989.054.01.003.

[261] Mengin-Lecreulx, D. & Lemaitre, B., "Structure and metabolism of peptidoglycan and molecular requirements allowing its detection by the Drosophila innate immune system," *J. Endotoxin Res.*, vol. 11, no. 2, pp. 105–111, 2005, doi: 10.1179/096805105X35233.

[262] Wheeler, R., Chevalier, G., Eberl, G., & Gomperts Boneca, I., "The biology of bacterial peptidoglycans and their impact on host immunity and physiology," *Cell. Microbiol.*, vol. 16, no. 7, pp. 1014–1023, Jul. 2014, doi: 10.1111/cmi.12304.

[263] Werner, T., Liu, G., Kang, D., Ekengren, S., Steiner, H., & Hultmark, D., "A family of peptidoglycan recognition proteins in the fruit fly Drosophila melanogaster," *Proc. Natl. Acad. Sci.*, vol. 97, no. 25, pp. 13772–13777, Dec. 2000, doi: 10.1073/pnas.97.25.13772.

[264] Kurata, S., "Peptidoglycan recognition proteins in Drosophila immunity," *Dev. Comp. Immunol.*, vol. 42, no. 1, pp. 36–41, Jan. 2014, doi: 10.1016/j.dci.2013.06.006.

[265] Liu, C., Xu, Z., Gupta, D., & Dziarski, R., "Peptidoglycan recognition proteins: A novel family of four human innate immunity pattern recognition molecules," *J. Biol. Chem.*, vol. 276, no. 37, pp. 34686–34694, Sep. 2001, doi: 10.1074/jbc.M105566200.

[266] Liu, C., Gelius, E., Liu, G., Steiner, H., & Dziarski, R., "Mammalian peptidoglycan recognition protein binds peptidoglycan with high affinity, is expressed in neutrophils, and inhibits bacterial growth," *J. Biol. Chem.*, vol. 275, no. 32, pp. 24490–24499, Aug.

2000, doi: 10.1074/jbc.M001239200.

[267] Rämet, M., Manfruelli, P., Pearson, A., Mathey-Prevot, B., & Ezekowitz, R. A. B., "Functional genomic analysis of phagocytosis and identification of a Drosophila receptor for E. Coli," *Nature*, vol. 416, no. 6881, pp. 644–648, Apr. 2002, doi: 10.1038/nature735.

[268] Gottar, M., Gobert, V., Michel, T., Belvin, M., Duyk, G., Hoffmann, J. A., Ferrandon, D., & Royet, J., "The Drosophila immune response against Gram-negative bacteria is mediated by a peptidoglycan recognition protein," *Nature*, vol. 416, no. 6881, pp. 640–644, Apr. 2002, doi: 10.1038/nature734.

[269] Choe, K. M., Werner, T., Stöven, S., Hultmark, D., & Anderson, K. V., "Requirement for a peptidoglycan recognition protein (PGRP) in relish activation and antibacterial immune responses in Drosophila," *Science (80-.).*, vol. 296, no. 5566, pp. 359–362, Apr. 2002, doi: 10.1126/science.1070216.

[270] Werner, T., Borge-Renberg, K., Mellroth, P., Steiner, H., & Hultmark, D., "Functional diversity of the Drosophila PGRP-LC gene cluster in the response to lipopolysaccharide and peptidoglycan," *J. Biol. Chem.*, vol. 278, no. 29, pp. 26319–26322, Jul. 2003, doi: 10.1074/jbc.C300184200.

[271] Chang, C. I., Chelliah, Y., Borek, D., Mengin-Lecreulx, D., & Deisanhofer, J., "Structure of tracheal cytotoxin in complex with a heterodimeric pattern-recognition receptor," *Science (80-.).*, vol. 311, no. 5768, pp. 1761–1764, Mar. 2006, doi: 10.1126/science.1123056.

[272] Chang, C. I., Ihara, K., Chelliah, Y., Mengin-Lecreulx, D., Wakatsuki, S., & Deisenhofer, J., "Structure of the ectodomain of Drosophila peptidoglycan-recognition protein LCa suggests a molecular mechanism for pattern recognition," *Proc. Natl. Acad. Sci. U. S. A.*, vol. 102, no. 29, pp. 10279–10284, Jul. 2005, doi: 10.1073/pnas.0504547102.

[273] Neyen, C., Poidevin, M., Roussel, A., & Lemaitre, B., " Tissue- and Ligand-Specific Sensing of Gram-Negative Infection in Drosophila by PGRP-LC Isoforms and PGRP-LE ," *J. Immunol.*, vol. 189, no. 4, pp. 1886–1897, Aug. 2012, doi: 10.4049/jimmunol.1201022.

[274] Kaneko, T. … Silverman, N., "PGRP-LC and PGRP-LE have essential yet distinct functions in the drosophila immune response to monomeric DAP-type peptidoglycan," *Nat. Immunol.*, vol. 7, no. 7, pp. 715–723, Jul. 2006, doi: 10.1038/ni1356.

[275] Takehana, A., Katsuyama, T., Yano, T., Oshima, Y., Takada, H., Aigaki, T., & Kurata, S., "Overexpression of a pattern-recognition receptor, peptidoglycan-recognition protein-LE, activates imd/relish-mediated antibacterial defense and the prophenoloxidase cascade in Drosophila larvae," *Proc. Natl. Acad. Sci. U. S. A.*, vol. 99, no. 21, pp. 13705–13710, Oct. 2002, doi: 10.1073/pnas.212301199.

[276] Yano, T. … Kurata, S., "Autophagic control of listeria through intracellular innate immune recognition in drosophila," *Nat. Immunol.*, vol. 9, no. 8, pp. 908–916, Aug. 2008, doi: 10.1038/ni.1634.

[277] Persson, C., Oldenvi, S., & Steiner, H., "Peptidoglycan recognition protein LF: A negative regulator of Drosophila immunity," *Insect Biochem. Mol. Biol.*, vol. 37, no. 12, pp. 1309–1316, Dec. 2007, doi: 10.1016/j.ibmb.2007.08.003.

[278] Basbous, N., Coste, F., Leone, P., Vincentelli, R., Royet, J., Kellenberger, C., & Roussel, A., "The Drosophila peptidoglycan-recognition protein LF interacts with peptidoglycan-recognition protein LC to downregulate the Imd pathway," *EMBO Rep.*, vol. 12, no. 4, pp. 327–333, Apr. 2011, doi: 10.1038/embor.2011.19.

[279] Gendrin, M., Zaidman-Rémy, A., Broderick, N. A., Paredes, J., Poidevin, M., Roussel, A., & Lemaitre, B., "Functional Analysis of PGRP-LA in Drosophila Immunity," *PLoS One*, vol. 8, no. 7, Jul. 2013, doi: 10.1371/journal.pone.0069742.

[280] Zaidman-Rémy, A. … Lemaitre, B., "The Drosophila Amidase PGRP-LB Modulates the Immune Response to Bacterial Infection," *Immunity*, vol. 24, no. 4, pp. 463–473, Apr. 2006, doi: 10.1016/j.immuni.2006.02.012.

[281] Mellroth, P., Karlsson, J., & Steiner, H., "A scavenger function for a Drosophila peptidoglycan recognition protein," *J. Biol. Chem.*, vol. 278, no. 9, pp. 7059–7064, Feb. 2003, doi: 10.1074/jbc.M208900200.

[282] Gendrin, M., Welchman, D. P., Poidevin, M., Hervé, M., & Lemaitre, B., "Long-range activation of systemic immunity through peptidoglycan diffusion in Drosophila," *PLoS Pathog.*, vol. 5, no. 12, Dec. 2009, doi: 10.1371/journal.ppat.1000694.

[283] Paredes, J. C., Welchman, D. P., Poidevin, M., & Lemaitre, B., "Negative regulation by Amidase PGRPs shapes the drosophila antibacterial response and protects the Fly from innocuous infection," *Immunity*, vol. 35, no. 5, pp. 770–779, Nov. 2011, doi: 10.1016/j.immuni.2011.09.018.

[284] Myllymaki, H., Valanne, S., & Ramet, M., "The Drosophila Imd Signaling Pathway," *J. Immunol.*, vol. 192, no. 8, pp. 3455–3462, Apr. 2014, doi: 10.4049/jimmunol.1303309.

[285] Dushay, M. S., Åsling, B., & Hultmark, D., "Origins of immunity: Relish, a compound rel-like gene in the antibacterial defense of Drosophila," *Proc. Natl. Acad. Sci. U. S. A.*, vol. 93, no. 19, pp. 10343–10347, Sep. 1996, doi: 10.1073/pnas.93.19.10343.

[286] Mellroth, P., Karlsson, J., Håkansson, J., Schultz, N., Goldman, W. E., & Steiner, H., "Ligand-induced dimerization of Drosophila peptidoglycan recognition proteins in vitro," *Proc. Natl. Acad. Sci. U. S. A.*, vol. 102, no. 18, pp. 6455–6460, May 2005, doi: 10.1073/pnas.0407559102.

[287] Georgel, P. … Hoffmann, J. A., "Drosophila Immune Deficiency (IMD) Is a Death Domain Protein that Activates Antibacterial Defense and Can Promote Apoptosis," *Dev. Cell*, vol. 1, no. 4, pp. 503–514, Oct. 2001, doi: 10.1016/S1534-5807(01)00059-4.

[288] Leulier, F., Vidal, S., Saigo, K., Ueda, R., & Lemaitre, B., "Inducible expression of double-stranded RNA reveals a role for dFADD in the regulation of the antibacterial response in Drosophila adults," *Curr. Biol.*, vol. 12, no. 12, pp. 996–1000, Jun. 2002, doi: 10.1016/S0960-9822(02)00873-4.

[289] Leulier, F., Rodriguez, A., Khush, R. S., Abrams, J. M., & Lemaitre, B., "The Drosophila caspase Dredd is required to resist Gram-negative bacterial infection," *EMBO Rep.*, vol. 1, no. 4, pp. 353–358, 2000, doi: 10.1093/embo-reports/kvd073.

[290] Leulier, F., Lhocine, N., Lemaitre, B., & Meier, P., "The Drosophila Inhibitor of Apoptosis Protein DIAP2 Functions in Innate Immunity and Is Essential To Resist Gram-Negative Bacterial Infection," *Mol. Cell. Biol.*, vol. 26, no. 21, pp. 7821–7831, Nov. 2006, doi: 10.1128/mcb.00548-06.

[291] Meinander, A. … Meier, P., "Ubiquitylation of the initiator caspase DREDD is required for innate immune signalling," *EMBO J.*, vol. 31, no. 12, pp. 2770–2783, Jun. 2012, doi: 10.1038/emboj.2012.121.

[292] Zhou, R., Silverman, N., Hong, M., Liao, D. S., Chung, Y., Chen, Z. J., & Maniatis, T., "The role of ubiquitination in Drosophila innate immunity," *J. Biol. Chem.*, vol. 280, no. 40, pp. 34048–34055, Oct. 2005, doi: 10.1074/jbc.M506655200.

[293] Paquette, N., Broemer, M., Aggarwal, K., Chen, L., Husson, M., Ertürk-Hasdemir, D., Reichhart, J. M., Meier, P., & Silverman, N., "Caspase-Mediated Cleavage, IAP Binding, and Ubiquitination: Linking Three Mechanisms Crucial for Drosophila NF-κB Signaling," *Mol. Cell*, vol. 37, no. 2, pp. 172–182, Jan. 2010, doi: 10.1016/j.molcel.2009.12.036.

[294] Silverman, N., Zhou, R., Erlich, R. L., Hunter, M., Bernstein, E., Schneider, D., & Maniatis, T., "Immune activation of NF-kappaB and JNK requires Drosophila TAK1.," *J. Biol. Chem.*, vol. 278, no. 49, pp. 48928–48934, Dec. 2003, doi: 10.1074/jbc.M304802200.

[295] Zhuang, Z. H., Sun, L., Kong, L., Hu, J. H., Yu, M. C., Reinach, P., Zang, J. W., & Ge, B. X., "Drosophila TAB2 is required for the immune activation of JNK and NF-kappaB," *Cell. Signal.*, vol. 18, no. 7, pp. 964–970, 2006, doi: 10.1016/j.cellsig.2005.08.020.

[296] Shibuya, H., Yamaguchi, K., Shirakabe, K., Tonegawa, A., Gotoh, Y., Ueno, N., Irie, K., Nishida, E., & Matsumoto, K., "TAB1 : An activator of the TAK1 MAPKKK in TGF-β signal transduction," *Science (80-.).*, vol. 272, no. 5265, pp. 1179–1182, May 1996, doi: 10.1126/science.272.5265.1179.

[297] Besse, A., Lamothe, B., Campos, A. D., Webster, W. K., Maddineni, U., Lin, S. C., Wu, H., & Darnay, B. G., "TAK1-dependent signaling requires functional interaction with TAB2/TAB3," *J. Biol. Chem.*, vol. 282, no. 6, pp. 3918–3928, Jan. 2007, doi: 10.1074/jbc.M608867200.

[298] Lu, Y., Wu, L. P., & Anderson, K. V., "The antibacterial arm of the Drosophila innate immune response requires an IκB kinase," *Genes Dev.*, vol. 15, no. 1, pp. 104–110, Jan. 2001, doi: 10.1101/gad.856901.

[299] Silverman, N., Zhou, R., Stöven, S., Pandey, N., Hultmark, D., & Maniatis, T., "A Drosophila IκB kinase complex required for relish cleavage and antibacterial immunity," *Genes Dev.*, vol. 14, no. 19, pp. 2461–2471, Oct. 2000, doi: 10.1101/gad.817800.

[300] Ertürk-Hasdemir, D. … Silverman, N., "Two roles for the Drosophila IKK complex in the activation of Relish and the induction of antimicrobial peptide genes," *Proc. Natl. Acad. Sci. U. S. A.*, vol. 106, no. 24, pp. 9779–9784, Jun. 2009, doi: 10.1073/pnas.0812022106.

[301] Bulet, P., Dimarcq, J. L., Hetru, C., Lagueux, M., Charlet, M., Hegy, G., Van Dorsselaer, A., & Hoffmann, J. A., "A novel inducible antibacterial peptide of Drosophila carries an O- glycosylated substitution," *J. Biol. Chem.*, vol. 268, no. 20, pp. 14893–14897, Jul. 1993.

[302] Åsling, B., Dushay, M. S., & Hultmark, D., "Identification of early genes in the Drosophila immune response by PCR-based differential display: the Attacin A gene and the evolution of attacin-like proteins," *Insect Biochem. Mol. Biol.*, vol. 25, no. 4, pp. 511–518, Apr. 1995, doi: 10.1016/0965-1748(94)00091-C.

[303] Reichhart, J.-M., Meister, M., Dimarcq, J.-L., Zachary, D., Hoffmann, D., Ruiz, C., Richards, G., & Hoffmann, J. A., "Insect immunity: developmental and inducible activity of the Drosophila diptericin promoter," 1992.

[304] Tanji, T., Hu, X., Weber, A. N. R., & Ip, Y. T., "Toll and IMD Pathways Synergistically Activate an Innate Immune Response in Drosophila melanogaster," *Mol. Cell. Biol.*, vol. 27, no. 12, pp. 4578–4588, Jun. 2007, doi: 10.1128/mcb.01814-06.

[305] Lemaitre, B., Reichhart, J. M., & Hoffmann, J. A., "Drosophila host defense: Differential induction of antimicrobial peptide genes after infection by various classes of microorganisms," *Proc. Natl. Acad. Sci. U. S. A.*, vol. 94, no. 26, pp. 14614–14619, Dec. 1997, doi: 10.1073/pnas.94.26.14614.

[306] Thevenon, D. … Fauvarque, M. O., "The Drosophila Ubiquitin-Specific Protease dUSP36/Scny Targets IMD to Prevent Constitutive Immune Signaling," *Cell Host Microbe*, vol. 6, no. 4, pp. 309–320, Nov. 2009, doi: 10.1016/j.chom.2009.09.007.

[307] Fernando, M. D. A., Kounatidis, I., & Ligoxygakis, P., "Loss of Trabid, a New Negative Regulator of the Drosophila Immune-Deficiency Pathway at the Level of TAK1, Reduces Life Span," *PLOS Genet.*, vol. 10, no. 2, p. e1004117, Feb. 2014.

[308] Tsuda, M., Langmann, C., Harden, N., & Aigaki, T., "The RING-finger scaffold protein Plenty of SH3s targets TAK1 to control immunity signalling in Drosophila," *EMBO Rep.*, vol. 6, no. 11, pp. 1082–1087, Nov. 2005, doi: 10.1038/sj.embor.7400537.

[309] Trompouki, E., Hatzivassillou, E., Tsichritzis, T., Farmer, H., Ashworth, A., & Mosialos, G., "CYLD is a deubiquitinating enzyme that negatively regulates NF-κB activation by TNFR family members," *Nature*, vol. 424, no. 6950, pp. 793–796, 2003, doi: 10.1038/nature01803.

[310] Tsichritzis, T., Gaentzsch, P. C., Kosmidis, S., Brown, A. E., Skoulakis, E. M., Ligoxygakis, P., & Mosialos, G., "A Drosophila ortholog of the human cylindromatosis tumor suppressor gene regulates triglyceride content and antibacterial defense," *Development*, vol. 134, no. 14, pp. 2605–2614, Jul. 2007, doi:

10.1242/dev.02859.

[311] Guntermann, S., Primrose, D. A., & Foley, E., "Dnr1-dependent regulation of the Drosophila immune deficiency signaling pathway," *Dev. Comp. Immunol.*, vol. 33, no. 1, pp. 127–134, Jan. 2009, doi: 10.1016/j.dci.2008.07.021.

[312] Kim, M., Lee, J. H., Lee, S. Y., Kim, E., & Chung, J., "Caspar, a suppressor of antibacterial immunity in Drosophila," *Proc. Natl. Acad. Sci. U. S. A.*, vol. 103, no. 44, pp. 16358–16363, Oct. 2006, doi: 10.1073/pnas.0603238103.

[313] Khush, R. S., Cornwell, W. D., Uram, J. N., & Lemaitre, B., "A ubiquitin-proteasome pathway represses the Drosophila immune deficiency signaling cascade," *Curr. Biol.*, vol. 12, no. 20, pp. 1728–1737, Oct. 2002, doi: 10.1016/S0960-9822(02)01214-9.

[314] Shibata, T., Sekihara, S., Fujikawa, T., Miyaji, R., Maki, K., Ishihara, T., Koshiba, T., & Kawabata, S. I., "Transglutaminase-catalyzed protein-protein cross-linking suppresses the activity of the NF-κB-like transcription factor relish," *Sci. Signal.*, vol. 6, no. 285, Jul. 2013, doi: 10.1126/scisignal.2003970.

[315] Lhocine, N. … Leulier, F., "PIMS Modulates Immune Tolerance by Negatively Regulating Drosophila Innate Immune Signaling," *Cell Host Microbe*, vol. 4, no. 2, pp. 147–158, Aug. 2008, doi: 10.1016/j.chom.2008.07.004.

[316] Kleino, A., Myllymäki, H., Kallio, J., Vanha-aho, L.-M., Oksanen, K., Ulvila, J., Hultmark, D., Valanne, S., & Rämet, M., "Pirk is a negative regulator of the Drosophila Imd pathway.," *J. Immunol.*, vol. 180, no. 8, pp. 5413–22, Apr. 2008, doi: 10.4049/JIMMUNOL.180.8.5413.

[317] Aggarwal, K., Rus, F., Vriesema-Magnuson, C., Ertürk-Hasdemir, D., Paquette, N., & Silverman, N., "Rudra interrupts receptor signaling complexes to negatively regulate the IMD pathway," *PLoS Pathog.*, vol. 4, no. 8, Aug. 2008, doi: 10.1371/journal.ppat.1000120.

[318] Buchon, N., Osman, D., David, F. P. A., Yu Fang, H., Boquete, J. P., Deplancke, B., & Lemaitre, B., "Morphological and Molecular Characterization of Adult Midgut Compartmentalization in Drosophila," *Cell Rep.*, vol. 3, no. 5, pp. 1725–1738, May 2013, doi: 10.1016/j.celrep.2013.04.001.

[319] Ren, C., Webster, P., Finkel, S. E., & Tower, J., "Increased Internal and External Bacterial Load during Drosophila Aging without Life-Span Trade-Off," *Cell Metab.*, vol. 6, no. 2, pp. 144–152, Aug. 2007, doi: 10.1016/j.cmet.2007.06.006.

[320] Ryu, J. H. … Lee, W. J., "Innate immune homeostasis by the homeobox gene Caudal and commensal-gut mutualism in Drosophila," *Science (80-.).*, vol. 319, no. 5864, pp. 777–782, Feb. 2008, doi: 10.1126/science.1149357.

[321] Buchon, N., Broderick, N. A., Chakrabarti, S., & Lemaitre, B., "Invasive and indigenous microbiota impact intestinal stem cell activity through multiple pathways in Drosophila," *Genes Dev.*, vol. 23, no. 19, pp. 2333–2344, Oct. 2009, doi: 10.1101/gad.1827009.

[322] Kovacs, E. J., Palmer, J. L., Fortin, C. F., Fülöp, T., Goldstein, D. R., & Linton, P. J.,

"Aging and innate immunity in the mouse: impact of intrinsic and extrinsic factors," *Trends in Immunology*, vol. 30, no. 7. Trends Immunol, pp. 319–324, Jul. 2009. doi: 10.1016/j.it.2009.03.012.

[323] Adler, A. S., Sinha, S., Kawahara, T. L. A., Zhang, J. Y., Segal, E., & Chang, H. Y., "Motif module map reveals enforcement of aging by continual NF-κB activity," *Genes Dev.*, vol. 21, no. 24, pp. 3244–3257, Dec. 2007, doi: 10.1101/gad.1588507.

[324] Zerofsky, M., Harel, E., Silverman, N., & Tatar, M., "Aging of the innate immune response in Drosophila melanogaster," *Aging Cell*, vol. 4, no. 2, pp. 103–108, Apr. 2005, doi: 10.1111/j.1474-9728.2005.00147.x.

[325] Broderick, N. A., Buchon, N., & Lemaitre, B., "Microbiota-induced changes in Drosophila melanogaster host gene expression and gut morphology," *MBio*, vol. 5, no. 3, May 2014, doi: 10.1128/mBio.01117-14.

[326] Guo, L., Karpac, J., Tran, S. L., & Jasper, H., "PGRP-SC2 promotes gut immune homeostasis to limit commensal dysbiosis and extend lifespan," *Cell*, vol. 156, no. 1–2, pp. 109–122, 2014, doi: 10.1016/j.cell.2013.12.018.

[327] Biteau, B., Hochmuth, C. E., & Jasper, H., "JNK activity in somatic stem cells causes loss of tissue homeostasis in the aging Drosophila gut.," *Cell Stem Cell*, vol. 3, no. 4, pp. 442–455, Oct. 2008, doi: 10.1016/j.stem.2008.07.024.

[328] Choi, N.-H., Kim, J.-G., Yang, D.-J., Kim, Y.-S., & Yoo, M.-A., "Age-related changes in Drosophila midgut are associated with PVF2, a PDGF/VEGF-like growth factor.," *Aging Cell*, vol. 7, no. 3, pp. 318–334, Jun. 2008, doi: 10.1111/j.1474-9726.2008.00380.x.

[329] Rera, M., Clark, R. I., & Walker, D. W., "Intestinal barrier dysfunction links metabolic and inflammatory markers of aging to death in Drosophila.," *Proc. Natl. Acad. Sci. U. S. A.*, vol. 109, no. 52, pp. 21528–21533, Dec. 2012, doi: 10.1073/pnas.1215849110.

[330] Cao, Y., Chtarbanova, S., Petersen, A. J., & Ganetzky, B., "Dnr1 mutations cause neurodegeneration in Drosophila by activating the innate immune response in the brain," *Proc. Natl. Acad. Sci. U. S. A.*, vol. 110, no. 19, pp. E1752–E1760, May 2013, doi: 10.1073/pnas.1306220110.

[331] Loch, G., Zinke, I., Mori, T., Carrera, P., Schroer, J., Takeyama, H., & Hoch, M., "Antimicrobial peptides extend lifespan in Drosophila," *PLoS One*, vol. 12, no. 5, May 2017, doi: 10.1371/journal.pone.0176689.

[332] Tzou, P., Reichhart, J. M., & Lemaitre, B., "Constitutive expression of a single antimicrobial peptide can restore wild-type resistance to infection in immunodeficient Drosophila mutants," *Proc. Natl. Acad. Sci. U. S. A.*, vol. 99, no. 4, pp. 2152–2157, Feb. 2002, doi: 10.1073/pnas.042411999.

[333] Rutschmann, S., Jung, A. C., Zhou, R., Silverman, N., Hoffmann, J. A., & Ferrandon, D., "Role of Drosophila IKKγ in a Toll-independent antibacterial immune response," *Nat. Immunol.*, vol. 1, no. 4, pp. 342–347, 2000, doi: 10.1038/79801.

[334] Bischof, J. & Basler, K., "Recombinases and their use in gene activation, gene

inactivation, and transgenesis.," *Methods Mol. Biol.*, vol. 420, pp. 175–195, 2008, doi: 10.1007/978-1-59745-583-1_10.

[335] Bradford, M., "A Rapid and Sensitive Method for the Quantitation of Microgram Quantities of Protein Utilizing the Principle of Protein-Dye Binding," *Anal. Biochem.*, vol. 72, no. 1–2, pp. 248–254, May 1976, doi: 10.1006/abio.1976.9999.

[336] Laemmli, U. K., "Cleavage of structural proteins during the assembly of the head of bacteriophage T4," *Nature*, vol. 227, no. 5259, pp. 680–685, 1970, doi: 10.1038/227680a0.

[337] Basset, A., Khush, R. S., Braun, A., Gardan, L., Boccard, F., Hoffmann, J. A., & Lemaitre, B., "The phytopathogenic bacteria Erwinia carotovora infects Drosophila and activates an immune response," *Proc. Natl. Acad. Sci.*, vol. 97, no. 7, pp. 3376–3381, Mar. 2000, doi: 10.1073/pnas.97.7.3376.

[338] Griffiths, E., "Effect of pH and haem compounds on the killing of Pasteurella septica by specific antiserum," *J. Gen. Microbiol.*, vol. 88, no. 2, pp. 345–354, 1975, doi: 10.1099/00221287-88-2-345.

[339] Kalvari, I., Tsompanis, S., Mulakkal, N. C., Osgood, R., Johansen, T., Nezis, I. P., & Promponas, V. J., "iLIR: A web resource for prediction of Atg8-family interacting proteins," *Autophagy*, vol. 10, no. 5. Taylor and Francis Inc., pp. 913–925, 2014. doi: 10.4161/auto.28260.

[340] Tusco, R., "Molecular mechanisms of selective autophagy in innate immunity," University of Warwick, 2017.

[341] Wild, P., McEwan, D. G., & Dikic, I., "The LC3 interactome at a glance," *J. Cell Sci.*, vol. 127, no. 1, pp. 3–9, Jan. 2014, doi: 10.1242/jcs.140426.

[342] Husnjak, K. & Dikic, I., "Ubiquitin-binding proteins: Decoders of ubiquitin-mediated cellular functions," *Annu. Rev. Biochem.*, vol. 81, pp. 291–322, Jul. 2012, doi: 10.1146/annurev-biochem-051810-094654.

[343] Schultz, J., Milpetz, F., Bork, P., & Ponting, C. P., "SMART, a simple modular architecture research tool: Identification of signaling domains," *Proc. Natl. Acad. Sci. U. S. A.*, vol. 95, no. 11, pp. 5857–5864, May 1998, doi: 10.1073/pnas.95.11.5857.

[344] Mistry, J. … Bateman, A., "Pfam: The protein families database in 2021," *Nucleic Acids Res.*, vol. 49, no. D1, pp. D412–D419, Jan. 2021, doi: 10.1093/nar/gkaa913.

[345] Blum, M. … Finn, R. D., "The InterPro protein families and domains database: 20 years on," *Nucleic Acids Res.*, vol. 49, no. D1, pp. D344–D354, Jan. 2021, doi: 10.1093/nar/gkaa977.

[346] Dosztányi, Z., Mészáros, B., & Simon, I., "ANCHOR: Web server for predicting protein binding regions in disordered proteins," *Bioinformatics*, vol. 25, no. 20, pp. 2745–2746, Oct. 2009, doi: 10.1093/bioinformatics/btp518.

[347] Fields, S. & Song, O. K., "A novel genetic system to detect protein-protein interactions," *Nature*, vol. 340, no. 6230, pp. 245–246, 1989, doi: 10.1038/340245a0.

[348] Brooks, D., Naeem, F., Stetsiv, M., Goetting, S. C., Bawa, S., Green, N., Clark, C., Bashirullah, A., & Geisbrecht, E. R., "Drosophila NUAK functions with Starvin/BAG3 in autophagic protein turnover," *PLoS Genet.*, vol. 16, no. 4, p. e1008700, Apr. 2020, doi: 10.1371/journal.pgen.1008700.

[349] Groth, A. C., Fish, M., Nusse, R., & Calos, M. P., "Construction of Transgenic Drosophila by Using the Site-Specific Integrase from Phage φC31," *Genetics*, vol. 166, no. 4, pp. 1775–1782, Apr. 2004, doi: 10.1534/genetics.166.4.1775.

[350] Bischof, J., Maeda, R. K., Hediger, M., Karch, F., & Basler, K., "An optimized transgenesis system for Drosophila using germ-line-specific φC31 integrases," *Proc. Natl. Acad. Sci. U. S. A.*, vol. 104, no. 9, pp. 3312–3317, Feb. 2007, doi: 10.1073/pnas.0611511104.

[351] Lőrincz, P., Mauvezin, C., & Juhász, G., "Exploring Autophagy in Drosophila," *Cells*, vol. 6, no. 3, p. 22, Jul. 2017, doi: 10.3390/cells6030022.

[352] Jacomin, A. C. & Nezis, I. P., "Using fluorescent reporters to monitor autophagy in the female germline cells in Drosophila melanogaster," in *Methods in Molecular Biology*, vol. 1457, Humana Press Inc., 2016, pp. 69–78. doi: 10.1007/978-1-4939-3795-0_5.

[353] Prabakaran, T. … Paludan, S. R., " Attenuation of c GAS - STING signaling is mediated by a p62/ SQSTM 1-dependent autophagy pathway activated by TBK1 ," *EMBO J.*, vol. 37, no. 8, p. e97858, Apr. 2018, doi: 10.15252/embj.201797858.

[354] Mauvezin, C., Ayala, C., Braden, C. R., Kim, J., & Neufeld, T. P., "Assays to monitor autophagy in Drosophila," vol. 68, no. 1, Jun. 2014, doi: 10.1016/j.ymeth.2014.03.014.

[355] Engström, Y., "Induction and regulation of antimicrobial peptides in Drosophila," *Dev. Comp. Immunol.*, vol. 23, no. 4, pp. 345–358, 1999, doi: https://doi.org/10.1016/S0145-305X(99)00016-6.

[356] Hanson, M. A., Dostálová, A., Ceroni, C., Poidevin, M., Kondo, S., & Lemaitre, B., "Synergy and remarkable specificity of antimicrobial peptides in vivo using a systematic knockout approach," *Elife*, vol. 8, Feb. 2019, doi: 10.7554/eLife.44341.

[357] Libert, S., Chao, Y., Chu, X., & Pletcher, S. D., "Trade-offs between longevity and pathogen resistance in Drosophila melanogaster are mediated by NFkappaB signaling.," *Aging Cell*, vol. 5, no. 6, pp. 533–543, Dec. 2006, doi: 10.1111/j.1474-9726.2006.00251.x.

[358] Giot, L. … Rothberg, J. M., "A Protein Interaction Map of Drosophila melanogaster," *Science (80-.).*, vol. 302, no. 5651, pp. 1727–1736, Dec. 2003, doi: 10.1126/science.1090289.

[359] Choi, H. … Nesvizhskii, A. I., "SAINT: Probabilistic scoring of affinity purificationg-mass spectrometry data," *Nat. Methods*, vol. 8, no. 1, pp. 70–73, Jan. 2011, doi: 10.1038/nmeth.1541.

[360] Liu, W. … Ren, J., "IBS: an illustrator for the presentation and visualization of biological sequences: Fig. 1.," *Bioinformatics*, vol. 31, no. 20, pp. 3359–3361, Oct. 2015, doi: 10.1093/bioinformatics/btv362.

[361] Truebestein, L. & Leonard, T. A., "Coiled-coils: The long and short of it," *BioEssays*, vol. 38, no. 9, pp. 903–916, Sep. 2016, doi: 10.1002/bies.201600062.

[362] Keown, J. R., Black, M. M., Ferron, A., Yap, M., Barnett, M. J., Grant Pearce, F., Stoye, J. P., & Goldstone, D. C., "A helical LC3-interacting region mediates the interaction between the retroviral restriction factor Trim5 and mammalian autophagy-related ATG8 proteins," *J. Biol. Chem.*, vol. 293, no. 47, pp. 18378–18386, Nov. 2018, doi: 10.1074/jbc.RA118.004202.

[363] Chen, L., Paquette, N., Mamoor, S., Rus, F., Nandy, A., Leszyk, J., Shaffer, S. A., & Silverman, N., "Innate immune signaling in Drosophila is regulated by transforming growth factor β (TGFβ)-activated kinase (Tak1)-triggered ubiquitin editing," *J. Biol. Chem.*, vol. 292, no. 21, pp. 8738–8749, May 2017, doi: 10.1074/jbc.M117.788158.

[364] Sato, S., Sanjo, H., Takeda, K., Ninomiya-Tsuji, J., Yamamoto, M., Kawai, T., Matsumoto, K., Takeuchi, O., & Akira, S., "Essential function for the kinase TAK1 in innate and adaptive immune responses," *Nat. Immunol.*, vol. 6, no. 11, pp. 1087–1095, Nov. 2005, doi: 10.1038/ni1255.

[365] Takatsu, Y., Nakamura, M., Stapleton, M., Danos, M. C., Matsumoto, K., O'Connor, M. B., Shibuya, H., & Ueno, N., "TAK1 Participates in c-Jun N-Terminal Kinase Signaling during Drosophila Development," *Mol. Cell. Biol.*, vol. 20, no. 9, pp. 3015–3026, May 2000, doi: 10.1128/mcb.20.9.3015-3026.2000.

[366] HuangFu, W. C., Omori, E., Akira, S., Matsumoto, K., & Ninomiya-Tsuji, J., "Osmotic stress activates the TAK1-JNK pathway while blocking TAK1-mediated NF-κB activation: TAO2 regulates TAK1 pathways," *J. Biol. Chem.*, vol. 281, no. 39, pp. 28802–28810, Sep. 2006, doi: 10.1074/jbc.M603627200.

[367] Tan, S. H. … Tan, N. S., "Regulation of cell proliferation and migration by TAK1 via transcriptional control of von Hippel-Lindau tumor suppressor," *J. Biol. Chem.*, vol. 284, no. 27, pp. 18047–18058, Jul. 2009, doi: 10.1074/jbc.M109.002691.

[368] Mihaly, S. R., Ninomiya-Tsuji, J., & Morioka, S., "TAK1 control of cell death," *Cell Death and Differentiation*, vol. 21, no. 11. Nature Publishing Group, pp. 1667–1676, Aug. 22, 2014. doi: 10.1038/cdd.2014.123.

[369] Lamothe, B., Lai, Y., Xie, M., Schneider, M. D., & Darnay, B. G., "TAK1 Is Essential for Osteoclast Differentiation and Is an Important Modulator of Cell Death by Apoptosis and Necroptosis," *Mol. Cell. Biol.*, vol. 33, no. 3, pp. 582–595, Feb. 2013, doi: 10.1128/mcb.01225-12.

[370] Mukhopadhyay, H. & Lee, N. Y., "Multifaceted roles of TAK1 signaling in cancer," *Oncogene*, vol. 39, no. 7. NIH Public Access, pp. 1402–1413, Feb. 13, 2020. doi: 10.1038/s41388-019-1088-8.

[371] Badinloo, M., Nguyen, E., Suh, W., Alzahrani, F., Castellanos, J., Klichko, V. I., Orr, W. C., & Radyuk, S. N., "Over-expression of antimicrobial peptides contributes to aging through cytotoxic effects in Drosophila tissues," *Arch. Insect Biochem. Physiol.*, vol. 98, no. 4, p. e21464, Aug. 2018, doi: 10.1002/ARCH.21464.

[372] Kehl, S. R., Soos, B. A., Saha, B., Choi, S. W., Herren, A. W., Johansen, T., &

Mandell, M. A., “TAK 1 converts Sequestosome 1/p62 from an autophagy receptor to a signaling platform,” *EMBO Rep.*, Jul. 2019, doi: 10.15252/embr.201846238.

[373] Van Weering, J. R. T., Sessions, R. B., Traer, C. J., Kloer, D. P., Bhatia, V. K., Stamou, D., Carlsson, S. R., Hurley, J. H., & Cullen, P. J., “Molecular basis for SNX-BAR-mediated assembly of distinct endosomal sorting tubules,” *EMBO J.*, vol. 31, no. 23, pp. 4466–4480, Nov. 2012, doi: 10.1038/emboj.2012.283.

[374] Paquette, N. … Silverman, N., “Serine/threonine acetylation of TGFβ-activated kinase (TAK1) by Yersinia pestis YopJ inhibits innate immune signaling,” *Proc. Natl. Acad. Sci. U. S. A.*, vol. 109, no. 31, pp. 12710–12715, Jul. 2012, doi: 10.1073/pnas.1008203109.